Stochastic models for $CD4^+$ T cells

Luis de la Higuera Romero

Submitted in accordance with the requirements for the degree of Doctor of Philosophy

The University of Leeds

Department of Applied Mathematics

November 2017

Everything existing in the universe is the fruit of chance and necessity.

DEMOCRITUS

Acknowledgements

I would like to acknowledge to the European Union for the economical support for this work. In particular, to the Quantitative T cell Immunology (QuanTI) Initial Training Network (ITN) for having trained me in Systems Immunology and giving me the opportunity of learning from lots of great experimental and theoretical scientists.

To my supervisors, Carmen Molina-París, Martín López-García and Grant Lythe, who have patiently guided me through my tasks, and to my whole research group from whom I could learn and receive support in the not so good moments.

I would also like to thank to Pasteur Institute and, in particular, to Antonio Freitas and Sary El Daker, for providing some data for my mathematical analysis and for their help in my immunological learning.

To Stuart Barber and John Paul Gosling, from the University of Leeds, for helping me out very kindly with the statistical analysis.

To my family and friends, whose company is my real motivation.

Abstract

In this thesis, we study the mechanisms involved in $CD4^+$ T cell activation focusing on the crucial role of costimulation for an effective immune response. For this purpose, interactions between receptors from T cells and ligands on the APCs, as well as the trafficking of these molecules, need to be analysed. At the same time, population models are developed to study their homeostatic behaviour and the role of IL-2, as well as quorum-sensing mechanisms in $CD4^+$ T cell maintenance. A multidisciplinary approach that combines statistical analysis of experimental data and mathematical models that describe the experiments, has been used that take into account the stochastic nature of these processes. We have combined deterministic methods when appropriate with stochastic ones, as well as made us of numerical simulations.

Related Publications

[1] **de la Higuera, L** and López-García, M and Lythe, G and Molina-París, C. *IL-2 Stimulation of Regulatory T Cells: A Stochastic and Algorithmic Approach*. In Modeling Cellular Systems, Springer (2017) (editors: Pahle J, Matthaus F, Graw F).

[2] **de la Higuera, L** and López-García, M and Lythe, G and Molina-París, C. *Stochastic model of CTLA-4 mediated ligand trans-endocytosis* Proceedings of the Royal Society of Edinburgh. *(To submit*).

[3] El Daker, S and **de la Higuera, L** and Molina-París, C and Freitas, AA. *In: Quorum-Sensing like mechanism of CD*4^+ *Tregs*. (In preparation).

Contents

List of figures

List of tables

Chapter 1

Introduction

1.1 Immunological motivation

1.1.1 The role of T cells in the immune system

Immunology is a relatively young area of research. It was only in 1983 that the precise nature of the T cell receptor that uniquely characterises T cells was discovered. It is in this sense, that we can say immunology is nowadays still evolving as a mature science. Therefore, having a clear structure of the events that take place in a host when an infection occurs, the main components involved and the characteristics of such a process should be the first steps to follow when introducing any particular topic in the field as in the case of the present work.

Once the initial physical and chemical barriers are run through, an infectious agent (**pathogen**) faces a combination of multiple cells and molecules in the organism whose ability to interact between themselves and against the invader will determine the outcome of the immune response. In fact, it is very common ([48] or [67] among others) to divide the functions of the immune response between those referring to recognise and even completely neutralise external pathogens, such as viruses or bacteria, and those tasks involving self-regulation, so the organism is not damaged when the response is taking place. Moreover, the ability of the immune system to learn from specific antigens so certain cells can keep the *memory* for subsequent attacks also plays a central role on the capacity of immune system to defend us.

1.1.2 Different cells for different responses.

Depending on the characteristics of the response, this can be described as **innate** or **adaptive** [65]. The former takes place within a matter of hours and it is not antigen specific, that is, it is produced disregarding the kind of molecule inducing immune response whereas the adaptive response might take days to be completed and involves a more complicated process of recognition between the host cell and the pathogen for the signal to be triggered. Although the current work focuses on the adaptive one, a proper overlap of both is essential when the innate response fails to deal the infection [46].

This adaptive response is mainly driven by **T lymphocytes** (T cells), which give *instructions* to other cells and between them about how to proceed when pathogens replicate in the body. T cell precursors originate in the bone marrow and mature in the thymus (undergoing positive and negative selection). Only around 3% of immature T cells entering the thymus complete the maturation process and are released into the periphery [66]. T cells in the periphery recognise pathogens during an infection by means of a specific molecule that they express on their surface, the **T cell receptor** (TCR). Maturation in the thymus ensures that the TCR is functional but, at the same time, will not mount a potential autoimmune response in the periphery.

T cells in the periphery have very different functions depending on the class they belong to. **Helper** T cells ($CD4^+$ T cells) assist other cells within the immune system, such as **B lymphocytes** (B cells) or **cytotoxic** T cells ($CD8^+$ T cells), during an immune response. Cytotoxic T cells are directly capable of killing virus-infected cells by recognising particular molecules expressed on the surface of these target cells. T cells which are released into the periphery and have not participated yet in an immune response are called **naive** T cells. Upon primary infection, naive T cells, which are able to recognise the corresponding pathogen, undergo proliferation and clonal expansion when their TCR bind a specific molecule (**peptide**), by means of the **major histocompatibility complexes** (pMHC) that is located in an **antigen presenting cells** (APCs) (see Figure 1.1).

After this occurs, a clonal contraction follows, which is tightly regulated by a subpopulation of $CD4^+$ T cells called **regulatory** T cells (Treg cells). Regulatory T cells are responsible for restraining the immune response within *safe* levels, as well as for avoiding the occurrence of potential autoimmune responses caused by T lymphocytes which may have erroneously escaped negative selection in the thymus; see [11]. After clonal contraction, a small pool of those T cells that participated in the immune response is selected to remain in the periphery, becoming

memory T cells. These will be able then to mount a faster immune response following a potential secondary exposure to the same pathogen [11].

1.1.3 Stages on an immune response.

It is commonly accepted that three different types of signal are generally involved in the whole process of T cell activation.

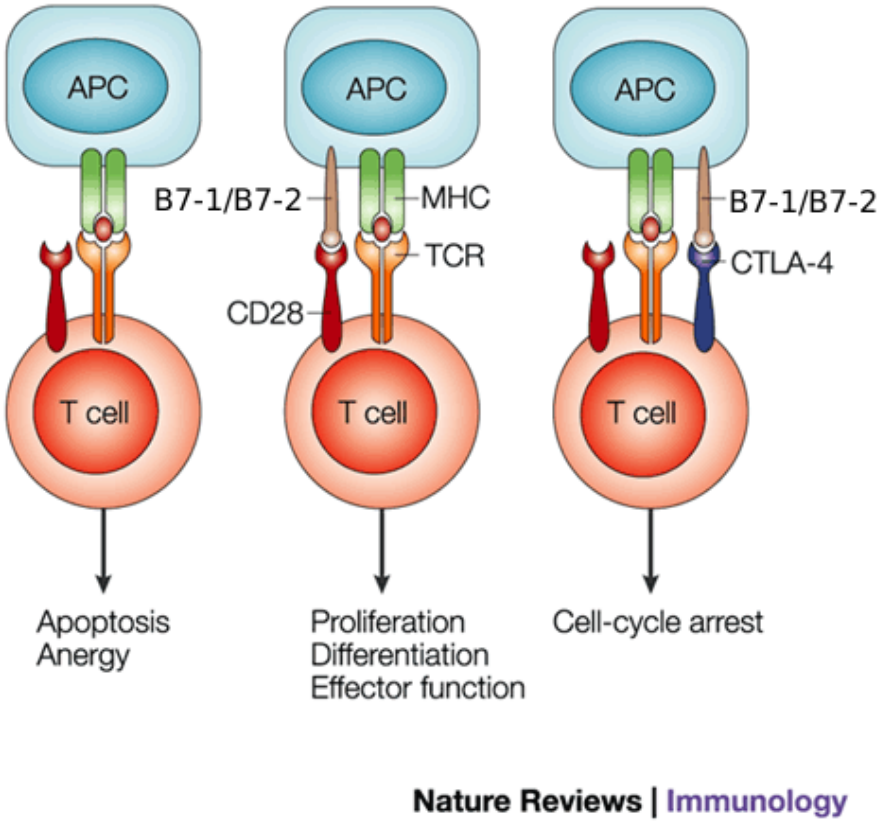

Figure 1.1: Diagram of different pathways within T cell activation process that might drive into apoptosis (death of the cell), in the absence of signal 2; into the third step, when the balance between co-receptor CD28 with ligands B7-1 and B7-2 (also referred as CD80 and CD86) is adequate or to an arrest of the cell-cycle, when the inhibitory signal produced by CTLA-4 is too high. Figure taken from [3].

Signal 1, which would trigger the other two, is mediated by the T-cell receptor and normally takes place in the peripheral lymphoid organs. This engagement might also be enforced by either co-receptor CD4 or CD8 [21] but it will not assure the activation of such a cell. Signal 2, arises

as a balance between inhibitory and promoting signals produced by co-receptors **CTLA-4** and **CD28**, respectively, located on the T cells, when binding certain members of the immunoglobulin superfamily, B7 molecules, which appear on the surface of APCs [36]. In particular, this so-called **co-stimulatory system** (see Figure 1.1) mainly involves the dynamics of the two co-receptor with ligands **B7-1** and **B7-2** (also called CD80 and CD86) which, with different particularities, might drive the immune response to distinct pathways as it will be observed later on. Although a more in detail explanation will head every chapter, there is a correspondence between some signals and the chapters of this thesis. Chapter 3 studies a co-stimulatory system model to understand and predict some of the characteristics of this signal 2.

Finally, signal 3 corresponds to certain **cytokines** (proteins released by activated cells which, once bound with specific receptors, they induce a particular response) called interleukins, which are produced in this case by a subpopulation of T cells. In particular, **interleukin-2** (IL-2), but also interleukin-7 (IL-7), are the key factors in an important process of self-regulation, called quorum-sensing, in which T cells replicate accordingly to the needs of the system by being capable of perceiving their own population levels [5].

Figure 1.2 shows a general diagram from the antigen-mediated activation to the differentiation of either $CD4^+$ or $CD8^+$ in an IL-2 mediation manner regulated by regulatory T cells. These cells are characterised by the presence of FOXP3, a transcription factor, and CD25, which is the high affinity IL-2 receptor. Thus, effector T cell, those IL-2 producer, together with regulatory T cells, mainly those which can bind IL-2, play an important role in the quorum-sensing process described in Chapter 4. At the same time, the main dynamics of IL-2 when trafficking within a regulatory T cell and binding IL-2R are stochastically described in Chapter 2.

Apparently, it seems evident that regulatory T cells have an important role in both signals 2 and 3. In fact, some experiments have shown that regulatory cells knockout mice, this is, mice whose regulatory cells have been removed, they end up with autoimmune diseases, inflammatory bowel diseases and tumour rejection [61]. Nevertheless, it is not clear the average levels of regulatory T cells at which the immune response might be optimised. In contrast to what has been done in the rest of the chapters, in which in vitro data have been taken from literature to calibrate the models, Chapter 4 appears as a result of a collaborative project with experimentalist partners from Pasteur Institute in Paris. Therefore, data come from in vivo mice in which population levels of this regulatory T cells, among others, were tracked under different scenarios as it will be described in the aforesaid chapter.

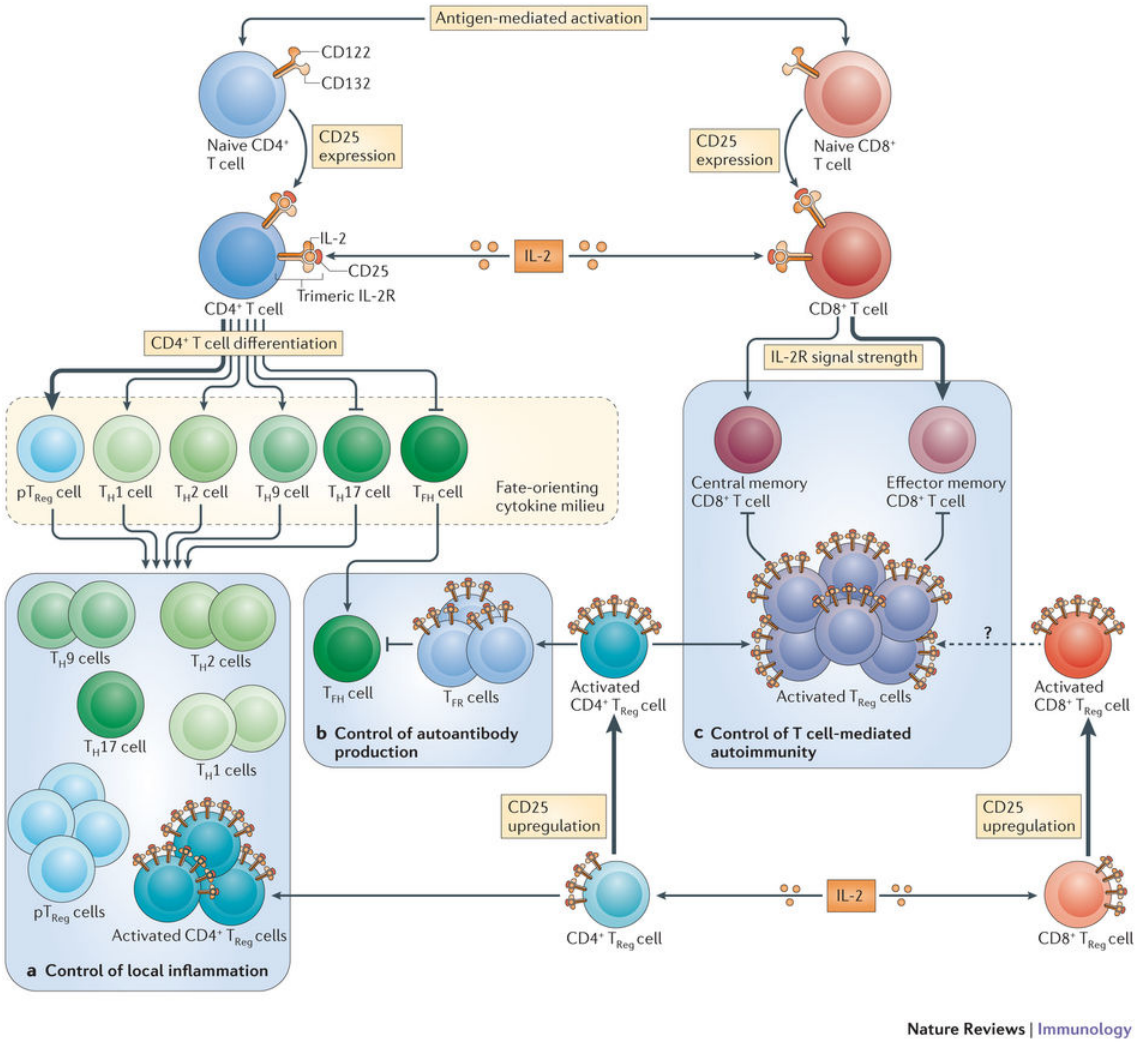

Figure 1.2: Once $CD4^+$ or $CD8^+$ become activated, their differentiation fate is affected by interleukins mediation, each of them related to a specific kind of effector T cell (T_H cells) which whole ream of possibilities will not be considered in this work. However, it is known that IL-2 and its high affinity receptor CD25 (IL-2R) affects the whole T cell fate process [71]. This IL-2 receptor is constitutively expressed in regulatory T cells and both take part of the quorum-sensing mechanism described in Chapter 4. Figure taken from [32].

The role of regulatory T cells in the immune system has been of particular interest when dealing with tumour scenarios. [20] or [49], among others, show how the progression of different cancers is highly correlated to a high expression level of regulatory T cells. In particular, their relative population levels together with effector $CD8^+$ cells seem to be an important factor for tumour prognosis [70]. In such situations, effector cells in charged of eliminating tumour cells, would be

blocked by a too high amount of T reg cells, allowing the tumour to spread. In Chapter 5, this quorum-sensing mechanism will be analysed to elucidate which conditions would drive a poor or a better tumours prognosis.

1.2 Mathematical introduction

From a mathematical perspective, stochastic processes are the main tool followed to canvass an important set of immunological issues in this work. More precisely, the particularities of the biological frames under study, make Markov processes an ideal candidate for approaching the main mechanisms that drive the nature of such systems, in which randomness plays an essential role. Therefore, the fact of not taking into account aleatory behaviour might sometimes disregard crucial features of the models. This can be addressed as a consequence of what is behind the Markovian approach; the idea that responses of a system can be predicted only by knowing the current situation of the process and that they do not depend on previous facts. Some examples of the applicability of such approach can be found in epidemiology, genetics, finance, telecommunications or genomics.

This scenario is also the case for Chapters 2 and 3, in which interactions of molecules from a certain type of T cell to another, or within a same cell, might take place. The purposes of this mathematical introduction are, primarily, to briefly introduce first and previous biological examples in which the main tool behind this stochastic approach, the matrix-analytic methods, was used. Secondly, to define some of the methodology that is used in those Sections, so the reader might find more straightforward the biological tales behind each of those approaches without an excessive overlapping with definitions and development of the mathematical structure. We will refer to the concepts made below during Chapters 2, 3 and 5 when needed.

Matrix-analytic methods were originally applied as a tool to deal with bi-dimensional systems, with some special properties, and verifying Markovian assumptions in an algorithmic and manipulable structure, as it will be seen by the end of this section. From its utility in queuing theory to broader applications in epidemiology or immunology, these methods rely on certain techniques to arrange states of given processes which allows the construction of algorithms. These arrangements permits transferring limitations to computational capacities by working from groups and sub-groups conveniently represented by blocks and sub-blocks of matrices.

1.2.1 Markov processes and the exponential distribution

Markov processes can be widely found in literature when approaching to biology and medicine. For instance, studies like [10] claim that the completion time for sequential macromolecules reactions can be exponentially distributed, and that this seems to be extended to more complex biochemical systems. This Markovian assumptions, which simplify the nature of the system for making it more tractable, have been then broadly used in immunology when analysing molecules and cells interactions. In particular, for modelling $CD4^+$ dynamics, References [26, 33, 55] could be used as examples. Let us start then with a definition:

Definition 1.2.1 *A* **continuous-time Markov chain** *(CTMC) is a continuous-time stochastic process* $\mathcal{X} = \{X(t) : t \geq 0\}$ *over the discrete state space* $\mathcal{S}$*, where* $t \in [0, +\infty)$ *continuous and where* $X(t)$ *is a discrete random variable with probability mass function* $\{p_i(t) : i \in \mathcal{S}\}$ *which satisfies the* **Markovian property***, that is,*

$$\mathbb{P}(X(t+s) = j | X(s) = i) = \mathbb{P}(X(t+s) = j | X(s) = i, X(u) = i_u, u \in [0, s)),$$

for all states $i, j \in \mathcal{S}$ *and all times* $s, t \geqslant 0$*.*

This implies that the probability for the process to move to a certain state j in the next movement only depends on where the process is at the present, state i, and not where it was in the past, states $\{i_u, u \in [0, s)\}$. If the process satisfies the time homogeneity property, as it will be assumed from now on, that is,

$$\mathbb{P}(X(t) = j | X(s) = i) = \mathbb{P}(X(t-s) = j | X(0) = i),$$

we can denote the transition probabilities $p_{ij}(t) = \mathbb{P}(X(t) = j | X(0) = i)$. The **transition matrix** $\mathbf{P}(t)$ of a CTMC $\mathcal{X}$ is then defined as

$$\mathbf{P}(t) = (p_{ij}(t))_{i,j \in \mathcal{S}}, \tag{1.1}$$

and satisfies

$$\begin{aligned} p_{ij}(t) &\geqslant 0, \\ \sum_{j=0}^{+\infty} p_{ij}(t) &= 1, \\ p_{ij}(t+s) &= \sum_{k\in\mathcal{S}} p_{ik}(t)p_{kj}(s), \end{aligned} \tag{1.2}$$

for all $i, j \in \mathcal{S}$ and for all $t, s \geqslant 0$. The third property is referred to as the **Chapman-Kolmogorov** equations. Moreover, $\mathbf{P}(t)$ is a right stochastic matrix, a real square matrix with each row summing up to 1, and there is a one-to-one relation between a Markov chain and its transition matrix.

A CTMC can be characterised by its initial distribution $\{p_i(0) = \mathbb{P}(X(0) = i) : i \in \mathcal{S}\}$ and $\mathbf{P}(t)$, for each $t \geqslant 0$. However, the probabilities $p_{ij}(t)$ and so the transition matrix are not always easy to obtain, see Example 1.2.3 in this Section. In these situations, as occurs later on in other chapters, an alternative construction of $\mathcal{X}$ can be given to describe the evolution of the system.

An alternative way of dealing with a CTMC requires the use of transition rates q_{ij}, where $i, j \in \mathcal{S}$, that can be derived from transition probabilities $p_{ij}(t)$, where $i, j \in \mathcal{S}$, as explained in next Definition 1.2.2.

Definition 1.2.2 *Given a CTMC $\mathcal{X} = \{X(t) : t \geq 0\}$ over the state space $\mathcal{S}$ with transition probabilities $p_{ij}(t)$, where $i, j \in \mathcal{S}$, continuous and differentiable for $t \geqslant 0$, and satisfying*

$$p_{ij}(0) = \begin{cases} 0, & \text{if } i \neq j, \\ 1, & \text{if } i = j, \end{cases}$$

the **transition rates** *q_{ij}, where $i, j \in \mathcal{S}$, can be defined as*

$$q_{ij} = \begin{cases} \lim\limits_{\Delta t\to 0^+} \frac{p_{ij}(\Delta t)-p_{ij}(0)}{\Delta t} = \lim\limits_{\Delta t\to 0^+} \frac{p_{ij}(\Delta t)}{\Delta t}, & \text{if } i \neq j, \\ \lim\limits_{\Delta t\to 0^+} \frac{p_{ii}(\Delta t)-p_{ii}(0)}{\Delta t} = \lim\limits_{\Delta t\to 0^+} \frac{p_{ij}(\Delta t)-1}{\Delta t}, & \text{if } i = j. \end{cases}$$

From Equation (1.2) and the fact that $q_{ij} \geqslant 0$ for $i \neq j$, it follows that

$$q_{ii} = -\sum_{j\in\mathcal{S};j\neq i} q_{ij} = -q_i, \quad i \in \mathcal{S}, \tag{1.3}$$

and thus the following property holds

$$\sum_{j\in\mathcal{S}} q_{ij} = 0, \quad i \in \mathcal{S}.$$

These transition rates, analogously to the transition probabilities in Equation (1.1), can be gathered in a matrix called the *infinitesimal generator* matrix, defined next.

Definition 1.2.3 *The* **infinitesimal generator Q** *of a given CTMC* $\mathcal{X} = \{X(t) : t \geq 0\}$ *with transition rates* q_{ij}, $i, j \in \mathcal{S}$, *is defined as*

$$\mathbf{Q} = (q_{ij})_{i,j\in\mathcal{S}}, \tag{1.4}$$

where q_{ij} *denotes the rate to move from state* i *to state* j.

The following relation can be then established.

Theorem 1.2.1 (Forward and backward Kolmogorov equations) *Let* $\mathbf{P}(t)$ *and* $\mathbf{Q}$ *be the transition matrix and the generating matrix of a CTMC* $\mathcal{X} = \{X(t) : t \geq 0\}$, *respectively. Then,* $\mathbf{P}(t)$ *is differentiable with respect to t and*

$$\frac{d\mathbf{P}(t)}{dt} = \mathbf{P}(t)\mathbf{Q} \tag{1.5}$$

and

$$\frac{d\mathbf{P}(t)}{dt} = \mathbf{Q}\mathbf{P}(t), \tag{1.6}$$

with the initial condition

$$\mathbf{P}(0) = \mathbf{I},$$

are called, respectively, the forward and backward Kolmogorov differential equations. $\frac{d\mathbf{P}(t)}{dt}$ *denotes the element-by-element derivative of* $\mathbf{P}(t)$ *with respect to t and* $\mathbf{I}$ *is the identity matrix of size* $\#\mathcal{S}$, *the cardinality of* $\mathcal{S}$.

In scalar form, Equation (1.5) can be rewritten as

$$\frac{dp_{ij}(t)}{dt} = \sum_{k=0}^{+\infty} p_{ik}(t)q_{kj}, \quad i, j \in \mathcal{S}, \quad t \geqslant 0,$$

which is usually referred to as the master equation of the CTMC $\mathcal{X}$. The solution of Equations (1.5)-(1.6) is given by

$$\mathbf{P}(t) = e^{\mathbf{Q}t}, \tag{1.7}$$

where

$$e^{\mathbf{Q}t} = \sum_{k=0}^{+\infty} \frac{(\mathbf{Q}t)^k}{k!}.$$

This convergent power series can be, in principle, computed in many ways depending on the characteristic of the matrix $\mathbf{Q}$. However the analytical expression is circumscribe to quite specific situations, as reported in [47], in which case numerical methods for solving differential equations need to be used. On the other hand, there are several approaches to obtain $\mathbf{P}(t)$ as an explicit function of t which are constrained to specific scenarios. For instance, when dealing with a CTMC $\mathcal{X} = \{X(t) : t \geq 0\}$ with a finite state space $\mathcal{S}$ and a diagonalizable generating matrix $\mathbf{Q}$, an explicit expression of $\mathbf{P}(t)$ can be obtained by dealing with the eigenvalues of $\mathbf{Q}$. The *uniformation method*, described in [77], is another useful approach which works only under specific situations for both finite and infinite state space $\mathcal{S}$. Based on stability and efficiency criteria, some of these approaches and others might be more appropriate. Reference [47] provides a full list of different methods when solving the exponential of a matrix.

The exponential distribution plays a crucial role when dealing with Markov processes.

Definition 1.2.4 *A random variable X has an* **exponential distribution** *with parameter λ, $X \sim exp(\lambda)$, if its probability distribution function is given by*

$$\mathcal{F}(x) = 1 - e^{-\lambda x}, \quad x \geqslant 0, \tag{1.8}$$

where $\lambda > 0$ is a fixed constant.

It can be shown [28] that exponential random variables are the only non-negative, continuous random variables that possess the *memoryless property*.

Definition 1.2.5 *The probability distribution of a random variable X has the* **memoryless property** *if*

$$\mathbb{P}(X > t + s | X > s) = \mathbb{P}(X > t), \tag{1.9}$$

for all $s, t \geqslant 0$.

Moreover, this property is behind the proof that exponential distribution is closed under the minimum operation. In particular, if $\{X_1, ..., X_n\}$ are independent exponentially distributed random variables with parameters $\{\lambda_j : 1 \leq j \leq n\}$ then

1. $X = \min\{X_1, ..., X_n\}$ has a exponential distribution with parameter $\sum_{j=1}^{n} \lambda_j$ and
2. $\mathbb{P}(X_j = \min\{X_1, ..., X_n\}) = \frac{\lambda_j}{\lambda_1 + \cdots + \lambda_n}$.

Let us recall that given a CTMC $\mathcal{X}$, from Equation (1.3), $q_i = \sum_{k \in \mathcal{S}: k \neq i} q_{ik}$ and let us denote $p_{ij} = \frac{q_{ij}}{\sum_{k \in \mathcal{S}: k \neq i} q_{ik}}$. Thus, an alternative definition of a CTMC is given in Definition 1.2.6.

Definition 1.2.6 *A* **continuous-time Markov chain** *(CTMC) is a continuous-time stochastic process $\mathcal{X} = \{X(t) : t \geq 0\}$ over the discrete state space $\mathcal{S}$ if and only if given the sequence of events $0 < S_1 < S_2 < \ldots$ of $\mathcal{X}$ where S_n, $n \geqslant 1$, is the time of the n_{th} transition, the process $\{X_0, (X_n, Y_n) : n \geqslant 1\}$ satisfies*

$$\mathbb{P}(X_{n+1} = j, Y_{n+1} > y | X_n = i, Y_n, X_{n-1}, Y_{n-1}, ..., X_1, Y_1, X_0) \quad = \quad p_{ij} e^{-q_i y}, \quad i, j \in \mathcal{S}, n \geqslant 0,$$

where $Y_n = S_n - S_{n-1}$ (with $S_0 = 0$) is called the n_{th} **sojourn time**, *and X_n the state of the system after the n_{th} transition.*

Alternative Definition 1.2.6 has the following interpretation. Given a CTMC $\mathcal{X} = \{X(t) : t \geq 0\}$ over the state space $\mathcal{S}$, if the process is at state $X(t) = i$, where $i \in \mathcal{S}$ at a given time $t \geqslant 0$, its dynamics can be studied as a competition of exponentially distributed random times. Thus, for those states $j \in \mathcal{S}$, $j \neq i$, which are directly accessible from i in one jump (for notation $j \in AC(i)$), such jump occurs after an exponentially distributed random time $exp(q_{ij})$, where q_{ij} is the infinitesimal transition rate from state i to state j. Then, this movement actually takes place with probability $p_{ij} = \frac{q_{ij}}{\sum_{k \in \mathcal{S}: k \neq i} q_{ik}}$ and the total time that the process $\mathcal{X}$ stays in state $i \in \mathcal{S}$ is exponentially distributed $exp(\sum_{k \in \mathcal{S}: k \neq i} q_{ik})$. This idea is the basis of the Gillespie algorithm for simulating Markov processes (Definition 1.2.7). More details can be found in [34, Chapter 4].

Definition 1.2.7 *The* **Gillespie algorithm** *for a given CTMC $\mathcal{X} = \{X(t) : t \geq 0\}$ with initial state $X(t_0 = 0) = n_0$ and a final simulation time $T > t_0$, follows the following steps:*

$n = n_0$;

$t = t_0$;

while $t < T$:

for k in $AC(n)$*:*

$u_k \sim U[0,1)$;

$e_k = -\frac{\log(1-u_k)}{q_{nk}}$;

$\tau = \min_{k \in AC(n)} \{e_k\}$;

$t = t + \tau$;

$n = argmin_{k \in AC(n)} \{e_k\}$;

where argmin is the index of the minimum value of $\{e_k : k \in AC(n)\}$.

A Gillespie python code is shown in the Appendices.

1.2.2 From Poisson processes to quasi-birth-and-death processes

Let us start with a simple example of a CTMC which is the Poisson process.

Example 1.2.1 *The Poisson process with parameter* λ *can be defined as a continuous-time Markov chain* $\mathcal{X} = \{X(t) : t \geq 0\}$ *over the state space* $\mathcal{S} = \mathbb{N}_0 = \mathbb{N} \cup \{0\}$ *satisfying*

1. $X(0) = 0$, *and*
2. *for h sufficiently small and for all* $i, j \in \mathcal{S}$,
   - $p_{i,i+1}(h) = \lambda h + o(h)$,
   - $p_{i,i}(h) = 1 - \lambda h + o(h)$,
   - $p_{i,j}(h) = o(h)$, *if* $j > i + 1$ *and*
   - $p_{i,j}(h) = 0$, *if* $j < i$,

where $\lim_{h \to 0} \frac{o(h)}{h} = 0$.

Figure 1.3 shows a diagram of the Poisson process with parameter λ.

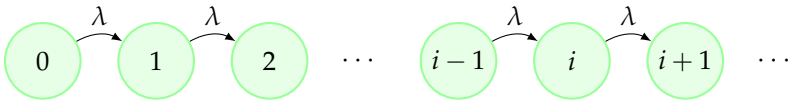

Figure 1.3: Diagrammatic representation of the Poisson process with parameter λ.

A more general extension of the Poisson process appears when allowing the system not only to increase, but to decrease. This leads to the general birth-and-death process.

Example 1.2.2 *The general birth-and-death process can be defined as a continuous-time Markov chain* $\mathcal{X} = \{X(t) : t \geq 0\}$ *over the state space* $\mathcal{S} = \mathbb{N}_0$ *satisfying*

1. $X(0) = 0$ *and*
2. *for* h *sufficiently small and for all* $i, j \in \mathcal{S}$,
   - $p_{i,i+1}(h) = \lambda_i h + o(h)$,
   - $p_{i,i-1}(h) = \mu_i h + o(h)$,
   - $p_{i,i}(h) = 1 - (\lambda_i + \mu_i)h + o(h)$,
   - $p_{i,j}(h) = o(h)$, *otherwise.*

Figure 1.4 shows a diagram of the birth-and-death process over the state space $\mathcal{S} = \mathbb{N}_0$, with parameters λ_i, for all $i \geqslant 0$, and μ_i, for all $i \geqslant 1$. Two particular cases of this process appear when only considering arrows in one direction. Thus, the *pure birth process* would satisfy $\mu_i = 0$, for all $i \geqslant 1$, whereas the *pure death process* fulfils $\lambda_i = 0$, for all $i \geqslant 0$.

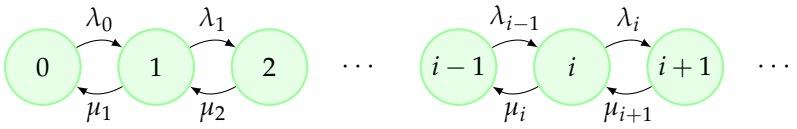

Figure 1.4: Diagram of the general birth-and-death process.

The corresponding generating matrices $\mathbf{Q}_P$ and $\mathbf{Q}_{BD}$ of the Poisson and the birth-and-death process, respectively, are given by the following expressions

$$\mathbf{Q}_P = \begin{pmatrix} -\lambda & \lambda & 0 & \dots \\ 0 & -\lambda & \lambda & \dots \\ 0 & 0 & -\lambda & \dots \\ \vdots & \vdots & \vdots & \ddots \end{pmatrix}$$

and

$$\mathbf{Q}_{BD} = \begin{pmatrix} -\lambda_0 & \lambda_0 & 0 & \dots \\ \mu_1 & -\lambda_1 - \mu_1 & \lambda_1 & \dots \\ 0 & \mu_2 & -\lambda_2 - \mu_2 & \dots \\ \vdots & \vdots & \vdots & \ddots \end{pmatrix}.$$

The following definition can be seen as an extension of the birth-and-death process which keeps some of its transitions structure.

Definition 1.2.8 *The* **quasi-birth-and-death process** *(QBD) is a two-dimensional continuous-time Markov process* $\{(\mathcal{N}(t), \mathcal{E}(t)) : t \geqslant 0\}$ *over the state space*

$$\mathcal{S} = \{(n, i) : n \geqslant 0, 1 \leq i \leq m\}, \quad \textit{where n and i are the level and the phase of the process,}$$

with level-restricted transitions to neighbour.

This means that from a state $(n, i) \in \mathcal{S}$, one-step transitions are only possible to $(n-1, j), (n, j), (n+1, j) \in \mathcal{S}$. The process can be analysed as a two dimensional process with a block structure by levels and an intra-block structure by phases. The generating matrix $\mathbf{Q}^{LI}_{QBD}$ for a level-independent QBD process has the form

$$\mathbf{Q}^{LI}_{QBD} = \begin{pmatrix} \mathbf{S} - \mathbf{\Lambda} & \mathbf{\Lambda} & \mathbf{0} & \dots \\ \mathbf{M} & \mathbf{S} - \mathbf{\Lambda} - \mathbf{M} & \mathbf{\Lambda} & \dots \\ \mathbf{0} & \mathbf{M} & \mathbf{S} - \mathbf{\Lambda} - \mathbf{M} & \dots \\ \vdots & \vdots & \vdots & \ddots \end{pmatrix}$$

where $\mathbf{S}$, $\mathbf{\Lambda}$ and $\mathbf{M}$ are $m \times m$ matrices, $\mathbf{S}$ is the generating matrix of $\{\mathcal{E}(t) : t \geqslant 0\}$, see Example 1.2.3.

For the cases in which transition matrices $\mathbf{S}$, $\mathbf{\Lambda}$ and $\mathbf{M}$ vary from one level to another, a different version of quasi-birth-and-death process arises. We refer this as a level-dependent QBD process, whose generating matrix $\mathbf{Q}_{QBD}^{LD}$, has the form

$$\mathbf{Q}_{QBD}^{LD} = \begin{pmatrix} \mathbf{S_{0,0}} - \mathbf{\Lambda_{0,1}} & \mathbf{\Lambda_{0,1}} & \mathbf{0} & \cdots \\ \mathbf{M_{1,0}} & \mathbf{S_{1,1}} - \mathbf{\Lambda_{1,2}} - \mathbf{M_{1,0}} & \mathbf{\Lambda_{1,2}} & \cdots \\ \mathbf{0} & \mathbf{M_{2,1}} & \mathbf{S_{2,2}} - \mathbf{\Lambda_{2,3}} - \mathbf{M_{2,1}} & \cdots \\ \vdots & \vdots & \vdots & \ddots \end{pmatrix}, \tag{1.10}$$

where submatrices satisfy the same conditions as in $\mathbf{Q}_{QBD}^{LI}$, but their elements might change from one level to another. These will be the type of generating matrices we will find in subsequent chapters. Intuitively, the similar tridiagonal structure of $\mathbf{Q}_{BD}$ and $\mathbf{Q}_{QBD}$ is behind the applicability of matrix-analytic methods, which allows to study characteristics of interest in these processes in an algorithmic manner. We note that generating matrices $\mathbf{Q}_{QBD}^{LI}$ and $\mathbf{Q}_{QBD}^{LD}$ encode the rates to move from each state to another state in $\mathcal{S}$ but, where states are ordered in the same way by rows and columns. It will be observed in some of the following chapters that the success of this matrix-analytic approach relies, to a large extend, on the election of this order, that is, how to arrange these infinitesimal generators. Additional details about matrix-analytic methods can be found in [28]- [35].

Example 1.2.3 *Suppose we are working with a quasi-birth-and-death process* $\{(\mathcal{N}(t), \mathcal{E}(t)) : t \geqslant 0\}$, *with* $m = 3$ *phases per level, over the state space*

$$\mathcal{S} = \{(n, i) : n \geqslant 0, 1 \leq i \leq 3\}, \quad \textit{where n and i are the level and the phase of the process}$$

with level-restricted transitions to neighbour and which diagrammatic representation is given in Figure 1.5.

Therefore, its generating matrix $\mathbf{Q}_{QBD}^{LI}$ *has the form*

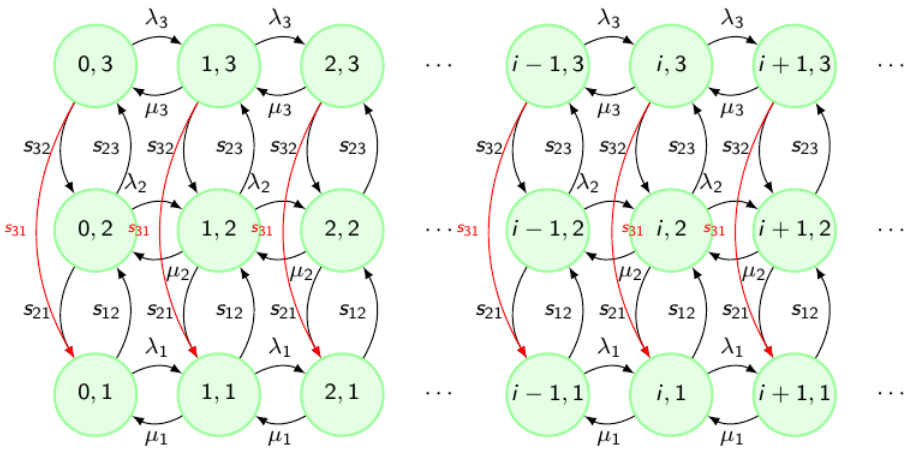

Figure 1.5: Diagrammatic representation of the level independent QBD process given in Example 1.2.3.

$$\mathbf{Q}^{LI}_{QBD} = \left(\begin{array}{ccc|ccc|ccc|c} q_1^o & s_{12} & 0 & \lambda_1 & 0 & 0 & 0 & 0 & 0 & \dots \\ s_{21} & q_2^o & s_{23} & 0 & \lambda_2 & 0 & 0 & 0 & 0 & \dots \\ s_{31} & s_{32} & q_3^o & 0 & 0 & \lambda_3 & 0 & 0 & 0 & \dots \\ \hline \mu_1 & 0 & 0 & q_1^* & s_{12} & 0 & \lambda_1 & 0 & 0 & \dots \\ 0 & \mu_2 & 0 & s_{21} & q_2^* & s_{23} & 0 & \lambda_2 & 0 & \dots \\ 0 & 0 & \mu_3 & s_{31} & s_{32} & q_3^* & 0 & 0 & \lambda_3 & \dots \\ \hline 0 & 0 & 0 & \mu_1 & 0 & 0 & q_1^* & s_{12} & 0 & \dots \\ 0 & 0 & 0 & 0 & \mu_2 & 0 & s_{21} & q_2^* & s_{23} & \dots \\ 0 & 0 & 0 & 0 & 0 & \mu_3 & s_{31} & s_{32} & q_3^* & \dots \\ \hline \vdots & \vdots & \vdots & \vdots & \vdots & \vdots & \vdots & \vdots & \vdots & \ddots \end{array}\right)$$

where $q_1^o = -s_{12} - \lambda_1$, $q_2^o = -s_{21} - s_{23} - \lambda_2$, $q_3^o = -s_{31} - s_{32} - \lambda_3$ *and* $q_1^* = -s_{12} - \lambda_1 - \mu_1$, $q_2^* = -s_{21} - s_{23} - \lambda_2 - \mu_2$, $q_3^o = -s_{31} - s_{32} - \lambda_3 - \mu_3$. *And the general form is then*

$$\mathbf{Q}^{LI}_{QBD} = \begin{pmatrix} \mathbf{S} - \mathbf{\Lambda} & \mathbf{\Lambda} & \mathbf{0} & \dots \\ \mathbf{M} & \mathbf{S} - \mathbf{\Lambda} - \mathbf{M} & \mathbf{\Lambda} & \dots \\ \mathbf{0} & \mathbf{M} & \mathbf{S} - \mathbf{\Lambda} - \mathbf{M} & \dots \\ \vdots & \vdots & \vdots & \ddots \end{pmatrix}$$

where $\mathbf{S}$, $\mathbf{\Lambda}$ *and* $\mathbf{M}$ *and* 3×3 *matrices,* $\mathbf{S}$ *is the generating matrix of* $\{\mathcal{E}(t) : t \geqslant 0\}$ *and* $\mathbf{\Lambda}$ *and* $\mathbf{M}$ *are diagonal matrices with* $\mathbf{\Lambda}_{ii} = \lambda_i$ *and* $\mathbf{M}_{ii} = \mu_i$ *for* $1 \leq i \leq 3$.

1.2.3 Classification of states and long-term behaviour

One of the aims when analysing a CTMC $\mathcal{X}$ over the state space $\mathcal{S}$ is usually to study its long-term behaviour; that is, the dynamics of $\{X(t) : t \geqslant 0\}$ when $t \to +\infty$. In order to carry out this analysis, one needs first to classify states within the state space $\mathcal{S}$.

Definition 1.2.9 *Given a CTMC* $\mathcal{X}$ *over the state space* $\mathcal{S}$*, a state* $i \in \mathcal{S}$ *can be called either* **instantaneous, stable** *or* **absorbing** *depending, respectively, on* $q_i = +\infty, 0 < q_i < +\infty$ *or* $q_i = 0$.

Definition 1.2.10 *A set of states* $C \subseteq \mathcal{S}$ *is called* **communicating class** *if all the states in* C *are accessible among them, that is,* $\forall i, j \in C$ *exists some* $t \geqslant 0$ *such that* $p_{ij}(t) > 0$*. Moreover, a communicating class is said to be* **closed** *if* $\forall i \in C$ *and* $\forall j \notin C$ $p_{ij}(t) = 0$*, for all* $t \geqslant 0$.

Definition 1.2.11 *A CTMC* $\mathcal{X}$ *over* $\mathcal{S}$ *is called* **irreducible** *if* $\mathcal{S}$ *is a closed communicating class.*

The following concepts are necessary for studying the behaviour of the process when t goes to infinity.

Definition 1.2.12 *Given a CTMC* $\mathcal{X}$ *over the state space* $\mathcal{S}$*, a state* $i \in \mathcal{S}$ *is called* **recurrent** *if* $u_i = 1$*, where*

$$u_i = \mathbb{P}(\inf\{t \geqslant Y_1 = S_1 : X(t) = i\} < +\infty | X(0) = i), i \in \mathcal{S};$$

that is, if the probability of the process $\mathcal{X}$ *to return to state* i *in finite time, starting at this state, is one. State* $i \in \mathcal{S}$ *is called* **transient** *if* $u_i < 1$*. Moreover,* $\mathcal{X}$ *is an irreducible transient or recurrent CTMC if all its states are transient or recurrent, respectively.*

Definition 1.2.13 *Given a CTMC* $\mathcal{X}$ *over the state space* $\mathcal{S}$*, a recurrent state* $i \in \mathcal{S}$ *is called* **positive recurrent** *if* $\mu_i < +\infty$*, where*

$$\mu_i = E\left[\inf\{t \geqslant Y_1 = S_1 : X(t) = i\} | X(0) = i\right], i \in \mathcal{S},$$

and **null recurrent** *if* $\mu_i = +\infty$.

Definition 1.2.14 *A positive recurrent and irreducible CTMC $\mathcal{X}$ is called* **ergodic**.

For ergodic CTMCs, the following results allows one to analyse its long-term behaviour

Theorem 1.2.2 *Let $\mathbf{Q}$ be the infinitesimal generator of an ergodic CTMC $\mathcal{X}$, and let $\boldsymbol{\pi} = \{\pi_j : j \in \mathcal{S}\}$ where $\pi_j = \lim_{t\to+\infty} \mathbb{P}(X(t) = j|X(0) = i)$, which does not depend on $i \in \mathcal{S}$. Then, $\boldsymbol{\pi}$ is given by*

$$\boldsymbol{\pi}\mathbf{Q} = \mathbf{0},$$
$$\boldsymbol{\pi}\mathbf{e} = 1,$$

where $\mathbf{e}$ is a column unity vector and $\mathbf{0}$ is a column vector of zeros.

1.2.4 First passage time and phase-type distributions

Let us consider now a non-ergodic CTMC $\mathcal{X}$ over $\mathcal{S}$. Let us assume that $\mathcal{X}$ is not irreducible because there is one absorbing state $i \in \mathcal{S}$. One can study the time until absorption of this absorbing CTMC $\mathcal{X}$. This time is related to the first passage time for any given state $i \in \mathcal{S}$.

Definition 1.2.15 *Given a CTMC $\{X(t) : t \geqslant 0\}$ defined over $\mathcal{S}$, and $i \in \mathcal{S}$, the* **first passage time** *to i is a random variable defined as*

$$\mathcal{T} = \min\{t \geqslant 0 : X(t) = i\}.$$

For the particular case in which state $i \in \mathcal{S}$ is absorbing, the first passage time to i is usually referred to as the absorption time into i. This time, for the cases in which $\mathcal{S}$ in finite, follows a phase-type distribution.

Definition 1.2.16 *A* **phase-type distribution** *$PH(\boldsymbol{\alpha}, \mathbf{T})$ is defined as the time until absorption in an absorbing CTMC over the state space $\mathcal{S} = \{1, 2, \cdots, m\} \cup \{0\}$, with 0 the absorbing state and with $\boldsymbol{\alpha}$ the vector of initial probabilities, where the generating matrix has the form*

$$\mathbf{Q} = \left(\begin{array}{c|c} \mathbf{T} & \mathbf{T}^0 \\ \hline \mathbf{0} & 0 \end{array}\right), \tag{1.11}$$

where $\mathbf{T}$ is an $m \times m$ matrix such that (i) all diagonal elements are negative, (ii) all non-diagonal elements are non-negative; (iii) all row sums are non-positive and (iv) $\mathbf{T}$ is invertible and where $\mathbf{T}^0 = -\mathbf{T}\mathbf{e}$, with $\mathbf{e}$ being an $m \times 1$ column vector of ones.

If a random variable X follows a phase-type distribution ($X \sim PH(\boldsymbol{\alpha}, \mathbf{T})$) where $\mathbf{T}$ is given in Definition 1.2.16 and $\boldsymbol{\alpha}$ is a probability vector, the distribution function of X is given by

$$\mathcal{F}(x) = 1 - \boldsymbol{\alpha} e^{\mathbf{T}x}\mathbf{e}, \quad x \geqslant 0, \tag{1.12}$$

the density function by

$$f(x) = \boldsymbol{\alpha} e^{\mathbf{T}x}\mathbf{T}^{\mathbf{0}}, \quad x \geqslant 0,$$

and the different order moments by

$$E\left[X^n\right] = (-1)^n n! \boldsymbol{\alpha}\mathbf{T}^{-n}\mathbf{e}, \quad x \geqslant 0.$$

It can be observed that the exponential distribution is a particular case of the phase-type distribution. For instance, by comparing the probability distribution function of both distributions, Equations (1.8) and (1.12), it can be seen that the exponential distribution arises when setting $m = 1$, so that the exponential distribution is the phase-type distribution with $\mathbf{T} = -\lambda$ and $\boldsymbol{\alpha} = 1$.

Example 1.2.4 *Let us consider the quasi-brith-and-death process* $\{(\mathcal{N}(t), \mathcal{E}(t)) : t \geqslant 0\}$ *given in Example 1.2.3, but with only* $N + 1$ *levels and an absorbing state Abs. Let us assume that state Abs is reachable only from level N, see the diagrammatic representation in Figure 1.6.*

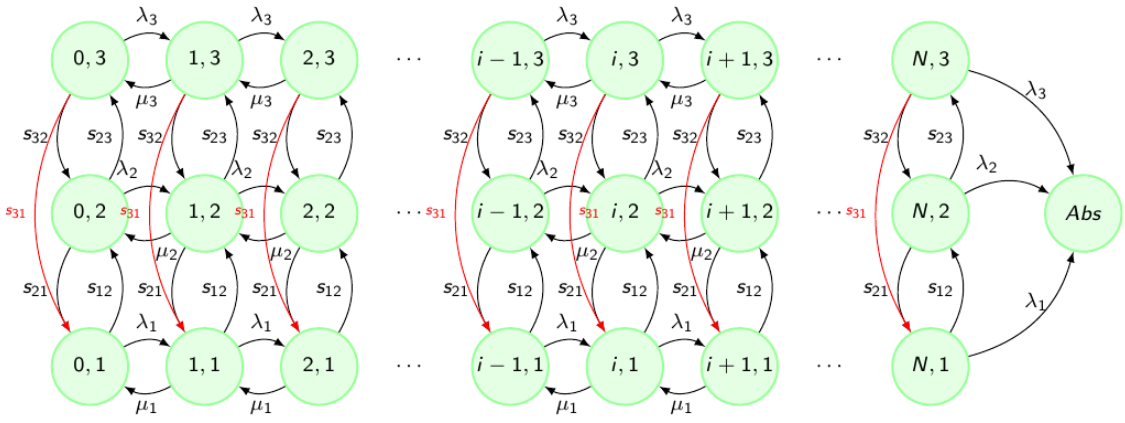

Figure 1.6: Diagrammatic representation of the level independent QBD process given in Example 1.2.4 with absorption at level *Abs*.

The generating matrix has the form

$$\mathbf{Q}_{QBD}^{LI} = \left(\begin{array}{cccc|c} \mathbf{S}-\mathbf{\Lambda} & \mathbf{\Lambda} & \mathbf{0} & \dots & \mathbf{0} \\ \mathbf{M} & \mathbf{S}-\mathbf{\Lambda}-\mathbf{M} & \mathbf{\Lambda} & \dots & \mathbf{0} \\ \mathbf{0} & \mathbf{M} & \mathbf{S}-\mathbf{\Lambda}-\mathbf{M} & \dots & \mathbf{0} \\ \vdots & \vdots & \vdots & \ddots & \mathbf{0} \\ \mathbf{0} & \mathbf{0} & \mathbf{M} & \mathbf{S}-\mathbf{\Lambda}-\mathbf{M} & \boldsymbol{\lambda} \\ \hline \mathbf{0} & \mathbf{0} & \mathbf{0} & \mathbf{0} & 0 \end{array}\right),$$

where $\mathbf{S}$, $\mathbf{\Lambda}$ *and* $\mathbf{M}$ *and* 3×3 *matrices,* $\mathbf{S}$ *is the generating matrix of* $\{\mathcal{E}(t) : t \geqslant 0\}$, $\mathbf{\Lambda}$ *and* $\mathbf{M}$ *are diagonal matrices with* $\mathbf{\Lambda}_{ii} = \lambda_i$ *and* $\mathbf{M}_{ii} = \mu_i$ *for* $1 \leq i \leq 3$, *and* $\boldsymbol{\lambda} = (\lambda_1, \lambda_2, \lambda_3)^T$; *the transpose of the vector containing transition rates from level N to absorption.*

We finish this section by defining the Laplace-Stieltjes transform of a random variable, which will be widely used in Chapters 2 and 3 when dealing with exponential, phase-type distributions and CTMCs.

Definition 1.2.17 *The* **Laplace-Stieltjes transform** *of a non-negative continuous random variable X is defined as*

$$\varphi_X(s) = \int_0^{+\infty} e^{-st} f(t) dt = E[e^{-sX}] \tag{1.13}$$

where $f(\cdot)$ *is the probability density function of X.*

When dealing with continuous random variables, the Laplace-Stieltjes transform plays a similar role as the generating function for the case of discrete-time random variables. In fact, there are two properties that will be useful in our analysis. The first one is that the Laplace-Stieltjes transform is closed under the sum, that is, if $\varphi_X(s)$ and $\varphi_Y(s)$ are the Laplace-Stieltjes transforms of the independently distributed random variables X and Y, respectively, then

$$\varphi_{X+Y}(s) = \varphi_X(s)\varphi_Y(s).$$

The second one is used to calculate the different order moments of a random variable X. Since if $\varphi_X(s)$ is the Laplace-Stieltjes transform of X, then

$$E[X^n] = (-1)^n \frac{d^n \varphi_X(s)}{ds^n}\bigg|_{s=0} = (-1)^n \varphi_X^{(n)}(0).$$

The mathematical framework reported in this section belongs to those tools that have been used in more than one chapter of this thesis, in particular, Chapters 2, 3 and 5. Other mathematical procedures used in these chapters and in Chapter 4, are explained in the aforesaid sections given that they are used for more specific situations.

1.3 State-of-the-art. Aims of the thesis

In this section, a general overview of the state-of-the-art regarding the role of IL-2 in T cell stimulation, the costimulatory system or regulatory T cells as a down-regulator subpopulation is presented. These have been used as a starting point for the motivation of the current work. The summary reported here, gathers investigations developed from different mathematical approaches, some of them also in the field of Markov processes.

Regarding intracellular dynamics of IL-2, discussed in Chapter 2, it is known [6] that this cytokine is required for regulatory cells homeostasis in peripheral pools. Reference [13] shows how the upregulation of IL-2R, IL-2 high-affinity receptor, provokes a positive feedback loop of this ligand signalling. IL-2 internal dynamics from an effector T cell to a regulatory cell were used in such a chapter, with slight alterations, to develop a matrix-analytic approach from a stochastic version of this phenomenon. Thus, quantitative information regarding this molecule wants to be analysed with accuracy. Nevertheless, IL-2 ability to regulate T cell expansion was translated, back in 2014, into the first reproducible effective human cancer immunotherapies [58].

However, population dynamics of T cells are not only driven by stimulatory signals, explained in Section 1.1.2, from which IL-2 is the main protagonist of signal 3, but for inhibitory activities in which regulatory T cells role needs to be studied separately. Already in Chapter 2, there is a distinction regarding this subpopulation which is due to their expression of IL-2R. But in addition to this, there is a characteristic that regulatory T cells have which has to do with the location of the inhibitory receptor CTLA-4. Several works like [68] state that this co-receptor is constitutively located mainly in intracellular compartments of conventional T cells whereas they are on the cell surface only in regulatory T cells [76] which, in principle, would result in a higher ability, or faster, for these regulatory T cells to inhibit others.

Moreover, a controversy between the mechanisms by which CTLA-4 would perform its restraining functions has emerged mainly after recent discoveries in vitro and in vivo. For instance, in [54], some experiments would support a CTLA-4 cell-extrinsic mediation in which, in

contrast between a cell-intrinsic one, APC ligands sources of T cell activation would be depleted via CTLA-4 internalisation within T cells. This hypothesis, would categorise APCs ability for T cell activation depending on if they have been in contact with CTLA-4^+ T cells before, this is, depending on the amount of ligands (B7-1 and B7-2) that they have left [76]. The need of an accurate quantitative analysis supports in Chapter 3 the use of matrix-analytic methods that might bring some light to some of the characteristics that drive this costimulatory system.

Identifying the key elements that explain T cell activation requires a perspective that takes into account different levels. Thus, the other two chapters jump from a molecular to a cellular and a population level. In Chapter 4, different results regarding subpopulation dynamics of T cells, in which IL-2 and regulatory cells were argued to have an important role, are used as a starting point for a quorum-sensing like hypothesis. Previous works in [5] or [57], suggest this mechanism to be behind homeostasis in T cells number by a process of perceiving the density of their own cell populations. To elucidate if failures in such process might result in autoimmunity or uncontrolled T cell activation, in vivo data is used in Chapter 4 to verify the efficiency of contrasted models suggesting, if possible, different alternatives.

Moreover, regulatory cells also have a crucial function in tumour scenarios. Lots of different researches (like [62] or [20]) correlate high FOXP3^+ T reg cell expression to diverse cancers in relation to other subpopulation of cells. In particular, the ratio between this cells and effector $CD8^+$ cells seems to be particularly important for tumour prognosis [70]. In Chapter 5, a tumour scenario is considered to keep investigating the quorum-sensing role. By several versions of a model, we try to illustrate the mechanisms by which regulatory T cells suppress effective antitumour immunity, causing tumour progression [49]. For this purpose, a stochastic and a deterministic approach will bring some conclusions regarding how the parameters of our models might have an impact on tumour prognosis.

Regarding the methodology most frequently used in this work, matrix-analytic methods, as stated in Section 1.2, have had a notorious impact during last decades thanks mainly to computational improvement. This method makes use of a matrix formalism, and was originally developed by Marcel F Neuts in the area of queueing theory [50]. Since then, it has been successfully applied during the last years in different areas of mathematical biology, such as population dynamics [23], epidemiology [18, 37], or cell and molecular biology [8, 38]. However, it has not been used yet for the specific purpose of this work.

Chapter 2

A stochastic model for intracellular trafficking of interleukin-2

2.1 Introduction

The proper functioning of the different T cell classes described in the introduction, and so the interaction between them, not only depends on the TCR and the pMHC complexes (see Figure 1.1), but on a group of cytokines called the *interleukin* family; proteins that mediate communication between cells regulating cell growth, differentiation and motility. The main target of this chapter resides in understanding the main dynamics of the molecule interleukin-2 (IL-2), a cytokine involved in different immunological processes (T cell thymic development [42, 43], immune response [11] and regulation of homeostatic levels of regulatory T cells [7, 44]). Regulatory T cell survival in the periphery depends on IL-2 molecules, as regulatory T cells are characterised by the constitutive expression of IL-2 receptor molecules on their cell surface. Since regulatory T cells are not capable of producing IL-2 in significant amounts, they directly depend on the production of background levels of IL-2 by other cells in the periphery, such as helper T cells [41]. As it will be studied in detail in Chapter 4, IL-2 is the key element on the called quorum-sensing mechanism, in which the immune system is capable of self-controlling its own population levels by the ability of some cells to produce IL-2, which implies T cell proliferation, and in particular, proliferation of regulatory T cell, and by the capacity of regulatory T cells to down-regulate T cell pool by inhibitory signals.

In particular, this chapter introduces, developes and analyses a stochastic version of the deterministic model presented in [13] for the interaction between a helper T cell and a regulatory T cell by means of the IL-2 molecule. When analysing a biological system like this one from a mathematical and computational perspective, deterministic or stochastic approaches can be followed. The advantage of a deterministic approach is that it allows one to elucidate the dynamics of the process in an analytical manner, whereas the mathematical analysis of the system is, in general, more plausible than in the stochastic approach. However, the stochastic approach is able to reproduce the intrinsic randomness that naturally arises in these processes, being specially desirable when small numbers of molecules are involved (e.g., T cell responses have been reported to be mediated only by around 10 IL-2/IL-2R molecules [17]). When analysing a stochastic model, the usual approach is to study the *master equation* of the process (a system of differential equations involving the probabilities of the process being at each possible state at any particular time, which is defined in Section 1.2.1). This system, which is usually referred to as the Kolmogorov equations in the field of stochastic processes [34], is usually non-solvable from an analytical point of view. Then, different approaches are implemented in the literature such as Gillespie simulations [22] (see Definition 1.2.7) or the application of moment-based approximations [75].

The aim here is therefore to illustrate the applicability of an alternative algorithmic method: the *matrix-analytic* approach. The analysis developed here relies in the introduction of *stochastic descriptors*, which are conveniently defined random variables providing detailed information about the dynamics of the process, but without requiring to analyse the time-dependent dynamics in the master equation.

The chapter is structured as follows: In Section 2.2, the stochastic version of the model in [13] is presented. Different stochastic descriptors are defined in Section 2.3 for analysing the rate at which IL-2/IL-2R complexes are formed on the regulatory T cell surface, as well as the rate at which IL-2R molecules are synthesised. These descriptors can be efficiently analysed by means of a matrix formalism developed in Section 2.4 which allows to work algorithmically to obtain certain quantities of interest. This algorithmical approach, discussed in Section 2.6, allows to analyse in an efficient manner these descriptors. Numerical results are obtained and discussed in Section 2.5, and a summary with main conclusions is given in Section 2.8. Finally, as an example of the different approaches mentioned before when solving Kolmogorov equations, a Van Kampen's expansion approximation is explained for the present model in Section 2.7

2.2 Stochastic model

The aim of this section is to develop a stochastic version of the deterministic model proposed in [13] for the interaction between a helper T cell and a regulatory T lymphocyte, mediated by the interleukin-2 cytokine (IL-2) and its receptor (IL-2R). Considerations are restricted to the dynamics of regulatory T cells: the synthesis of IL-2R by regulatory T cells is induced by IL-2 that is secreted by helper T cells, but sensed by regulatory T cells in a paracrine fashion.

The mathematical model introduced in [13], and generalised here with a stochastic approach, considers the following variables: IL-2 cytokine or free ligand molecules (L), IL-2 receptors (R) on the regulatory T cell surface, bound IL-2/IL-2R complexes on the cell surface (C), and bound complexes in the endosome of regulatory T cells (E). The model under study is then represented in Figure 2.1, and involves the analysis of the following random variables:

$$\begin{aligned} R(t) &= \text{“}\textit{Number of free IL-2R on the cell surface at time } t\text{”}, \\ C(t) &= \text{“}\textit{Number of IL-2/IL-2R complexes on the cell surface at time } t\text{”}, \\ E(t) &= \text{“}\textit{Number of IL-2/IL-2R complexes in the endosome at time } t\text{”}, \\ L(t) &= \text{“}\textit{Number of free extra-cellular IL-2 ligands at time } t\text{”}, \end{aligned}$$

for any $t \geq 0$, where an initial number of IL-2 molecules (ligand) $L(0) = n_L$ and free IL-2 receptors $R(0) = n_R$ are assumed, with $C(0) = E(0) = 0$. In what follows, and given that the dynamics of helper T cells, their IL-2 secretion, or the spatial diffusion of IL-2 from helper T cells to regulatory T cells are not explicitly modelled, a constant background of ligand is postulated so that $L(t) = n_L$ $\forall t \geq 0$, in the spirit of [27], and justified by the similar dynamics observed in previous simulations under different initial values (results not shown here). Finally, let us consider that the total number of receptors per cell is bounded by a *carrying capacity* of regulatory T cells. Thus, it is assumed that

$$R(t) + C(t) + E(t) \leq n_R^{max} \ ,$$

for all $t \geq 0$, so that $n_R \leq n_R^{max}$.

Once the variables of the model have been described, the set of reactions considered in the model (see Figure 2.1) can be introduced as:

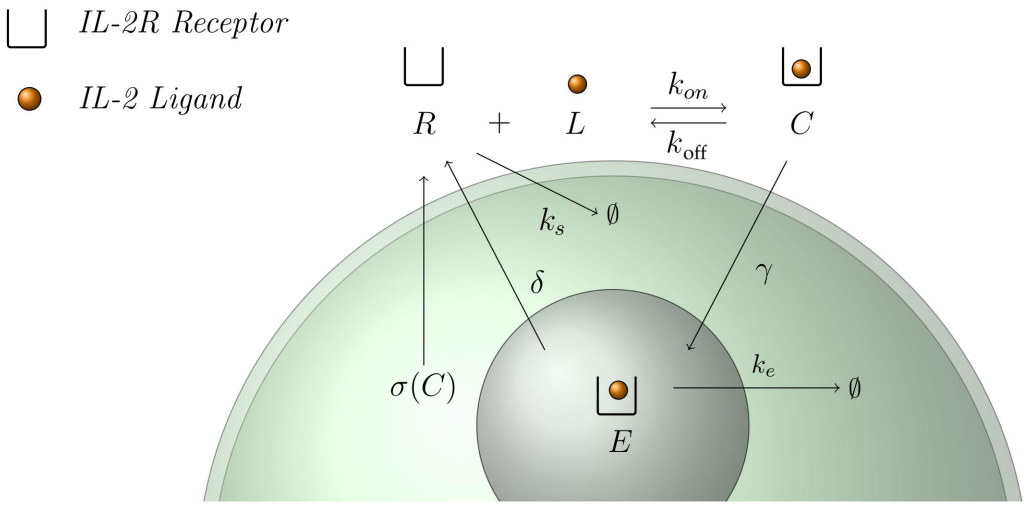

Figure 2.1: Model for IL-2 stimulation of a regulatory T cell where $\sigma(\cdot)$ encodes the ligand-induced synthesis rate by a Hill function (see reaction $(\mathbb{R}_3)$ below).

$(\mathbb{R}_1)$ **Binding of ligand to receptor**

Extra-cellular IL-2 molecules can bind to IL-2R on the surface of regulatory T cells, forming IL-2/IL-2R complexes, with rate k_{on},

$$R + L \xrightarrow{k_{\text{on}}} C\,.$$

$(\mathbb{R}_2)$ **Dissociation of ligand and receptor**

Bound complexes C can dissociate with rate k_{off},

$$C \xrightarrow{k_{\text{off}}} R + L\,.$$

$(\mathbb{R}_3)$ **Synthesis of IL-2R**

Both constitutive and IL-2 induced synthesis of new IL-2R molecules,

$$\varnothing \xrightarrow{\nu_0+\nu_1\sigma(x)} R\,.$$

are taken into account. The synthesis of new receptors occurs at rate

$$v_0 + v_1\sigma(x) \quad = \quad v_0 + v_1\frac{x^3}{x^3 + K_c^3}\ ,$$

where x is the number of bound complexes on the cell surface at a given time, v_0 is the constitutive synthesis rate and v_1 is the ligand-induced synthesis rate. The positive feedback of bound complexes on IL-2R synthesis is represented by a Hill function with half-saturation constant $K_c = 10^3$ and Hill coefficient $m = 3$ [13].

($\mathbb{R}_4$) **Internalisation of bound complexes**

IL-2/IL-2R complexes are internalised from the membrane of the cell into the endosome with rate γ,

$$C \xrightarrow{\gamma} E\ .$$

($\mathbb{R}_5$) **Endosomal degradation**

Internalised IL-2/IL-2R complexes are degraded in the endosome with rate k_e,

$$E \xrightarrow{k_e} \emptyset\ .$$

($\mathbb{R}_6$) **Receptor recycling**

IL-2R recycling takes place from internalised IL-2/IL-2R complexes with rate δ,

$$E \xrightarrow{\delta} R\ .$$

($\mathbb{R}_7$) **Surface receptor degradation**

Free IL-2R on the cell surface are degraded with rate k_s,

$$R \xrightarrow{k_s} \emptyset\ .$$

Under Markovian assumptions, let us introduce a continuous-time Markov process (see Definition 1.2.1) $\mathcal{X}(t) = \{(R(t), C(t), E(t)) : t \geq 0\}$ defined over the space of states $\mathcal{S} = \{(n_1, n_2, n_3) \in \mathbb{N}^3 : n_1 + n_2 + n_3 \leq n_R^{max}\}$, with non-null infinitesimal transition rates, according

to mass-action kinetics, given by

$$q_{(n_1,n_2,n_3),(n_1',n_2',n_3')} = \begin{cases} k_{\text{on}}\, n_1 n_L\,, & \text{if } (n_1',n_2',n_3') = (n_1-1,n_2+1,n_3), \\ k_{\text{off}}\, n_2\,, & \text{if } (n_1',n_2',n_3') = (n_1+1,n_2-1,n_3), \\ k_s\, n_1\,, & \text{if } (n_1',n_2',n_3') = (n_1-1,n_2,n_3), \\ \gamma\, n_2\,, & \text{if } (n_1',n_2',n_3') = (n_1,n_2-1,n_3+1), \\ \delta\, n_3\,, & \text{if } (n_1',n_2',n_3') = (n_1+1,n_2,n_3-1), \\ k_e\, n_3\,, & \text{if } (n_1',n_2',n_3') = (n_1,n_2,n_3-1), \\ \nu_0+\nu_1\sigma(n_2)\,, & \text{if } (n_1',n_2',n_3') = (n_1+1,n_2,n_3), \end{cases} \tag{2.1}$$

for $(n_1,n_2,n_3),(n_1',n_2',n_3') \in \mathcal{S}$. In Section 2.5 the values for all the rates are discussed.

If we note $\mathbf{n} = (n_1,n_2,n_3)$, the dynamics of this process can be analysed in terms of the probabilities $\{\mathbb{P}_{\mathbf{n}}(t) : t \geq 0,\ \mathbf{n} \in \mathcal{S}\}$, where $\mathbb{P}_{\mathbf{n}}(t) = \mathbb{P}((R(t),C(t),E(t)) = \mathbf{n})$ is the probability of the process being at state $\mathbf{n}$ at time t, for a given initial state $\mathbf{n}_0 = (n_R,0,0)$. These probabilities verify the master equation corresponding to the Markov process under consideration [34]:

$$\frac{d\mathbb{P}_{\mathbf{n}}(t)}{dt} = \sum_{\mathbf{n}'\in\mathcal{S}\,,\mathbf{n}'\neq\mathbf{n}} q_{(\mathbf{n}',\mathbf{n})}\,\mathbb{P}_{\mathbf{n}'}(t) - \sum_{\mathbf{n}'\in\mathcal{S}\,,\mathbf{n}'\neq\mathbf{n}} q_{(\mathbf{n},\mathbf{n}')}\,\mathbb{P}_{\mathbf{n}}(t)\,, \quad \forall \mathbf{n} \in \mathcal{S}\,. \tag{2.2}$$

This system of differential equations cannot, in general, be solved analytically. Different methods have been proposed and used in the literature to study the Kolmogorov equations of a given Markov process, such as carrying out Gillespie simulations [22] or making use of expansion techniques like Van Kampen's approximation [75] that turns the Kolmogorov equations into a combination of macroscopic fluctuations and concentrations; Fokker-Planck equation, in what is called a system-size expansion. This procedure is used in Section 2.7 for the master Equation (2.2).

Our objective here is to propose, in Section 2.3, an alternative approach: the introduction of new stochastic descriptors, which are random variables of interest to the process under consideration. This approach, based on a matrix formalism, requires arranging the space of states $\mathcal{S}$ in groups of states, and the use of several algorithmic techniques, known as the matrix-analytic approach [28].

2.3 Stochastic descriptors

Further to previous elucidations, this section has the purpose of introducing and analysing a continuous and a discrete stochastic descriptor that permit to study the joint role of the rate at which IL-2/IL-2R bound complexes are formed and the rate at which IL-2R molecules are synthesised in the dynamics of the process. For this objective, let us introduce:

1. the time to reach a threshold number, B, of bound complexes simultaneously present on the cell surface, and
2. the number of newly synthesised receptors during that time.

The first descriptor gives an absolute measure of the rate at which bound complexes are formed and maintained to reach a threshold number on the cell surface, while the second descriptor enables relating this threshold number with its direct output, the synthesis of new receptors. In order to analyse the stochastic descriptors, it is necessary to arrange the space of states $\mathcal{S}$ by *levels* as follows:

$$\mathcal{S} \;=\; \bigcup_{k=0}^{n_R^{max}} L(k)\;,$$

where each level, $L(k) = \{(n_1, n_2, n_3) \in \mathcal{S} :\; n_2 = k\}$, is organised in sub-levels

$$L(k) \;=\; \bigcup_{r=0}^{n_R^{max}-k} l(k;r)\;, \quad 0 \leq k \leq n_R^{max}\;,$$

with $l(k;r) = \{(n_1, n_2, n_3) \in L(k) :\; n_1 = r\}$. That is, level $L(k)$ is the group of states within $\mathcal{S}$ representing a total number of bound complexes on the cell surface equal to k, while each sub-level $l(k;r)$ is formed by those states within $L(k)$ representing a total number of free receptors equal to r, for $0 \leq r \leq n_R^{max} - k$ and $0 \leq k \leq n_R^{max}$, as Figure 2.2 shows. Finally, it can be proved that

$$\begin{aligned} J(k) \;&=\; \#L(k) \;=\; \frac{(n_R^{max}-k+1)(n_R^{max}-k+2)}{2}\;, \\ J(k;r) \;&=\; \#l(k;r) \;=\; n_R^{max}-k-r+1\;, \end{aligned}$$

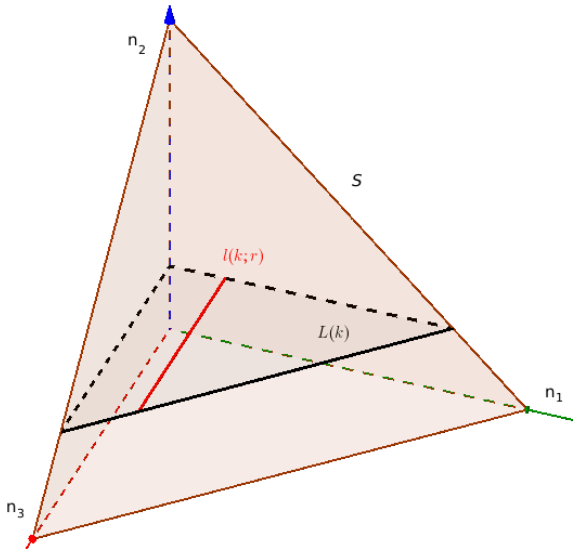

Figure 2.2: Space of states $\mathcal{S}$ subdivided by *levels* $L(k)$ and *sublevels* $l(k;r)$.

for $0 \leq k \leq n_R^{max}$ and $0 \leq r \leq n_R^{max} - k$.

This organisation of $\mathcal{S}$ precedes an algorithmic approach when analysing the descriptors under study. This analysis is based on the use of first-step arguments, Laplace-Stieltjes transforms and probability generating functions, and is developed in the following sections. In Section 2.3.1 the time to reach a total threshold number B of bound complexes simultaneously present on the cell surface is studied as a random variable, where its Laplace-Stieltjes transform is obtained and its order moments are computed. In Section 2.3.2, what it is analysed is the probability generating function of the random variable representing the number of receptors synthesised during the time it takes to reach a threshold number B of bound complexes simultaneously present on the cell surface. Not only the different order moments of this random variable are obtained but also an algorithmic approach for computing its probability mass function.

2.3.1 Time to reach a threshold number B of bound complexes on the cell surface

The time to reach a threshold number B of bound complexes simultaneously present on the cell surface can be analysed in terms of the random variable

$$\begin{aligned} T^B_{(n_1,n_2,n_3)} &= \text{“Time to reach a threshold number } B \text{ of bound complexes} \\ &\quad \text{simultaneously present on the cell surface, given the current state} \\ &\quad \text{of the process } (n_1,n_2,n_3) \in \mathcal{S}\text{”} \end{aligned}$$

or, mathematically,

$$T^B_{(n_1,n_2,n_3)} = \inf\{t \geqslant 0 : C(t) = B\},$$

for values $n_2 \leq B \leq n_R^{max}$, with $T^{n_2}_{(n_1,n_2,n_3)} = 0$. In order to study this random variable, Let us make use of its Laplace-Stieltjes transform [34, Appendix F] (see Definition 1.2.17)

$$\varphi^B_{(n_1,n_2,n_3)}(z) = E\left[e^{-z\, T^B_{(n_1,n_2,n_3)}}\right], \quad \Re(z) \geq 0\,,$$

which uniquely determines the distribution of the random variable and allows to compute its order moments by successive differentiation, as follows

$$m^{B,(l)}_{(n_1,n_2,n_3)} = E\left[(T^B_{(n_1,n_2,n_3)})^l\right] = (-1)^l \left.\frac{d^l}{dz^l}\varphi^B_{(n_1,n_2,n_3)}(z)\right|_{z=0}, \quad l \geq 1\,.$$

The Laplace-Stieltjes transform $\varphi^B_{(n_1,n_2,n_3)}(z)$ can be obtained by a first-step argument

$$\begin{aligned} (z+\Delta_{(n_1,n_2,n_3)})\varphi^B_{(n_1,n_2,n_3)}(z) &= k_{\text{on}}\, n_1 n_L \varphi^B_{(n_1-1,n_2+1,n_3)}(z) + k_{\text{off}}\, n_2 \varphi^B_{(n_1+1,n_2-1,n_3)}(z) \\ &\quad + k_s\, n_1 \varphi^B_{(n_1-1,n_2,n_3)}(z) + \gamma\, n_2 \varphi^B_{(n_1,n_2-1,n_3+1)}(z) \\ &\quad + \delta\, n_3 \varphi^B_{(n_1+1,n_2,n_3-1)}(z) + k_e\, n_3 \varphi_{(n_1,n_2,n_3-1)}(z) \\ &\quad + (1-\delta_{n_1+n_2+n_3,n_R^{max}})\,(\nu_0 + \nu_1\sigma(n_2)) \\ &\quad \times \varphi^B_{(n_1+1,n_2,n_3)}(z)\,, \end{aligned} \tag{2.3}$$

where $\Delta_{(n_1,n_2,n_3)} = k_{\text{on}}\ n_1 n_L + k_{\text{off}}\ n_2 + k_s\ n_1 + \gamma\ n_2 + \delta\ n_3 + k_e\ n_3 + (1 - \delta_{n_1+n_2+n_3,n_R^{max}})$ $\times (\nu_0 + \nu_1\sigma(n_2))$, and $\delta_{i,j}$ represents the Kronecker's delta (which is equal to 1 if $i = j$ and 0 otherwise). Equation (2.3) yields a system of equations involving the Laplace-Stieltjes transforms corresponding to states $(n_1, n_2, n_3) \in \cup_{k=0}^{B-1} L(k)$, with boundary conditions $\varphi^B_{(n_1,B,n_3)}(z) = 1$ for states $(n_1, B, n_3) \in L(B)$. This system of equations can be efficiently solved by working with a matrix formalism, while exploiting the structure of $\mathcal{S}$. This procedure is shown in some detail in Section 2.6.

Once the Laplace-Stieltjes transforms are in hand, the different order moments can be obtained by successive differentiation of Equation (2.3) with respect to z, and setting $z = 0$, as follows

$$\begin{aligned}
\Delta_{(n_1,n_2,n_3)} m^{B,(l)}_{(n_1,n_2,n_3)} \quad = \quad & k_{\text{on}}\ n_1 n_L m^{B,(l)}_{(n_1-1,n_2+1,n_3)} + k_{\text{off}}\ n_2 m^{B,(l)}_{(n_1+1,n_2-1,n_3)} \\
& + k_s\ n_1 m^{B,(l)}_{(n_1-1,n_2,n_3)} + \gamma\ n_2 m^{B,(l)}_{(n_1,n_2-1,n_3+1)} \\
& + \delta\ n_3 m^{B,(l)}_{(n_1+1,n_2,n_3-1)} + k_e\ n_3 m^{B,(l)}_{(n_1,n_2,n_3-1)} \\
& + (1 - \delta_{n_1+n_2+n_3,n_R^{max}})\ (\nu_0 + \nu_1\sigma(n_2)) m^{B,(l)}_{(n_1+1,n_2,n_3)} \\
& + l m^{B,(l-1)}_{(n_1,n_2,n_3)}\ , \qquad (2.4)
\end{aligned}$$

so that moments of order l can be obtained, in an algorithmic manner, from previously computed moments of order $l - 1$, starting with $m^{B,(0)}_{(n_1,n_2,n_3)} = \varphi^B_{(n_1,n_2,n_3)}(0)$, computed from Equation (2.3). This procedure makes use of a similar matrix formalism to the one mentioned for solving Equation (2.3), and is briefly discussed in Section 2.4.

2.3.2 Number of receptors synthesised during the time to reach a threshold number B of bound complexes on the cell surface

Let us now focus on analysing the random variable

$$\begin{aligned}
N^B_{(n_1,n_2,n_3)} \quad = \quad & \textit{"Number of newly synthesised receptors during the time it takes to} \\
& \textit{reach a threshold number B of bound complexes simultaneously} \\
& \textit{present on the cell surface, given the current state of the system} \\
& (n_1, n_2, n_3) \in \mathcal{S}\textit{"}
\end{aligned}$$

which is defined for values $n_2 \leq B \leq n_R^{max}$. In order to analyse this random variable, Let us consider its probability generating function

$$\phi^B_{(n_1,n_2,n_3)}(s) \quad = \quad E\left[s^{N^B_{(n_1,n_2,n_3)}}\right] \ , \quad |s| \leq 1 \ ,$$

which characterises the random variable, while allowing at the same time to compute any pth order factorial moment as

$$\begin{aligned} n^{B,(p)}_{(n_1,n_2,n_3)} &= E\left[N^B_{(n_1,n_2,n_3)}(N^B_{(n_1,n_2,n_3)}-1)(N^B_{(n_1,n_2,n_3)}-2)\ldots(N^B_{(n_1,n_2,n_3)}-p+1)\right] \\ &= \frac{d^p}{ds^p}\phi^B_{(n_1,n_2,n_3)}(s)\Big|_{s=1} \ , \quad p \geq 0 \ . \end{aligned} \tag{2.5}$$

A particular advantage of using the probability generating function is that it allows us to compute the probability mass function of the random variable under study as

$$\alpha^B_{(n_1,n_2,n_3)}(a) \quad = \quad \mathbf{P}(N^B_{(n_1,n_2,n_3)} = a) \ = \ \frac{1}{a!}\frac{d^a}{ds^a}\phi^B_{(n_1,n_2,n_3)}(s)\Big|_{s=0} \ , \quad a \geq 0 \ . \tag{2.6}$$

The probability generating function can be obtained by following a first-step argument, in a similar manner to that discussed in Section 2.3.1. In particular,

$$\begin{aligned} \Delta_{(n_1,n_2,n_3)}\phi^B_{(n_1,n_2,n_3)}(s) &= k_{\text{on}}\, n_1 n_L \phi^B_{(n_1-1,n_2+1,n_3)}(s) + k_{\text{off}}\, n_2 \phi^B_{(n_1+1,n_2-1,n_3)}(s) \\ &\quad + k_s\, n_1 \phi^B_{(n_1-1,n_2,n_3)}(s) + \gamma\, n_2 \phi^B_{(n_1,n_2-1,n_3+1)}(s) \\ &\quad + \delta\, n_3 \phi^B_{(n_1+1,n_2,n_3-1)}(s) + k_e\, n_3 \phi^B_{(n_1,n_2,n_3-1)}(s) \\ &\quad + (1-\delta_{n_1+n_2+n_3,n_R^{max}})\,(\nu_0 + \nu_1\sigma(n_2))\, s \\ &\quad \times \phi^B_{(n_1+1,n_2,n_3)}(s) \ , \end{aligned} \tag{2.7}$$

for states $(n_1,n_2,n_3) \in \cup_{k=0}^{B-1} L(k)$, with boundary conditions $\phi^B_{(n_1,B,n_3)}(s) = 1$ for states $(n_1,B,n_3) \in L(B)$. Equation (2.7) yields a system of equations that can be efficiently solved by following the same matrix formalism as in Section 2.3.1 and that is discussed in Section 2.4.

A direct application of Equations (2.5)-(2.7) leads to a system of equations corresponding to the desired factorial moments and the probability mass function. In particular,

$$
\begin{aligned}
\Delta_{(n_1,n_2,n_3)} n^{B,(p)}_{(n_1,n_2,n_3)} &= k_{\text{on}}\, n_1 n_L n^{B,(p)}_{(n_1-1,n_2+1,n_3)} + k_{\text{off}}\, n_2 n^{B,(p)}_{(n_1+1,n_2-1,n_3)} \\
&\quad + k_s\, n_1 n^{B,(p)}_{(n_1-1,n_2,n_3)} + \gamma\, n_2 n^{B,(p)}_{(n_1,n_2-1,n_3+1)} \\
&\quad + \delta\, n_3 n^{B,(p)}_{(n_1+1,n_2,n_3-1)} + k_e\, n_3 n^{B,(p)}_{(n_1,n_2,n_3-1)} \\
&\quad + (1-\delta_{n_1+n_2+n_3,n_R^{max}})\,(\nu_0+\nu_1\sigma(n_2))(n^{B,(p)}_{(n_1+1,n_2,n_3)} \\
&\quad + p\, n^{B,(p-1)}_{(n_1+1,n_2,n_3)})\,, \quad p \geq 1\,, \\
\Delta_{(n_1,n_2,n_3)} \alpha^B_{(n_1,n_2,n_3)}(a) &= k_{\text{on}}\, n_1 n_L \alpha^B_{(n_1-1,n_2+1,n_3)}(a) + k_{\text{off}}\, n_2 \alpha^B_{(n_1+1,n_2-1,n_3)}(a) \\
&\quad + k_s\, n_1 \alpha^B_{(n_1-1,n_2,n_3)}(a) + \gamma\, n_2 \alpha^B_{(n_1,n_2-1,n_3+1)}(a) \\
&\quad + \delta\, n_3 \alpha^B_{(n_1+1,n_2,n_3-1)}(a) + k_e\, n_3 \alpha^B_{(n_1,n_2,n_3-1)}(a) \\
&\quad + (1-\delta_{n_1+n_2+n_3,n_R^{max}})(1-\delta_{a,0})\,(\nu_0+\nu_1\sigma(n_2)) \\
&\quad \times \alpha^B_{(n_1+1,n_2,n_3)}(a-1)\,, \quad a \geq 0\,.
\end{aligned}
$$

Boundary conditions for the equations above are $n^{B,(p)}_{(n_1,B,n_3)} = 0$, for all $p \geq 1$ and $(n_1, B, n_3) \in L(B)$, and $\alpha^B_{(n_1,B,n_3)}(a) = 0$ for all $a \geq 1$, and $\alpha^B_{(n_1,B,n_3)}(0) = 1$. Efficient methods to solve the previous systems of equations can be developed by following the matrix formalism presented earlier and mathematical details are explained in Section 2.4.

2.4 Matrix formalism

For efficiently analysing the first descriptor studied in Section 2.3.1, we express the system of equations given by Equation (2.3), in matrix form as

$$\boldsymbol{\varphi}(z) = \mathbf{A}(z)\boldsymbol{\varphi}(z) + \mathbf{b}(z), \tag{2.8}$$

where the constant B is omitted here for the ease of notation. The vector of *unknowns* $\boldsymbol{\varphi}(z)$ is structured, due to the organization of $\mathcal{S}$ in levels and sub-levels, by blocks as

$$
\boldsymbol{\varphi}(z) = \begin{pmatrix} \boldsymbol{\varphi}_0(z) \\ \boldsymbol{\varphi}_1(z) \\ \vdots \\ \boldsymbol{\varphi}_{B-1}(z) \end{pmatrix}, \quad \boldsymbol{\varphi}_k(z) = \begin{pmatrix} \boldsymbol{\varphi}^k_0(z) \\ \boldsymbol{\varphi}^k_1(z) \\ \vdots \\ \boldsymbol{\varphi}^k_{n_R^{max}-k}(z) \end{pmatrix}, \quad 0 \leq k \leq B-1,
$$

with $\boldsymbol{\varphi}_r^k(z) = (\varphi_{(r,k,0)}(z), \ldots, \varphi_{(r,k,n_R^{max}-r-k)}(z))^T$, and where ^{T} represents the transpose operator. In a similar way, the organisation of states within $\mathcal{S}$ by levels and sub-levels, and the consideration of transition rates in Equation (2.1), yield

$$\mathbf{A}(z) = \begin{pmatrix} \mathbf{A}_{0,0}(z) & \mathbf{A}_{0,1}(z) & \mathbf{0} & \ldots & \mathbf{0} & \mathbf{0} \\ \mathbf{A}_{1,0}(z) & \mathbf{A}_{1,1}(z) & \mathbf{A}_{1,2}(z) & \ldots & \mathbf{0} & \mathbf{0} \\ \mathbf{0} & \mathbf{A}_{2,1}(z) & \mathbf{A}_{2,2}(z) & \ldots & \mathbf{0} & \mathbf{0} \\ \vdots & \vdots & \vdots & \ddots & \vdots & \vdots \\ \mathbf{0} & \mathbf{0} & \mathbf{0} & \ldots & \mathbf{A}_{B-2,B-2}(z) & \mathbf{A}_{B-2,B-1}(z) \\ \mathbf{0} & \mathbf{0} & \mathbf{0} & \ldots & \mathbf{A}_{B-1,B-2}(z) & \mathbf{A}_{B-1,B-1}(z) \end{pmatrix},$$

where the sub-matrix $\mathbf{A}_{k,k'}(z)$ contains in an ordered fashion those coefficients in the System (2.3) related with transitions from states at level $L(k)$ towards states at level $L(k')$. The specific structure by sub-levels yields the expressions

$$\mathbf{A}_{k,k}(z) = \begin{pmatrix} \mathbf{B}_{0,0}^{k,k}(z) & \mathbf{B}_{0,1}^{k,k}(z) & \mathbf{0} & \ldots & \mathbf{0} & \mathbf{0} \\ \mathbf{B}_{1,0}^{k,k}(z) & \mathbf{B}_{1,1}^{k,k}(z) & \mathbf{B}_{1,2}^{k,k}(z) & \ldots & \mathbf{0} & \mathbf{0} \\ \mathbf{0} & \mathbf{B}_{2,1}^{k,k}(z) & \mathbf{B}_{2,2}^{k,k}(z) & \ldots & \mathbf{0} & \mathbf{0} \\ \vdots & \vdots & \vdots & \ddots & \vdots & \vdots \\ \mathbf{0} & \mathbf{0} & \mathbf{0} & \ldots & \mathbf{B}_{n_R^{max}-k-1,n_R^{max}-k-1}^{k,k}(z) & \mathbf{B}_{n_R^{max}-k-1,n_R^{max}-k}^{k,k}(z) \\ \mathbf{0} & \mathbf{0} & \mathbf{0} & \ldots & \mathbf{B}_{n_R^{max}-k,n_R^{max}-k-1}^{k,k}(z) & \mathbf{B}_{n_R^{max}-k,n_R^{max}-k}^{k,k}(z) \end{pmatrix},$$

$$\mathbf{A}_{k,k-1}(z) = \begin{pmatrix} \mathbf{B}_{0,0}^{k,k-1}(z) & \mathbf{B}_{0,1}^{k,k-1}(z) & \mathbf{0} & \ldots & \mathbf{0} & \mathbf{0} \\ \mathbf{0} & \mathbf{B}_{1,1}^{k,k-1}(z) & \mathbf{B}_{1,2}^{k,k-1}(z) & \ldots & \mathbf{0} & \mathbf{0} \\ \mathbf{0} & \mathbf{0} & \mathbf{B}_{2,2}^{k,k-1}(z) & \ldots & \mathbf{0} & \mathbf{0} \\ \vdots & \vdots & \vdots & \ddots & \vdots & \vdots \\ \mathbf{0} & \mathbf{0} & \mathbf{0} & \ldots & \mathbf{B}_{n_R^{max}-k-1,n_R^{max}-k}^{k,k-1}(z) & \mathbf{0} \\ \mathbf{0} & \mathbf{0} & \mathbf{0} & \ldots & \mathbf{B}_{n_R^{max}-k,n_R^{max}-k}^{k,k-1}(z) & \mathbf{B}_{n_R^{max}-k,n_R^{max}-k+1}^{k,k-1}(z) \end{pmatrix},$$

$$\mathbf{A}_{k,k+1}(z) = \begin{pmatrix} \mathbf{0} & \mathbf{0} & \mathbf{0} & \ldots & \mathbf{0} & \mathbf{0} \\ \mathbf{B}_{1,0}^{k,k+1}(z) & \mathbf{0} & \mathbf{0} & \ldots & \mathbf{0} & \mathbf{0} \\ \mathbf{0} & \mathbf{B}_{2,1}^{k,k+1}(z) & \mathbf{0} & \ldots & \mathbf{0} & \mathbf{0} \\ \vdots & \vdots & \vdots & \ddots & \vdots & \vdots \\ \mathbf{0} & \mathbf{0} & \mathbf{0} & \ldots & \mathbf{B}_{n_R^{max}-k-1,n_R^{max}-k-2}^{k,k+1}(z) & \mathbf{0} \\ \mathbf{0} & \mathbf{0} & \mathbf{0} & \ldots & \mathbf{0} & \mathbf{B}_{n_R^{max}-k,n_R^{max}-k-1}^{k,k+1}(z) \end{pmatrix},$$

where the dimensions of sub-blocks **0** in previous expressions are omitted. However, dimensions of a sub-block **0** corresponding to those rows related with sub-level $l(k;r)$ and those columns related with sub-level $l(k';r')$ are $J(k;r) \times J(k';r')$. Expressions for sub-matrices $\mathbf{B}^{k,k'}_{r,r'}(z)$ are obtained from Equation (2.3) as

$$(\mathbf{B}^{k,k-1}_{r,r}(z))_{ij} = \begin{cases} \gamma k(z+\Delta_{(r,k,i)})^{-1}, & \text{if } j = i+1, \\ 0, & \text{otherwise,} \end{cases}$$

where $1 \leq i \leq J(k;r)$, $1 \leq j \leq J(k-1;r)$, $1 \leq k \leq B-1$ and $0 \leq r \leq n_R^{max} - k$;

$$(\mathbf{B}^{k,k-1}_{r,r+1}(z))_{ij} = \begin{cases} k_{off} k(z+\Delta_{(r,k,i)})^{-1}, & \text{if } j = i, \\ 0, & \text{otherwise,} \end{cases}$$

where $1 \leq i \leq J(k;r)$, $1 \leq j \leq J(k-1;r+1)$, $1 \leq k \leq B-1$ and $0 \leq r \leq n_R^{max} - k - 1$;

$$(\mathbf{B}^{k,k}_{r,r-1}(z))_{ij} = \begin{cases} k_s r(z+\Delta_{(r,k,i)})^{-1}, & \text{if } j = i, \\ 0, & \text{otherwise,} \end{cases}$$

where $1 \leq i \leq J(k;r)$, $1 \leq j \leq J(k;r-1)$, $0 \leq k \leq B-1$ and $1 \leq r \leq n_R^{max} - k$;

$$(\mathbf{B}^{k,k}_{r,r}(z))_{ij} = \begin{cases} k_e i(z+\Delta_{(r,k,i)})^{-1}, & \text{if } j = i-1, \\ 0, & \text{otherwise,} \end{cases}$$

where $1 \leq i \leq J(k;r)$, $1 \leq j \leq J(k;r)$, $0 \leq k \leq B-1$ and $0 \leq r \leq n_R^{max} - k$;

$$(\mathbf{B}^{k,k}_{r,r+1}(z))_{ij} = \begin{cases} \sigma(k)(z+\Delta_{(r,k,i)})^{-1}, & \text{if } j = i, \\ \delta i(z+\Delta_{(r,k,i)})^{-1}, & \text{if } j = i-1, \\ 0, & \text{otherwise,} \end{cases}$$

where $1 \leq i \leq J(k;r)$, $1 \leq j \leq J(k;r+1)$, $0 \leq k \leq B-1$ and $0 \leq r \leq n_R^{max} - k - 1$; and

$$(\mathbf{B}^{k,k+1}_{r,r-1}(z))_{ij} = \begin{cases} k_{on} r n_L(z+\Delta_{(r,k,i)})^{-1}, & \text{if } j = i, \\ 0, & \text{otherwise,} \end{cases}$$

where $1 \leq i \leq J(k;r)$, $1 \leq j \leq J(k+1;r-1)$, $0 \leq k \leq B-2$ and $1 \leq r \leq n_R^{max} - k$. Finally, the

expression for vector $\mathbf{b}(z)$ in Equation (2.8) is given by

$$\mathbf{b}(z) = \begin{pmatrix} \mathbf{0} \\ \mathbf{0} \\ \vdots \\ \mathbf{0} \\ \mathbf{A}_{B-1,B}(z)\mathbf{e}_{J(B)} \end{pmatrix},$$

where $\mathbf{e}_j$ represents a column vector of ones with dimension j.

Then, following a forward elimination backward substitution method suggested by Ciarlet [15, p. 144], Algorithm 1 is obtained which permits to compute all the Laplace-Stieltjes transforms in Equation (2.3) in an efficient and recursive manner.

2.5 Numerical results

In this section, we carry out a numerical study of the the descriptors previously introduced for the IL-2 stimulation of regulatory T cells. In order to do so, we propose to make use of the physiological parameters and kinetic rates provided in [13] and reported in Table 2.1. We are interested in the stimulation dynamics of a regulatory T cell under three different regimes, characterised by the availability of IL-2 (low, medium, high), given by $n_L \in \{10^3, 5 \cdot 10^3, 10^4\}$, respectively. These values, chosen for illustrative purposes, have been selected taking into account that a helper T cell has an antigen induced IL-2R synthesis rate in the range of $(0, 2) \cdot 10^4$ $molecules \cdot h^{-1}$ [13] (where h is hours). Initial conditions for our process are then given by $R(0) = v_0/k_s$, $C(0) = E(0) = 0$, which represent the state of the regulatory T cell before stimulation. We have assumed that in the absence of IL-2, the initial number of IL-2R on the surface of a regulatory T cell is given by the balance between receptor synthesis and degradation. We restrict ourselves to the first 60 minutes post-stimulation and for computational convenience, we consider the dynamics occurring on $f = 1\%$ of the cell surface, without loss of generality. Thus, $n_L \in \{10, 50, 100\}$, $n_R = 15$ and the kinetic rates have been transformed accordingly. Over this model, molecules are considered not to move in a way they could interact to each other as long as they are located in the synapse. New approaches including mobility are suggested for further analysis as explained in Chapter 6. The binding rate, k_{on} (see Figure 2.1) is obtained from

$\tilde{k}_{\text{on}}$ in Table 2.1 as follows

$$k_{\text{on}} = \frac{\tilde{k}_{\text{on}}}{f\ d\ s_c\ N_A}\ ,$$

where d is the distance to the source of IL-2 (helper T cells), s_c is the regulatory T cell surface area and N_A is Avogadro's number. Finally, preliminary Gillespie simulations allow us to set $n_R^{max} = 6\ R(0)$. This value is chosen so that the total number of receptors in the system, $R(t) + C(t) + E(t)$, for $t \in [0, 60]$min, does not exceed the value n_R^{max} with a probability greater than 0.99.

Parameter	**Value**
Regulatory T cell surface area, s_c	$3 \times 10^{-10} m^2$
Distance to a helper T cell secreting IL-2, d	$1 \times 10^{-3} m$
Antigen induced IL-2R synthesis rate in a regulatory T cell, v_0	$10^3\ molecules \cdot h^{-1}$
IL-2 induced IL-2R synthesis rate in a regulatory T cell, v_1	$8 \times 10^3\ molecules \cdot h^{-1}$
IL-2 association rate constant to IL-2R, $\tilde{k}_{\text{on}}$	$111.6 nM^{-1} h^{-1}$
IL-2 dissociation rate constant to IL-2R, k_{off}	$0.83 h^{-1}$
Internalisation rate constant of IL-2R, k_s	$0.64 h^{-1}$
Internalisation rate constant of IL-2/IL-2R complexes, γ	$1.7 h^{-1}$
Recycling rate constant of endosomal IL-2R, δ	$9 h^{-1}$
Endosomal degradation constant, k_e	$5 h^{-1}$

Table 2.1: Physiological parameters and kinetic rates from [13] where nM^{-1} are nanomoles.

We note that the aim of the numerical experiments to be carried out in this section is to investigate the main hypothesis of the mathematical model, and originally considered in [13]. Namely, that IL-2R ligand-induced synthesis is driven by a positive feedback from the IL-2/IL-2R complexes on the cell surface. However, a number of other possible alternatives need to be considered, for example, a positive feedback from the IL-2/IL-2R complexes in the endosome, or a synergistic positive feedback from the IL-2/IL-2R complexes on the surface and those in the endosome. Thus, we propose here three possible alternatives for the synthesis rate considered in reaction $(\mathbb{R}_3)$ in Section 2.2. In particular, we consider three different arguments for the function σ.

$$\begin{aligned} \sigma(C) &= \frac{C^3}{C^3 + K_c^3}\ , \\ \sigma(E) &= \frac{E^3}{E^3 + K_c^3}\ , \\ \sigma(C+E) &= \frac{(C+E)^3}{(C+E)^3 + K_c^3}\ , \end{aligned}$$

where C and E represent the number of surface complexes and endosomal complexes at a given

time, respectively. In fact, for the $\sigma(C+E)$ case, making the function Hill depends on two Hill functions instead of the sum of two of them was proof not to substantially alter the results (not shown here).

In Figure 2.3, we plot the average time $E[T^B_{(15,0,0)}]$ to reach a threshold number B of bound complexes on the cell surface $\pm$ its standard deviation. We plot these times as a function of B, for different ligand concentrations $n_L \in \{10, 50, 100\}$, and for the three synthesis hypothesis, $\sigma(C)$, $\sigma(E)$ and $\sigma(C+E)$, respectively. In the first instance (Figure 2.3 *top*, $\sigma(C)$), the average time to reach B bound complexes on the cell surface is approximately equal to one hour for values of B equal to $B = 4$, $B = 21$ and $B = 39$, for concentrations $n_L = 10$, $n_L = 50$ and $n_L = 100$, respectively. That is, higher ligand concentrations lead to a larger number of bound receptors on the surface, that induce synthesis of new IL-2 receptors, thus enhancing further IL-2 binding to IL-2R. In the third model (Figure 2.3 *bottom*, $\sigma(C+E)$), the corresponding values of B for an average time of one hour are $B = 4$, $B = 23$ and $B = 41$, for concentrations $n_L = 10$, $n_L = 50$ and $n_L = 100$, respectively. This illustrates the small but additional positive feedback that endosomal complexes provide to the number of surface complexes, if they are explicitly considered in the synthesis rate. On the other hand, the second hypothesis corresponding to $\sigma(E)$ (Figure 2.3 *middle*), which assumes that only endosomal complexes induce positive feedback for the synthesis of new receptors, significantly changes the timescales of the threshold. In particular, values of B corresponding to an average time, $E[T^B_{(15,0,0)}]$, approximately equal to one hour are $B = 4$, $B = 10$ and $B = 13$, for concentrations $n_L = 10$, $n_L = 50$ and $n_L = 100$, respectively. That is, if only endosomal complexes were to give positive feedback for the synthesis of new receptors, the stimulation of the regulatory T cell, and in particular the rate at which complexes are formed in its surface, would significantly decrease.

A similar analysis can be made regarding the second descriptor, the average number $E[N^B_{(15,0,0)}]$ of synthesised receptors during the time it takes for B complexes to be present on the cell surface. The descriptor is analysed in Figure 2.4 and plotted as a function of B. We study the behaviour of this discrete descriptor for different ligand concentrations and considering a number, $E[N^B_{(15,0,0)}]$, to be approximately equal to 40. If we assume the first hypothesis, corresponding to $\sigma(C)$ (Figure 2.4 *top*), the threshold value of IL-2/IL-2R corresponds to $B = 7$, $B = 19$ and $B = 26$, for concentrations $n_L = 10$, $n_L = 50$ and $n_L = 100$, respectively. If we assume the third hypothesis, corresponding to $\sigma(C+E)$ (Figure 2.4 *bottom*), the threshold values are then equal to $B = 7$, $B = 19$ and $B = 27$, for concentrations $n_L = 10$, $n_L = 50$ and $n_L = 100$, respectively. This means that there is a slight enhancement contribution of endosomal complexes in $\sigma(C+E)$ in comparison

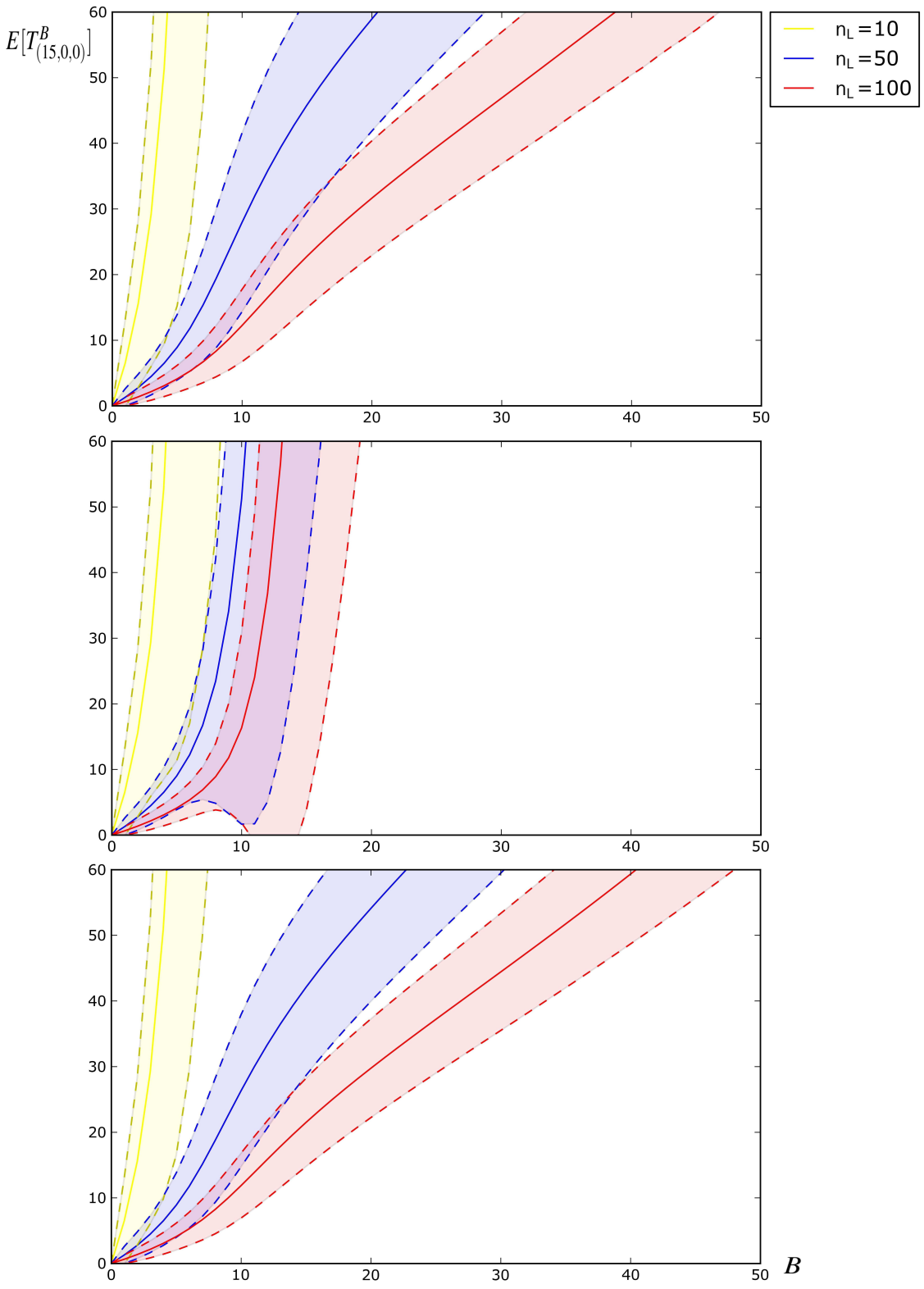

Figure 2.3: Mean time $E[T^B_{(15,0,0)}]$ (in minutes), $\pm$ its standard deviation, to reach a threshold number B of bound complexes on the cell surface, as a function of B, for different number of IL-2 molecules, $n_L \in \{10, 50, 100\}$. The synthesis rate hypothesis considered in the process amounts to (from *top* to *bottom*) $\sigma(C)$, $\sigma(E)$ and $\sigma(C+E)$. (Python code for obtaining the blue curves, $n_L = 50$, when $\sigma(C+E)$ is included in Appendix A).

with $\sigma(C)$, which allows the regulatory T cell to synthesise receptors slightly faster.

On the other hand, the hypothesis corresponding to $\sigma(E)$ (Figure 2.4 *middle*) significantly changes the stimulatory dynamics, and corresponding values of B are approximately equal to $B = 7$, $B = 14$ and $B = 17$, for concentrations $n_L = 10$, $n_L = 50$ and $n_L = 100$, respectively. We point out that results in Figure 2.4 need to be carefully interpreted in relation with results in Figure 2.3, since they are intrinsically related. In particular, since we plot in Figure 2.4 the number of synthesised receptors to reach a threshold number B of bound complexes on the cell surface, this number directly depends on the time to reach this threshold, which is plotted in Figure 2.3. This explains some behaviours shown in Figure 2.4. For example, in Figure 2.4 *middle*, the number $E[N^B_{(15,0,0)}]$ of receptors synthesised to reach $B = 14$ complexes on the cell surface, for a concentration $n_L = 50$, is equal to $E[N^B_{(15,0,0)}] \sim 44$. This large number of receptors synthesised (in comparison, for example, with the same case in Figure 2.4 *top*, $E[N^B_{(15,0,0)}] \sim 23$), can be explained by noting that $B = 14$ complexes on the cell surface are only obtained in this case after a time significantly larger than one hour (see Figure 2.4 *middle*).

From previous comments it is clear that, when endosomal complexes are considered in the synthesis rate, their contribution to this synthesis is negligible during the one hour time interval considered in this section. However, it is not possible from previous results to quantify how much the contribution of the ligand-induced pathway is, in comparison with the constitutive pathway, to the receptors synthesis. This can be addressed by noting that, regardless of the particular $\sigma(x)$ considered (with $x \in \{C, E, C+E\}$), the total number of synthesised receptors to reach a threshold number B of surface bound complexes, $N^B_{(n_R,0,0)}$, can be split as

$$N^B_{(n_R,0,0)} \quad = \quad N^B_{(n_R,0,0)}(CS) + N^B_{(n_R,0,0)}(LIS),$$

where $N^B_{(n_R,0,0)}(CS)$ represents those receptors which are constitutively synthesised, while $N^B_{(n_R,0,0)}(LIS)$ represents those receptors which are ligand-induced synthesised. It is clear then that

$$E[N^B_{(n_R,0,0)}] \quad = \quad E[N^B_{(n_R,0,0)}(CS)] + E[N^B_{(n_R,0,0)}(LIS)],$$

where values $E[N^B_{(n_R,0,0)}]$ are those ones considered in Figure 2.4. Values $E[N^B_{(n_R,0,0)}(CS)]$ can be

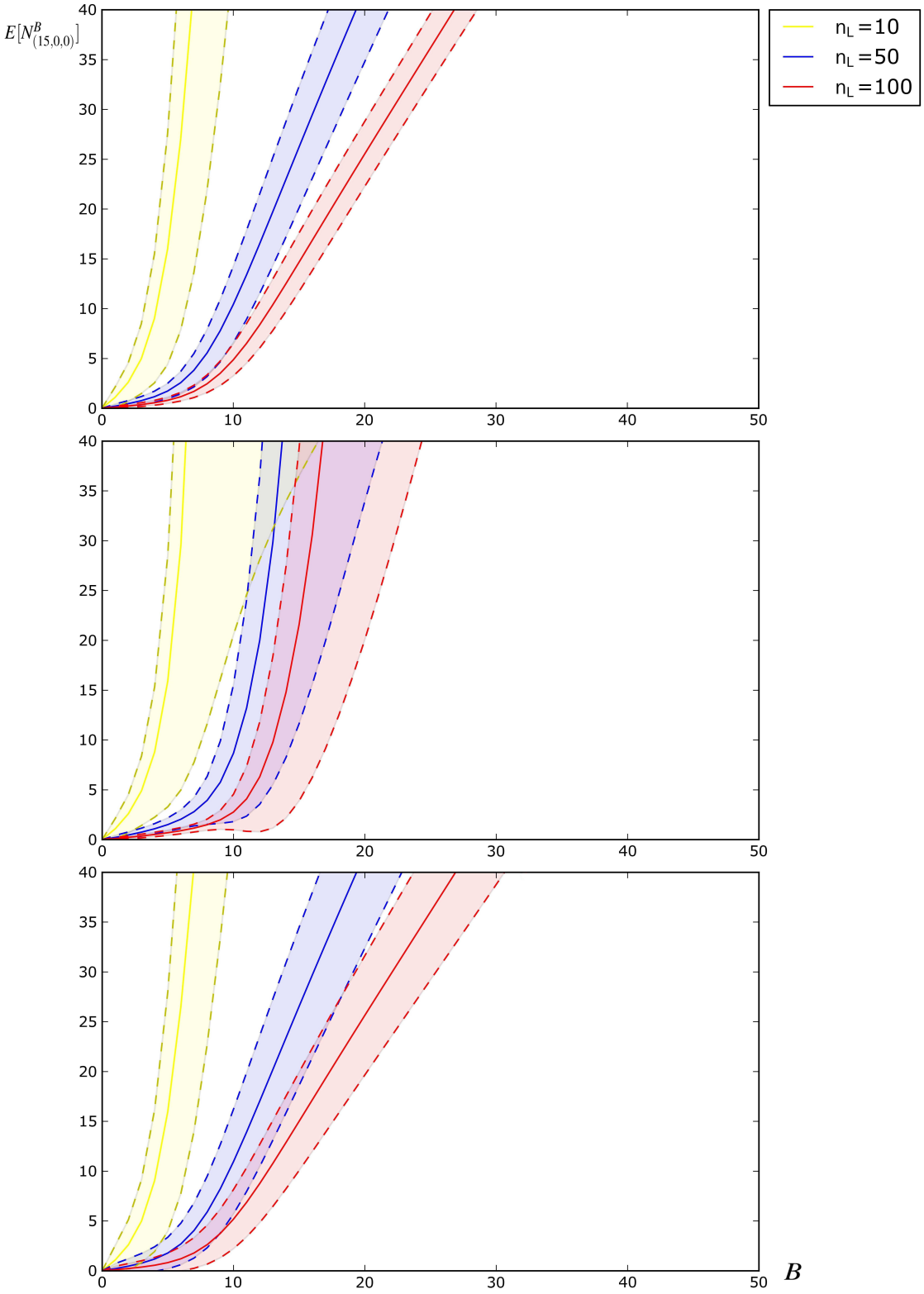

Figure 2.4: Mean number $E[N^B_{(15,0,0)}]$ of receptors synthesised, plus and minus its standard deviation, to reach a threshold number B of bound complexes on the cell surface, versus B, for different ligand concentrations $n_L \in \{10, 50, 100\}$. Synthesis rate hypothesis considered in the process amounts to (from *top* to *bottom*) $\sigma(C)$, $\sigma(E)$ or $\sigma(C+E)$.

obtained by slightly modifying our arguments in Section 2.3. In particular, if we define

$$\phi^B_{(n_1,n_2,n_3)}(s;CS) \;=\; E\left[s^{N^B_{(n_1,n_2,n_3)}(CS)}\right], \quad |s| \leq 1,$$

Equation (2.7) is replaced by

$$\begin{aligned}\Delta_{(n_1,n_2,n_3)}\phi^B_{(n_1,n_2,n_3)}(s;CS) \;=\;& k_{\text{on}} n_1 n_L \phi^B_{(n_1-1,n_2+1,n_3)}(s;CS) + k_{\text{off}} n_2 \phi^B_{(n_1+1,n_2-1,n_3)}(s;CS)\\ &+k_s n_1 \phi^B_{(n_1-1,n_2,n_3)}(s;CS) + \gamma n_2 \phi^B_{(n_1,n_2-1,n_3+1)}(s;CS)\\ &+\delta n_3 \phi^B_{(n_1+1,n_2,n_3-1)}(s;CS) + k_e n_3 \phi^B_{(n_1,n_2,n_3-1)}(s;CS)\\ &+(1-\delta_{n_1+n_2+n_3,n_R^{max}})\left(v_0 s + v_1 \frac{x^3}{x^3+K_c^3}\right)\phi^B_{(n_1+1,n_2,n_3)}(s;CS),\end{aligned}$$

where $x \in \{n_2, n_3, n_2+n_3\}$ for synthesis rates given by $\sigma(C)$, $\sigma(E)$ and $\sigma(C+E)$, respectively. Thus, moments of $N^B_{(n_R,0,0)}(CS)$ (and, similarly, of $N^B_{(n_R,0,0)}(LIS)$) can be obtained by reproducing our arguments in Section 2.3.

We compute in Table 2.2 not only the mean number $E[N^B_{(15,0,0)}]$ of synthesised receptors to reach a threshold number B of bound complexes under different scenarios, but also the percentage contribution to this synthesis of constitutive and ligand-induced synthesis pathways. For the hypothesis corresponding to synthesis rate given by $\sigma(C)$, we observe that larger amounts of ligands represent a more important role played by ligand-induced synthesis, which was expected. However, a saturation behaviour can be observed between concentrations $n_L = 50$ and $n_L = 100$, which seems to indicate that ligand concentrations above a particular threshold do not lead to higher ligand-induced synthesis. Of course, this is directly related with the Hill function assumed in [13] for $\sigma(x)$. Similar comments can be made for hypothesis corresponding to $\sigma(C+E)$. Moreover, differences between values of $E[N^B_{(15,0,0)}]$ in Table 2.2 for the cases $\sigma(C)$ and $\sigma(C+E)$, and even for $\sigma(E)$, are negligible for $B = 5$. This indicates that the ligand-induced synthesis pathway does not play a significant role, in absolute terms, in the short-term dynamics of the system. This is not the case for $B = 10$, which shows a significant different behaviour for $\sigma(E)$ with respect to $\sigma(C)$ or $\sigma(C+E)$, meaning that ligand-induced synthesis plays a major role in mid- and long-term dynamics. Finally, we point out that several values shown in Table 2.2 have to be carefully interpreted by looking at the same time at Figures 2.3 and 2.4. For example, the value $E[N^B_{(15,0,0)}] \sim 670$ for $B = 10$, synthesis rate given by $\sigma(E)$, and ligand concentration $n_L = 10$, can be explained by noting that, under these settings, $B = 10$ bound complexes on the cell surface are only reached in the long-term, significantly after the first hour of the experiment (see Figure 2.3).

B	$\sigma(x)$	n_L	$E[T^B_{(15,0,0)}]$	$E[N^B_{(15,0,0)}]$	$100\frac{E[N^B_{(15,0,0)}(CS)]}{E[N^B_{(15,0,0)}]}\%$	$100\frac{E[N^B_{(15,0,0)}(LIS)]}{E[N^B_{(15,0,0)}]}\%$
5	$\sigma(C)$	10	86.52	15.97	90.33%	9.67%
		50	8.91	1.73	86.06%	13.94%
		100	4.10	0.80	85.66%	14.34%
	$\sigma(E)$	10	95.26	15.92	99.72%	0.28%
		50	9.00	1.50	99.73%	0.27%
		100	4.11	0.69	99.84%	0.16%
	$\sigma(C+E)$	10	84.12	15.98	87.72%	12.28%
		50	8.88	1.78	83.02%	16.98%
		100	4.09	0.82	83.46%	16.54%
10	$\sigma(C)$	10	408.35	107.32	63.43%	36.57%
		50	27.93	10.41	44.75%	55.25%
		100	12.23	4.85	42.00%	58.00%
	$\sigma(E)$	10	3993.32	669.99	99.36%	0.64%
		50	51.13	8.67	98.33%	1.67%
		100	16.31	2.76	98.36%	1.64%
	$\sigma(C+E)$	10	316.02	92.79	56.77%	43.23%
		50	26.32	10.95	40.05%	59.95%
		100	11.87	5.18	38.21%	61.79%

Table 2.2: Values of $E[T^B_{(15,0,0)}]$ (in *minutes*), $E[N^B_{(15,0,0)}]$, $100\frac{E[N^B_{(15,0,0)}(CS)]}{E[N^B_{(15,0,0)}]}\%$ (that is, % corresponding to constitutive synthesis), and $100\frac{E[N^B_{(15,0,0)}(LIS)]}{E[N^B_{(15,0,0)}]}\%$ (that is, % corresponding to ligand-induced synthesis), for different concentrations $n_L \in \{10, 50, 100\}$ and different values of $B \in \{5, 10\}$. Synthesis rates given by $\sigma(C)$, $\sigma(E)$ and $\sigma(C+E)$ considered.

2.6 Algorithms

Algorithm 1 (for obtaining the Laplace-Stieltjes transforms $\varphi^B_{(n_1,n_2,n_3)}(z)$)

$\mathbf{H}_0(z) = \mathbf{I}_{J(0)} - \mathbf{A}_{0,0}(z)$;

For $k = 1, \ldots, B-1$:

$\mathbf{H}_k(z) = \mathbf{I}_{J(k)} - \mathbf{A}_{k,k}(z) - \mathbf{A}_{k,k-1}(z)\mathbf{H}^{-1}_{k-1}(z)\mathbf{A}_{k-1,k}(z)$;

$\boldsymbol{\varphi}_{B-1}(z) = \mathbf{H}^{-1}_{B-1}(z)\mathbf{A}_{B-1,B}(z)\mathbf{e}_{J(B)}$;

For $k = B-2, \ldots, 0$:

$\boldsymbol{\varphi}_k(z) = \mathbf{H}^{-1}_k(z)\mathbf{A}_{k,k+1}(z)\boldsymbol{\varphi}_{k+1}(z)$;

Finally, the different order moments $m^{B,(l)}_{(n_1,n_2,n_3)}$ of the random variable $T^B_{(n_1,n_2,n_3)}$ can be obtained by means of applying a similar matrix formalism to Equation (2.4). In particular, system given by

Equation (2.4) can be expressed in matrix form as

$$\mathbf{m}^{(l)} \quad = \quad \mathbf{A}(0)\mathbf{m}^{(l)} + \tilde{\mathbf{b}}^{l},$$

with

$$(\tilde{\mathbf{b}}^{l})_i \quad = \quad l\frac{1}{\Delta_i}(\mathbf{m}^{(l-1)})_i, \quad 0 \leq i \leq \sum_{k=0}^{B-1} \#L(k),$$

where Δ_i represents the value $\Delta_{(n_1,n_2,n_3)}$ for the state (n_1, n_2, n_3) corresponding to row i. Vector $\tilde{\mathbf{b}}^{l}$ can be structured by blocks as

$$\tilde{\mathbf{b}}^{l} \quad = \quad \begin{pmatrix} \tilde{\mathbf{b}}_0^{l} \\ \tilde{\mathbf{b}}_1^{l} \\ \vdots \\ \tilde{\mathbf{b}}_{B-2}^{l} \\ \tilde{\mathbf{b}}_{B-1}^{l} \end{pmatrix}.$$

Then, similar arguments than those ones applied for obtaining Algorithm 1 yield Algorithm 1 (continuation), which allows us to compute moments in vector $\mathbf{m}^{(p)}$ from previously computed moments in vector $\mathbf{m}^{(p-1)}$, starting at $\mathbf{m}^{(0)} = \boldsymbol{\varphi}(0)$ and until the desired order $p = l$ is reached.

Algorithm 1 (Continuation) (for obtaining the l-th order moments $m^{B,(l)}_{(n_1,n_2,n_3)}$)

For $k = 0, 1, \ldots, B-1$*:*

$\mathbf{m}_k^{(0)} \;=\; \boldsymbol{\varphi}_k(0)$*;*

For $p = 1, \ldots, l$*:*

$\mathbf{J}_0^{(p)} \;=\; \tilde{\mathbf{b}}_0^{p}$*;*

For $j = 1, \ldots, B-1$*:*

$\mathbf{J}_j^{(p)} \;=\; \mathbf{A}_{j,j-1}(0)\mathbf{H}_{j-1}^{-1}(0)\mathbf{J}_{j-1}^{(p)} + \tilde{\mathbf{b}}_j^{p}$*;*

$\mathbf{m}_{B-1}^{(p)} \;=\; \mathbf{H}_{B-1}^{-1}(0)\mathbf{J}_{B-1}^{(p)}$*;*

For $j = B-2, \ldots, 1, 0$*:*

$$\mathbf{m}_j^{(p)} \;=\; \mathbf{H}_j^{-1}(0)\left(\mathbf{J}_j^{(p)} + \mathbf{A}_{j,j+1}(0)\mathbf{m}_{j+1}^{(p)}\right);$$

Regarding the second descriptor analysed in Section 2.3.2, Equation (2.8) can be expressed in matrix form as

$$\boldsymbol{\phi}(s) \;=\; \overline{\mathbf{A}}(s)\boldsymbol{\phi}(s) + \overline{\mathbf{b}}, \tag{2.9}$$

where we are omitting again B in the notation, and where probability generating functions $\phi^B_{(n_1,n_2,n_3)}(s)$ for $(n_1,n_2,n_3) \in \cup_{k=0}^{B-1} L(k)$ are stored in a column vector $\boldsymbol{\phi}(s)$ which is organised in sub-vectors following the structure by levels and sub-levels of $\mathcal{S}$, in a similar way than our arguments with vector $\boldsymbol{\varphi}(z)$. Moreover, from a direct comparison between Equations (2.3) and (2.8) it is straightforward to check that $\overline{\mathbf{A}}(s) = \mathbf{A}(z=0)$, except for sub-blocks $\mathbf{B}^{k,k}_{r,r+1}(z)$ which should be replaced by $\overline{\mathbf{B}}^{k,k}_{r,r+1}(s)$ given by

$$(\mathbf{B}^{k,k}_{r,r+1}(s))_{ij} \;=\; \begin{cases} \sigma(k)s\Delta^{-1}_{(r,k,i)}, & \text{if } j=i, \\ \delta i\Delta^{-1}_{(r,k,i)}, & \text{if } j=i-1, \\ 0, & \text{otherwise}, \end{cases}$$

for $1 \le i \le J(k;r)$, $1 \le j \le J(k;r+1)$, $0 \le k \le B-1$ and $0 \le r \le n_R^{max} - k - 1$. Finally, vector $\overline{\mathbf{b}} = \mathbf{b}(z=0)$, and Algorithm 1 directly applies for computing vector $\boldsymbol{\phi}(s)$ from Equation (2.9). Factorial moments $n^{B,(p)}_{(n_1,n_2,n_3)}$ and probabilities $\alpha^B_{(n_1,n_2,n_3)}(a)$ of random variable $N^B_{(n_1,n_2,n_3)}$ can then be computed following similar arguments than before, and are omitted here.

2.7 Van Kampen's expansion approximation

For the cases in which the chemical master equation is not an exact procedure (when Lindeberg condition is not obeyed), an approximation procedure procures an analytical complement to numerical simulations. Accordingly, in the limit of infinitely large systems, several approaches have associated the solutions of the master equation to the one for the reaction rate equation (RRE) of the aforesaid system. In the present section, for instance, by separating macroscopic fluctuation y_i from the macroscopic concentration ϕ_i, the Master equation can be turned into a Fokker-Planck equation kind [74] when expanding the total number of the i^{th} species, n_i, in inverse powers of the square root of the system size Ω in what it is called a "system-size expansion". This approximation, proved by Van Kampen [31], provides more precise solutions for the master

equation in a systematic way by adding perturbations to the solution of the RRE. Linear noise approximation refers to the first perturbation term in Van Kampen's expansion which, as it will be shown in the present section, plays the central role in this procedure. Let us then define

$$n_i = \Omega\phi_i + \Omega^{\frac{1}{2}} y_i.$$

A step operator that increases or decreases the i^{th} species in 1 over the function f can be also defined for our purpose as

$$\mathbb{E}_i(f(n_i)) = f(n_i + 1)$$

and

$$\mathbb{E}_i^{-1} := \mathbb{F}_i(f(n_i)) = f(n_i - 1).$$

Given that the previous operator hardly affects the macroscopic scale, Taylor series properly describe it, in the limit of $\Omega \gg 1$. For instance, if the operator is applied to $f(n_i) = n_i$ ending as

$$\begin{aligned} \mathbb{E}_i^{\pm 1} n_i &= n_i \pm 1, \\ \mathbb{E}_i^{\pm 1} n_i^2 &= n_i^2 + 1^2 \pm 2n_i, \\ &\vdots \quad , \end{aligned}$$

so the operator can be approximated by a Taylor series,

$$\mathbb{E}_i^{\pm 1} = 1 \pm \frac{\partial}{\partial n_i} + \frac{1}{2}\frac{\partial^2}{\partial n_i^2} \pm \ldots,$$

and, applying the chain rule for

$$\begin{aligned} \frac{\partial}{\partial y_i} f(n_i(y_i)) &= \frac{\partial n_i}{\partial y_i}\frac{\partial}{\partial n_i} f(n_i(y_i)), \\ \frac{\partial}{\partial n_i} &= (\frac{\partial n_i}{\partial y_i})^{-1}\frac{\partial}{\partial y_i}, \end{aligned}$$

the following expression holds

$$\mathbb{E}_i^{\pm 1} = 1 \pm (\Omega)^{-\frac{1}{2}}\frac{\partial}{\partial y_i} + \frac{1}{2}\Omega^{-1}\frac{\partial^2}{\partial y_i^2} \pm .... \tag{2.10}$$

Transforming from the old variables (n_1, n_2, n_3) to (y_1, y_2, y_3), we have the relations:

$$P_{(n_1,n_2,n_3)}(t) \longrightarrow \Pi_{(y_1,y_2,y_3)}(t),$$

$$\Omega^{\frac{1}{2}} \frac{\partial}{\partial n_i} P_{(n_1,n_2,n_3)}(t) = \frac{\partial}{\partial y_i} \Pi_{(y_1,y_2,y_3)}(t).$$

Thus, our master equation from Equation (2.2) given by

$$\begin{aligned}
\frac{dp_{(n_1,n_2,n_3)}}{dt} &= \kappa_{on} n_L (n_1+1) p_{(n_1+1,n_2-1,n_3)} + \kappa_{off}(n_2+1) p_{(n_1-1,n_2+1,n_3)} \\
&\quad + \kappa_s (n_1+1) p_{(n_1+1,n_2,n_3)} + \gamma (n_2+1) p_{(n_1,n_2+1,n_3-1)} \\
&\quad + \delta (n_3+1) p_{(n_1-1,n_2,n_3+1)} + \kappa_e (n_3+1) p_{(n_1,n_2,n_3+1)} \\
&\quad + (\nu_0 + \nu_1 \sigma(n_2)) p_{(n_1-1,n_2,n_3)} - \Big(\kappa_{on} n_L n_1 \\
&\quad + \kappa_{off} n_2 + \kappa_s n_1 + \gamma n_2 + \delta n_3 + \kappa_e n_3 + (\nu_0 + \nu_1 \sigma(n_2)) \Big) p_{(n_1,n_2,n_3)},
\end{aligned}$$

may be rewritten in terms of these operators as

$$\begin{aligned}
\frac{\partial}{\partial t} \Pi_{(y_1,y_2,y_3)}(t) &= (\mathbb{E}_1 \mathbb{F}_2 - \mathbb{I}) \kappa_{on} n_L n_1 + (\mathbb{F}_1 \mathbb{E}_2 - \mathbb{I}) \kappa_{off} n_2 + (\mathbb{E}_1 - \mathbb{I}) \kappa_s n_1 + (\mathbb{E}_2 \mathbb{F}_3 - \mathbb{I}) \gamma n_2 \\
&\quad + (\mathbb{F}_1 \mathbb{E}_3 - \mathbb{I}) \delta n_3 + (\mathbb{E}_3 - \mathbb{I}) \kappa_e n_3 + (\mathbb{F}_1 - \mathbb{I})(\nu_0 + \nu_1 \sigma(n_2)), \qquad (2.11)
\end{aligned}$$

where $\mathbb{I}$ is the identity operator and where

$$\mathbb{E}_i \mathbb{F}_j = \mathbb{F}_j \mathbb{E}_i = 1 + \Omega^{-\frac{1}{2}} \left(\frac{\partial}{\partial y_i} - \frac{\partial}{\partial y_j} \right) + \Omega^{-1} \frac{1}{2} \left(\frac{\partial}{\partial y_i} - \frac{\partial}{\partial y_j} \right)^2. \qquad (2.12)$$

Ignoring terms with Ω^i when $i < -1$. Finally, using identities (2.10), (2.11) and (2.12):

$$\begin{aligned}
\frac{\partial}{\partial t}\Pi &- \sqrt{\Omega} \frac{d\phi_1}{dt} \frac{\partial \Pi}{\partial y_1} - \sqrt{\Omega} \frac{d\phi_2}{dt} \frac{\partial \Pi}{\partial y_2} - \sqrt{\Omega} \frac{d\phi_3}{dt} \frac{\partial \Pi}{\partial y_3} = \Big[\kappa_{on} n_L \left(\frac{Y_1 - Y_2}{\sqrt{\Omega}} + \frac{(Y_1 - Y_2)^2}{2\Omega} \right) \left(\sqrt{\Omega} y_1 + \Omega \phi_1 \right) \\
&+ \kappa_{off} \left(\frac{Y_2 - Y_1}{\sqrt{\Omega}} + \frac{(Y_2 - Y_1)^2}{2\Omega} \right) \left(\sqrt{\Omega} y_2 + \Omega \phi_2 \right) + \kappa_s \left(\frac{Y_1}{\sqrt{\Omega}} + \frac{Y_1^2}{2\Omega} \right) \left(\sqrt{\Omega} y_1 + \Omega \phi_1 \right) \\
&+ \gamma \left(\frac{Y_2 - Y_3}{\sqrt{\Omega}} + \frac{(Y_2 - Y_3)^2}{2\Omega} \right) \left(\sqrt{\Omega} y_2 + \Omega \phi_2 \right) + \delta \left(\frac{Y_3 - Y_1}{\sqrt{\Omega}} + \frac{(Y_3 - Y_1)^2}{2\Omega} \right) \left(\sqrt{\Omega} y_3 + \Omega \phi_3 \right) \\
&+ \kappa_e \left(\frac{Y_3}{\sqrt{\Omega}} + \frac{Y_3^2}{2\Omega} \right) \left(\sqrt{\Omega} y_3 + \Omega \phi_3 \right) + \left(\nu_0 + \nu_1 \sigma(\sqrt{\Omega} y_2 + \Omega \phi_2) \right) \left(- \frac{Y_1}{\sqrt{\Omega}} + \frac{Y_1^2}{2\Omega} \right) \Big] \Pi, \qquad (2.13)
\end{aligned}$$

where $Y_i^n = \frac{\partial^n}{\partial y_i^n}$. Therefore, for the case $\nu_1 = 0$, and expanding the last expression according to $\sqrt{\Omega}$, the three differential equations for the macroscopic behaviour hold for the terms with $\sqrt{\Omega}$,

$$\begin{aligned}
\frac{d\phi_1}{dt} &= -\kappa_{on} n_L \phi_1 + \kappa_{off}\phi_2 - \kappa_s \phi_1 + \delta\phi_3, \\
\frac{d\phi_2}{dt} &= \kappa_{on} n_L \phi_1 - \kappa_{off}\phi_2 - \gamma\phi_2, \\
\frac{d\phi_3}{dt} &= \gamma\phi_2 - \delta\phi_3 - \kappa_e\phi_3,
\end{aligned}$$

in which the steady state is the trivial $(n_1, n_2, n_3)_0^* = (0, 0, 0)$. When $\nu_1 \neq 0$, an unsolvable situation to obtain a polynomial expression in terms of $\Omega^{-\frac{1}{2}}$ holds. It can be supposed, however, that a coefficient $\overline{\nu_1}$ approximates the value of the synthesis. In such a scenario, in order to obtain the steady state, the following system needs to be solved

$$\begin{aligned}
0 &= -\kappa_{on} n_L \phi_1 + \kappa_{off}\phi_2 - \kappa_s \phi_1 + \delta\phi_3 + \overline{\nu_1}, \\
0 &= \kappa_{on} n_L \phi_1 - \kappa_{off}\phi_2 - \gamma\phi_2, \\
0 &= \gamma\phi_2 - \delta\phi_3 - \kappa_e\phi_3,
\end{aligned} \tag{2.14}$$

and the steady state can be shown to satisfy

$$(n_1, n_2, n_3)^* = \left(\frac{(\delta + \kappa_e)(\gamma + \kappa_{off})\overline{\nu_1}}{T}, \frac{(\delta + \kappa_e)\kappa_{on} n_L \overline{\nu_1}}{T}, \frac{\gamma\kappa_{on} n_L \overline{\nu_1}}{T} \right),$$

where $T = \gamma\delta\kappa_s + \gamma\kappa_e\kappa_s + \delta\kappa_{off}\kappa_s + \kappa_e\kappa_{off}\kappa_s + \gamma\kappa_e\kappa_{on} n_L$. To prove its stability, the Jacobian $\mathbf{J}$ is computed,

$$\mathbf{J} = \begin{pmatrix} -\kappa_{on} n_L - \kappa_s & \kappa_{off} & \delta \\ \kappa_{on} n_L & -\kappa_{off} - \gamma & 0 \\ 0 & \gamma & -\delta - \kappa_e \end{pmatrix}.$$

Thus, defining $\mathbf{M} = \mathbf{J} - \lambda \mathbf{I}_{3\times 3}$ and expressing the determinant of $\mathbf{M}$ as a polynomial in λ

$$|\mathbf{M}| = \lambda^3 + \lambda^2 a_1 + \lambda a_2 + a_3,$$

it can be shown that $a_1, a_2, a_3 > 0$ and $a_1 a_2 > a_3$ regardless of the value of the parameters

(assuming they are all positive), and so $(n_1, n_2, n_3)^*$ is stable. Let us approximate $\overline{\nu_1} = 1.3333$, disregarding for a moment the $\frac{x^3}{x^3+\kappa_C^3}$ term. In such a case, using the values of the parameters modified from [13] and given in Table 2.1, the time dynamics can be plotted in Figure 2.5, and

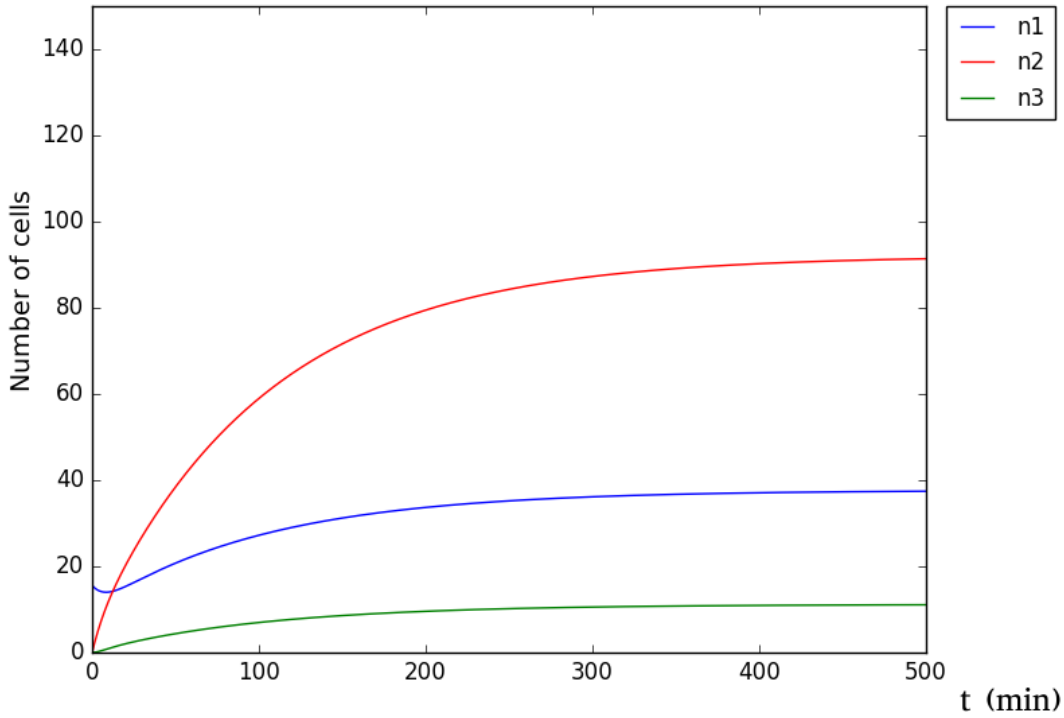

Figure 2.5: Time dynamics (in minutes) for System (2.14). $\overline{\nu_1} = 1.3333$. Parameter values modified from Table 2.1 as explained in Section 2.5, this is, $\kappa_{off} = 0.0138 min^{-1}$, $\kappa_s = 0.0107 min^{-1}$, $\delta = 0.15 min^{-1}$, $\nu_0 = 0.1667 min^{-1}$, $\gamma = 0.0283 min^{-1}$, $\kappa_e = 0.0833 min^{-1}$, and $\kappa_{on} \approx 0.001$. Case $N_L = 100$. Initial conditions also given in Section 2.5 are $(n_1(0), n_2(0), n_3(0)) = (\frac{\nu_0}{\kappa_s}, 0, 0)$.

the positive steady state that results is

$$(n_1, n_2, n_3)^* = (37.66, 92.07, 11.17),$$

where its stability has been proved.

From the lowest order in Equation (2.13), the following Fokker-Plank equation is also obtained to characterise the fluctuations

$$\frac{\partial \Psi}{\partial t} = -\sum_{i,j} A_{ij} \frac{\partial}{\partial y_i}(y_j \Psi) + \frac{1}{2} \sum_{i,j} B_{ij} \frac{\partial^2 \Psi}{\partial y_i \partial y_j}, \tag{2.15}$$

with

$$\mathbf{A} = \begin{pmatrix} -\kappa_{on} n_L - \kappa_s + \overline{\nu_1} & \kappa_{off} & \delta \\ \kappa_{on} n_L & -\kappa_{off} - \gamma & 0 \\ 0 & \gamma & -\delta - \kappa_e \end{pmatrix}$$

and

$$\mathbf{B} = \begin{pmatrix} \kappa_{on} n_L \phi_1 + \kappa_{off} \phi_2 + \kappa_s \phi_1 + \delta \phi_3 + \overline{\nu_1} & -2\kappa_{on} n_L \phi_1 - 2\kappa_{off} \phi_2 & -2\delta \phi_3 \\ -2\kappa_{on} n_L \phi_1 - 2\kappa_{off} \phi_2 & \kappa_{on} n_L \phi_1 + \kappa_{off} \phi_2 + \gamma \phi_2 & -2\gamma \phi_2 \\ -2\delta \phi_3 & -2\gamma \phi_2 & \gamma \phi_2 + \delta \phi_3 + \kappa_e \phi_3 \end{pmatrix},$$

so the first moment and the variance of the fluctuation can be obtained from Equation (2.15):

$$\begin{aligned} \frac{d\langle y_i \rangle}{dt} &= \sum_j A_{ij} \langle y_j \rangle, \\ \frac{d\langle y_i y_j \rangle}{dt} &= \sum_m A_{im} \langle y_m y_j \rangle + \sum_n A_{jn} \langle y_i y_n \rangle + B_{ij}. \end{aligned}$$

In particular,

$$\begin{aligned} \frac{d\langle y_1 \rangle}{dt} &= (-\kappa_{on} n_L - \kappa_s + \overline{\nu_1}) \langle y_1 \rangle + \kappa_{off} \langle y_2 \rangle + \delta \langle y_3 \rangle, \\ \frac{d\langle y_2 \rangle}{dt} &= \kappa_{on} n_L \langle y_1 \rangle + (-\kappa_{off} - \gamma) \langle y_2 \rangle, \\ \frac{d\langle y_3 \rangle}{dt} &= \gamma \langle y_2 \rangle + (-\delta - \kappa_e) \langle y_3 \rangle, \end{aligned}$$

and the second order moments are given as

$$\begin{aligned}
\frac{d\langle y_1^2\rangle}{dt} &= 2(-\kappa_{on}n_L - \kappa_s + \overline{\nu_1})\langle y_1^2\rangle + 2\kappa_{off}\langle y_1y_2\rangle + 2\delta\langle y_1y_3\rangle + \kappa_{on}n_L\phi_1 \\
&\quad +\kappa_{off}\phi_2 + \kappa_s\phi_1 + \delta\phi_3 + \overline{\nu_1}, \\
\frac{d\langle y_2^2\rangle}{dt} &= 2\kappa_{on}n_L\langle y_1y_2\rangle - 2(\kappa_{off}+\gamma)\langle y_2^2\rangle + \kappa_{on}n_L\phi_1 + \kappa_{off}\phi_2 + \gamma\phi_2, \\
\frac{d\langle y_3^2\rangle}{dt} &= 2\gamma\langle y_2y_3\rangle - 2(\delta+\kappa_e)\langle y_3^2\rangle + \gamma\phi_2 + \delta\phi_3 + \kappa_e\phi_3, \\
\frac{d\langle y_1y_2\rangle}{dt} &= \kappa_{on}n_L\langle y_1^2\rangle + (-\kappa_{on}n_L - \kappa_s - \kappa_{off} - \gamma + \overline{\nu_1})\langle y_1y_2\rangle + \kappa_{off}\langle y_2^2\rangle \\
&\quad +\delta\langle y_2y_3\rangle - 2\kappa_{on}n_L\phi_1 - 2\kappa_{off}\phi_2, \\
\frac{d\langle y_1y_3\rangle}{dt} &= \gamma\langle y_1y_2\rangle + (-\kappa_{on}n_L - \kappa_s - \delta - \kappa_e + \overline{\nu_1})\langle y_1y_3\rangle + \kappa_{off}\langle y_2y_3\rangle + \delta\langle y_3^2\rangle - 2\delta\phi_3, \\
\frac{d\langle y_2y_3\rangle}{dt} &= \kappa_{on}n_L\langle y_1y_3\rangle + \gamma\langle y_2^2\rangle - (\kappa_{off}+\gamma+\delta+\kappa_e)\langle y_2y_3\rangle - 2\gamma\phi_2,
\end{aligned}$$

which in steady state, the sign is calculated, resulting in

$$\begin{aligned}
\langle y_1^2\rangle, \langle y_2^2\rangle, \langle y_3^2\rangle, \langle y_1y_2\rangle, \langle y_1y_3\rangle &> 0, \quad \text{and} \\
\langle y_2y_3\rangle &< 0,
\end{aligned}$$

and we can conclude that only complexes on the cell surface and those in the endosome have negative correlation.

2.8 Discussion

We have developed a stochastic version of the deterministic model introduced in [13], for the stimulation of a regulatory T cell by IL-2. Instead of solving the master equation associated with the Markovian process, or of carrying out Gillespie simulations, we have defined two random variables to analyse the rate at which IL-2/IL-2R bound complexes are formed and stay on the cell surface, as well as the rate at which IL-2R is synthesised. We have computed the Laplace-Stieltjes transforms and the probability generating functions of these random variables by appropriately arranging the space of states and making use of first-step arguments.

The authors in [13] hypothesise that IL-2R synthesis is induced by the presence of bound IL-

2/IL-2R complexes on the cell surface. We have further generalised this hypothesis, and have also considered the role of internalised IL-2/IL-2R complexes in the IL-2R synthesis rate. We have made use of numerical experiments to compare these two different hypotheses. Our numerical results suggest that if endosomal complexes contribute to the induced synthesis rate, their effect would be negligible when considering the time to reach a certain signalling threshold (encoded by the number of bound IL-2/IL-2R complexes on the surface of a regulatory T cell). Moreover, considering only endosomal complexes as the signalling units for IL-2R synthesis would significantly change the dynamics of the process.

On the other hand, slight modifications in our stochastic descriptors allow us to address the role played by the constitutive and the ligand-induced pathways in the synthesis of IL-2R molecules. A particular conclusion from Table 2.2 is that ligand-induced synthesis is not significantly important for short-term dynamics of the system, in which constitutive receptor synthesis seems to play the central role. On the other hand, under high ligand concentrations, ligand-induced synthesis plays a major role, and the hypothesis regarding the nature of the synthesis rate needs to be carefully analysed. While including endosomal complexes in the synthesis rate (together with surface complexes) seems to not change main behaviours of the process, considering only these complexes into the synthesis rate gives significantly different results. On the other hand, while increasing ligand concentrations gives an increasing role of the ligand-induced synthesis, a saturation behaviour is clearly observed, so that above particular ligand concentration thresholds no significant more ligand-induced synthesis should be expected.

Finally, we need to point out that, although the algorithmic approach followed here allows us to obtain analytical results regarding the dynamics of the process, it also has its own computational limitations. Thus, the focus on algorithmic efficiency made in Section 2.6 is essential for the computation of numerical results. In general, a balance between computational limitations and model complexity needs to be considered, and alternative procedures should prevail under higher dimensional models for more complex processes.

Chapter 3

CTLA-4 in the co-stimulatory system

3.1 Introduction

As mentioned in Section 1.1.2, T cells require at least two different signals to become fully activated; the antigen-specific, involving the T-cell receptor, and the co-stimulatory signal; an antigen nonspecific interaction between molecules (ligands) on APC (antigen presenting cell), and receptors from the T cell. The balance between stimulatory and inhibitory co-signals, CD28 and CTLA-4 (cytotoxic T lymphocyte antigen 4) bindings respectively, determines the nature of the latter. Since these receptors bind the same two ligands B7-1 and B7-2 (also referred to as CD80 and CD86, respectively), dynamics when forming complexes need to be established. Failures on co-stimulation may result in T cell anergy.

This chapter is accomplished through the study of mathematical models for simulating the synaptic accumulation of these four molecules. For this purpose, some data about their nature such as mobility, expression levels, binding affinity or endocytic and exocytic procedures must be analysed to estimate the parameters of the models.

The first step is to develop some preliminary stochastic models involving specific phases of the whole process and disregarding partakers if needed. Thus, for the binding stage, several models are elaborated in Section 3.2 for CD28 with the two ligands and for B7-1 with both receptors having into account the monomeric and dimeric structure of B7-2 and B7-1, respectively, and the monovalence and bivalence of CD28 and CTLA-4 each to each. After that, another model for CTLA-4 endocytosis is developed in Section 3.3. Its emerging role as a cell-extrinsic regulator and

the relevance of this until now not well-known process to immune system tolerance lead to claim that a proper understanding about the behavior of this inhibitory receptor can be crucial.

Through continuous time trivariate Markov processes, the stochastic equations are derived for all the models and so the Kolmogorov equation. By using this master equation and partial differential equations for the moment generating function first and second moments are then obtained for each case. To move from this stochastic approach to the deterministic one, the master equation is developed using the Van Kampen expansion. With moment closure techniques the approximated solution of the moments can be also found. For the internalisation model, a matrix analytic method will be described to study in an analytical manner the distribution of certain variables.

In this Chapter, the aim is to analyse the interaction dynamics of molecules CTLA-4, B7-1 and B7-2 when intracellular trafficking of CTLA-4 is taken into account, by considering a stochastic Markovian framework. Then, a matrix formalism, based on the matrix-analytic approach [35], is proposed which allows us to analyse in an exact way the dynamics of the process involving the interaction of this receptor with a single ligand type within the synapse, and different characteristics of the underlying Markov process are studied by means of stochastic descriptors (conveniently defined random variables which allow one to analyse the main dynamics in the process). This matrix formalism not only allows to analyse these dynamics, but also to identify the role played by each kinetic rate in the characteristics under study.

Moreover, a whole picture scenario can be also analysed by expanding the one-to-one molecule model, leading to a general model with four compartments representing the interaction dynamics between CTLA-4, CD28, B7-1 and B7-2. By means of Gillespie simulations, our numerical results suggest that co-receptor CD28 and ligand B7-2 play, in a synergistic manner, a crucial role in co-stimulation when they are simultaneously present within the synapse, having a significant impact on the B7-1 ligand depletion timescales, as well as on the formation dynamics of CTLA-4/B7-1 bound complexes. On the other hand, B7-2 ligand depletion dynamics, which are highly affected by the total number of CTLA-4 receptors on the cell surface, do not seem to be noticeable affected by competitor molecules (CD28 and B7-1). Moreover, saturation scenarios are identified when the synthesis of co-receptor CTLA-4 is represented in our process by means of a proportional increase of molecular levels on the cell surface upon T cell activation.

The chapter is organised as follows. Section 3.2 introduces several stochastic models describing the interactions between ligands and receptors on cell surface. In Section 3.3, a stochastic model is

proposed in which the interaction dynamics of CTLA-4 with one ligand are represented. In order to analyse these dynamics, we introduce several stochastic descriptors (Section 3.3.2), which can be efficiently analysed in terms of the matrix formalism proposed in that section. In this matrix-analytic approach, the focus is on constructing iterative procedures for computing the quantities of interest, leading to the construction of algorithmic procedures. A sensitivity analysis is also developed in Section 3.3.2.5 in order to quantitatively address the role played by each kinetic rate (these rates being discussed in Section 3.3.3) in the dynamics of our process. Numerical results involving B7-1 and CTLA-4 interactions are obtained in Section 3.3.4 regarding the internalisation (ligand depletion) timescales, the rate of receptor-ligand complex formation on the synapse and the sensitivity analysis mentioned above. Equivalent results related to B7-2 ligand instead of B7-1 are also presented in this section. Finally, in Section 3.4, we propose a general model in which the four main molecules in charge of the co-stimulatory system (B7-1, B7-2, CTLA-4 and CD28) are considered. This model is constructed in terms of compartments, so that the impact of each molecule on the system dynamics can be addressed.

3.2 Cell surface models

CTLA-4 and CD28 are glycoproteins expressed by both $CD8^+$ and $CD4^+$ T cells. However, while CD28 is constitutively expressed on the plasma membrane of both resting and activated conventional T cells, CTLA-4 only does it constitutively in $CD4^+CD25^+FOXP3^+$ T regs (regulatory T cells), whereas it is not expressed by resting conventional T cell until 2 days after cell-activation in both mice and humans. Furthermore, in the resting immune system the expression of CTLA-4 is normally to T reg cells. According to several studies, CD28-deficient mice have considerably impaired T cell responses to antigen. In contrast with this co-stimulatory function, blockade of CTLA-4 increases T cell response in a wide range of systems.

In terms of the morphology of these molecules, B7-1 and B7-2 have a dimeric and a monomeric crystal structure respectively. CD28 is a dimer but its binding are thought to be monovalent due to steric inhibition. Finally, CTLA-4 is also a dimer and binds as a bivalent molecule. One of the most interesting parts of this process, in addition to the quantification of the balance between positive and negative signals from the receptor, is CTLA-4 fate after endocytosis. On one hand, because of the lack of information to this respect, and on the other, due to its emerging role as an extrinsic regulator of T cell response, in which this receptor would deplete the ligands from the APC so for future interactions, this APC would not be able to stimulate in the same way. Having

said that, several aspects about CTLA-4 trafficking need to be also taken into consideration for a better understanding.

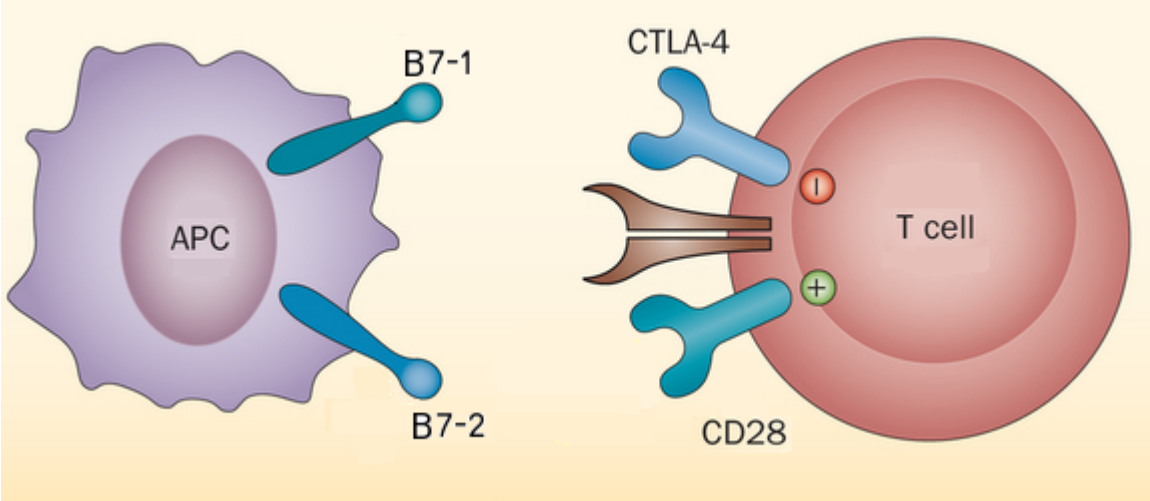

Figure 3.1: Co-stimulatory system between and APC and a T cell. Our models contemplate the dynamics between the co-receptors CD28 and CTLA-4 expressed by a T cell and ligands B7-1 and B7-2 presented on an APC. Figure taken from [19].

One of the first things to take into account when buiding our models, and in particular for the parametrisation stage, has to do with CTLA-4 endocytosis. It is stated that this process is consitutive and independent of ligand bindings [76, 73], which indicates that it is the receptor itself driving this trafficking move. At the same time, it is well known that trafficking pool of CTLA-4 is regulated by both recycling and degradation pathways [73] which reduces the amount of kinetic rates for us to consider when building up the models. In this same study, it was found that whilst CTLA-4 traffic is increased following stimulation, no change in endocytosis is apparent.

Regarding the spatial location of this receptor, it is believed that the majority of surface CTLA-4 (more than 80%) internalise within 5 minutes [76] and that only a small fraction of them is expressed on the surface at any given time. Moreover, recent studies suggest that CTLA-4 acts as an effector molecule to inhibit CD28 co-stimulation by the cell-extrinsic depletion of ligands [54], this means that somehow, ligands in charge of stimulate T cells are depleted from APCs by CTLA-4 so that APCs ability to re-stimulate in the future will be considerably, although still not quantified, reduced. This new hypothesis is particularly analysed in Section 3.4.1.

The two models proposed in this subsection are mainly studied from an stochastic point of view and can be defined as three dimensional Continuous Time Markov Processes. Given the state vector $W(t) = (n_1, n_2, n_3)$, which values correspond to the number of each molecule involved in the reaction at time t, three elements defined in Chapter 1.2 need to be established to characterise every model; the states space, the transition rates and the infinitesimal generator matrix.

3.2.1 CD28 binding B7-1 and B7-2 model

In this first part, a stochastical model for simulating the synaptic accumulation of the co-stimulatory molecules CD28, B7-1, and B7-2 is presented. Due to the almost negligible amount of CTLA-4 on the surface before the TCR signalling befalls, similar conditions could be supposed at commencement of co-stimulation. For this purpose, we assume a constant receptor and ligands concentration; R_1, L_1 and L_2 respectively. In this first approach, considerations about diffusion on cells are ignored. Given that, three different complexes $X_1(t)$, $X_2(t)$ and $X_3(t)$ can be formed as follows:

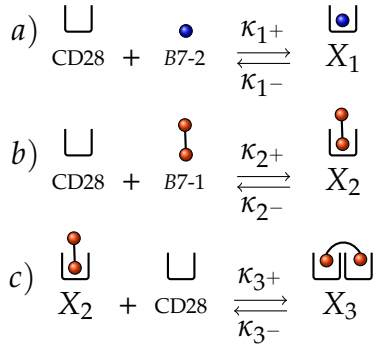

Figure 3.2: Diagram for a CD28 binding B7-1 and B7-2 dynamics model.

Figure 3.2 shows the diagram of the kinetics between co-receptor CD28 and ligands B7-1 and B7-2. In particular, κ_{1+} encodes the binding rate between the monovalent B7-2 ligand and CD28 which, once bound forming complex X_1, it can be dissociated with rate rate κ_{1-}. Analogously, κ_{2+} and κ_{2-} give the association and dissociation rates between CD28 and ligand B7-1. Given that this ligand is bivalent, when binding with receptor CD28 a factor of two needs to be included, as it can be seen in the rates given in Equation (3.1). Finally, monomer X_2 can bind another CD28 receptor to form a dimer X_3 with rate κ_{3+} which dissociates with rate κ_{3-} also by a factor of two.

Thus, if $\overline{n} = (n_1, n_2, n_3)$ represents the number of molecules X_1, X_2 and X_3, for each random

vector *W(t) = ($X_1(t)$, $X_2(t)$, $X_3(t)$)* a probability distribution $\mathbb{P}_n(t)$= $\mathbb{P}(X_1(t) = n_1,\ X_2(t) = n_2,\ X_3(t) = n_3)$ is associated and we can describe our model with the six reactions below:

$$\begin{aligned} \Delta W_1 &= (1,0,0), & \Delta W_4 &= (0,-1,0),\\ \Delta W_2 &= (-1,0,0), & \Delta W_5 &= (0,-1,1),\\ \Delta W_3 &= (0,1,0), & \Delta W_6 &= (0,1,-1). \end{aligned}$$

For which of them we can obtain the following infinitesimal transition rates $q_{\Delta W_i}(n_1,n_2,n_3) = \lim_{\Delta t\to 0} \mathbb{P}(W(t+\Delta t) = (n_1,n_2,n_3) + \Delta W_i \mid W(t) = (n_1,n_2,n_3))$, respectively:

$$\begin{aligned} q_{\Delta W_1}(n_1,n_2,n_3) &= \kappa_{1_+}(L_1-n_1)(R_1-n_1-n_2-2n_3),\\ q_{\Delta W_2}(n_1,n_2,n_3) &= \kappa_{1_-}n_1,\\ q_{\Delta W_3}(n_1,n_2,n_3) &= 2\kappa_{2_+}(L_2-n_2-n_3)(R_1-n_1-n_2-2n_3),\\ q_{\Delta W_4}(n_1,n_2,n_3) &= \kappa_{2_-}n_2,\\ q_{\Delta W_5}(n_1,n_2,n_3) &= \kappa_{3_+}n_2(R_1-n_1-n_2-2n_3),\\ q_{\Delta W_6}(n_1,n_2,n_3) &= 2\kappa_{3_-}n_3. \end{aligned} \tag{3.1}$$

For convenience, in the special case $\Delta W_0 = (0,0,0)$ we write $q_{\Delta W_0} = 1 - \sum_{i=1}^{6} q_{\Delta W_i}$. Hence, we get the expression

$$\mathbb{P}_{\overline{n}}(t) = \sum_{\Delta W_i} q_{\Delta W_i}(\overline{n})\mathbb{P}_{\overline{n}}(t+\Delta t),$$

where the state space is $\mathcal{S} = \{(n_1,n_2,n_3) \in (\mathbb{N}\cup\{0\})^3;\ n_1+n_2+2n_3 \le R_1\ ,\ n_2+n_3 \le L_2\ \}$ which may give distinguishable cases for the nature of $\mathcal{S}$ depending on the relation between R_1 and L_2. For notation simplicity, we write $\mathbb{P}_{\overline{n}}(t) = \mathbb{P}_{\overline{n}}$, and the master equation of this model can be deduced

$$\begin{aligned} \frac{dp_{(n_1,n_2,n_3)}}{dt} &= \kappa_{1_-}(n_1+1)p_{(n_1+1,n_2,n_3)} + \kappa_{1_+}(L_1-n_1+1)(R_1-n_1+1-n_2-2n_3)p_{(n_1-1,n_2,n_3)}\\ &\quad + \kappa_{2_-}(n_2+1)p_{(n_1,n_2+1,n_3)} + 2\kappa_{2_+}(L_2-n_2+1-n_3)(R_1-n_1-n_2+1-2n_3)p_{(n_1,n_2-1,n_3)}\\ &\quad + 2\kappa_{3_-}(n_3+1)p_{(n_1,n_2-1,n_3+1)} + \kappa_{3_+}(n_2+1)(R_1-n_1-n_2+1-2n_3)p_{(n_1,n_2+1,n_3-1)}\\ &- \Big((R_1-n_1-n_2-2n_3)[\kappa_{1_+}(L_1-n_1) + 2\kappa_{2_+}(L_2-n_2-n_3) + \kappa_{3_+}n_2] + \kappa_{1_-}n_1 + \kappa_{2_-}n_2 + 2\kappa_{3_-}n_3 + 1\Big)p_{(n_1,n_2,n_3)}, \end{aligned}$$

from which the different order moments $m_i = E\left[X_i(t)\right]$ and $m_{ij} = E\left[X_i(t)X_j(t)\right]$, with $i, j \in \{1, 2, 3\}$ can be obtained. Those of order one are given below

$$
\begin{aligned}
\tfrac{dm_1}{dt} &= \kappa_{1_+} R_1 L_1 - (\kappa_{1_+} R_1 + \kappa_{1_-}) m_1 - \kappa_{1_+}(L_1 - m_1)(m_1 + m_2 + 2m_3) \\
&\quad + \kappa_{1_+}(m_{11} - m_1^2 + m_{12} - m_1 m_2 + 2m_{13} - 2m_1 m_3), \\
\tfrac{dm_2}{dt} &= 2\kappa_{2_+} L_2 R_1 - 2\kappa_{2_+}(L_2 - m_2 - m_3) m_1 - [2\kappa_{2_+} L_2 - \kappa_{3_+} m_1 + (2\kappa_{2_+} + \kappa_{3_+})(R_1 - m_2 - 3m_3) \\
&\quad + \kappa_{2_-} + \kappa_{3_+} m_3] m_2 - (2\kappa_{2_+}(m_{12} + m_{13} - m_1 m_2 - m_1 m_3) + \kappa_{3_+}(m_{12} - m_1 m_2) \\
&\quad + (2\kappa_{2_+} + \kappa_{3_+})(m_{22} - m_2^2) + (6\kappa_{2_+} + 2\kappa_{3_+})(m_{23} - m_2 m_3) + 4\kappa_{2_+}(m_{33} - m_3^2), \\
\tfrac{dm_3}{dt} &= (R_1 - m_1 - m_2 - 2m_3)\kappa_{3_+} m_2 - 2\kappa_{3_-} m_3 - \kappa_{3_+}(m_{12} - m_1 m_2 + m_{22} - m_2^2 + 2m_{23} - 2m_2 m_3).
\end{aligned}
$$

3.2.2 CTLA-4 and CD28 competing for B7-2 model

The following scenario could occur when receptors CTLA-4 have been already recycled to the synapse and they are in a position of binding ligands. Thus, the competition with CD28 for binding to B7-2 is studied here. In order to analyse possible variations with the presence of B7-1, this second approach provides an indication about what would occur in its absence. For this purpose, we assume a constant ligand and receptors concentration; L_1, R_1 and R_2 respectively. It can be noticed, that this model is symmetric to model in Figure 3.2, so variations will be due to the name of the variables and the rates considered later on in Section 3.3.3 so only the main characteristics will be enunciated here. Again, considerations about the mobility on cells are ignored. Given that, three different complex $X_1'(t)$, $X_2'(t)$ and $X_3'(t)$ can be formed as follows:

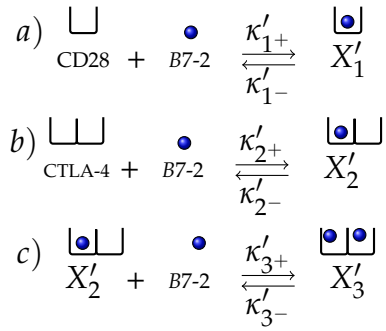

Figure 3.3: Diagram for a B7-2 binding CD28 and CTLA-4 dynamics model.

Similarly to the previous case, the increment vectors linked to *i*th reaction can be defined

$$\Delta W_1 = (1,0,0), \qquad \Delta W_4 = (0,-1,0),$$
$$\Delta W_2 = (-1,0,0), \qquad \Delta W_5 = (0,-1,1),$$
$$\Delta W_3 = (0,1,0), \qquad \Delta W_6 = (0,1,-1).$$

For which of them we can obtain the infinitesimal transition rates, respectively,

$$\begin{aligned}
q_{\Delta W_1}(n_1,n_2,n_3) &= \kappa'_{1_+}(R_1-n_1)(L_1-n_1-n_2-2n_3),\\
q_{\Delta W_2}(n_1,n_2,n_3) &= \kappa'_{1_-}n_1,\\
q_{\Delta W_3}(n_1,n_2,n_3) &= 2\kappa'_{2_+}(R_2-n_2-n_3)(L_1-n_1-n_2-2n_3),\\
q_{\Delta W_4}(n_1,n_2,n_3) &= \kappa'_{2_-}n_2,\\
q_{\Delta W_5}(n_1,n_2,n_3) &= \kappa'_{3_+}n_2(L_1-n_1-n_2-2n_3),\\
q_{\Delta W_6}(n_1,n_2,n_3) &= 2\kappa'_{3_-}n_3.
\end{aligned}$$

In this second model, the state space is $S = \{(n_1,n_2,n_3)\ ;\ n_1+n_2+2n_3 \leq L_1\ ,\ n_2+n_3 \leq R_2\ \}$ and the master equation is as follows:

$$\begin{aligned}
\frac{dp_{(n_1,n_2,n_3)}}{dt} &= \kappa'_{1_-}(n_1+1)p_{(n_1+1,n_2,n_3)} + \kappa'_{1_+}(R_1-n_1+1)(L_1-n_1+1-n_2-2n_3)p_{(n_1-1,n_2,n_3)}\\
&+ \kappa'_{2_-}(n_2+1)p_{(n_1,n_2+1,n_3} + 2\kappa'_{2_+}(R_2-n_2+1-n_3)(L_1-n_1-n_2+1-2n_3)p_{(n_1,n_2-1,n_3)}\\
&+ 2\kappa'_{3_-}(n_3+1)p_{(n_1,n_2-1,n_3+1)} + \kappa'_{3_+}(n_2+1)(L_1-n_1-n_2+1-2n_3)p_{(n_1,n_2+1,n_3-1)}\\
&- \Big((L_1-n_1-n_2-2n_3)[\kappa'_{1_+}(R_1-n_1)+2\kappa'_{2_+}(R_2-n_2-n_3)+\kappa'_{3_+}n_2] + \kappa'_{1_-}n_1+\kappa'_{2_-}n_2+2\kappa'_{3_-}n_3+1\Big)p_{(n_1,n_2,n_3)}.
\end{aligned}$$

Finally, the first order moment in this situation are given by the expressions

$$\begin{aligned}
\tfrac{dm_1}{dt} &= \kappa'_{1_+}L_1R_1 - (\kappa'_{1_+}L_1+\kappa'_{1_-})m_1 - \kappa'_{1_+}(R_1-m_1)(m_1+m_2+2m_3)\\
&\quad +\kappa'_{1_+}(m_{11}-m_1^2+m_{12}-m_1m_2+2m_{13}-2m_1m_3),\\
\tfrac{dm_2}{dt} &= 2\kappa'_{2_+}R_2L_1 - 2\kappa'_{2_+}(R_2-m_2-m_3)m_1 - [2\kappa'_{2_+}R_2-\kappa'_{3_+}m_1+(2\kappa'_{2_+}+\kappa'_{3_+})(L_1-m_2-3m_3)\\
&\quad +\kappa'_{2_-}+\kappa'_{3_+}m_3]m_2 - (2\kappa'_{2_+}(m_{12}+m_{13}-m_1m_2-m_1m_3)+\kappa'_{3_+}(m_{12}-m_1m_2)\\
&\quad +(2\kappa'_{2_+}+\kappa'_{3_+})(m_{22}-m_2^2)+(6\kappa'_{2_+}+2\kappa'_{3_+})(m_{23}-m_2m_3)+4\kappa'_{2_+}(m_{33}-m_3^2),\\
\tfrac{dm_3}{dt} &= (L_1-m_1-m_2-2m_3)\kappa'_{3_+}m_2 - 2\kappa'_{3_-}m_3 - \kappa'_{3_+}(m_{12}-m_1m_2+m_{22}-m_2^2+2m_{23}-2m_2m_3)
\end{aligned}.$$

Several simulations for the binding models are included in Section 3.2.3 and so the explanation regarding the parameters taken in Section 3.3.3.

3.2.3 Numerical results

Once the kinetic rates for CTLA-4 and ligands B7-1 and B7-2 are in hand in Section 3.3.3, and those involving CD28 in Section 3.4, the binding models described before can be numerically studied to have a better understanding of dynamics surface. Following these cited rates, which will be explained in Section 3.3.3, gathered for a better tracking in Table 3.1, Gillespie simulations were run for monitoring the main dynamics of these four molecules when *i)* CLTA-4 is missing and *ii)* there is an absence of B7-1.

Mature APC		**Activated T cell after**		**Kinetic rates**					
B7-1	**B7-2**	**CD28**	**CTLA-4**	$\kappa_{1+}, \kappa'_{1+}$	$\kappa_{1-}, \kappa'_{1-}$	κ_{2+}, κ_{3+}	κ_{2-}, κ_{3-}	$\kappa'_{2+}, \kappa'_{3+}$	$\kappa'_{2-}, \kappa'_{3-}$
20	431	256	110	$0.061s^{-1}$	$28s^{-1}$	$0.034s^{-1}$	$1.6s^{-1}$	$0.087s^{-1}$	$5.1s^{-1}$

Table 3.1: Total numbers L_1 and L_2 of ligands (B7-1 or B7-2) provided by a mature and receptors R_1 and R_2 (CD28 or CTLA-4) for an activated T cell and kinetic rates for models in Figures 3.2 and 3.3.

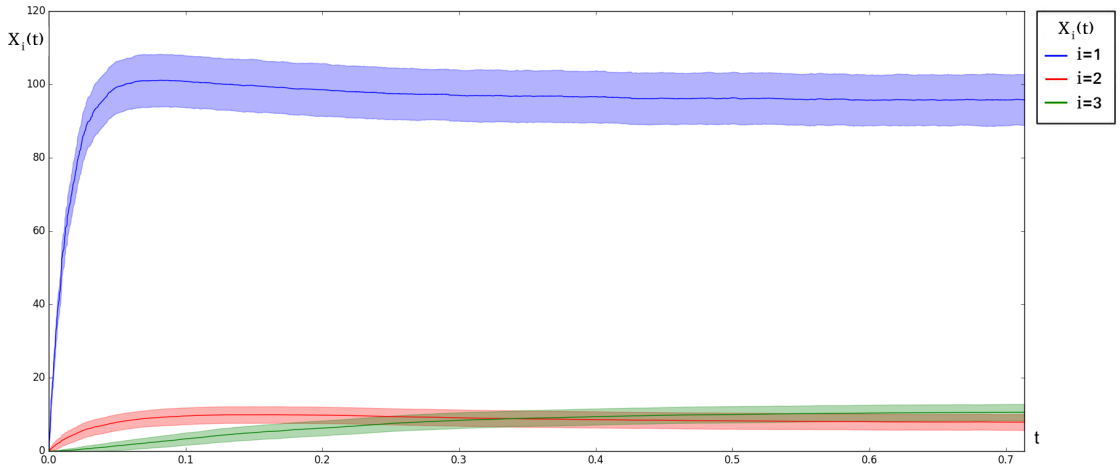

Figure 3.4: Gillespie simulations for model given in Figure 3.2 with rates taken from Table 3.1 regarding binding kinetics between CD28 with B7-1 and B7-2. X_1 correspond to bound CD28/B7-2 complexes, X_2 are CD28/B7-1 monomers and X_3, CD28/B7-1 dimers. Time in seconds.

Binding kinetics have a much faster performance than trafficking states. Whereas ligand internalisation occurs at the order of $\approx 4 \cdot 10^3 - 9 \cdot 10^4$ seconds (see Section 3.3.4) depending on the ligand and on the scenario, steady state for complex formation is reached in less than a second. This justifies a separate study of molecular interactions on the surface without necessarily considering internalisation or recycling. Figures 3.4 and 3.5 also show a similar qualitative behavior for complex formation in both models. This was forseen since, as mentioned before,

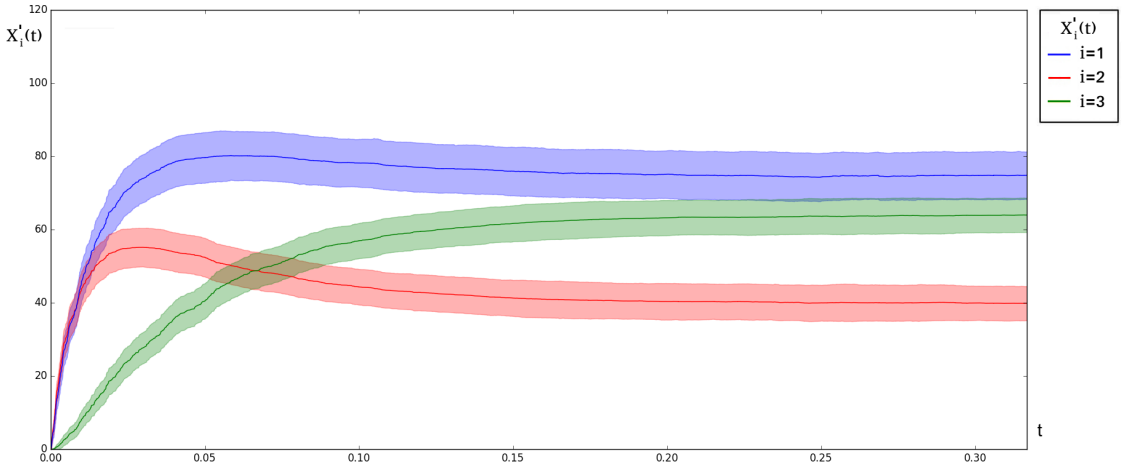

Figure 3.5: Gillespie simulations for model given in Figure 3.3 with rates taken from Table 3.1 regarding binding kinetics between B7-2 with CD28 and CTLA-4. X_1' correspond to bound CD28/B7-2 complexes, X_2' are CTLA-4/B7-2 monomers and X_3', CTLA-4/B7-2 dimers. Time in seconds.

both models are symmetric. monomers X_2 and X_2' have a quicker formation than dimers X_3 and X_3' but, after some time, the laters overtake the formers and so they remain ready for internalising.

3.3 CTLA-4 transendocytosis dynamics

3.3.1 Stochastic model

In this section we construct a stochastic model for the interaction dynamics of receptor R (CTLA-4) with ligand L (B7-1 or B7-2), represented in Figure 3.6. The system under study consists of a T cell containing a total number n_R of receptors which can interact with a total number n_L of ligands provided by a donor cell placed next to the T cell under consideration. Receptors in the system can be found into the endosome (species R_E), on the cell surface (species R_S, where we only consider receptors present on the synapse, which is where these interaction dynamics take place) or forming bound complexes with the ligand on the synapse (species B). Receptors on the synapse can be endocytosed with rate γ_R, becoming receptors into the endosome. On the other hand, internalised receptors can be recycled towards the synapse, which occurs with rate δ. Ligands on the synapse are internalised by means of their combination with free receptors, this binding occurring at rate α_+, forming bound complexes B which eventually become internalised with rate γ_B. Finally, bound complexes B on the synapse can also be dissociated with rate α_-, and

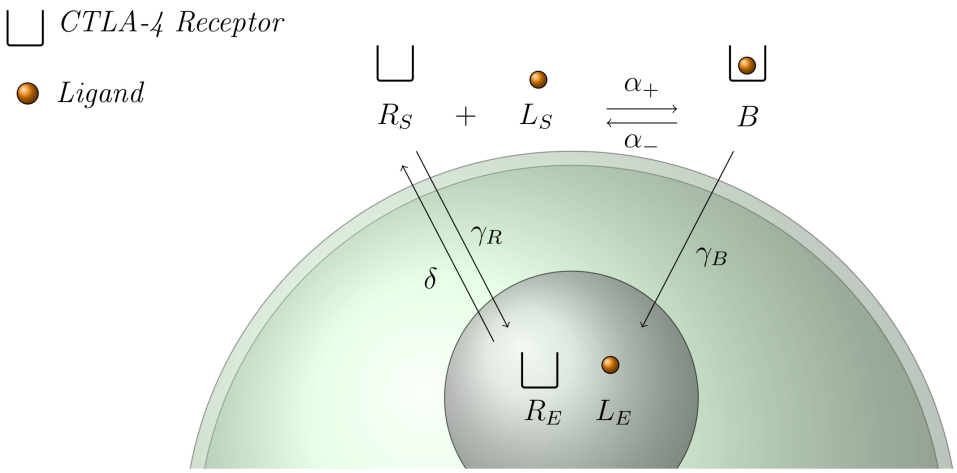

Figure 3.6: Diagram of the stochastic model for the interaction between a receptor and a ligand on the synapse between a T cell and an APC.

this dissociation is assumed to occur instantaneously once the bound complex is internalised, representing an acidic endosomal environment [64]; see Figure 3.6. In order to study this process from the stochastic point of view, we consider the random variables

$$\begin{aligned}
R_E(t) &= \text{“Number of free receptors in the endosome at time } t\text{”},\\
B(t) &= \text{“Number of bound } R+L \text{ complexes on the synapse at time } t\text{”},\\
L_E(t) &= \text{“Number of ligands in the endosome at time } t\text{”},\\
L_S(t) &= \text{“Number of ligands on the synapse at time } t\text{”},\\
R_S(t) &= \text{“Number of free receptors on the synapse at time } t\text{”},
\end{aligned}$$

for $t \geq 0$, with initial conditions

$$\begin{aligned}
B(0) = L_E(0) &= 0,\\
L_S(0) &= n_L,\\
R_E(0) + R_S(0) &= n_R.
\end{aligned}$$

That is, zero ligands are considered to be initially internalised, representing the beginning of the T cell/APC interaction. On the other hand, the number of receptors initially on the synapse and

in the endosome can vary between different situations. It is clear then that

$$\begin{aligned} n_L &= L_S(0) = L_S(t) + L_E(t) + B(t), \\ n_R &= R_S(0) + R_E(0) = R_S(t) + R_E(t) + B(t), \end{aligned}$$

for all $t \geq 0$, which yields

$$\begin{aligned} L_S(t) &= n_L - L_E(t) - B(t), \\ R_S(t) &= n_R - R_E(t) - B(t), \end{aligned} \tag{3.2}$$

for all $t \geq 0$.

We consider a continuous-time Markov chain (CTMC) $\mathcal{X} = \{\mathbf{X}(t) = (R_E(t), B(t), L_E(t)) : t \geq 0\}$ modelling our process. From Equation (3.2) it is clear that $\mathcal{X}$ is defined over the state space $\mathcal{S} = \{(n_1, n_2, n_3) \in (\mathbb{N} \cup \{0\})^3 : n_1 + n_2 \leq n_R, n_2 + n_3 \leq n_L\}$. From a straightforward analysis of the geometric shape of $\mathcal{S}$, it is observable that there are two distinguishable cases for the nature of $\mathcal{S}$ depending on the relation between n_R and n_L. We assume from now on that $n_L \leq n_R$, which drives us to consider only ligand B7-1 for carrying out this analysis; see CTLA-4, B7-1 and B7-2 copy numbers in Section 3.3.3. However, we note here that all the arguments developed in this paper can be easily adapted to the case $n_L > n_R$ and therefore this approach would be valid for B7-2 ligand.

When describing the transitions between states in $\mathcal{X}$, we note that, from one state (n_1, n_2, n_3) in the interior of $\mathcal{S}$, there are five possible transitions towards adjacent states, from a direct analysis of Figure 3.6. These transitions represent formation and dissociation of bound complexes on the synapse, internalisation of these, as well as internalisation and recycling of free receptors between the synapse and the endosome. A transition from a state $\mathbf{n} = (n_1, n_2, n_3)$ to a state $\mathbf{n}' = (n_1', n_2', n_3')$ is governed by the infinitesimal transition rate

$$q_{\mathbf{n},\mathbf{n}'} = \begin{cases} (n_R - n_1 - n_2)\gamma_R, & \text{if } (n_1', n_2', n_3') = (n_1 + 1, n_2, n_3), \\ n_1\delta, & \text{if } (n_1', n_2', n_3') = (n_1 - 1, n_2, n_3), \\ (n_R - n_1 - n_2)(n_L - n_2 - n_3)\alpha_+, & \text{if } (n_1', n_2', n_3') = (n_1, n_2 + 1, n_3), \\ n_2\alpha_-, & \text{if } (n_1', n_2', n_3') = (n_1, n_2 - 1, n_3), \\ n_2\gamma_B, & \text{if } (n_1', n_2', n_3') = (n_1 + 1, n_2 - 1, n_3 + 1), \end{cases} \tag{3.3}$$

summarised in Figure 3.7. For states in the boundary of $\mathcal{S}$, those transitions inwards $\mathcal{S}$ are

considered in the same way than in Equation (3.3), discarding any transition outwards $\mathcal{S}$. Transition rates in Equation (3.3) are directly obtained by mass-action kinetics from the reactions considered in the process and by pointing out that, if $(R_E(t), B(t), L_E(t)) = (n_1, n_2, n_3)$ at a certain epoch $t \geq 0$, the number of free receptors and free ligands on the synapse at that instant is $n_R - n_1 - n_2$ and $n_L - n_2 - n_3$, respectively. For example, process $\mathcal{X}$ can move from state (n_1, n_2, n_3) to state $(n_1 + 1, n_2, n_3)$ if a CTLA-4 receptor molecule becomes internalised from the synapse into the endosome, a transition that occurs with infinitesimal transition rate $q_{(n_1,n_2,n_3),(n_1+1,n_2,n_3)} = \gamma_R(n_R - n_1 - n_2)$, since any of the $n_R - n_1 - n_2$ available free receptors on the synapse internalises with rate γ_R according to Figure 3.6.

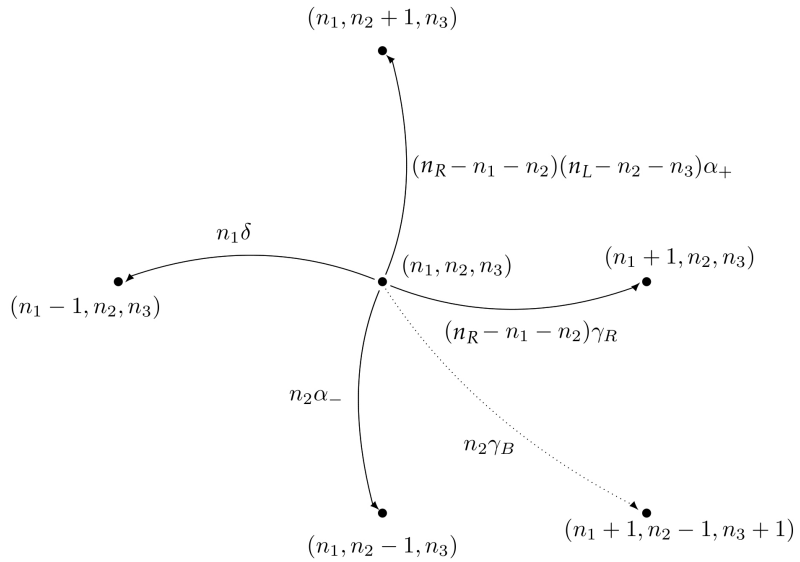

Figure 3.7: Transitions diagram for process $\mathcal{X}$.

The dynamics of the process $\mathcal{X}$ can be analysed in terms of its master equation given by

$$\frac{d\mathbb{P}_{\mathbf{n}}(t)}{dt} = \sum_{\mathbf{n}' \in S, \mathbf{n}' \neq \mathbf{n}} q_{\mathbf{n}',\mathbf{n}}\, \mathbb{P}_{\mathbf{n}'}(t) - \sum_{\mathbf{n}' \in S, \mathbf{n}' \neq \mathbf{n}} q_{\mathbf{n},\mathbf{n}'}\, \mathbb{P}_{\mathbf{n}}(t)\,, \quad \forall \mathbf{n} \in \mathcal{S},$$

with $\mathbf{n} = (n_1, n_2, n_3)$ representing a particular state of the process, and $\mathbb{P}_{\mathbf{n}}(t) = \mathbb{P}(\mathbf{X}(t) = \mathbf{n})$. Since it is rarely possible to analitically solve a master equation of this type, different approximative techniques such as the Van Kampen approach [75] or Gillespie simulations are often implemented in the literature instead. However, given particular characteristics of

our process $\mathcal{X}$, analytic approaches can be followed in order to exactly compute a number of quantities of interest regarding this process. In particular, we analyse in Section 3.3.2 a number of summary statistics, here referred to as stochastic descriptors, by means of first-step arguments, the usage of auxiliary absorbing Markov chains and Laplace-Stieltjes transforms, and the implementation of a matrix-analytic approach.

3.3.2 Stochastic descriptors

The interest in this section is in a number of characteristics of interest in our process related to the internalisation (ligand depletion) timescales, and the rate of receptor-ligand bound complex formation on the synapse. This is because the time to reach a given threshold number of ligands internalised may be identified with the initiation of different signalling cascades [2, 69]. However, this time may not only depend on the ligand concentration provided by the donor cell (that is, the amount of ligand on the synapse), but also on the particular binding affinity of the ligand considered, the spatial distribution of receptors (surface/endosome) within the T cell when this co-stimulatory process takes place, or the presence of other molecular competitors (*e.g.*, co-receptor CD28) on the synapse at the same time. These factors will be considered in our numerical experiments in Sections 3.3.4 and 3.3.5.

Secondly, it is also of interest to analyse the rate at which receptor-ligand complexes are formed on the cell surface, and how these binding events occur while internalisation is taking place. This is because the initiation of a cellular reponse may not only depend on the individual signal provided by every bound complex on the synapse during time, but on this signal being produced by complexes simultaneously present at any given time. In particular, the internalisation of ligand may occur after a considerably accumulation of bound complexes on the synapse occurs, so that at some given time in our process one may find many bound complexes simultaneously present on the synapse, or alternatively internalisation of bound complexes could occur in a more sequential manner, having only few bound complexes simultaneously present on the synapse at any given time.

Finally, we also analyse the steady-state spatial configuration of CTLA-4 receptors in our system without ligand stimulation, since it allows us to inform our models from experimental knowledge. In particular, we can link the steady-state spatial configuration of CTLA-4 receptors without ligand stimulation with the internalisation and recycling rates of this receptor, and then make use of well-known quantitative experimental information in order to approximate

these rates. Lastly, it is of interest to analyse what is the role played by each parameter $\theta \in \{\alpha_+, \alpha_-, \gamma_R, \gamma_B, \delta\}$ in process $\mathcal{X}$, regarding the behavior of the characteristics mentioned above. This can be done by means of a local sensitivity analysis for the parameters, which is carried out in Section 3.3.2.5 by extending and adapting arguments in [14]. In particular, an adaptation of arguments in [14] recently carried out in [25] for developing local sensitivity analysis in structured Markov chains, allows one to identify the most crucial parameters for each particular stochastic descriptor under study, in a neighbourhood of a particular selection $(\alpha_+, \alpha_-, \gamma_R, \gamma_B, \delta)$.

3.3.2.1 Matrix-analytic approach

The analysis of the stochastic descriptors is carried out here by means of the matrix-analytic approach [35], which mainly consists of thinking on the Markov chain under consideration as a stochastic process evolving over groups or levels of states inside $\mathcal{S}$, instead of over particular states $(n_1, n_2, n_3) \in \mathcal{S}$. This leads to the analysis of systems of linear equations by following a matrix formalism, where matrices involved in these systems can be structured by blocks. The structure by blocks of these matrices is crucial when developing efficient algorithms in order to obtain the different order moments and distributions of the random variables under analysis. Then, a strong focus on algorithmic issues is made all over this Section, and all the algorithmic procedures constructed are provided in Section 3.3.2.6.

First, we propose to organise the space of states $\mathcal{S}$ of $\mathcal{X}$ by levels and sub-levels. Specifically,

$$\mathcal{S} \;=\; \bigcup_{k=0}^{n_L} L(k), \text{ with } L(k) \;=\; \bigcup_{r=0}^{n_L-k} l(k;r),$$

where the level $L(k)$ is formed by all the states in $\mathcal{S}$ with a total number of ligands into the endosome equal to k, that is, $L(k) = \{(n_1, n_2, n_3) \in \mathcal{S} : n_3 = k\}$. Moreover, each level $L(k)$ is divided into sub-levels so that each sub-level $l(k;r)$ contains those states with a total number of ligands into the endosome equal to k and a total number of bound complexes on the cell surface equal to r, that is, $l(k;r) = \{(n_1, n_2, n_3) \in \mathcal{S} : n_2 = r, n_3 = k\} = \{(0, r, k), (1, r, k), \ldots, (n_R - r, r, k)\}$. Then, $\#l(k;r) = n_R - r + 1$ and straightforward algebra yields $J(k) = \#L(k) = \sum_{r=0}^{n_L-k} \#l(k;r) = \frac{(n_L-k+1)(2n_R-n_L+k+2)}{2}$. It is obvious that the state space's cardinality is $\#\mathcal{S} = \sum_{k=0}^{n_L} \#L(k)$.

An analysis of possible transitions in Figure 3.7 indicates that transitions from one sub-level $l(k;r)$ only occur towards adjacent sub-levels $l(k';r')$ with $(k', r') \in \{(k, r-1), (k, r), (k, r+1), (k+1, r-$

$1)\}$. This yields the following infinitesimal generator $\mathbf{Q}$ for the CTMC $\mathcal{X}$ structured by blocks,

$$\mathbf{Q} = \begin{pmatrix} \mathbf{A}_{0,0} & \mathbf{A}_{0,1} & \mathbf{0}_{J(0)\times J(2)} & \cdots & \mathbf{0}_{J(0)\times J(n_L-1)} & \mathbf{0}_{J(0)\times J(n_L)} \\ \mathbf{0}_{J(1)\times J(0)} & \mathbf{A}_{1,1} & \mathbf{A}_{1,2} & \cdots & \mathbf{0}_{J(1)\times J(n_L-1)} & \mathbf{0}_{J(1)\times J(n_L)} \\ \mathbf{0}_{J(2)\times J(0)} & \mathbf{0}_{J(2)\times J(1)} & \mathbf{A}_{2,2} & \cdots & \mathbf{0}_{J(2)\times J(n_L-1)} & \mathbf{0}_{J(2)\times J(n_L)} \\ \vdots & \vdots & \vdots & \ddots & \vdots & \vdots \\ \mathbf{0}_{J(n_L-1)\times J(0)} & \mathbf{0}_{J(n_L-1)\times J(1)} & \mathbf{0}_{J(n_L-1)\times J(2)} & \cdots & \mathbf{A}_{n_L-1,n_L-1} & \mathbf{A}_{n_L-1,n_L} \\ \mathbf{0}_{J(n_L)\times J(0)} & \mathbf{0}_{J(n_L)\times J(1)} & \mathbf{0}_{J(n_L)\times J(2)} & \cdots & \mathbf{0}_{J(n_L)\times J(n_L-1)} & \mathbf{A}_{n_L,n_L} \end{pmatrix},$$

where the matrix $\mathbf{A}_{k,k'}$ contains the transition rates corresponding to transitions from states of $L(k)$ to states of $L(k')$, $k' \in \{k, k+1\}$. Due to transitions between sub-levels we have that

$$\mathbf{A}_{k,k} = \begin{pmatrix} \mathbf{B}_{0,0}^{k,k} & \mathbf{B}_{0,1}^{k,k} & \mathbf{0} & \cdots & \mathbf{0} & \mathbf{0} \\ \mathbf{B}_{1,0}^{k,k} & \mathbf{B}_{1,1}^{k,k} & \mathbf{B}_{1,2}^{k,k} & \cdots & \mathbf{0} & \mathbf{0} \\ \mathbf{0} & \mathbf{B}_{2,1}^{k,k} & \mathbf{B}_{2,2}^{k,k} & \cdots & \mathbf{0} & \mathbf{0} \\ \vdots & \vdots & \vdots & \ddots & \vdots & \vdots \\ \mathbf{0} & \mathbf{0} & \mathbf{0} & \cdots & \mathbf{B}_{n_L-k-1,n_L-k-1}^{k,k} & \mathbf{B}_{n_L-k-1,n_L-k}^{k,k} \\ \mathbf{0} & \mathbf{0} & \mathbf{0} & \cdots & \mathbf{B}_{n_L-k,n_L-k-1}^{k,k} & \mathbf{B}_{n_L-k,n_L-k}^{k,k} \end{pmatrix}, \quad 0 \le k \le n_L, \tag{3.4}$$

$$\mathbf{A}_{k,k+1} = \begin{pmatrix} \mathbf{0} & \mathbf{0} & \mathbf{0} & \cdots & \mathbf{0} & \mathbf{0} \\ \mathbf{B}_{1,0}^{k,k+1} & \mathbf{0} & \mathbf{0} & \cdots & \mathbf{0} & \mathbf{0} \\ \mathbf{0} & \mathbf{B}_{2,1}^{k,k+1} & \mathbf{0} & \cdots & \mathbf{0} & \mathbf{0} \\ \vdots & \vdots & \vdots & \ddots & \vdots & \vdots \\ \mathbf{0} & \mathbf{0} & \mathbf{0} & \cdots & \mathbf{0} & \mathbf{0} \\ \mathbf{0} & \mathbf{0} & \mathbf{0} & \cdots & \mathbf{B}_{n_L-k,n_L-k-1}^{k,k+1} & \mathbf{0} \end{pmatrix}, \quad 0 \le k \le n_L - 1.$$

Dimensions of blocks $\mathbf{0}$ are omitted in the previous expressions, but a block $\mathbf{0}$ representing transitions from states in $l(k;r)$ towards states in $l(k';r')$ has dimensions $(n_R - r + 1) \times (n_R - r' + 1)$. Expressions for matrices $\mathbf{B}_{r,r'}^{k,k'}$ in Equation (3.4) are as follows:

- For $0 \leq r \leq n_L - k$, $0 \leq k \leq n_L$,

$$\left(\mathbf{B}^{k,k}_{r,r}\right)_{ij} = \begin{cases} i\delta, & \text{if } j = i-1, \\ -A_{(i,r,k)}, & \text{if } j = i, \\ (n_R - i - r)\gamma_R, & \text{if } j = i+1, \\ 0, & \text{otherwise,} \end{cases}$$

  where $A_{(i,r,k)} = (n_R - i - r)\gamma_R + i\delta + (n_R - i - r)(n_L - r - k)\alpha_+ + r\alpha_- + r\gamma_B$ and where $0 \leq i \leq n_R - r$, $0 \leq j \leq n_R - r$.

- For $0 \leq r \leq n_L - k - 1$, $0 \leq k \leq n_L$,

$$\left(\mathbf{B}^{k,k}_{r,r+1}\right)_{ij} = \begin{cases} (n_R - r - i)(n_L - r - k)\alpha_+, & \text{if } j = i, \\ 0, & \text{otherwise,} \end{cases}$$

  where $0 \leq i \leq n_R - r$, $0 \leq j \leq n_R - r - 1$.

- For $1 \leq r \leq n_L - k$, $0 \leq k \leq n_L$,

$$\left(\mathbf{B}^{k,k}_{r,r-1}\right)_{ij} = \begin{cases} r\alpha_-, & \text{if } j = i, \\ 0, & \text{otherwise,} \end{cases}$$

  where $0 \leq i \leq n_R - r$, $0 \leq j \leq n_R - r + 1$.

- For $1 \leq r \leq n_L - k$, $0 \leq k \leq n_L - 1$,

$$\left(\mathbf{B}^{k,k+1}_{r,r-1}\right)_{ij} = \begin{cases} r\gamma_B, & \text{if } j = i+1, \\ 0, & \text{otherwise,} \end{cases}$$

  where $0 \leq i \leq n_R - r$, $0 \leq j \leq n_R - r + 1$.

3.3.2.2 Steady-state spatial CTLA-4 configuration

Because the amount of ligands n_L in our model is constant and, once internalised, ligands can not be recycled to the synapse, the system in the long-term (in particular, once $L_E(t) = n_L$) only describes the trafficking of CTLA-4 between the endosome and the synapse. That is, once $L_E(T) = n_L$ at some time T, the dynamics of $\mathcal{X}$ are reduced to the process $\hat{\mathcal{X}} = \{R_E(t) : t \geq T\}$, since

given a total number n_R of CTLA-4 receptors in the system it is clear that $R_S(t) = n_R - R_E(t)$ for any $t \geq T$. This leads to the birth-and-death process $\hat{\mathcal{X}}$ defined over $\hat{\mathcal{S}} = \{0, 1, \ldots, n_R\}$ and represented in Figure 3.8, and the long-term dynamics of this process can be analysed in terms of its stationary distribution, which does not depend on the initial state of this process.

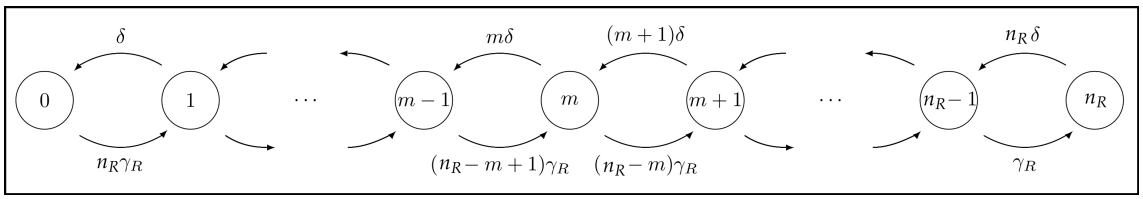

Figure 3.8: Transitions diagram of process $\hat{\mathcal{X}}$.

The infinitesimal generator $\hat{\mathbf{Q}}$ of $\hat{\mathcal{X}}$ is given by

$$\begin{pmatrix} -n_R\gamma_R & n_R\gamma_R & 0 & \ldots & 0 \\ \delta & -(\delta + (n_R - 1)\gamma_R) & (n_R - 1)\gamma_R & \ldots & 0 \\ 0 & 2\delta & -(2\delta + (n_R - 2)\gamma_R) & \ldots & 0 \\ \vdots & \vdots & \vdots & \ddots & \vdots \\ 0 & 0 & 0 & \ldots & \gamma_R \\ 0 & 0 & 0 & \ldots & -n_R\delta \end{pmatrix},$$

and the stationary distribution $\hat{\boldsymbol{\pi}} = (\hat{\pi}_m : 0 \leq m \leq n_R)$ of $\hat{\mathcal{X}}$ can be easily obtained as the solution of

$$\begin{aligned} \hat{\boldsymbol{\pi}}\hat{\mathbf{Q}} &= \mathbf{0}_{n_R+1}, \\ \hat{\boldsymbol{\pi}}\mathbf{e}_{n_R+1} &= 1, \end{aligned}$$

where $\mathbf{0}_a$ represents a column vector of zeros with dimension a and $\mathbf{e}_b$ represents a column vector of ones with dimension b. Finally, straightforward algebra yields

$$\hat{\pi}_m = \lim_{t \to +\infty} \mathbb{P}(R_E(t) = m) = \binom{n_R}{m} \left(\frac{\gamma_R}{\delta + \gamma_R}\right)^m \left(\frac{\delta}{\delta + \gamma_R}\right)^{n_R - m}, \quad 0 \leq m \leq n_R.$$

Obviously, we can obtain different features regarding the state of the process $\mathcal{X}$ in the long-term from $\hat{\boldsymbol{\pi}}$. Of particular interest is the mean number of receptors into the endosome of the T cell in

the long-term, which is given by

$$\hat{m} \;=\; \sum_{m=0}^{n_R} m\hat{\pi}_m \;=\; \frac{n_R\gamma_R}{\delta+\gamma_R}. \tag{3.5}$$

3.3.2.3 Time to reach a threshold number I of internalisations of ligands

In this Section, our aim is to study the time to reach a total threshold number I of ligands internalised during the process. This characteristic in the process, given an initial state $(n_1, n_2, n_3) \in \mathcal{S}$, can be analysed in terms of the continuous random variable

$$\begin{aligned} T^I_{(n_1,n_2,n_3)} \;=\; & \text{“}\textit{Time to reach a threshold number } I \textit{ of internalised ligands in the process} \\ & \mathcal{X}\textit{, given the current state } (n_1,n_2,n_3)\text{”} \;=\; \inf\{t \geqslant 0 : L_E(t) = I\}; \end{aligned}$$

that is, the first time to have $L_E(t) = I$ given the initial state $(n_1, n_2, n_3) \in \mathcal{S}$. We point out here that, given an initial value n_3, we consider only the relevant case $n_3 \leq I \leq n_L$.

In order to analyse this random variable, we split the state space as

$$\mathcal{S} \;=\; \mathcal{C} \cup \hat{\mathcal{C}},$$

with $\mathcal{C} = \{(n_1, n_2, n_3) \in \mathcal{S} : \; n_3 \leq I-1\}$ and $\hat{\mathcal{C}} = \{(n_1, n_2, n_3) \in \mathcal{S} : \; n_3 \geq I\}$. Then, given an initial state $(n_1, n_2, n_3) \in \mathcal{C}$, the time $T^I_{(n_1,n_2,n_3)}$ to have a threshold number I of internalised ligands is the time until the process $\mathcal{X}$ reaches the sub-set $\hat{\mathcal{C}}$. In order to analyse this time, we construct an auxiliary process $\mathcal{X}(I)$ defined over the truncated state space

$$\mathcal{S}(I) \;=\; \mathcal{C} \cup \{\bar{I}\},$$

where $\bar{I}$ is a macro-state constructed by lumping all the states within $\hat{\mathcal{C}}$. We maintain all the transitions between states in $\mathcal{C}$, and transitions from states in $\mathcal{C}$ towards the macro-state $\bar{I}$ are obtained by lumping transitions from $\mathcal{C}$ towards $\hat{\mathcal{C}}$ in the original process. Moreover, we consider $\bar{I}$ as an absorbing macro-state, so that when the auxiliary process $\mathcal{X}(I)$ enters into $\bar{I}$, the process ends. From the construction of $\mathcal{X}(I)$, it is clear that the time to reach the absorbing state $\bar{I}$ in the auxiliary process is exactly the time $T^I_{(n_1,n_2,n_3)}$ to reach a threshold number I of ligands internalised in the original process $\mathcal{X}$. Thus, this time can now be studied as the time until absorption in a CTMC with a finite irreducible class $\mathcal{C}$ of transient states, and one absorbing state $\bar{I}$, so that

$T^I_{(n_1,n_2,n_3)}$ follows a continuous phase-type distribution; see [34, Section 6.13].

It is advisable here to work with the Laplace-Stieltjes transform of $T^I_{(n_1,n_2,n_3)}$ so that any order moment of the random variable under study can be obtained in an efficient manner. The definition of the Laplace-Stieltjes transform allows us to work in an algorithmic way, which is strongly recommendable when the size of the state space can become a challenge from the computational point of view, as it occurs here. Moreover, we point out that, although it is beyond the objectives of this Section, the probability distribution of $T^I_{(n_1,n_2,n_3)}$ is unequivocally determined by its Laplace-Stieltjes transform, and that it is possible to approximate this distribution by means of the numerical inversion of the transform; see [24] where this procedure was applied regarding a random variable representing the survival time of an individual in a competition process, and [1] for a presentation and comparison of several numerical inversion techniques.

We define then the Laplace-Stieltjes transform of $T^I_{(n_1,n_2,n_3)}$ as

$$\phi^I_{(n_1,n_2,n_3)}(z) = E\left[e^{-zT^I_{(n_1,n_2,n_3)}}\right], \quad Re(z) \geq 0,$$

and, once this transform is in hand, the different l-th order moments $\tau^{I,(l)}_{(n_1,n_2,n_3)} = E\left[\left(T^I_{(n_1,n_2,n_3)}\right)^l\right]$ can be obtained by successive differentiation as

$$\tau^{I,(l)}_{(n_1,n_2,n_3)} = (-1)^l \frac{d^l}{dz^l}\phi^I_{(n_1,n_2,n_3)}(z)\Big|_{z=0}, \quad l \geq 1.$$

In order to obtain the Laplace-Stieltjes transform for the initial state $(n_1, n_2, n_3) \in \mathcal{C}$, we can apply a first-step argument so that a system of equations is obtained relating the transforms for the different possible initial states in $\mathcal{C}$. Specifically,

$$\begin{aligned}
\phi^I_{(n_1,n_2,n_3)}(z) = {} & \frac{(n_R - n_1 - n_2)\gamma_R}{A_{(n_1,n_2,n_3)} + z}(1 - \delta_{n_1,n_R-n_2})\phi^I_{(n_1+1,n_2,n_3)}(z) + \frac{n_1\delta}{A_{(n_1,n_2,n_3)} + z} \\
& \times (1 - \delta_{n_1,0})\phi^I_{(n_1-1,n_2,n_3)}(z) + \frac{(n_R - n_1 - n_2)(n_L - n_2 - n_3)\alpha_+}{A_{(n_1,n_2,n_3)} + z} \\
& \times (1 - \delta_{n_2,n_L-n_3})(1 - \delta_{n_2,n_R-n_1})\phi^I_{(n_1,n_2+1,n_3)}(z) + \frac{n_2\alpha_-}{A_{(n_1,n_2,n_3)} + z} \\
& \times (1 - \delta_{n_2,0})\phi^I_{(n_1,n_2-1,n_3)}(z) + \frac{n_2\gamma_B}{A_{(n_1,n_2,n_3)} + z}\left((1 - \delta_{n_2,0})\right. \\
& \left. \times (1 - \delta_{n_3,I-1})\phi^I_{(n_1+1,n_2-1,n_3+1)}(z) + \delta_{n_3,I-1}\right),
\end{aligned} \tag{3.6}$$

for any $(n_1, n_2, n_3) \in \mathcal{C}$, where $A_{(i,r,k)} = (n_R - i - r)\gamma_R + i\delta + (n_R - i - r)(n_L - r - k)\alpha_+ + r\alpha_- + r\gamma_B$ and $\delta_{i,j}$ represents Kronecker's delta (which equals 1 if and only if $i = j$, and 0 otherwise). We present later a matrix formalism which allows us to work in an algorithmic manner when solving Equation (3.6), yielding Algorithm 2 (Part 1) provided in Section 3.3.2.6 for computing the Laplace-Stieltjes transforms $\phi^I_{(n_1,n_2,n_3)}(z)$.

Once transforms $\phi^I_{(n_1,n_2,n_3)}(z)$ are in hand, the l-th order moments of $T^I_{(n_1,n_2,n_3)}$ can be obtained by successive differentiation of Equation (3.6),

$$\begin{aligned} A_{(n_1,n_2,n_3)}\tau^{I,(l)}_{(n_1,n_2,n_3)} &= l\tau^{I,(l-1)}_{(n_1,n_2,n_3)} + (n_R - n_1 - n_2)\gamma_R(1 - \delta_{n_1,n_R-n_2})\tau^{I,(l)}_{(n_1+1,n_2,n_3)} \\ &+ n_1\delta(1 - \delta_{n_1,0})\tau^{I,(l)}_{(n_1-1,n_2,n_3)} + (n_R - n_1 - n_2)(n_L - n_2 - n_3) \\ &\times\alpha_+(1 - \delta_{n_2,n_L-n_3})(1 - \delta_{n_2,n_R-n_1})\tau^{I,(l)}_{(n_1,n_2+1,n_3)} + n_2\alpha_- \\ &\times(1 - \delta_{n_2,0})\tau^{I,(l)}_{(n_1,n_2-1,n_3)} + n_2\gamma_B(1 - \delta_{n_2,0})(1 - \delta_{n_3,I-1}) \\ &\times\tau^{I,(l)}_{(n_1+1,n_2-1,n_3+1)}, \end{aligned} \tag{3.7}$$

and where Equation (3.7) is algorithmically solved in Section 3.3.2.6. A by following the same matrix formalism than the one followed for solving Equation (3.6), so that Algorithm 2 (Part 2) is built and provided in Section 3.3.2.6.

The state space $\mathcal{S}(I)$ of $\mathcal{X}(I)$ inherits the structure by levels from $\mathcal{S}$,

$$\mathcal{S}(I) = \mathcal{C} \cup \{\bar{I}\} = \bigcup_{k=0}^{I-1} L(k) \cup \{\bar{I}\},$$

so that Equation (3.6) can be written in matrix form as

$$\mathbf{g}^{(I)}(z) = \mathbf{A}^{(I)}(z)\mathbf{g}^{(I)}(z) + \mathbf{a}^{(I)}(z). \tag{3.8}$$

It is obvious that the size of the previous system and, thus, the dimensions of the matrix $\mathbf{A}^{(I)}(z)$ and the column vectors $\mathbf{g}^{(I)}(z)$ and $\mathbf{a}^{(I)}(z)$ depend on the value I. However, we omit for simplicity the superscript I in the notation from now on. The column vector $\mathbf{g}(z)$ contains the Laplace-Stieltjes transforms $\phi^I_{(n_1,n_2,n_3)}(z)$ for states (n_1, n_2, n_3) in $\mathcal{S}(I)$ in an ordered manner, and the matrix $\mathbf{A}(z)$ and the column vector $\mathbf{a}(z)$ are straightforwardly obtained from Equation (3.6). Specifically, for $Re(z) \geq 0$, $\mathbf{g}(z) = \left(\mathbf{g}_0(z)^T, \mathbf{g}_1(z)^T, \ldots, \mathbf{g}_{I-2}(z)^T, \mathbf{g}_{I-1}(z)^T\right)^T$, where $\mathbf{g}_k(z) = \Big(\mathbf{g}^k_0(z)^T, \mathbf{g}^k_1(z)^T, \ldots, \mathbf{g}^k_{n_L-k-1}(z)^T, \mathbf{g}^k_{n_L-k}(z)^T\Big)^T$ for $0 \leq k \leq I-1$. Finally, $\mathbf{g}^k_r(z) = (\phi^I_{(0,r,k)}(z), \phi^I_{(1,r,k)}(z),$

$\ldots, \phi^I_{(n_R-r-1,r,k)}(z), \phi^I_{(n_R-r,r,k)}(z))^T$, for $0 \leq r \leq n_L - k$, $0 \leq k \leq I-1$.

We point out that, with the proposed structure, the column vector $\mathbf{g}_k(z)$ contains the Laplace-Stieltjes transforms corresponding to initial states in the level $L(k)$, and the column sub-vector $\mathbf{g}^k_r(z)$ contains the Laplace-Stieltjes transforms corresponding to initial states in the sub-level $l(k;r) \subset L(k)$. From Equation (3.6), it is clear that

$$\mathbf{A}(z) = \begin{pmatrix} \mathbf{A}_{0,0}(z) & \mathbf{A}_{0,1}(z) & \mathbf{0}_{J(0)\times J(2)} & \cdots & \mathbf{0}_{J(0)\times J(I-2)} & \mathbf{0}_{J(0)\times J(I-1)} \\ \mathbf{0}_{J(1)\times J(0)} & \mathbf{A}_{1,1}(z) & \mathbf{A}_{1,2}(z) & \cdots & \mathbf{0}_{J(1)\times J(I-2)} & \mathbf{0}_{J(1)\times J(I-1)} \\ \mathbf{0}_{J(2)\times J(0)} & \mathbf{0}_{J(2)\times J(1)} & \mathbf{A}_{2,2}(z) & \cdots & \mathbf{0}_{J(2)\times J(I-2)} & \mathbf{0}_{J(2)\times J(I-1)} \\ \vdots & \vdots & \vdots & \ddots & \vdots & \vdots \\ \mathbf{0}_{J(I-2)\times J(0)} & \mathbf{0}_{J(I-2)\times J(1)} & \mathbf{0}_{J(I-2)\times J(2)} & \cdots & \mathbf{A}_{I-2,I-2}(z) & \mathbf{A}_{I-2,I-1}(z) \\ \mathbf{0}_{J(I-1)\times J(0)} & \mathbf{0}_{J(I-1)\times J(1)} & \mathbf{0}_{J(I-1)\times J(2)} & \cdots & \mathbf{0}_{J(I-1)\times J(I-2)} & \mathbf{A}_{I-1,I-1}(z) \end{pmatrix},$$

where matrices $\mathbf{A}_{k,k'}(z)$ have the same structure than matrices $\mathbf{A}_{k,k'}$ in the infinitesimal generator $\mathbf{Q}$, but with sub-matrices $\mathbf{B}^{k,k'}_{r,r'}$ replaced by sub-matrices $\mathbf{B}^{k,k'}_{r,r'}(z)$, where the latter are obtained from the former as

$$\left(\mathbf{B}^{k,k'}_{r,r'}(z)\right)_{ij} = \begin{cases} 0, & \text{if } k'=k,\ r'=r \text{ and } i=j, \\ \frac{1}{A_{(i,r,k)}+z}\left(\mathbf{B}^{k,k'}_{r,r'}\right)_{ij}, & \text{otherwise.} \end{cases}$$

Finally, $\mathbf{a}(z) = \left(\mathbf{0}^T_{J(0)}, \mathbf{0}^T_{J(1)}, \ldots, \mathbf{0}^T_{J(I-2)}, \mathbf{a}_{I-1}(z)^T\right)^T$, with $\mathbf{a}_{I-1}(z) = \left(\mathbf{0}^T_{n_R+1}, \mathbf{a}^{I-1}_1(z)^T, \ldots, \mathbf{a}^{I-1}_{n_L-I}(z)^T, \mathbf{a}^{I-1}_{n_L-I+1}(z)^T\right)^T$, where $\mathbf{a}^{I-1}_r(z) = r\gamma_B\left(\frac{1}{z+A_{(0,r,I-1)}}, \frac{1}{z+A_{(1,r,I-1)}}, \ldots, \frac{1}{z+A_{(n_R-r-1,r,I-1)}}, \frac{1}{z+A_{(n_R-r,r,I-1)}}\right)^T$, for $1 \leq r \leq n_L - I + 1$.

We can express system in Equation (3.8) in terms of levels as

$$\begin{aligned} \mathbf{g}_0(z) &= \mathbf{A}_{0,0}(z)\mathbf{g}_0(z) + \mathbf{A}_{0,1}(z)\mathbf{g}_1(z), \\ \mathbf{g}_1(z) &= \mathbf{A}_{1,1}(z)\mathbf{g}_1(z) + \mathbf{A}_{1,2}(z)\mathbf{g}_2(z), \\ &\vdots \\ \mathbf{g}_{I-2}(z) &= \mathbf{A}_{I-2,I-2}(z)\mathbf{g}_{I-2}(z) + \mathbf{A}_{I-2,I-1}(z)\mathbf{g}_{I-1}(z), \\ \mathbf{g}_{I-1}(z) &= \mathbf{A}_{I-1,I-1}(z)\mathbf{g}_{I-1}(z) + \mathbf{a}_{I-1}(z), \end{aligned} \tag{3.9}$$

which can be solved in an algorithmic manner. In particular, a straightforward analysis of

Equation (3.9) permits to construct Algorithm 1, given in Section 3.3.2.6, which solves the system by working with the levels structure with an specialised block-Gaussian elimination procedure. However, we recall here that the dimension of a level $L(k)$ (and, therefore, of the matrices $A_{k,k}(z)$ in Equation (3.9)) is given by $J(k) = \frac{(n_L-k+1)(2n_R-n_L+k+2)}{2}$, while the dimension of a sub-level is $\#l(k;r) = n_R - r + 1$. This encourages the development of efficient alternatives to Algorithm 1 which take advantage of the special sub-level structure of $\mathcal{S}(I)$. In particular, the equation corresponding to a particular level $L(k)$ in Equation (3.9), for any $0 \leq k \leq I-1$, can be rewritten in terms of sub-levels as

$$\begin{aligned}
\mathbf{g}_0^k(z) &= \mathbf{B}_{0,0}^{k,k}(z)\mathbf{g}_0^k(z) + \mathbf{B}_{0,1}^{k,k}(z)\mathbf{g}_1^k(z), \\
\mathbf{g}_1^k(z) &= \mathbf{B}_{1,0}^{k,k}(z)\mathbf{g}_0^k(z) + \mathbf{B}_{1,1}^{k,k}(z)\mathbf{g}_1^k(z) + \mathbf{B}_{1,2}^{k,k}(z)\mathbf{g}_2^k(z) + (1-\delta_{k,I-1})\mathbf{B}_{1,0}^{k,k+1}(z) \\
&\quad \times \mathbf{g}_0^{k+1}(z) + \delta_{k,I-1}\mathbf{a}_1^{I-1}(z), \\
\vdots &= \vdots \\
\mathbf{g}_{n_L-k-1}^k(z) &= \mathbf{B}_{n_L-k-1,n_L-k-2}^{k,k}(z)\mathbf{g}_{n_L-k-2}^k(z) + \mathbf{B}_{n_L-k-1,n_L-k-1}^{k,k}(z)\mathbf{g}_{n_L-k-1}^k(z) \\
&\quad + \mathbf{B}_{n_L-k-1,n_L-k}^{k,k}(z)\mathbf{g}_{n_L-k}^k(z) + (1-\delta_{k,I-1})\mathbf{B}_{n_L-k-1,n_L-k-2}^{k,k+1}(z) \\
&\quad \times \mathbf{g}_{n_L-k-2}^{k+1}(z) + \delta_{k,I-1}\mathbf{a}_{n_L-I}^{I-1}(z), \\
\mathbf{g}_{n_L-k}^k(z) &= \mathbf{B}_{n_L-k,n_L-k-1}^{k,k}(z)\mathbf{g}_{n_L-k-1}^k(z) + \mathbf{B}_{n_L-k,n_L-k}^{k,k}(z)\mathbf{g}_{n_L-k}^k(z) + (1-\delta_{k,I-1}) \\
&\quad \times \mathbf{B}_{n_L-k,n_L-k-1}^{k,k+1}(z)\mathbf{g}_{n_L-k-1}^{k+1}(z) + \delta_{k,I-1}\mathbf{a}_{n_L-I+1}^{I-1}(z).
\end{aligned} \tag{3.10}$$

It is clear from Equation (3.10) that, by assuming that transforms $\mathbf{g}_{k+1}(z)$ corresponding to the level $L(k+1)$ are in hand, we can obtain transforms $\mathbf{g}_k(z)$ of the level $L(k)$ with a similar procedure than in Algorithm 1. Then, by initializing this procedure in the last level $L(I-1)$, where the transforms $\mathbf{g}_{I-1}(z)$ can be directly obtained from Equation (3.10), we can work in an algorithmic manner obtaining the transforms in $\mathbf{g}_k(z)$ for $k = I-1, I-2, \ldots, 1, 0$, which yields Algorithm 2 (Part 1) in Section 3.3.2.6. We recall here that the computational challenge in Algorithm 2 (Part 1) lays on the calculation of inverses of matrices with size $n_R - r + 1$, whereas in Algorithm 1 it lays on the calculation of inverses of matrices with size $J(k) = \frac{(n_L-k+1)(2n_R-n_L+k+2)}{2}$.

In order to solve Equation (3.7), we organise the moments $\tau_{(n_1,n_2,n_3)}^{I,(l)}$ in column vectors in a similar manner than with the Laplace-Stieltjes transforms, so that quantities $\tau_{(n_1,n_2,n_3)}^{I,(l)}$ for the different possible initial states are stored in a column vector $\mathbf{m}^{(l)} = (\mathbf{m}_0^{(l)T}, \mathbf{m}_1^{(l)T}, \ldots, \mathbf{m}_{I-2}^{(l)T}, \mathbf{m}_{I-1}^{(l)T})^T$, where $\mathbf{m}_k^{(l)} = (\mathbf{m}_0^{k,(l)T}, \mathbf{m}_1^{k,(l)T}, \ldots, \mathbf{m}_{n_L-k-1}^{k,(l)T}, \mathbf{m}_{n_L-k}^{k,(l)T})^T$, for $0 \leq k \leq I-1$. Finally, $\mathbf{m}_r^{k,(l)} =$

$(\tau^{I,(l)}_{(0,r,k)}, \tau^{I,(l)}_{(1,r,k)}, \dots, \tau^{I,(l)}_{(n_R-r-1,r,k)}, \tau^{I,(l)}_{(n_R-r,r,k)})^T$, for $0 \leq r \leq n_L - k$ and $0 \leq k \leq I-1$. Then, Equation (3.7) yields the system in matrix form

$$\mathbf{m}^{(l)} = \mathbf{A}(0)\mathbf{m}^{(l)} + \sum_{i=1}^{l} \binom{l}{i} \mathbf{A}^{(i)}(0)\mathbf{m}^{(l-i)} + (-1)^l \mathbf{a}^{(l)}(0), \tag{3.11}$$

that can be rewritten in terms of levels and sub-levels in a similar way than system in Equation (3.8), so that Algorithm 2 (Part 2) is obtained and given in Section 3.3.2.6. We point out here that Algorithm 2 (Part 2) works in an efficient algorithmic manner by calculating the i-th order moments stored in $\mathbf{m}^{(i)}$ by using the $(i-1)$-th order moments $\mathbf{m}^{(i-1)}$ computed in the previous step, and starting at $\mathbf{m}^{(0)} = \mathbf{g}(0)$. Expressions for the derivatives of matrices $\mathbf{B}^{k,k'}_{r,r'}(z)$ and sub-vectors $\mathbf{a}^{I-1}_r(z)$ with respect to z, at $z = 0$, appearing in Algorithm 2 (Part 2) are given as

$$\begin{aligned}
\left(\mathbf{B}^{k,k',(p)}_{r,r'}(0)\right)_{ij} &= (-1)^p p! \frac{1}{A^{p+1}_{(i,r,k)}} \left(\mathbf{B}^{k,k'}_{r,r'}(0)\right)_{ij}, \\
\left(\mathbf{a}^{I-1,(p)}_r(0)\right)_i &= (-1)^p p! \frac{1}{A^{p+1}_{(i,r,k)}} \left(\mathbf{a}^{I-1}_r(0)\right)_i,
\end{aligned}$$

for any possible values of i, j, r, k, and p, and where we are making use of the matrix calculus notation $\mathbf{A}^{(p)}(0) = \frac{d^p}{dz^p}\mathbf{A}(z)\Big|_{z=0}$.

3.3.2.4 Maximum number of bound complexes B

The aim in this section is to develop a wide analysis of the peak reached by $B(t)$ during the process; that is, the peak number of bound complexes obtained by the T cell on the synapse after ligand stimulation. In order to analyse both the stimulation intensity and its speed, we propose to study the related random variables

$$\begin{aligned}
B^{max}_{(n_1,n_2,n_3)} &= \text{“}\textit{Maximum number of bound complexes simultaneously present on the synapse of the T cell during the whole process, given the current state } (n_1,n_2,n_3) \in \mathcal{S}\text{”} = \max\{B(t) : 0 \leq t \leq T^{n_L}_{(n_1,n_2,n_3)}\}, \\
TB^{b}_{(n_1,n_2,n_3)} &= \text{“}\textit{Time to reach b bound complexes simultaneously present on the synapse of the T cell, given the current state } (n_1,n_2,n_3) \in \mathcal{S}\text{”} \\
&= \inf\{t \geq 0 : B(t) = b\},
\end{aligned}$$

where we consider only non-trivial cases given by values $n_2 \leq b \leq n_L$. We first note that the random variable $TB^b_{(n_1,n_2,n_3)}$ is defective, since $\mathbb{P}(TB^b_{(n_1,n_2,n_3)} \to +\infty) > 0$, representing the case in which every ligand becomes internalised without $\mathcal{X}$ ever showing b bound complexes simultaneously on the synapse. Moreover, variable $B^{max}_{(n_1,n_2,n_3)}$ is directly related to $TB^b_{(n_1,n_2,n_3)}$ since $\mathbb{P}(TB^b_{(n_1,n_2,n_3)} < +\infty) = \mathbb{P}(B^{max}_{(n_1,n_2,n_3)} \geq b)$, so that the analysis of the random variable $TB^b_{(n_1,n_2,n_3)}$ yields the distribution of $B^{max}_{(n_1,n_2,n_3)}$.

In order to analyse the random variable $TB^b_{(n_1,n_2,n_3)}$, we can focus on its different order moments. However, we point out that for any value $n_2 \leq b \leq n_L$ we can split its l-th order moment as

$$\begin{aligned} E\left[\left(TB^b_{(n_1,n_2,n_3)}\right)^l\right] &= E\left[\left(TB^b_{(n_1,n_2,n_3)}\right)^l \middle| B^{max}_{(n_1,n_2,n_3)} \geq b\right] \mathbb{P}\left(B^{max}_{(n_1,n_2,n_3)} \geq b\right) \\ &\quad + E\left[\left(TB^b_{(n_1,n_2,n_3)}\right)^l \middle| B^{max}_{(n_1,n_2,n_3)} < b\right] \mathbb{P}\left(B^{max}_{(n_1,n_2,n_3)} < b\right) \to +\infty, \end{aligned} \tag{3.12}$$

since $\mathbb{P}(B^{max}_{(n_1,n_2,n_3)} < b) > 0$ and $E[(TB^b_{(n_1,n_2,n_3)})^l | B^{max}_{(n_1,n_2,n_3)} < b] \to +\infty$. We focus then on the first term in Equation (3.12), which provides us information about the time to reach a total number b of bound complexes simultaneously on the synapse restricted to the case that this number is in fact reached, as well as about the probability of this event taking place. The time until reaching the value b in those cases in which this value is not reached at all is obviously infinite and, thus, irrelevant. Moreover, the analysis of the first addend in Equation (3.12) allows us to compute the probability mass function of $B^{max}_{(n_1,n_2,n_3)}$. In order to analyse the first contribution in Equation (3.12), we consider the Laplace-Stieltjes transform of the time to reach a total number b of bound complexes simultaneously on the synapse of the T cell, restricted to the fact that this number is achieved, which is given by

$$\begin{aligned} \bar{\phi}^b_{(n_1,n_2,n_3)}(z) &= E\left[e^{-zTB^b_{(n_1,n_2,n_3)}}; B^{max}_{(n_1,n_2,n_3)} \geq b\right] \\ &= E\left[e^{-zTB^b_{(n_1,n_2,n_3)}} \middle| B^{max}_{(n_1,n_2,n_3)} \geq b\right] \mathbb{P}\left(B^{max}_{(n_1,n_2,n_3)} \geq b\right), \end{aligned}$$

so that this Laplace-Stieltjes transform does not accumulate mass 1 at $z = 0$, but we have instead $\bar{\phi}^b_{(n_1,n_2,n_3)}(0) = \mathbb{P}(B^{max}_{(n_1,n_2,n_3)} \geq b)$.

Let us note that, from an analysis of $\mathcal{S}$, if $L_E(t) = n_L - b + 1$ at some time during the process before $B(t)$ reaching the value b, then it will not be possible to have $B(t) = b$ in the future any more, because of ligand scarcity on the cell surface (since at this time there are only $b - 1$ ligands available on the synapse). This means that the process to reach b bound complexes on the synapse

of the T cell or until being certain that this value will not be ever reached can be analysed by means of an auxiliary process $\mathcal{X}(b)$ over

$$\mathcal{S}(b) \quad = \quad \mathcal{C}(b) \cup \{\bar{b}\} \cup \{\overline{n_L - b + 1}\},$$

where $\mathcal{C}(b) = \{(n_1, n_2, n_3) \in \mathcal{S} : n_2 < b, n_3 < n_L - b + 1\}$ is an irreducible class of transient states, the macro-state $\bar{b}$ is obtained by lumping all the states in $\{(n_1, n_2, n_3) \in \mathcal{S} : b \leq n_2 \leq n_L\}$, and $\overline{n_L - b + 1}$ is obtained by lumping all the states in $\{(n_1, n_2, n_3) \in \mathcal{S} : n_L - b + 1 \leq n_3 \leq n_L\}$, with $\bar{b}$ and $\overline{n_L - b + 1}$ being considered as absorbing states in $\mathcal{X}(b)$. We maintain from the original process $\mathcal{X}$ all the transitions between states in $\mathcal{C}(b)$, and those transitions from states in $\mathcal{C}(b)$ towards states in $\{(n_1, n_2, n_3) \in \mathcal{S} : b \leq n_2 \leq n_L\}$ or in $\{(n_1, n_2, n_3) \in \mathcal{S} : n_L - b + 1 \leq n_3 \leq n_L\}$ become, in $\mathcal{X}(b)$, transitions from $\mathcal{C}(b)$ towards state $\bar{b}$ or $\overline{n_L - b + 1}$, respectively. Then, the time to reach b bound complexes in the original process restricted to the sample paths where b is actually reached is the time to reach the absorbing state $\bar{b}$ in the auxiliary process, restricted to the sample paths where absorption actually occurs in $\bar{b}$ and not in $\overline{n_L - b + 1}$. This means that, if we extend the definition of the restricted Laplace-Stieltjes transforms to the auxiliary process $\mathcal{X}(b)$, we have that $\bar{\phi}^b_{\bar{b}}(z) \equiv 1$ and $\bar{\phi}^b_{\overline{n_L - b + 1}}(z) \equiv 0, \forall Re(z) \geq 0$.

We can obtain, by a first-step argument, a system of equations regarding the restricted Laplace-Stieltjes transforms $\bar{\phi}^b_{(n_1,n_2,n_3)}(z)$ as

$$\begin{aligned}(z + A_{(n_1,n_2,n_3)})\bar{\phi}^b_{(n_1,n_2,n_3)}(z) \quad = \quad & (1 - \delta_{n_1,n_R-n_2})(n_R - n_1 - n_2)\gamma_R \bar{\phi}^b_{(n_1+1,n_2,n_3)}(z) \\ & + (1 - \delta_{n_1,0})n_1\delta\bar{\phi}^b_{(n_1-1,n_2,n_3)}(z) + (1 - \delta_{n_2,0})n_2\alpha_- \\ & \times \bar{\phi}^b_{(n_1,n_2-1,n_3)}(z) + (1 - \delta_{n_2,0})(1 - \delta_{n_3,n_L-b})n_2\gamma_B \\ & \times \bar{\phi}^b_{(n_1+1,n_2-1,n_3+1)}(z) + (n_R - n_1 - n_2)(n_L - n_2 - n_3) \\ & \times \alpha_+ \left((1 - \delta_{n_2,b-1})\bar{\phi}^b_{(n_1,n_2+1,n_3)}(z) + \delta_{n_2,b-1}\right), \end{aligned} \tag{3.13}$$

for any $0 \leq n_2 \leq b - 1$, $0 \leq n_3 \leq n_L - b$, $0 \leq n_1 \leq n_R - n_2$ and $Re(z) \geq 0$. Equation (3.13) can be solved in an algorithmic way, so that Algorithm 3 (Part 1) is constructed in Section 3.3.2.6. Since $\bar{\phi}^b_{(n_1,n_2,n_3)}(z) = E[e^{-zTB^b_{(n_1,n_2,n_3)}}; B^{max}_{(n_1,n_2,n_3)} \geq b]$, the distribution of $B^{max}_{(n_1,n_2,n_3)}$ is given in terms of $\bar{\phi}^b_{(n_1,n_2,n_3)}(0) = \mathbb{P}(B^{max}_{(n_1,n_2,n_3)} \geq b)$.

Once the restricted Laplace-Stieltjes transforms are in hand, the restricted moments $\bar{\tau}^{b,(l)}_{(n_1,n_2,n_3)} = E[(TB^b_{(n_1,n_2,n_3)})^l; TB^b_{(n_1,n_2,n_3)} < +\infty]$ of the random variable $TB^b_{(n_1,n_2,n_3)}$ can be computed by successive differentiation of Equation (3.13), and Algorithm 3 (Part 2), given in Section 3.3.2.6,

is obtained by following similar matrix-analytic arguments.

The state space of the auxiliary process $\mathcal{X}(b)$ inherits the structure by levels and sub-levels from $\mathcal{S}$. Specifically,

$$\mathcal{C}(b) \quad = \quad \bigcup_{k=0}^{n_L-b} L^b(k),$$

where a level $L^b(k)$ is given as $L^b(k) = \cup_{r=0}^{b-1} l(k;r)$, where sub-levels $l(k;r)$ are those ones defined in the original process $\mathcal{X}$. That is, a level $L^b(k)$ in the auxiliary process differs from a level $L(k)$ in the original process only in the fact that it contains less sub-levels, in particular it only contains those sub-levels $l(k;r)$ with values $r \in \{0,\ldots,b-1\}$, instead of $r \in \{0,\ldots,n_L-k\}$ as it was in the original process.

Equation (3.13) yields the system in matrix form

$$\bar{\mathbf{g}}(z) \quad = \quad \bar{\mathbf{A}}(z)\bar{\mathbf{g}}(z) + \bar{\mathbf{a}}(z), \tag{3.14}$$

where for the ease of notation we are omitting from now on the value b in the notation. However, it is important to point out that the vector $\bar{\mathbf{g}}(z)$ in Equation (3.14), as well as other quantities obtained later, directly depend on the particular value of b, so that we would have in fact $\bar{\mathbf{g}}(z;b)$. Then, if our interest is in obtaining the Laplace-Stieltjes transforms $\bar{\phi}^b_{(n_1,n_2,n_3)}(z)$ for different values of b, we need to solve the system in Equation (3.14) for all those different values of b.

In a similar way than in Section 3.3.2.3, $\bar{\mathbf{g}}(z)$ is a column vector containing the restricted Laplace-Stieltjes transforms $\bar{\phi}^b_{(n_1,n_2,n_3)}(z)$ for states $(n_1,n_2,n_3) \in \mathcal{C}(b)$, in an ordered manner. The particular structure of $\bar{\mathbf{g}}(z)$ is omitted here since it follows the steps given in Section 3.3.2.3 for $\mathbf{g}(z)$. However, it is clear that $\bar{\mathbf{g}}(z)$ contains sub-vectors $\bar{\mathbf{g}}_k(z)$ storing the Laplace-Stieltjes transforms corresponding to states in level $L^b(k)$. At the same time, any sub-vector $\bar{\mathbf{g}}_k(z)$ is structured in sub-vectors $\bar{\mathbf{g}}^k_r(z)$ which contain the Laplace-Stieltjes transforms for states in sub-level $l(k;r) \subset L^b(k)$.

The special structure of $\mathcal{S}(b)$ means that the matrix $\bar{\mathbf{A}}(z)$ is similar to matrix $\mathbf{A}(z)$ in Equation

(3.8). Specifically, we can write

$$\bar{\mathbf{A}}(z) = \begin{pmatrix} \bar{\mathbf{A}}_{0,0}(z) & \bar{\mathbf{A}}_{0,1}(z) & \cdots & \mathbf{0}_{\bar{J}(0)\times\bar{J}(n_L-b-1)} & \mathbf{0}_{\bar{J}(0)\times\bar{J}(n_L-b)} \\ \mathbf{0}_{\bar{J}(1)\times\bar{J}(0)} & \bar{\mathbf{A}}_{1,1}(z) & \cdots & \mathbf{0}_{\bar{J}(1)\times\bar{J}(n_L-b-1)} & \mathbf{0}_{\bar{J}(1)\times\bar{J}(n_L-b)} \\ \mathbf{0}_{\bar{J}(2)\times\bar{J}(0)} & \mathbf{0}_{\bar{J}(2)\times\bar{J}(1)} & \cdots & \mathbf{0}_{\bar{J}(2)\times\bar{J}(n_L-b-1)} & \mathbf{0}_{\bar{J}(2)\times\bar{J}(n_L-b)} \\ \vdots & \vdots & \ddots & \vdots & \vdots \\ \mathbf{0}_{\bar{J}(n_L-b-1)\times\bar{J}(0)} & \mathbf{0}_{\bar{J}(n_L-b-1)\times\bar{J}(1)} & \cdots & \bar{\mathbf{A}}_{n_L-b-1,n_L-b-1}(z) & \bar{\mathbf{A}}_{n_L-b-1,n_L-b}(z) \\ \mathbf{0}_{\bar{J}(n_L-b)\times\bar{J}(0)} & \mathbf{0}_{\bar{J}(n_L-b)\times\bar{J}(1)} & \cdots & \mathbf{0}_{\bar{J}(n_L-b)\times\bar{J}(n_L-b-1)} & \bar{\mathbf{A}}_{n_L-b,n_L-b}(z) \end{pmatrix},$$

where now $\#L^b(k) = \bar{J}(k) = \sum_{r=0}^{b-1} \#l(k;r)$. Matrices $\bar{\mathbf{A}}_{k,k'}(z)$ have the same structure than $\mathbf{A}_{k,k'}(z)$ in Equation (3.9) but removing those rows and columns related to sub-levels $l(k;r)$ with $b \leq r \leq n_L - k$, and they are thus omitted. Finally, the vector $\bar{\mathbf{a}}(z)$ is given by

$$\bar{\mathbf{a}}(z) = \begin{pmatrix} \bar{\mathbf{a}}_0(z) \\ \bar{\mathbf{a}}_1(z) \\ \vdots \\ \bar{\mathbf{a}}_{n_L-b-1}(z) \\ \bar{\mathbf{a}}_{n_L-b}(z) \end{pmatrix}, \text{ with } \bar{\mathbf{a}}_k(z) = \begin{pmatrix} \mathbf{0}_{n_R+1} \\ \mathbf{0}_{n_R} \\ \vdots \\ \mathbf{0}_{n_R-b+3} \\ \bar{\mathbf{a}}^k_{b-1}(z) \end{pmatrix}, \quad 0 \leq k \leq n_L - b,$$

where $\bar{\mathbf{a}}^k_{b-1}(z) = (\frac{(n_R-b+1)(n_L-b+1-k)\alpha_+}{z+A_{(0,b-1,k)}}, \frac{(n_R-b)(n_L-b+1-k)\alpha_+}{z+A_{(1,b-1,k)}}, \ldots, \frac{(n_L-b+1-k)\alpha_+}{z+A_{(n_R-b,b-1,k)}}, 0)^T$, for $0 \leq k \leq n_L - b$.

A similar system than the one given by Equation (3.9) can be obtained in terms of the levels $L^b(k)$, and then re-expressed in terms of sub-levels as in Equation (3.10). Moreover, system in Equation (3.14) can be iteratively differentiated so that the restricted different order moments of our random variables $TB^b_{(n_1,n_2,n_3)}$, $\bar{\tau}^{b,(l)}_{(n_1,n_2,n_3)} = E[(TB^b_{(n_1,n_2,n_3)})^l; B^{max}_{(n_1,n_2,n_3)} \geq b]$, $l \geq 1$, can be computed. In particular, by following a similar approach than in Algorithm 2, Algorithm 3 is constructed and given in Section 3.3.2.6, which permits to obtain the restricted Laplace-Stieltjes transforms of the random variables $TB^b_{(n_1,n_2,n_3)}$ (stored in the column vector $\bar{\mathbf{g}}(z)$), and the restricted different order moments of $TB^b_{(n_1,n_2,n_3)}$ (stored in a column vector $\bar{\mathbf{m}}^{(l)}$ structured in sub-vectors regarding levels and sub-levels). Finally, for an initial state $(n_1, n_2, n_3) \in \mathcal{S}$, the distribution of $B^{max}_{(n_1,n_2,n_3)}$ is stored in the column vectors $\bar{\mathbf{g}}(0)$, obtained by application of Algorithm 3 when varying the value $b \leq n_L$.

3.3.2.5 Sensitivity analysis

In this section we carry out a local sensitivity analysis of the characteristics studied in the previous sections with respect parameters $\{\alpha_+, \alpha_-, \gamma_R, \gamma_B, \delta\}$. Once the descriptors of interest are in hand, we address the question about the particular contribution of each parameter to each of these descriptors. Specifically, we propose here to carry out a local sensitivity analysis in terms of the computation of the partial derivatives of each of the descriptors in this section with respect to each parameter.

The local sensitivity analysis permits to study which kind of changes we should expect regarding the descriptors of interest from slight perturbations in one of the parameters - these perturbations can represent either an error in its approximation or a slight change in the experiment conditions. Moreover, it allows us to know, in an neighbourhood of the specific selection $(\alpha_+, \alpha_-, \gamma_R, \gamma_B, \delta)$, which is the contribution of each parameter to the results obtained for each descriptor, by observing the sign and the relative magnitudes of the partial derivatives.

We propose here to follow the arguments in [25], which generalise arguments in [14] for perturbation analysis of absorbing CTMCs to structured Markov chains of the same type than the ones analysed in this paper. Specifically, in [14] known properties of matrix calculus [39, 40] are used in order to obtain the derivatives of different descriptors in absorbing Markov chains with respect parameters appearing in the transition rates of these Markov chains. Roughly speaking, the arguments in [14, 25] basically lay on the idea that the main properties of scalar calculus - such as the *chain rule* - also apply to matrix calculus, and in the fact that, given a matrix that depends on some parameter, $\mathbf{A}(\theta)$, it is possible to obtain the derivative of $\mathbf{A}(\theta)^{-1}$ with respect to θ as

$$\frac{d\left(\mathbf{A}(\theta)^{-1}\right)}{d\theta} = -\mathbf{A}(\theta)^{-1}\frac{d\mathbf{A}(\theta)}{d\theta}\mathbf{A}(\theta)^{-1}.$$

In fact, the arguments in [14] do not require the Markov chain being absorbing, and it is possible then to generalise arguments in [14, 39, 40] to more general structured Markov chains as the ones analysed in this paper, as shown in [25]. In particular, we can obtain the derivatives of our descriptors - quantities stored in $\mathbf{m}^{(l)}$ in Algorithm 2, and in $\bar{\mathbf{g}}(0)$ and $\bar{\mathbf{m}}(l)$ in Algorithm 3 - with respect each parameter $\theta \in \{\alpha_+, \alpha_-, \gamma_R, \gamma_B, \delta\}$. Specifically, Algorithms 2S and 3S are obtained in Section 3.3.2.6, where these derivatives are stored, respectively, in vectors $\mathbf{m}^{(l,\theta)}$, $\bar{\mathbf{g}}^{(\theta)}(0)$ and $\bar{\mathbf{m}}^{(l,\theta)}$. We note here that Algorithms 2S and 3S use data obtained from Algorithms 2 and 3, and have to be implemented after them.

Once Algorithms 2S and 3S have been developed, the partial derivatives of the components of vectors $\mathbf{m}^{(l)}$ (corresponding to the l-th order moments of the time $T^{I}_{(n_1,n_2,n_3)}$ to reach some threshold number I of ligands internalised), $\bar{\mathbf{g}}(0)$ (corresponding to the probabilities of reaching some maximum number of bound complexes simultaneously on the synapse, $\mathbb{P}(B^{max}_{(n_1,n_2,n_3)} \geq b)$), and $\bar{\mathbf{m}}^{(l)}$ (corresponding to the restricted l-th order moments of the time to reach a total number b of bound complexes simultaneously on the synapse) with respect each parameter $\theta \in \{\alpha_+, \alpha_-, \gamma_R, \gamma_B, \delta\}$ are stored in vectors $\mathbf{m}^{(l,\theta)}$, $\bar{\mathbf{g}}^{(\theta)}(0)$ and $\bar{\mathbf{m}}^{(l,\theta)}$, respectively. Then, regarding the time $T^{I}_{(n_1,n_2,n_3)}$ to reach some threshold number I of ligands internalised, we can obtain the partial derivative of any of its different l-th order moments $\tau^{I,(l)}_{(n_1,n_2,n_3)}$ with respect each parameter $\theta \in \{\alpha_+, \alpha_-, \gamma_R, \gamma_B, \delta\}$, $\frac{\partial \tau^{I,(l)}_{(n_1,n_2,n_3)}}{\partial \theta}$, which is directly stored in the (n_1, n_2, n_3)-th component of the vector $\mathbf{m}^{(l,\theta)}$ obtained from Algorithm 2S. Regarding the maximum number of bound complexes simultaneously present on the synapse during the process, $B^{max}_{(n_1,n_2,n_3)}$, we can analyse its l-th order moment as

$$E\left[\left(B^{max}_{(n_1,n_2,n_3)}\right)^l\right] = \sum_{b=n_2}^{n_L} b^l \mathbb{P}(B^{max}_{(n_1,n_2,n_3)} = b),$$

so that its partial derivatives are given by

$$\frac{\partial E\left[\left(B^{max}_{(n_1,n_2,n_3)}\right)^l\right]}{\partial \theta} = \sum_{b=n_2}^{n_L} b^l \frac{\partial \mathbb{P}(B^{max}_{(n_1,n_2,n_3)} = b)}{\partial \theta},$$

where the partial derivatives of the probabilities in the expression above are straightforwardly obtained from derivatives $\frac{\partial \mathbb{P}(B^{max}_{(n_1,n_2,n_3)} \geq b)}{\partial \theta}$, stored in the (n_1, n_2, n_3)-th component of the vector $\bar{\mathbf{g}}^{(\theta)}(0)$ obtained in Algorithm 3S for the particular value b.

Finally, partial derivatives of the probabilities $\hat{\pi}_m$, $0 \leq m \leq n_R$, regarding the stationary distribution of the CTMC, can be straightforwardly computed by direct differentiation so that if $\hat{m}$ represents the mean number of receptors into the endosome in steady-state, we have

$$\frac{\partial \hat{m}}{\partial \theta} = \sum_{m=0}^{n_R} m \frac{\partial \hat{\pi}_m}{\partial \theta} = \begin{cases} 0, & \text{if } \theta \in \{\alpha_+, \alpha_-, \gamma_B\}, \\ \frac{n_R \delta}{(\delta+\gamma_R)^2}, & \text{if } \theta = \gamma_R, \\ -\frac{n_R \gamma_R}{(\delta+\gamma_R)^2}, & \text{if } \theta = \delta, \end{cases}$$

where, in the expression above, partial derivatives for quantities $\hat{\pi}_m$ are given by

$$\frac{\partial \hat{\pi}_m}{\partial \theta} = \begin{cases} 0, & \text{if } \theta \in \{\alpha_+, \alpha_-, \gamma_B\}, \\ \hat{\pi}_m \left(\frac{m}{\gamma_R} - \frac{n_R}{\delta+\gamma_R} \right), & \text{if } \theta = \gamma_R, \\ \hat{\pi}_m \left(\frac{n_R \gamma_R}{\delta(\delta+\gamma_R)} - \frac{m}{\delta} \right), & \text{if } \theta = \delta, \end{cases}$$

for $0 \leq m \leq n_R$.

3.3.2.6 Algorithms

Algorithm 1

(Laplace-Stieltjes transforms $\phi^I_{(n_1,n_2,n_3)}(z)$ computed from Equation (3.9))

$\mathbf{H}_0(z) = \mathbf{I}_{J(0)} - \mathbf{A}_{0,0}(z)$;

For $k = 1, \ldots, I-1$*:*

$\mathbf{H}_k(z) = \mathbf{I}_{J(k)} - \mathbf{A}_{k,k}(z)$;

$\mathbf{g}_{I-1}(z) = \mathbf{H}_{I-1}(z)^{-1}\mathbf{a}_{I-1}(z)$;

For $k = I-2, \ldots, 1, 0$*:*

$\mathbf{g}_k(z) = \mathbf{H}_k(z)^{-1}\mathbf{A}_{k,k+1}(z)\mathbf{g}_{k+1}(z)$;

Algorithm 2

Part 1 (Laplace-Stieltjes transforms $\phi^I_{(n_1,n_2,n_3)}(z)$ computed from Equation (3.10))

$\mathbf{H}_0^{I-1}(z) = \mathbf{I}_{n_R+1} - \mathbf{B}_{0,0}^{I-1,I-1}(z)$; $\mathbf{J}_0^{I-1,(0)}(z) = \mathbf{0}_{n_R+1}$;

For $r = 1, \ldots, n_L - I + 1$*:*

$\mathbf{H}_r^{I-1}(z) = \mathbf{I}_{n_R-r+1} - \mathbf{B}_{r,r}^{I-1,I-1}(z) - \mathbf{B}_{r,r-1}^{I-1,I-1}(z)\mathbf{H}_{r-1}^{I-1}(z)^{-1}\mathbf{B}_{r-1,r}^{I-1,I-1}(z)$;

$\mathbf{J}_r^{I-1,(0)}(z) = \mathbf{B}_{r,r-1}^{I-1,I-1}(z)\mathbf{H}_{r-1}^{I-1}(z)^{-1}\mathbf{J}_{r-1}^{I-1,(0)}(z) + \mathbf{a}_r^{I-1}(z)$;

$\mathbf{g}_{n_L-I+1}^{I-1}(z) = \mathbf{H}_{n_L-I+1}^{I-1}(z)^{-1}\mathbf{J}_{n_L-I+1}^{I-1,(0)}(z)$; $\mathbf{m}_{n_L-I+1}^{I-1,(0)} = \mathbf{g}_{n_L-I+1}^{I-1}(0)$;

For $r = n_L - I, \ldots, 1, 0$*:*

$$\mathbf{g}_r^{I-1}(z) \;=\; \mathbf{H}_r^{I-1}(z)^{-1}\left(\mathbf{B}_{r,r+1}^{I-1,I-1}(z)\mathbf{g}_{r+1}^{I-1}(z)+\mathbf{J}_r^{I-1,(0)}(z)\right);\; \mathbf{m}_r^{I-1,(0)} \;=\; \mathbf{g}_r^{I-1}(0);$$

For $k = I-2,\ldots,1,0$*:*

$$\mathbf{H}_0^k(z) \;=\; \mathbf{I}_{n_R+1}-\mathbf{B}_{0,0}^{k,k}(z);\; \mathbf{J}_0^{k,(0)}(z) \;=\; \mathbf{0}_{n_R+1};$$

For $r = 1,\ldots,n_L-k$*:*

$$\mathbf{H}_r^k(z) \;=\; \mathbf{I}_{n_R-r+1}-\mathbf{B}_{r,r}^{k,k}(z)-\mathbf{B}_{r,r-1}^{k,k}(z)\mathbf{H}_{r-1}^k(z)^{-1}\mathbf{B}_{r-1,r}^{k,k}(z);$$

$$\mathbf{J}_r^{k,(0)}(z) \;=\; \mathbf{B}_{r,r-1}^{k,k}(z)\mathbf{H}_{r-1}^k(z)^{-1}\mathbf{J}_{r-1}^{k,(0)}(z)+\mathbf{B}_{r,r-1}^{k,k+1}(z)\mathbf{g}_{r-1}^{k+1}(z);$$

$$\mathbf{g}_{n_L-k}^k(z) \;=\; \mathbf{H}_{n_L-k}^k(z)^{-1}\mathbf{J}_{n_L-k}^{k,(0)}(z);\; \mathbf{m}_{n_L-k}^{k,(0)} \;=\; \mathbf{g}_{n_L-k}^k(0);$$

For $r = n_L-k-1,\ldots,1,0$*:*

$$\mathbf{g}_r^k(z) \;=\; \mathbf{H}_r^k(z)^{-1}\left(\mathbf{B}_{r,r+1}^{k,k}(z)\mathbf{g}_{r+1}^k(z)+\mathbf{J}_r^{k,(0)}(z)\right);\; \mathbf{m}_r^{k,(0)} \;=\; \mathbf{g}_r^k(0);$$

Part 2 (Moments $\tau_{(n_1,n_2,n_3)}^{I,(l)} = E\left[\left(T_{(n_1,n_2,n_3)}^I\right)^l\right]$ computed from Equation (3.11))

For $i = 1,\ldots,l$*:*

For $k = I-1,\ldots,1,0$*:*

$$\mathbf{J}_0^{k,(i)}(0) \;=\; \sum_{p=1}^{i}\binom{i}{p}(-1)^p\left(\mathbf{B}_{0,0}^{k,k,(p)}(0)\mathbf{m}_0^{k,(i-p)}+\mathbf{B}_{0,1}^{k,k,(p)}(0)\mathbf{m}_1^{k,(i-p)}\right);$$

For $r = 1,\ldots,n_L-k$*:*

$$\begin{aligned}\mathbf{J}_r^{k,(i)}(0) \;=\;& \mathbf{B}_{r,r-1}^{k,k}(0)\mathbf{H}_{r-1}^k(0)^{-1}\mathbf{J}_{r-1}^{k,(i)}(0)+(1-\delta_{k,I-1})\mathbf{B}_{r,r-1}^{k,k+1}(0)\mathbf{m}_{r-1}^{k+1,(i)}\\ &+\sum_{p=1}^{i}\binom{i}{p}(-1)^p\left(\mathbf{B}_{r,r-1}^{k,k,(p)}(0)\mathbf{m}_{r-1}^{k,(i-p)}+\mathbf{B}_{r,r}^{k,k,(p)}(0)\mathbf{m}_r^{k,(i-p)}\right.\\ &+(1-\delta_{r,n_L-k})\mathbf{B}_{r,r+1}^{k,k,(p)}(0)\mathbf{m}_{r+1}^{k,(i-p)}+(1-\delta_{k,I-1})\mathbf{B}_{r,r-1}^{k,k+1,(p)}(0)\\ &\left.\times\mathbf{m}_{r-1}^{k+1,(i-p)}\right)+\delta_{k,I-1}(-1)^i\mathbf{a}_r^{I-1,(i)}(0);\end{aligned}$$

$$\mathbf{m}_{n_L-k}^{k,(i)} \;=\; \mathbf{H}_{n_L-k}^k(0)^{-1}\mathbf{J}_{n_L-k}^{k,(i)}(0);$$

For $r = n_L-k-1,\ldots,1,0$*:*

$$\mathbf{m}_r^{k,(i)} \;=\; \mathbf{H}_r^k(0)^{-1}\left(\mathbf{B}_{r,r+1}^{k,k}(0)\mathbf{m}_{r+1}^{k,(i)}+\mathbf{J}_r^{k,(i)}(0)\right);$$

Algorithm 3 (Truncated Laplace-Stieltjes transforms $\bar{\phi}_{(n_1,n_2,n_3)}^b(z)$ and the truncated l-th order moments $E[(TB_{(n_1,n_2,n_3)}^b)^l; B_{(n_1,n_2,n_3)}^{max} \geq b]$)

$\bar{\mathbf{H}}_0^{n_L-b}(z) \;=\; \mathbf{I}_{n_R+1} - \mathbf{B}_{0,0}^{n_L-b,n_L-b}(z)$; $\bar{\mathbf{J}}_0^{n_L-b,(0)}(z) \;=\; \mathbf{0}_{n_R+1}$;

For $r = 1, \ldots, b-1$*:*

$$\bar{\mathbf{H}}_r^{n_L-b}(z) \;=\; \mathbf{I}_{n_R-r+1} - \mathbf{B}_{r,r}^{n_L-b,n_L-b}(z) - \mathbf{B}_{r,r-1}^{n_L-b,n_L-b}(z)\bar{\mathbf{H}}_{r-1}^{n_L-b}(z)^{-1}\mathbf{B}_{r-1,r}^{n_L-b,n_L-b}(z);$$

$$\bar{\mathbf{J}}_r^{n_L-b,(0)}(z) \;=\; \mathbf{B}_{r,r-1}^{n_L-b,n_L-b}(z)\bar{\mathbf{H}}_{r-1}^{n_L-b}(z)^{-1}\bar{\mathbf{J}}_{r-1}^{n_L-b,(0)}(z) + \delta_{r,b-1}\bar{\mathbf{a}}_{b-1}^{n_L-b}(z);$$

$\bar{\mathbf{g}}_{b-1}^{n_L-b}(z) \;=\; \bar{\mathbf{H}}_{b-1}^{n_L-b}(z)^{-1}\bar{\mathbf{J}}_{b-1}^{n_L-b,(0)}(z)$; $\bar{\mathbf{m}}_{b-1}^{n_L-b,(0)} \;=\; \bar{\mathbf{g}}_{b-1}^{n_L-b}(0)$;

For $r = b-2, \ldots, 1, 0$*:*

$$\bar{\mathbf{g}}_r^{n_L-b}(z) \;=\; \bar{\mathbf{H}}_r^{n_L-b}(z)^{-1}\left(\mathbf{B}_{r,r+1}^{n_L-b,n_L-b}(z)\bar{\mathbf{g}}_{r+1}^{n_L-b}(z) + \bar{\mathbf{J}}_r^{n_L-b,(0)}(z)\right);\; \bar{\mathbf{m}}_r^{n_L-b,(0)} \;=\; \bar{\mathbf{g}}_r^{n_L-b}(0);$$

For $k = n_L - b - 1, \ldots, 1, 0$*:*

$\bar{\mathbf{H}}_0^{k}(z) \;=\; \mathbf{I}_{n_R+1} - \mathbf{B}_{0,0}^{k,k}(z)$; $\bar{\mathbf{J}}_0^{k,(0)}(z) \;=\; \mathbf{0}_{n_R+1}$;

For $r = 1, \ldots, b-1$*:*

$$\bar{\mathbf{H}}_r^{k}(z) \;=\; \mathbf{I}_{n_R-r+1} - \mathbf{B}_{r,r}^{k,k}(z) - \mathbf{B}_{r,r-1}^{k,k}(z)\bar{\mathbf{H}}_{r-1}^{k}(z)^{-1}\mathbf{B}_{r-1,r}^{k,k}(z);$$

$$\bar{\mathbf{J}}_r^{k,(0)}(z) \;=\; \mathbf{B}_{r,r-1}^{k,k}(z)\bar{\mathbf{H}}_{r-1}^{k}(z)^{-1}\bar{\mathbf{J}}_{r-1}^{k,(0)}(z) + \mathbf{B}_{r,r-1}^{k,k+1}(z)\bar{\mathbf{g}}_{r-1}^{k+1}(z) + \delta_{r,b-1}\bar{\mathbf{a}}_{b-1}^{k}(z);$$

$\bar{\mathbf{g}}_{b-1}^{k}(z) \;=\; \bar{\mathbf{H}}_{b-1}^{k}(z)^{-1}\bar{\mathbf{J}}_{b-1}^{k,(0)}(z)$; $\bar{\mathbf{m}}_{b-1}^{k,(0)} \;=\; \bar{\mathbf{g}}_{b-1}^{k}(0)$;

For $r = b-2, \ldots, 1, 0$*:*

$$\bar{\mathbf{g}}_r^{k}(z) \;=\; \bar{\mathbf{H}}_r^{k}(z)^{-1}\left(\mathbf{B}_{r,r+1}^{k,k}(z)\bar{\mathbf{g}}_{r+1}^{k}(z) + \bar{\mathbf{J}}_r^{k,(0)}(z)\right);\; \bar{\mathbf{m}}_r^{k,(0)} \;=\; \bar{\mathbf{g}}_r^{k}(0);$$

For $i = 1, \ldots, l$*:*

For $k = n_L - b, \ldots, 1, 0$*:*

$$\bar{\mathbf{J}}_0^{k,(i)}(0) \;=\; \sum_{p=1}^{i} \binom{i}{p}(-1)^p\left(\mathbf{B}_{0,0}^{k,k,(p)}(0)\bar{\mathbf{m}}_0^{k,(i-p)} + \mathbf{B}_{0,1}^{k,k,(p)}(0)\bar{\mathbf{m}}_1^{k,(i-p)}\right);$$

For $r = 1, \ldots, b-1$*:*

$$\begin{aligned}\bar{\mathbf{J}}_r^{k,(i)}(0) \;=\;& \mathbf{B}_{r,r-1}^{k,k}(0)\bar{\mathbf{H}}_{r-1}^{k}(0)^{-1}\bar{\mathbf{J}}_{r-1}^{k,(i)}(0) + (1-\delta_{k,n_L-b})\mathbf{B}_{r,r-1}^{k,k+1}(0)\bar{\mathbf{m}}_{r-1}^{k+1,(i)} \\ &+ \sum_{p=1}^{i}\binom{i}{p}(-1)^p\left(\mathbf{B}_{r,r-1}^{k,k,(p)}(0)\bar{\mathbf{m}}_{r-1}^{k,(i-p)} + \mathbf{B}_{r,r}^{k,k,(p)}(0)\bar{\mathbf{m}}_{r}^{k,(i-p)} + \right. \\ &(1-\delta_{r,b-1})\mathbf{B}_{r,r+1}^{k,k,(p)}(0)\bar{\mathbf{m}}_{r+1}^{k,(i-p)} + (1-\delta_{k,n_L-b})\mathbf{B}_{r,r-1}^{k,k+1,(p)}(0) \\ &\left.\times\bar{\mathbf{m}}_{r-1}^{k+1,(i-p)}\right) + \delta_{r,b-1}(-1)^i\mathbf{a}_{b-1}^{k,(i)}(0);\end{aligned}$$

$$\bar{\mathbf{m}}_{b-1}^{k,(i)} \;=\; \bar{\mathbf{H}}_{b-1}^{k}(0)^{-1}\bar{\mathbf{J}}_{b-1}^{k,(i)}(0);$$

For $r = b-2,\ldots,1,0$*:*

$$\bar{\mathbf{m}}_{r}^{k,(i)} \;=\; \bar{\mathbf{H}}_{r}^{k}(0)^{-1}\left(\mathbf{B}_{r,r+1}^{k,k}(0)\bar{\mathbf{m}}_{r+1}^{k,(i)} + \bar{\mathbf{J}}_{r}^{k,(i)}(0)\right);$$

Algorithm 2S (Sensitivity analysis for quantities computed in Algorithm 2)

$$\mathbf{H}_{0}^{I-1,(\theta)}(z) \;=\; -\mathbf{B}_{0,0}^{I-1,I-1,(\theta)}(z);\; \mathbf{J}_{0}^{I-1,(0,\theta)}(z) \;=\; \mathbf{0}_{n_R+1};$$

For $r = 1,\ldots,n_L - I + 1$*:*

$$\begin{aligned}\mathbf{H}_{r}^{I-1,(\theta)}(z) \;=\; & -\mathbf{B}_{r,r}^{I-1,I-1,(\theta)}(z) - \Big(\mathbf{B}_{r,r-1}^{I-1,I-1,(\theta)}(z)\mathbf{H}_{r-1}^{I-1}(z)^{-1}\mathbf{B}_{r-1,r}^{I-1,I-1}(z) - \mathbf{B}_{r,r-1}^{I-1,I-1}(z)\\ & \times\mathbf{H}_{r-1}^{I-1}(z)^{-1}\mathbf{H}_{r-1}^{I-1,(\theta)}(z)\mathbf{H}_{r-1}^{I-1}(z)^{-1}\mathbf{B}_{r-1,r}^{I-1,I-1}(z) + \mathbf{B}_{r,r-1}^{I-1,I-1}(z)\mathbf{H}_{r-1}^{I-1}(z)^{-1}\\ & \times\mathbf{B}_{r-1,r}^{I-1,I-1,(\theta)}(z)\Big);\\ \mathbf{J}_{r}^{I-1,(0,\theta)}(z) \;=\; & \mathbf{B}_{r,r-1}^{I-1,I-1,(\theta)}(z)\mathbf{H}_{r-1}^{I-1}(z)^{-1}\mathbf{J}_{r-1}^{I-1,(0)}(z) - \mathbf{B}_{r,r-1}^{I-1,I-1}(z)\mathbf{H}_{r-1}^{I-1}(z)^{-1}\mathbf{H}_{r-1}^{I-1,(\theta)}(z)\\ & \times\mathbf{H}_{r-1}^{I-1}(z)^{-1}\mathbf{J}_{r-1}^{I-1,(0)}(z) + \mathbf{B}_{r,r-1}^{I-1,I-1}(z)\mathbf{H}_{r-1}^{I-1}(z)^{-1}\mathbf{J}_{r-1}^{I-1,(0,\theta)}(z)\\ & +\mathbf{a}_{r}^{I-1,\theta}(z);\end{aligned}$$

$$\mathbf{g}_{n_L-I+1}^{I-1,(\theta)}(z) \;=\; -\mathbf{H}_{n_L-I+1}^{I-1}(z)^{-1}\mathbf{H}_{n_L-I+1}^{I-1,(\theta)}(z)\mathbf{H}_{n_L-I+1}^{I-1}(z)^{-1}\mathbf{J}_{n_L-I+1}^{I-1,(0)}(z) + \mathbf{H}_{n_L-I+1}^{I-1}(z)^{-1}\mathbf{J}_{n_L-I+1}^{I-1,(0,\theta)}(z);$$

$$\mathbf{m}_{n_L-I+1}^{I-1,(0,\theta)} \;=\; \mathbf{g}_{n_L-I+1}^{I-1,(\theta)}(0);$$

For $r = n_L - I,\ldots,1,0$*:*

$$\begin{aligned}\mathbf{g}_{r}^{I-1,(\theta)}(z) \;=\; & -\mathbf{H}_{r}^{I-1}(z)^{-1}\mathbf{H}_{r}^{I-1,(\theta)}(z)\mathbf{H}_{r}^{I-1}(z)^{-1}\left(\mathbf{B}_{r,r+1}^{I-1,I-1}(z)\mathbf{g}_{r+1}^{I-1}(z) + \mathbf{J}_{r}^{I-1,(0)}(z)\right)\\ & +\mathbf{H}_{r}^{I-1}(z)^{-1}\left(\mathbf{B}_{r,r+1}^{I-1,I-1,(\theta)}(z)\mathbf{g}_{r+1}^{I-1}(z) + \mathbf{B}_{r,r+1}^{I-1,I-1}(z)\mathbf{g}_{r+1}^{I-1,(\theta)}(z)\right.\\ & \left.+\mathbf{J}_{r}^{I-1,(0,\theta)}(z)\right);\; \mathbf{m}_{r}^{I-1,(0,\theta)} \;=\; \mathbf{g}_{r}^{I-1,(\theta)}(0);\end{aligned}$$

For $k = I-2,\ldots,1,0$*:*

$$\mathbf{H}_{0}^{k,(\theta)}(z) \;=\; -\mathbf{B}_{0,0}^{k,k,(\theta)}(z);\; \mathbf{J}_{0}^{k,(0,\theta)}(z) \;=\; \mathbf{0}_{n_R+1};$$

For $r = 1,\ldots,n_L - k$*:*

$$\mathbf{H}_{r}^{k,(\theta)}(z) \;=\; -\mathbf{B}_{r,r}^{k,k,(\theta)}(z) - \Big(\mathbf{B}_{r,r-1}^{k,k,(\theta)}(z)\mathbf{H}_{r-1}^{k}(z)^{-1}\mathbf{B}_{r-1,r}^{k,k}(z) - \mathbf{B}_{r,r-1}^{k,k}(z)\mathbf{H}_{r-1}^{k}(z)^{-1}\mathbf{H}_{r-1}^{k,(\theta)}(z)$$

$$\times \mathbf{H}_{r-1}^{k}(z)^{-1}\mathbf{B}_{r-1,r}^{k,k}(z) + \mathbf{B}_{r,r-1}^{k,k}(z)\mathbf{H}_{r-1}^{k}(z)^{-1}\mathbf{B}_{r-1,r}^{k,k,(\theta)}(z)\Big);$$

$$\mathbf{J}_{r}^{k,(0,\theta)}(z) = \mathbf{B}_{r,r-1}^{k,k,(\theta)}(z)\mathbf{H}_{r-1}^{k}(z)^{-1}\mathbf{J}_{r-1}^{k,(0)}(z) - \mathbf{B}_{r,r-1}^{k,k}(z)\mathbf{H}_{r-1}^{k}(z)^{-1}\mathbf{H}_{r-1}^{k,(\theta)}(z)\mathbf{H}_{r-1}^{k}(z)^{-1}\mathbf{J}_{r-1}^{k,(0)}(z)$$

$$+\mathbf{B}_{r,r-1}^{k,k}(z)\mathbf{H}_{r-1}^{k}(z)^{-1}\mathbf{J}_{r-1}^{k,(0,\theta)}(z) + \mathbf{B}_{r,r-1}^{k,k+1,(\theta)}(z)\mathbf{g}_{r-1}^{k+1}(z) + \mathbf{B}_{r,r-1}^{k,k+1}(z)\mathbf{g}_{r-1}^{k+1,(\theta)}(z);$$

$$\mathbf{g}_{n_L-k}^{k,(\theta)}(z) = -\mathbf{H}_{n_L-k}^{k}(z)^{-1}\mathbf{H}_{n_L-k}^{k,(\theta)}(z)\mathbf{H}_{n_L-k}^{k}(z)^{-1}\mathbf{J}_{n_L-k}^{k,(0)}(z) + \mathbf{H}_{n_L-k}^{k}(z)^{-1}\mathbf{J}_{n_L-k}^{k,(0,\theta)}(z);$$

$$\mathbf{m}_{n_L-k}^{k,(0,\theta)} = \mathbf{g}_{n_L-k}^{k,\theta}(0);$$

For $r = n_L - k - 1, \ldots, 1, 0$*:*

$$\mathbf{g}_{r}^{k,(\theta)}(z) = -\mathbf{H}_{r}^{k}(z)^{-1}\mathbf{H}_{r}^{k,(\theta)}(z)\mathbf{H}_{r}^{k}(z)^{-1}\left(\mathbf{B}_{r,r+1}^{k,k}(z)\mathbf{g}_{r+1}^{k}(z) + \mathbf{J}_{r}^{k,(0)}(z)\right)$$

$$+\mathbf{H}_{r}^{k}(z)^{-1}\left(\mathbf{B}_{r,r+1}^{k,k,(\theta)}(z)\mathbf{g}_{r+1}^{k}(z) + \mathbf{B}_{r,r+1}^{k,k}(z)\mathbf{g}_{r+1}^{k,(\theta)}(z) + \mathbf{J}_{r}^{k,(0,\theta)}(z)\right);$$

$$\mathbf{m}_{r}^{k,(0,\theta)} = \mathbf{g}_{r}^{k,(\theta)}(0);$$

For $i = 1, \ldots, l$*:*

For $k = I - 1, \ldots, 1, 0$*:*

$$\mathbf{J}_{0}^{k,(i,\theta)}(0) = \sum_{p=1}^{i}\binom{i}{p}(-1)^{p}\left(\mathbf{B}_{0,0}^{k,k,(p,\theta)}(0)\mathbf{m}_{0}^{k,(i-p)} + \mathbf{B}_{0,0}^{k,k,(p)}(0)\mathbf{m}_{0}^{k,(i-p,\theta)} + \mathbf{B}_{0,1}^{k,k,(p,\theta)}(0)\mathbf{m}_{1}^{k,(i-p)}\right.$$

$$\left.+\mathbf{B}_{0,1}^{k,k,(p)}(0)\mathbf{m}_{1}^{k,(i-p,\theta)}\right);$$

For $r = 1, \ldots, n_L - k$*:*

$$\mathbf{J}_{r}^{k,(i,\theta)}(0) = \mathbf{B}_{r,r-1}^{k,k,(\theta)}(0)\mathbf{H}_{r-1}^{k}(0)^{-1}\mathbf{J}_{r-1}^{k,(i)}(0) - \mathbf{B}_{r,r-1}^{k,k}(0)\mathbf{H}_{r-1}^{k}(0)^{-1}\mathbf{H}_{r-1}^{k,(\theta)}(0)\mathbf{H}_{r-1}^{k}(0)^{-1}\mathbf{J}_{r-1}^{k,(i)}(0)$$

$$+\mathbf{B}_{r,r-1}^{k,k}(0)\mathbf{H}_{r-1}^{k}(0)^{-1}\mathbf{J}_{r-1}^{k,(i,\theta)}(0) + (1-\delta_{k,I-1})\left(\mathbf{B}_{r,r-1}^{k,k+1,(\theta)}(0)\mathbf{m}_{r-1}^{k+1,(i)}\right.$$

$$\left.+\mathbf{B}_{r,r-1}^{k,k+1}(0)\mathbf{m}_{r-1}^{k+1,(i,\theta)}\right) + \sum_{p=1}^{i}\binom{i}{p}(-1)^{p}\left(\mathbf{B}_{r,r-1}^{k,k,(p,\theta)}(0)\mathbf{m}_{r-1}^{k,(i-p)} + \mathbf{B}_{r,r-1}^{k,k,(p)}(0)\mathbf{m}_{r-1}^{k,(i-p,\theta)}\right.$$

$$\left.+\mathbf{B}_{r,r}^{k,k,(p,\theta)}(0)\mathbf{m}_{r}^{k,(i-p)} + \mathbf{B}_{r,r}^{k,k,(p)}(0)\mathbf{m}_{r}^{k,(i-p,\theta)} + (1-\delta_{r,n_L-k})\left(\mathbf{B}_{r,r+1}^{k,k,(p,\theta)}(0)\mathbf{m}_{r+1}^{k,(i-p)}\right.\right.$$

$$\left.\left.+\mathbf{B}_{r,r+1}^{k,k,(p)}(0)\mathbf{m}_{r+1}^{k,(i-p,\theta)}\right) + (1-\delta_{k,I-1})\left(\mathbf{B}_{r,r-1}^{k,k+1,(p,\theta)}(0)\mathbf{m}_{r-1}^{k+1,(i-p)} + \mathbf{B}_{r,r-1}^{k,k+1,(p)}(0)\right.\right.$$

$$\left.\left.\times\mathbf{m}_{r-1}^{k+1,(i-p,\theta)}\right)\right) + \delta_{k,I-1}(-1)^{i}\mathbf{a}_{r}^{I-1,(i,\theta)}(0);$$

$$\mathbf{m}_{n_L-k}^{k,(i,\theta)} = -\mathbf{H}_{n_L-k}^{k}(0)^{-1}\mathbf{H}_{n_L-k}^{k,(\theta)}(0)\mathbf{H}_{n_L-k}^{k}(0)^{-1}\mathbf{J}_{n_L-k}^{k,(i)}(0) + \mathbf{H}_{n_L-k}^{k}(0)^{-1}\mathbf{J}_{n_L-k}^{k,(i,\theta)}(0);$$

For $r = n_L - k - 1, \ldots, 1, 0$*:*

$$\mathbf{m}_{r}^{k,(i,\theta)} = -\mathbf{H}_{r}^{k}(0)^{-1}\mathbf{H}_{r}^{k,(\theta)}(0)\mathbf{H}_{r}^{k}(0)^{-1}\left(\mathbf{B}_{r,r+1}^{k,k}(0)\mathbf{m}_{r+1}^{k,(i)} + \mathbf{J}_{r}^{k,(i)}(0)\right)$$

$$+\mathbf{H}_r^k(0)^{-1}\left(\mathbf{B}_{r,r+1}^{k,k,(\theta)}(0)\mathbf{m}_{r+1}^{k,(i)}+\mathbf{B}_{r,r+1}^{k,k}(0)\mathbf{m}_{r+1}^{k,(i,\theta)}+\mathbf{J}_r^{k,(i,\theta)}(0)\right);$$

Algorithm 3S (Sensitivity analysis for quantities computed in Algorithm 3)

$$\bar{\mathbf{H}}_0^{n_L-b,(\theta)}(z) = -\mathbf{B}_{0,0}^{n_L-b,n_L-b,(\theta)}(z);\ \bar{\mathbf{J}}_0^{n_L-b,(0,\theta)}(z) = \mathbf{0}_{n_R+1};$$

For $r=1,\ldots,b-1$*:*

$$\begin{aligned}\bar{\mathbf{H}}_r^{n_L-b,(\theta)}(z) &= -\mathbf{B}_{r,r}^{n_L-b,n_L-b,(\theta)}(z)-\Big(\mathbf{B}_{r,r-1}^{n_L-b,n_L-b,(\theta)}(z)\bar{\mathbf{H}}_{r-1}^{n_L-b}(z)^{-1}\mathbf{B}_{r-1,r}^{n_L-b,n_L-b}(z)\\ &\quad-\mathbf{B}_{r,r-1}^{n_L-b,n_L-b}(z)\bar{\mathbf{H}}_{r-1}^{n_L-b}(z)^{-1}\bar{\mathbf{H}}_{r-1}^{n_L-b,(\theta)}(z)\bar{\mathbf{H}}_{r-1}^{n_L-b}(z)^{-1}\mathbf{B}_{r-1,r}^{n_L-b,n_L-b}(z)\\ &\quad+\mathbf{B}_{r,r-1}^{n_L-b,n_L-b}(z)\bar{\mathbf{H}}_{r-1}^{n_L-b}(z)^{-1}\mathbf{B}_{r-1,r}^{n_L-b,n_L-b,(\theta)}(z)\Big);\\ \bar{\mathbf{J}}_r^{n_L-b,(0,\theta)}(z) &= \mathbf{B}_{r,r-1}^{n_L-b,n_L-b,(\theta)}(z)\bar{\mathbf{H}}_{r-1}^{n_L-b}(z)^{-1}\bar{\mathbf{J}}_{r-1}^{n_L-b,(0)}(z)-\mathbf{B}_{r,r-1}^{n_L-b,n_L-b}(z)\bar{\mathbf{H}}_{r-1}^{n_L-b}(z)^{-1}\\ &\quad\times\bar{\mathbf{H}}_{r-1}^{n_L-b,(\theta)}(z)\bar{\mathbf{H}}_{r-1}^{n_L-b}(z)^{-1}\bar{\mathbf{J}}_{r-1}^{n_L-b,(0)}(z)+\mathbf{B}_{r,r-1}^{n_L-b,n_L-b}(z)\bar{\mathbf{H}}_{r-1}^{n_L-b}(z)^{-1}\bar{\mathbf{J}}_{r-1}^{n_L-b,(0,\theta)}(z)\\ &\quad+\delta_{r,b-1}\bar{\mathbf{a}}_{b-1}^{n_L-b,(\theta)}(z);\end{aligned}$$

$$\bar{\mathbf{g}}_{b-1}^{n_L-b,(\theta)}(z) = -\bar{\mathbf{H}}_{b-1}^{n_L-b}(z)^{-1}\bar{\mathbf{H}}_{b-1}^{n_L-b,(\theta)}(z)\bar{\mathbf{H}}_{b-1}^{n_L-b}(z)^{-1}\bar{\mathbf{J}}_{b-1}^{n_L-b,(0)}(z)+\bar{\mathbf{H}}_{b-1}^{n_L-b}(z)^{-1}\bar{\mathbf{J}}_{b-1}^{n_L-b,(0,\theta)}(z);$$

$$\bar{\mathbf{m}}_{b-1}^{n_L-b,(0,\theta)} = \bar{\mathbf{g}}_{b-1}^{n_L-b,(\theta)}(0);$$

For $r=b-2,\ldots,1,0$*:*

$$\begin{aligned}\bar{\mathbf{g}}_r^{n_L-b,(\theta)}(z) &= -\bar{\mathbf{H}}_r^{n_L-b}(z)^{-1}\bar{\mathbf{H}}_r^{n_L-b,(\theta)}(z)\bar{\mathbf{H}}_r^{n_L-b}(z)^{-1}\left(\mathbf{B}_{r,r+1}^{n_L-b,n_L-b}(z)\bar{\mathbf{g}}_{r+1}^{n_L-b}(z)+\bar{\mathbf{J}}_r^{n_L-b,(0)}(z)\right)\\ &\quad+\bar{\mathbf{H}}_r^{n_L-b}(z)^{-1}\left(\mathbf{B}_{r,r+1}^{n_L-b,n_L-b,(\theta)}(z)\bar{\mathbf{g}}_{r+1}^{n_L-b}(z)+\mathbf{B}_{r,r+1}^{n_L-b,n_L-b}(z)\bar{\mathbf{g}}_{r+1}^{n_L-b,(\theta)}(z)\right.\\ &\quad\left.+\bar{\mathbf{J}}_r^{n_L-b,(0,\theta)}(z)\right);\ \bar{\mathbf{m}}_r^{n_L-b,(0,\theta)} = \bar{\mathbf{g}}_r^{n_L-b,(\theta)}(0);\end{aligned}$$

For $k=n_L-b-1,\ldots,1,0$*:*

$$\bar{\mathbf{H}}_0^{k,(\theta)}(z) = -\mathbf{B}_{0,0}^{k,k,(\theta)}(z);\ \bar{\mathbf{J}}_0^{k,(0,\theta)}(z) = \mathbf{0}_{n_R+1};$$

For $r=1,\ldots,b-1$*:*

$$\begin{aligned}\bar{\mathbf{H}}_r^{k,(\theta)}(z) &= -\mathbf{B}_{r,r}^{k,k,(\theta)}(z)-\Big(\mathbf{B}_{r,r-1}^{k,k,(\theta)}(z)\bar{\mathbf{H}}_{r-1}^{k}(z)^{-1}\mathbf{B}_{r-1,r}^{k,k}(z)-\mathbf{B}_{r,r-1}^{k,k}(z)\bar{\mathbf{H}}_{r-1}^{k}(z)^{-1}\bar{\mathbf{H}}_{r-1}^{k,(\theta)}(z)\\ &\quad\times\bar{\mathbf{H}}_{r-1}^{k}(z)^{-1}\mathbf{B}_{r-1,r}^{k,k}(z)+\mathbf{B}_{r,r-1}^{k,k}(z)\bar{\mathbf{H}}_{r-1}^{k}(z)^{-1}\mathbf{B}_{r-1,r}^{k,k,(\theta)}(z)\Big);\\ \bar{\mathbf{J}}_r^{k,(0,\theta)}(z) &= \mathbf{B}_{r,r-1}^{k,k,(\theta)}(z)\bar{\mathbf{H}}_{r-1}^{k}(z)^{-1}\bar{\mathbf{J}}_{r-1}^{k,(0)}(z)-\mathbf{B}_{r,r-1}^{k,k}(z)\bar{\mathbf{H}}_{r-1}^{k}(z)^{-1}\bar{\mathbf{H}}_{r-1}^{k,(\theta)}(z)\bar{\mathbf{H}}_{r-1}^{k}(z)^{-1}\bar{\mathbf{J}}_{r-1}^{k,(0)}(z)\\ &\quad+\mathbf{B}_{r,r-1}^{k,k}(z)\bar{\mathbf{H}}_{r-1}^{k}(z)^{-1}\bar{\mathbf{J}}_{r-1}^{k,(0,\theta)}(z)+\mathbf{B}_{r,r-1}^{k,k+1,(\theta)}(z)\bar{\mathbf{g}}_{r-1}^{k+1}(z)+\mathbf{B}_{r,r-1}^{k,k+1}(z)\bar{\mathbf{g}}_{r-1}^{k+1,(\theta)}(z)\end{aligned}$$

$$+\delta_{r,b-1}\bar{\mathbf{a}}_{b-1}^{k,(\theta)}(z);$$

$$\bar{\mathbf{g}}_{b-1}^{k,(\theta)}(z) = -\bar{\mathbf{H}}_{b-1}^{k}(z)^{-1}\bar{\mathbf{H}}_{b-1}^{k,(\theta)}(z)\bar{\mathbf{H}}_{b-1}^{k}(z)^{-1}\bar{\mathbf{J}}_{b-1}^{k,(0)}(z) + \bar{\mathbf{H}}_{b-1}^{k}(z)^{-1}\bar{\mathbf{J}}_{b-1}^{k,(0,\theta)}(z);$$

$$\bar{\mathbf{m}}_{b-1}^{k,(0,\theta)} = \bar{\mathbf{g}}_{b-1}^{k,(\theta)}(0);$$

For $r = b-2,\ldots,1,0$*:*

$$\bar{\mathbf{g}}_{r}^{k,(\theta)}(z) = -\bar{\mathbf{H}}_{r}^{k}(z)^{-1}\bar{\mathbf{H}}_{r}^{k,(\theta)}(z)\bar{\mathbf{H}}_{r}^{k}(z)^{-1}\left(\mathbf{B}_{r,r+1}^{k,k}(z)\bar{\mathbf{g}}_{r+1}^{k}(z)+\bar{\mathbf{J}}_{r}^{k,(0)}(z)\right)$$
$$+\bar{\mathbf{H}}_{r}^{k}(z)^{-1}\left(\mathbf{B}_{r,r+1}^{k,k,(\theta)}(z)\bar{\mathbf{g}}_{r+1}^{k}(z)+\mathbf{B}_{r,r+1}^{k,k}(z)\bar{\mathbf{g}}_{r+1}^{k,(\theta)}(z)+\bar{\mathbf{J}}_{r}^{k,(0,\theta)}(z)\right);$$

$$\bar{\mathbf{m}}_{r}^{k,(0,\theta)} = \bar{\mathbf{g}}_{r}^{k,(\theta)}(0);$$

For $i = 1,\ldots,l$*:*

For $k = n_L - b,\ldots,1,0$*:*

$$\bar{\mathbf{J}}_{0}^{k,(i,\theta)}(0) = \sum_{p=1}^{i}\binom{i}{p}(-1)^{p}\left(\mathbf{B}_{0,0}^{k,k,(p,\theta)}(0)\bar{\mathbf{m}}_{0}^{k,(i-p)}+\mathbf{B}_{0,0}^{k,k,(p)}(0)\bar{\mathbf{m}}_{0}^{k,(i-p,\theta)}+\mathbf{B}_{0,1}^{k,k,(p,\theta)}(0)\bar{\mathbf{m}}_{1}^{k,(i-p)}\right.$$
$$\left.+\mathbf{B}_{0,1}^{k,k,(p)}(0)\bar{\mathbf{m}}_{1}^{k,(i-p,\theta)}\right);$$

For $r = 1,\ldots,b-1$*:*

$$\bar{\mathbf{J}}_{r}^{k,(i,\theta)}(0) = \mathbf{B}_{r,r-1}^{k,k,(\theta)}(0)\bar{\mathbf{H}}_{r-1}^{k}(0)^{-1}\bar{\mathbf{J}}_{r-1}^{k,(i)}(0)-\mathbf{B}_{r,r-1}^{k,k}(0)\bar{\mathbf{H}}_{r-1}^{k}(0)^{-1}\bar{\mathbf{H}}_{r-1}^{k,(\theta)}(0)\bar{\mathbf{H}}_{r-1}^{k}(0)^{-1}\bar{\mathbf{J}}_{r-1}^{k,(i)}(0)$$
$$+\mathbf{B}_{r,r-1}^{k,k}(0)\bar{\mathbf{H}}_{r-1}^{k}(0)^{-1}\bar{\mathbf{J}}_{r-1}^{k,(i,\theta)}(0)+(1-\delta_{k,n_L-b})\left(\mathbf{B}_{r,r-1}^{k,k+1,(\theta)}(0)\bar{\mathbf{m}}_{r-1}^{k+1,(i)}+\mathbf{B}_{r,r-1}^{k,k+1}(0)\right.$$
$$\left.\times\bar{\mathbf{m}}_{r-1}^{k+1,(i,\theta)}\right)+\sum_{p=1}^{i}\binom{i}{p}(-1)^{p}\left(\mathbf{B}_{r,r-1}^{k,k,(p,\theta)}(0)\bar{\mathbf{m}}_{r-1}^{k,(i-p)}+\mathbf{B}_{r,r-1}^{k,k,(p)}(0)\bar{\mathbf{m}}_{r-1}^{k,(i-p,\theta)}\right.$$
$$+\mathbf{B}_{r,r}^{k,k,(p,\theta)}(0)\bar{\mathbf{m}}_{r}^{k,(i-p)}+\mathbf{B}_{r,r}^{k,k,(p)}(0)\bar{\mathbf{m}}_{r}^{k,(i-p,\theta)}+(1-\delta_{r,b-1})\left(\mathbf{B}_{r,r+1}^{k,k,(p,\theta)}(0)\right.$$
$$\left.\left.\times\bar{\mathbf{m}}_{r+1}^{k,(i-p)}+\mathbf{B}_{r,r+1}^{k,k,(p)}(0)\bar{\mathbf{m}}_{r+1}^{k,(i-p,\theta)}\right)\right.\quad+\quad(1\quad-$$
$$\delta_{k,n_L-b})\left(\mathbf{B}_{r,r-1}^{k,k+1,(p,\theta)}(0)\bar{\mathbf{m}}_{r-1}^{k+1,(i-p)}\right.$$
$$\left.\left.+\mathbf{B}_{r,r-1}^{k,k+1,(p)}(0)\bar{\mathbf{m}}_{r-1}^{k+1,(i-p,\theta)}\right)\right)+\delta_{r,b-1}(-1)^{i}\mathbf{a}_{b-1}^{k,(i,\theta)}(0);$$

$$\bar{\mathbf{m}}_{b-1}^{k,(i,\theta)} = -\bar{\mathbf{H}}_{b-1}^{k}(0)^{-1}\bar{\mathbf{H}}_{b-1}^{k,(\theta)}(0)\bar{\mathbf{H}}_{b-1}^{k}(0)^{-1}\bar{\mathbf{J}}_{b-1}^{k,(i)}(0)+\bar{\mathbf{H}}_{b-1}^{k}(0)^{-1}\bar{\mathbf{J}}_{b-1}^{k,(i,\theta)}(0);$$

For $r = b-2,\ldots,1,0$*:*

$$\bar{\mathbf{m}}_{r}^{k,(i,\theta)} = -\bar{\mathbf{H}}_{r}^{k}(0)^{-1}\bar{\mathbf{H}}_{r}^{k,(\theta)}(0)\bar{\mathbf{H}}_{r}^{k}(0)^{-1}\left(\mathbf{B}_{r,r+1}^{k,k}(0)\bar{\mathbf{m}}_{r+1}^{k,(i)}+\bar{\mathbf{J}}_{r}^{k,(i)}(0)\right)$$
$$+\bar{\mathbf{H}}_{r}^{k}(0)^{-1}\left(\mathbf{B}_{r,r+1}^{k,k,(\theta)}(0)\bar{\mathbf{m}}_{r+1}^{k,(i)}+\mathbf{B}_{r,r+1}^{k,k}(0)\bar{\mathbf{m}}_{r+1}^{k,(i,\theta)}+\bar{\mathbf{J}}_{r}^{k,(i,\theta)}(0)\right);$$

Note that expressions for matrices $\mathbf{B}_{r,r'}^{k,k',(\theta)}(z)$, $\bar{\mathbf{a}}_r^{I-1,(i,\theta)}(z)$ and $\bar{\mathbf{a}}_{b-1}^{k,(i,\theta)}(z)$ in Algorithms 2S and 3S are straightforwardly obtained by direct differentiation of matrices $\mathbf{B}_{r,r'}^{k,k'}(z)$, $\bar{\mathbf{a}}_r^{I-1,(i)}(z)$ and $\bar{\mathbf{a}}_{b-1}^{k,(i)}(z)$ with respect to $\theta \in \{\alpha_+, \alpha_-, \gamma_R, \gamma_B, \delta\}$, and are thus omitted here.

3.3.3 Kinetic rates and molecular levels

Firstly, we present in Table 3.2 association and dissociation rates for receptor CTLA-4 and ligands B7-1 and B7-2, obtained from those reported in [30]. In particular, we denote by α_{i+} and α_{i-} the association and dissociation rates, respectively, for molecule B7-i ($i \in 1, 2$) with receptor CTLA-4. Then, dissociation rates α_{i-} are directly obtained from [30], while association rates α_{i+} are computed by dividing binding rates α_i ($i \in \{1, 2\}$), defined and computed in [30], by the area of the synapse. Moreover, association rates α_{i+} have been multiplied by a factor $f \in \{2, 4\}$ depending on the nature of the two molecules B7-i involved in the reaction; that is, taking into account the bivalent structure of CTLA-4 and B7-1, and the monomeric structure of B7-2.

Lack of experimental data in the literature regarding endocytosis and recycling rates for receptor CTLA-4 forces us here to estimate them by making use of results obtained in Section 3.3.2 together with well-known characteristics of CTLA-4 trafficking. In particular, we assume here that CTLA-4 internalises in a completely ligand-independent manner [53, 76], so that $\gamma_R = \gamma_B$ both for B7-1 and B7-2 ligands in Figure 3.6. On the other hand, it has been estimated that 90% of CTLA-4 is intracellular at any given time [68], so that Equation (3.5) directly yields $\gamma_R = \gamma_B = 9\delta$. Finally, it is also known that when analysing trafficking dynamics, more than 80% of surface CTLA-4 at any time is internalised within 5 minutes [76]. We use this information as follows: we consider a situation where 100 CTLA-4 receptors are marked on the cell surface, and consider the time $T(85)$ for 85 of these receptors being internalised. In the absence of ligand, this yields the birth-and-death process in Figure 3.8 (with $n_R = 100$, $\gamma_R = 9\delta$), and $T(85)$ corresponds to the time to reach state $m = 85$ starting at state 0. We denote the mean of this time as τ_0, which can be computed by

θ	**Definition**	**Rate**
α_{1+}	CTLA-4/B7-1 association rate	$4 \cdot 0.094\ s^{-1}$
α_{1-}	CTLA-4/B7-1 dissociation rate	$0.43\ s^{-1}$
α_{2+}	CTLA-4/B7-2 association rate	$2 \cdot 0.087\ s^{-1}$
α_{2-}	CTLA-4/B7-2 dissociation rate	$5.1\ s^{-1}$

Table 3.2: Binding and dissociation rates considered for CTLA-4, B7-1 and B7-2, obtained from [30].

following a first-step argument. In particular, we can write the system

$$\begin{aligned}
\tau_0 &= \tau_1 + \frac{1}{900\delta}, \\
\tau_1 &= \frac{891}{892}\tau_2 + \frac{1}{892}\tau_0 + \frac{1}{892\delta}, \\
\vdots &= \vdots \\
\tau_m &= \frac{9(100-m)}{9(100-m)+m}\tau_{m+1} + \frac{m}{9(100-m)+m}\tau_{m-1} + \frac{1}{(9(100-m)+m)\delta}, \\
\vdots &= \vdots \\
\tau_{84} &= \frac{84}{228}\tau_{83} + \frac{1}{228\delta},
\end{aligned}$$

where $\tau_i = E[T(85)]$ for the initial state $i \in \{0, \ldots, 84\}$. Finally, we look for the value of δ so that $\tau_0 = 300s$, which is approximately $\delta = 9.0255 \cdot 10^{-4} s^{-1}$.

On the other hand, the amounts of each type of molecule in our process are obtained by conveniently transforming physiological parameters presented in Table 3.3, which are directly taken from [30]. To work with the correct amount of B7-1 and B7-2 ligands, homogeneous spatial distribution of these molecules is supposed in both T cells and APCs. Therefore, only a proportional part of these molecules is present on the synapse. This can be calculated by dividing the area of the synapse by the area of the specific cell (the T cell or the APC) which the molecules we are considering belong to. For the CTLA-4 receptor, we first note that its spatial distribution corresponds to $90\% - 10\%$ (endosome-surface) in non-regulatory T cells at any given time. Thus, 400 CTLA-4 receptors are considered on the cell surface (of which ~ 11 correspond to receptors on the synapse, according to synapse area and T cell radius), while 3600 are into the endosome (~ 100 corresponding to those ones trafficking to the synapse). Following T cell activation CTLA-4 is synthesised, resulting in a temporary proportional increase at the cell surface [68]. To represent different time instants after activation when synthesis may have occurred, we consider total numbers of CTLA-4 receptors within the synapse equal to 11, 22, 55 and 110

Molecular levels	**Rate**	**Cell dimension**	**Rate**
Total CTLA-4 on surface of T cell	$4 \cdot 10^2$	Radius of T cell	6 μm
Total B7-1 in Immature APC	$1 \cdot 10^3$	Radius of APC	10 μm
Total B7-1 in Mature APC	$2 \cdot 10^3$	Area of synapse	12.6 μm^2
Total B7-2 in Immature APC	$2 \cdot 10^4$		
Total B7-2 in Mature APC	$4.3 \cdot 10^4$		

Table 3.3: Molecular levels and cell dimension data from [30].

	$R_E(0)$	$R_S(0)$
Activated T cell	100	11
Activated T cell after CTLA-4 synthesis	100	22,55,110

Table 3.4: Initial numbers $R_E(0)$ and $R_S(0)$ of receptors in the endosome and on the synapse, respectively. We recall $n_R = R_E(0) + R_S(0)$.

(representing 2-, 5- or 10-fold increases with respect steady-state conditions before activation, respectively). We note that these higher surface receptor levels could also be considered when analysing the interaction between a regulatory T cell and an APC, since it is known that CTLA-4 is constitutively expressed by regulatory T cells [76]. These assumptions yield the total number of co-receptors given in Table 3.4, and their initial spatial distribution. Number of ligands provided by the donor cell are given in Table 3.5, and have been computed also by taking into account the APC surface area, the synapse area, and the quantities reported in [30].

3.3.4 Results

In this section, we study the trafficking dynamics upon stimulation of non-regulatory activated T cells by mature and immature APCs. In particular, our interest is in the interaction of receptor CTLA-4 with ligands B7-1 and B7-2 provided by these APCs. For these dynamics when considering only one ligand type (either B7-1 or B7-2), shown in Figure 3.6 and developed in Section 3.3.2 (for the case $n_R \geq n_L$ which includes ligand B7-1 but an analogous development can be done for B7-2 considering $n_R < n_L$), the exact analysis in Section 3.3.2 is applied, so that

Mature APC		**Immature APC**	
B7-1	**B7-2**	**B7-1**	**B7-2**
20	431	10	201

Table 3.5: Total number n_L of ligand (B7-1 or B7-2) provided by a mature or an immature APC on the synapse.

our results should be considered as exact in this situation. This exact analysis has the particular feature that it allows to develop a sensitivity analysis for parameters (Section 3.3.2.5), so that the role played by each parameter in our process can be exactly quantified, related to the stochastic descriptors analysed in Section 3.3.2.

3.3.4.1 Ligand depletion timescales

We focus in this section on the timescales of B7-1 depletion, which are analysed here in terms of the random variable $T^I_{\mathbf{n}}$, defined in Section 3.3.2.3. For these dynamics, B7-1 ligand depletion timescales can be analysed by computing $E[T^{n_L-I}_{\mathbf{n}}]$ (where $\mathbf{n} = (n_1, n_2, n_3)$ is the initial state, and n_L refers to the amount of B7-1 ligand on the synapse according to Table 3.5), when only ligand B7-1 is considered. This represents the mean time to reach a threshold number $n_L - I$ of internalised B7-1 ligands, so that I ligands remain on the synapse at that time instant. For $I = n_L$, $E[T^{n_L-I}_{\mathbf{n}}]$ is trivially 0 representing that no ligand depletion has occurred at the beginning of the process. On the other hand, $E[T^{n_L-I}_{\mathbf{n}}]$ for $I = 0$ represents the average first time at which all ligand (n_L) molecules have been internalised by the T cell.

To quantify the B7-1 internalisation ability of the T cell we analyse in Figure 3.9 the mean time to reach a threshold number $n_L - I$ of B7-1 ligands internalised for different values of I. In particular, we plot $E[T^{n_L-I}_{\mathbf{n}}]$ versus $1 \leq I \leq n_L$ for different numbers of CTLA-4 receptors initially on the synapse, and for a mature or an immature APC interacting with a T cell. These quantities of interest can be exactly computed by following arguments in Section 3.3.2, and in particular by means of Algorithm 2 in Section 3.3.2.6. A significant variation in $E[T^{n_L-I}_{\mathbf{n}}]$ cannot be noticeable between the different synapse receptor levels considered, although higher differences are shown when the T cell interacts with a mature APC. Interestingly, what can be observed when contrasting the kind of APC involved in the T cell activation (which means doubling the amount of available B7-1 ligands in the mature APC in comparison with the immature APC, see Table 3.5) is an increase in the internalisation time of just around a 25% in the immature case with respect the mature case (e.g. $E[T^{n_L}_{\mathbf{n}}] = 413.49s$ for $R_S(0) = 11$, and a T cell interacting with an immature APC, while $E[T^{n_L}_{\mathbf{n}}] = 548.84s$ in the mature case). A saturation behavior can be clearly identified with respect the total number $R_S(0)$ of CTLA-4 receptors initially on the synapse: while synthesis of CTLA-4 resulting in doubling the number of receptors (represented by $R_S(0) = 22$ in Figure 3.9) helps to reduce the timescales of ligand depletion, higher levels of receptors on the synapse ($R_S(0) \in \{55, 110\}$) do not seem to have a significant additional effect.

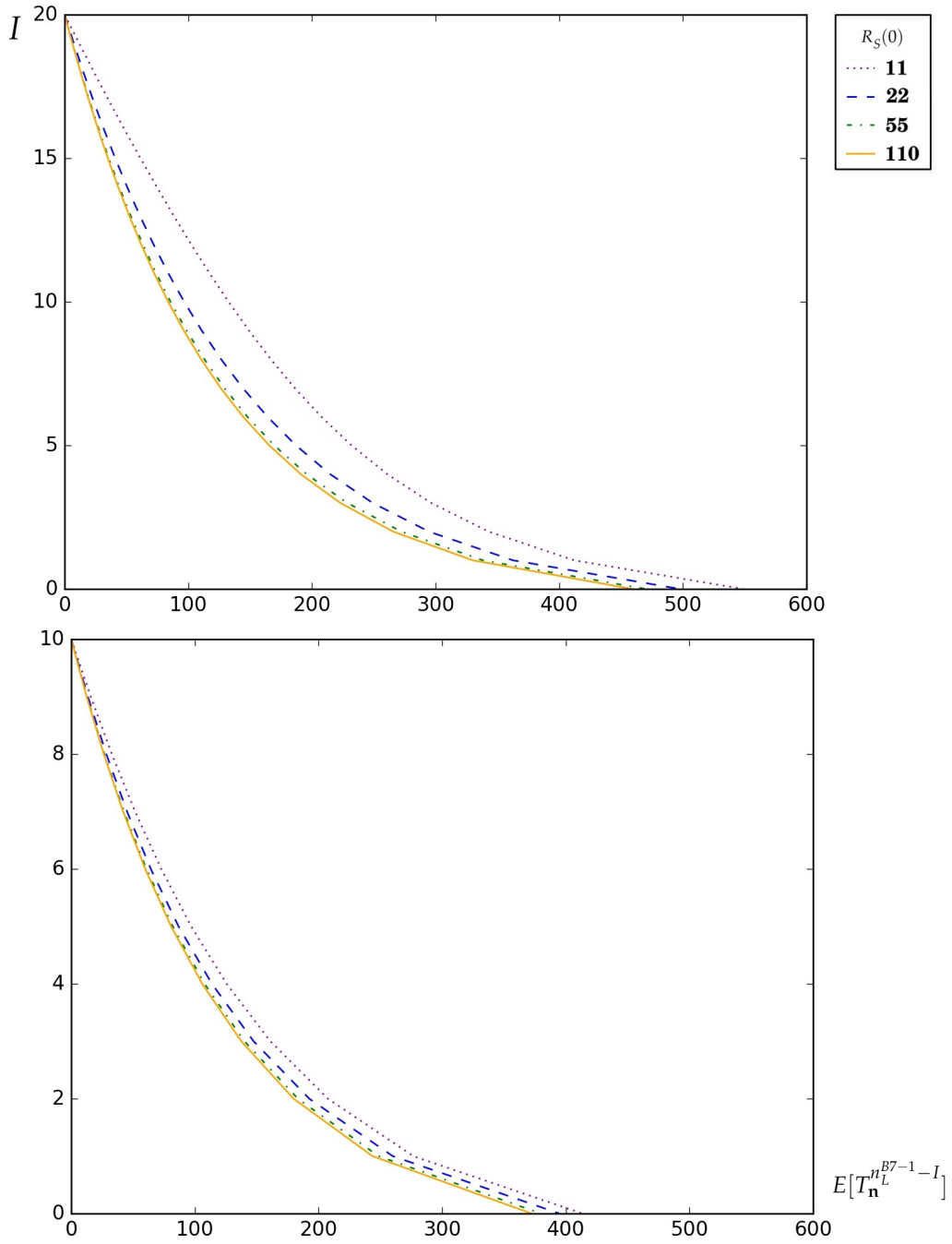

Figure 3.9: Ligand depletion represented by the mean time $E[T_{\mathbf{n}}^{n_L-I}]$ (in *seconds*) to reach a threshold number $n_L - I$ of internalised B7-1 ligands through CTLA-4 binding, versus $1 \leq I \leq n_L$. Consideration of a T cell interacting with a mature (*top*) or an immature (*bottom*) APC, for initial CTLA-4 receptor numbers on the synapse equal to 11, 22, 55 and 110.

	Mature APC				**Immature APC**			
$R_S(0)$	**11**	**22**	**55**	**110**	**11**	**22**	**55**	**110**
$E[TB_{\mathbf{n}}^{0.5n_L}]$	0.5186	0.1114	0.0361	0.0170	0.2111	0.0888	0.0328	0.0160

Table 3.6: Restricted mean time $E[TB_{\mathbf{n}}^{0.5n_L}]$ (in *seconds*) until having 50% of the B7-1 ligands simultaneously bound to CTLA-4 co-receptors on the synapse.

3.3.4.2 Receptor-ligand complex formation

The aim in this section is to develop a wide analysis of the peak reached by receptor-ligand complexes during the process; that is, the peak number of bound complexes obtained by the T cell on the synapse after ligand stimulation, taking into account definitions in Section 3.3.2.4 of $B_{\mathbf{n}}^{max}$ and $TB_{\mathbf{n}}^{b}$.

In particular, we analyse in Figure 3.10 the maximum number of bound CTLA-4/B7-1 complexes simultaneously present on the synapse during the process. More specifically, the probability mass function of $B_{\mathbf{n}}^{max}$ (when only ligand B7-1 is considered), for the initial state $\mathbf{n}$ obtained from molecular levels in Section 3.3.3 (in particular, $\mathbf{n} = (R_E(0), B_1(0), L_E(0)) = (100, 0, 0)$), is plotted under eight possible scenarios regarding interaction of B7-1 on either a mature or immature APC with CTLA-4 co-receptor under distinct instants of T cell activation, which correspond to four different receptor levels on the synapse ($R_S(0) \in \{11, 22, 55, 110\}$) reported in Table 3.4. These different initial receptor levels result in a manifest distinction between the probability distribution of $B_{\mathbf{n}}^{max}$ (Figure 3.10) when interacting with either an immature or mature APC. In order to explain these results, we first note the relatively short time needed for CTLA-4 co-receptors to bind B7-1 ligands, specially under high synapse receptor levels, in comparison with the internalisation timescales. This can be easily noticed by comparing the values of the restricted mean time $E[TB_{\mathbf{n}}^{0.5n_L}]$ to have 50% of the B7-1 ligands simultaneously bound to CTLA-4 co-receptors on the synapse, computed from Algorithm 3 in Section 3.3.2.6 and given in Table 3.6, with values in Figure 3.9 for the mean time $E[T_{\mathbf{n}}^{n_L-I}]$ to reach a threshold number $n_L - I$ of B7-1 ligands internalised, for varying values of I. We note here that the restricted mean time $E[TB_{\mathbf{n}}^{0.5n_L}]$ reported here is in fact $E[TB_{\mathbf{n}}^{0.5n_L} | TB_{\mathbf{n}}^{0.5n_L} < +\infty]$; that is, we compute the mean time to have a total number $0.5n_L$ of bound complexes simultaneously formed, assuming that this number is reached. This is related to the fact that the random variable $TB_{\mathbf{n}}^{b}$ is defective, see Section 3.3.2.4.

Results in Figure 3.10 show that, when analysing the interaction of a T cell with a mature APC, a limited number of CTLA-4 receptors on the cell surface avoids the accummulation of bound complexes on the cell surface, these being internalised in a more sequential way as they are

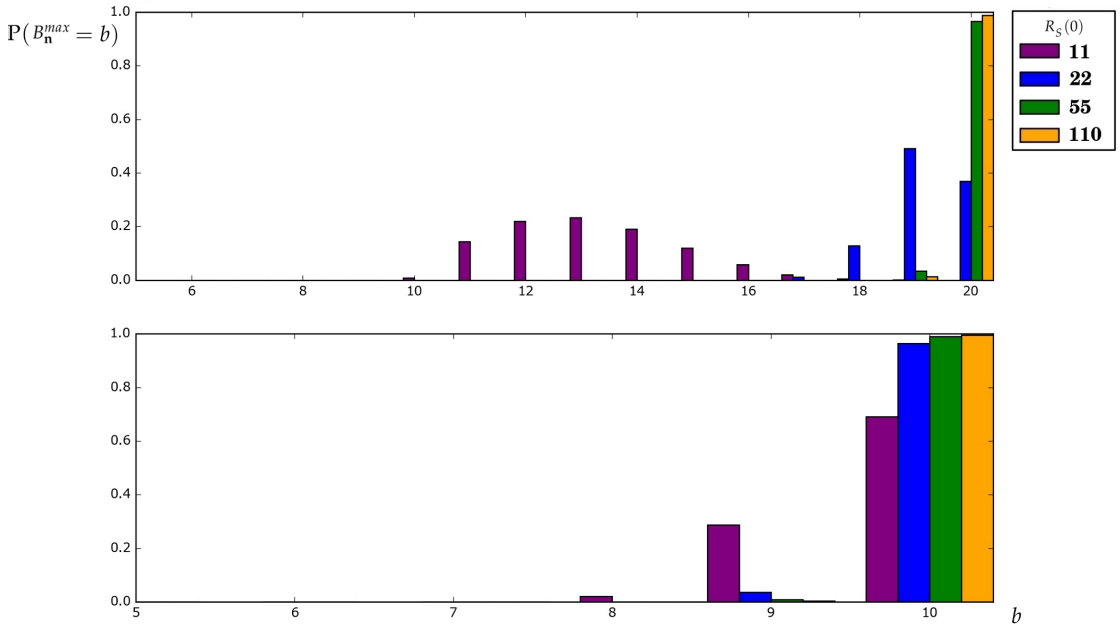

Figure 3.10: Probability mass function of the maximum number $B_{\mathbf{n}}^{max}$ of CTLA-4/B7-1 bound complexes simultaneously present on the synapse. T cell interacting with a mature (*top*) or an immature (*bottom*) APC, for initial CTLA-4 receptor numbers on the synapse equal to 11, 22, 55 and 110.

formed. On the other hand, if more CTLA-4 receptors are initially present on the synapse, all the available B7-1 ligands rapidly join these receptors forming a maximum number of $\sim$ 20 bound complexes on the synapse. This is also observable in the immature APC case, although here the amount of ligands (only 10 B7-1 ligands on the synapse) acts as the limiting factor when forming these bound complexes. These comments are also supported by results in Table 3.7, where summary statistics (mean and standard deviation) of these maximum numbers are reported.

	Mature APC				Immature APC			
$R_S(0)$	**11**	**22**	**55**	**110**	**11**	**22**	**55**	**110**
$E[B_{\mathbf{n}}^{max}]$	13.19	19.22	19.97	19.99	9.67	9.96	9.99	10
$SD[B_{\mathbf{n}}^{max}]$	1.57	0.71	0.17	0.36	0.51	0.2	0.1	0

Table 3.7: Mean and standard deviation of the maximum number $B_{\mathbf{n}}^{max}$ of CTLA-4/B7-1 bound complexes present on the synapse for the stochastic model, and for a mature or an immature APC interacting with T cell with 11, 22, 55 or 110 CTLA-4 receptors initially on the synapse.

Partial Derivative	θ	**Mature APC**		**Immature APC**	
		11 receptors	**110 receptors**	**11 receptors**	**110 receptors**
$\frac{\frac{\partial E[T^I_{\mathbf{n}}]}{\partial\theta}}{\frac{E[T^I_{\mathbf{n}}]}{\theta}}$	α_{1+}	$-1.28\cdot10^{-1}$	$-1.74\cdot10^{-2}$	$-1.49\cdot10^{-1}$	$-1.62\cdot10^{-2}$
	α_{1-}	$1.25\cdot10^{-1}$	$1.71\cdot10^{-2}$	$1.45\cdot10^{-1}$	$1.59\cdot10^{-2}$
	γ_R	$4.11\cdot10^{-2}$	$6.56\cdot10^{-3}$	$4.00\cdot10^{-2}$	$6.57\cdot10^{-3}$
	γ_B	$-7.74\cdot10^{-1}$	-1.00	$-9.50\cdot10^{-1}$	-1.00
	δ	$-2.64\cdot10^{-1}$	$-1.30\cdot10^{-3}$	$-8.59\cdot10^{-2}$	$-1.28\cdot10^{-3}$
$\frac{\frac{\partial E[B^{max}_{\mathbf{n}}]}{\partial\theta}}{\frac{E[B^{max}_{\mathbf{n}}]}{\theta}}$	α_{1+}	2.13	$5.68\cdot10^{-3}$	$1.16\cdot10^{-1}$	$5.98\cdot10^{-3}$
	α_{1-}	$-6.06\cdot10^{-1}$	$-3.80\cdot10^{-5}$	$-1.08\cdot10^{-2}$	$-3.91\cdot10^{-5}$
	γ_R	$-3.23\cdot10^{-1}$	$-6.83\cdot10^{-7}$	$-3.58\cdot10^{-4}$	$-8.29\cdot10^{-7}$
	γ_B	$-2.04\cdot10^{-1}$	$-1.13\cdot10^{-6}$	$-6.28\cdot10^{-4}$	$-1.37\cdot10^{-6}$
	δ	$6.72\cdot10^{-1}$	$7.10\cdot10^{-8}$	$3.51\cdot10^{-4}$	$8.43\cdot10^{-8}$

Table 3.8: Elasticities of the descriptors $E[B^{max}_{\mathbf{n}}]$ and $E[T^I_{\mathbf{n}}]$ with $I = 0.5n_L$, with respect rate $\theta \in \{\alpha_{1+}, \alpha_{1-}, \gamma_R, \gamma_B, \delta\}$. Different scenarios regarding interaction between a T cell at different stages of activation (11 and 110 receptors initially on the synapse) with an immature or mature APC. Receptor CTLA-4 and ligand B7-1.

3.3.4.3 Sensitivity analysis for B7-1/CTLA-4 complexes

In this Section, our aim is to address the impact that a perturbation in the parameter values has on the descriptors of interest, as an analytical tool for quantifying the role played by each parameter on the ligand depletion timescales and on the signal peak. To this end, we compute in Table 3.8 the partial derivatives of the descriptors $E[T^I_{\mathbf{n}}]$ (for $I = 0.5n_L$ representing the internalisation of 50% of available B7-1 ligands) and $E[B^{max}_{\mathbf{n}}]$ with respect to each parameter $\theta \in \{\alpha_{1+}, \alpha_{1-}, \gamma_R, \gamma_B, \delta\}$. In particular, elasticities (*normalised* and *dimensionless* partial derivatives) $(\partial E[T^I_{\mathbf{n}}]/\partial\theta)/(E[T^I_{\mathbf{n}}]/\theta)$ and $(\partial E[B^{max}_{\mathbf{n}}]/\partial\theta)/(E[B^{max}_{\mathbf{n}}]/\theta)$ are reported in Table 3.8.

A comprehensive analysis of values in Table 3.8 lead to the following insights: (i) value -1.00 for the elasticity of $E[T^I_{\mathbf{n}}]$ with respect the internalisation rate γ_B of bound complexes indicates the linear relationship between the timescales for the internalisation of bound complexes and the rate corresponding to this reaction (specially in the case of higher synapse receptor levels, $R_S(0) = 110$, which results in faster complex formation); (ii) while internalisation rate γ_B is shown to be the one playing the most important role for these timescales, second more crucial rates for this descriptor are binding/dissociation rates α_{1+} and α_{1-}, with similar elasticities (but with different elasticity sign, representing the fact that faster binding leads to shorter timescales, while faster dissociation leads to longer timescales); (iii) the recycling of receptors from the endosome

can have an important role for the timescales of ligand depletion under low synapse availability of receptors, which corresponds to the mature case when no receptor synthesis has occurred yet ($R_S(0) = 11$); (iv) the binding rate α_{1+} is the most important parameter in order to explain the signal peak represented by descriptor $E[B_{\mathbf{n}}^{max}]$, so that its corresponding elasticity is, at least, one order of magnitude larger than the elasticities corresponding to the rest of parameters; (v) the second most important parameter regarding this descriptor corresponds to the dissociation rate α_{1-}, while the role played by other rates (γ_R, γ_B and δ) is only significant under low surface receptor levels; (vi) all the parameters in the system play a more important role on the signal peak under low synapse receptor levels (mature APC with no receptor synthesis represented by $R_S(0) = 11$), while the role played by these parameters highly decreases under high receptor levels.

3.3.4.4 Analogous results for B7-2 ligand

In the present Section, we show the results we obtained by applying our model in Figure 3.6 when considering ligand B7-2 instead of B7-1, so that now n_L represents the amount of B7-2 ligand according to Table 3.5. As previously discussed, the whole procedure developed in Section 3.3.2, can be readjusted in a straightforward but wearisome manner after swapping the condition $n_L \leq n_R$ by $n_L > n_R$. Thus, taking into account values in Tables 3.4-3.5, B7-2 could be used as the ligand in our model. We carry out instead here Gillespie simulations as an approximation of the corresponding analytical values when considering this ligand.

In order to test how the B7-2 ligand depletion dynamics are affected by the total number of CLTA-4 receptors initially on the T cell surface, we plot in Figure 3.11 the B7-2 ligand depletion timescales for a mature APC interacting with a T cell, for different values $R_S(0) \in \{11, 22, 55, 110\}$ of CTLA-4 receptors on the cell surface. These timescales are computed and plotted in Figure 3.11 in terms of the average time $E[T_{\mathbf{n}}^{n_L - I}]$ to have $n_L - I$ B7-2 ligands internalised, for $1 \leq I \leq n_L$, which is computed here by means of Gillespie simulations. We note first that timescales for B7-2 ligand depletion are significantly larger than the timescales for B7-1 ligand depletion ($7.5 - 9$ minutes for total B7-1 ligand depletion in Figure 3.9 (top), versus $65 - 150$ minutes for total B7-2 ligand depletion in Figure 3.11). We point out here that this difference in these timescales seems to be caused by the different internalisation ability (via CTLA-4) of ligands B7-1 and B7-2. Total B7-1 ligand depletion occurs always in less than 10 minutes, regardless of the CTLA-4 surface receptor levels and the type of APC under study. For ligand B7-2, the saturation behavior observed for

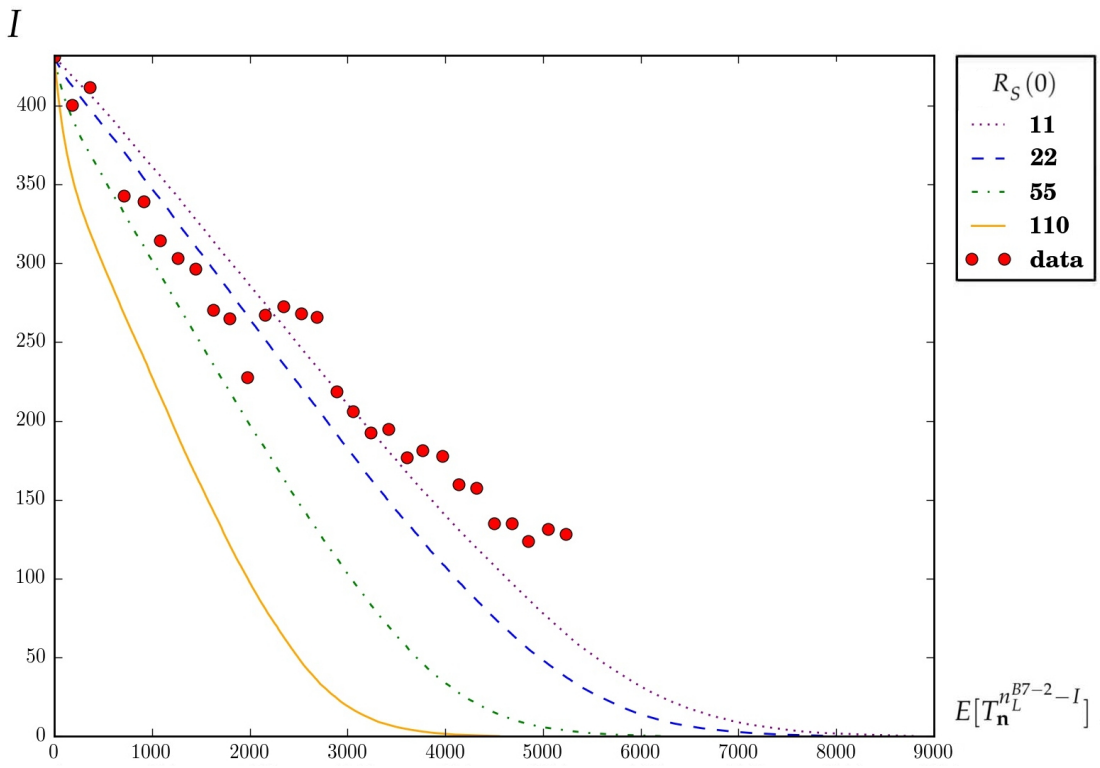

Figure 3.11: Ligand depletion represented by the mean time $E[T_{\mathbf{n}}^{n_L-I}]$ (in *seconds*) to reach a threshold number $n_L - I$ of internalised B7-2 ligands through CTLA-4 binding, versus $1 \leq I \leq n_L$. Consideration of a T cell interacting with a mature APC, for initial CTLA-4 receptor numbers on the synapse equal to 11, 22, 55 and 110. Data from [54, Supplementary Material, Figure S4 B (left)] are also plotted with only first dot is fitted.

B7-1 regarding the surface receptor levels is not observed, and higher synapse CTLA-4 receptor levels always result in a reduction for the timescales of B7-2 ligand depletion. In particular, a 10-fold increase for the CTLA-4 receptor levels via synthesis can result in a reduction of more than 50% for the time to total B7-2 ligand depletion ($\sim$ 150 minutes for $R_S(0) = 11$ against less than 75 minutes for $R_S(0) = 110$ in Figure 3.11).

Moreover, Figure 3.11 allows us to compare the B7-2 ligand depletion timescales obtained from our model with data in [54, Supplementary Material, Figure S4 B (left)]. In these experiments, mean B7-2 GFP fluorescence was measured and plotted in an intensity scale on the APC varying from 35 to 10 over the same timescale represented in Figure 3.11. By comparing the amount of ligands lost from the APC to that internalised by the T cell in the model and assuming a

correspondance from what happens in the synapse on a one to one interaction to what occurs in the whole cell when a bunch of them are cultured in the experiment, a similar slope can be appreciate, at least, in a qualitative manner. Moreover, some of the quantitative differences between our model predictions and the data might be explained by the role played by the other players (B7-1 and CD28) in the co-stimulatory system, as discussed in Section 3.3.5.

In Figure 3.12 the probability distribution for the maximum number $B_{\mathbf{n}}^{max}$ of CTLA-4/B7-2 bound complexes simultaneously present on the synapse is plotted for different initial CTLA-4 synapse levels, and for a T cell interacting with a mature or immature APC. Formation of CTLA-4/B7-2 bound complexes is limited in these scenarios by the availability of CTLA-4 receptors on the synapse. Thus, increasing the initial number of CTLA-4 receptors on the synapse clearly increases this maximum. On the other hand, some contribution for the formation of these complexes is given by the recycling of receptors from the endosome to the synapse, which can be noticed from the fact that, when a total number $R_S(0) = 11$ of CTLA-4 receptors is considered initially on the synapse, the distribution of $B_{\mathbf{n}}^{max}$ concentrates among values 15 to 30, which necessary implies as a prerequisite the recycling of some receptors. Formation of bound complexes does not significantly changes between the mature and immature case, although some differences can be noticed for higher numbers of CTLA-4 receptors initially on the synapse. This is related to the fact that, once availability of CTLA-4 receptors on the synapse is ensured, the availability of B7-2 ligands plays a more important role (and the immature APC contains less than half of the B7-2 ligands than the mature APC). Moreover, and as expected, a more deterministic behavior can be observed for the different distributions corresponding to larger amounts of molecules in Figure 3.12, given by smaller variances for these distributions.

3.3.5 Discussion

In the present Chapter, we introduce a stochastic model to study, in an analytical way, diverse dynamics of the main inhibitory co-receptor when interacting with ligands from an APC. In Section 3.3 we have carried out a detailed analysis for studying the ligand depletion timescales and the receptor-ligand complex formation dynamics, when a mature or an immature APC interacts with a T cell, and when this co-stimulation process occurs at different activation stages resulting in different CTLA-4 molecular levels on the synapse. We could observe in Section 3.3.4 that increasing CTLA-4 receptor levels result in a decrease of the timescales for B7-1 ligand depletion (Figure 3.9), where saturation scenarios are found for CTLA-4 receptor levels increases

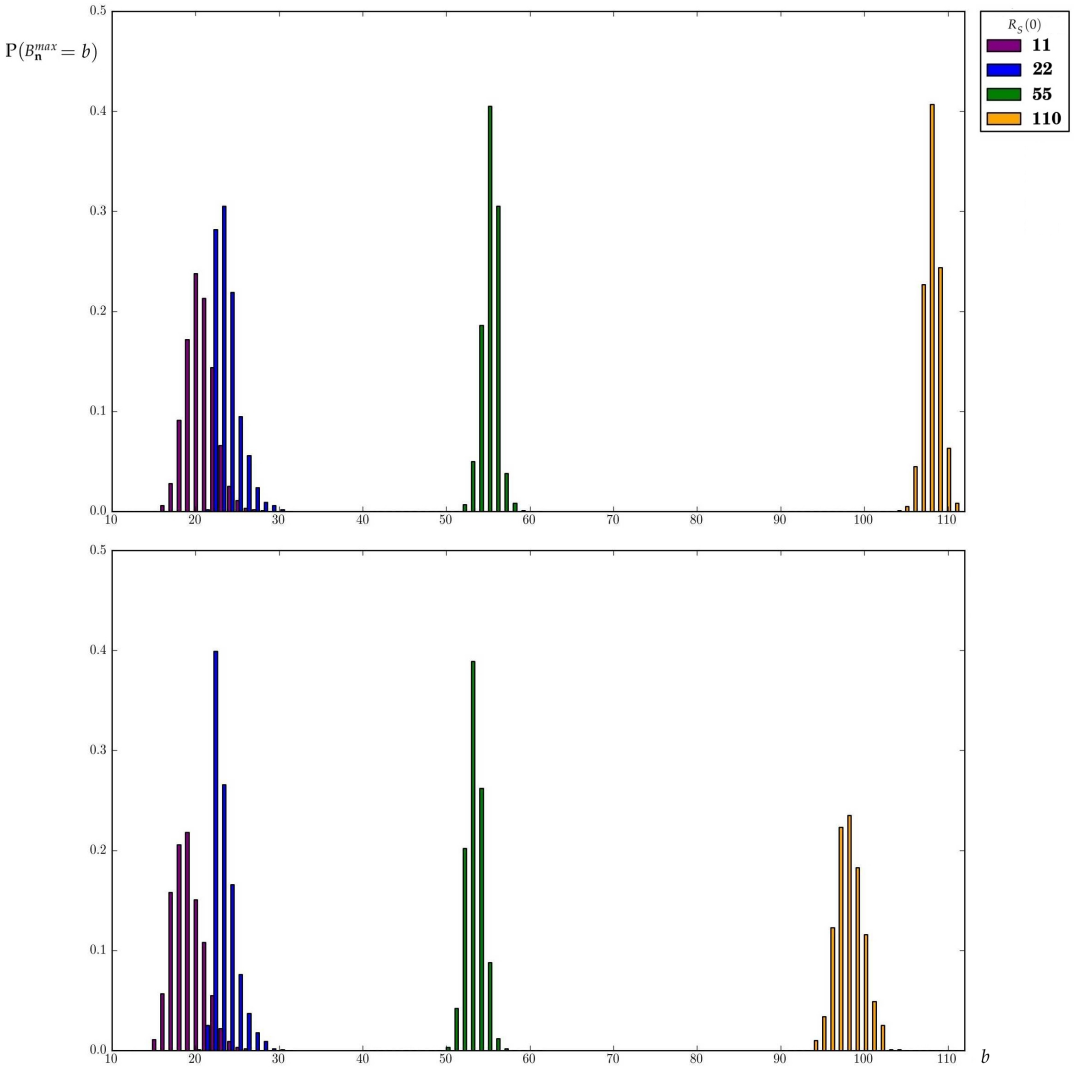

Figure 3.12: Probability mass function of the maximum number $B^{max}_{\mathbf{n}}$ of CTLA-4/B7-2 bound complexes simultaneously present on the synapse, for a T cell interacting with a mature (*top*) or immature (*bottom*) APC, and for initial CTLA-4 receptor numbers on the synapse equal to $R_S(0) \in \{11, 22, 55, 110\}$. Initial conditions $\mathbf{n}$ for the total number of each molecule chosen according to values in Tables 3.4-3.5.

higher than 2-fold ($R_S(0) \in \{55, 110\}$). This saturation behavior is not observed when analysing B7-2 ligand depletion (Figure 3.11), where increases in the CTLA-4 receptor levels always result in decreases for the ligand depletion timescales.

When analysing CTLA-4/B7-1 complex formation, our results in Figure 3.10 show a significant variation in the way CTLA-4 binds B7-1 depending on the initial synapse receptor levels. Given that association and dissociation rates for these molecules are much higher than CTLA-4 intracellular trafficking rates, the initial location of this receptor before ligand stimulation makes a significant difference in the dynamics analysed in Figure 3.10, which can be shown by studying the values of $E[B_{\mathbf{n}}^{max}]$ and $Var[B_{\mathbf{n}}^{max}]$ in Table 3.7 as a summary of the distributions plotted in Figure 3.10, where $Var[X]$ represents the variance of the random variable X. High synapse receptor levels correspond to a mean maximum amount $E[B_{\mathbf{n}}^{max}] \sim n_L$ of ligands simultaneously bound on the synapse, whereas the behavior for low levels regarding this descriptor varies depending on the kind of APC participating in the interaction.

Our results regarding B7-1 ligand depletion timescales in Figure 3.9 suggest that the lifetime of the last ligand present on the synapse is below ten minutes, while we have in just five minutes around 80% of them internalised into the endosome, which agrees with previous experimental knowledge [76]. Diverse scenarios involving different types of APCs and different T cell synapse receptor levels produce very similar timescales regarding this internalisation process, which is particularly striking when doubling the number of available ligands. This would imply that the time until having an inhibitory signal, if this signal depended on the complete internalisation of the available B7-1 ligands via binding the co-receptor CTLA-4, would be more affected by the concentration of CTLA-4 than by the concentration of B7-1.

Finally, results in Table 3.8 allow us to analyse the effect that each kinetic rate has on the descriptors previously computed. When analysing the role played by each kinetic rate on the CTLA-4/B7-1 interaction dynamics, kinetic rate α_{1+} seems to play a crucial role, specially under low receptor levels. Moreover, the recycling rate δ plays an important role under low CTLA-4 receptor levels on the cell surface, since recycling is, under these scenarios, a prerequisite for other interactions to take place. On the other hand, if an enough number of CTLA-4 receptors is initially on the synapse ($R_S(0) = 110$ due to synthesis), the importance of recycling dynamics clearly decreases.

3.4 A four compartment model

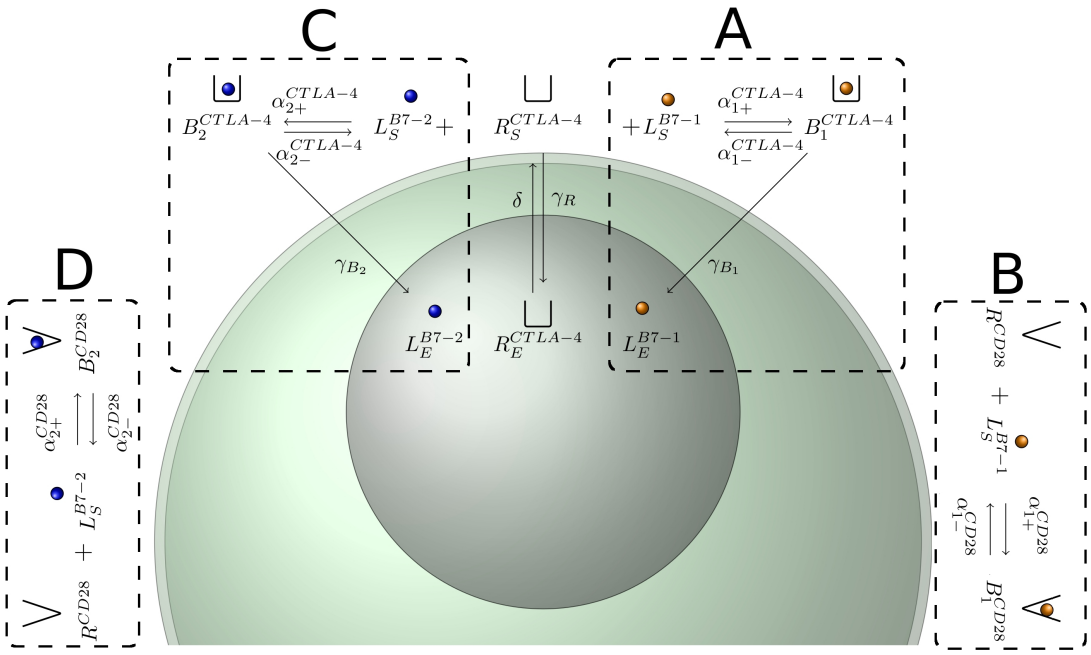

Figure 3.13: Compartmentalised stochastic model. **A**: formation and internalisation of bound CTLA-4/B7-1 complexes. **C**: formation and internalisation of bound CTLA-4/B7-2 complexes. **B**: formation of bound CD28/B7-1 complexes. **D**: formation of bound CD28/B7-2 complexes. Molecular levels from Tables in Section 3.3.3, where now n_L^{B7-1}, n_L^{B7-2}, n_R^{CD28} and n_R^{CTLA-4} refer to levels for B7-1 and B7-2 ligands, and CD28 and CTLA-4 receptors, respectively.

Understanding the mechanisms which allow CTLA-4 and CD28 to regulate T cell responses requires a mathematical procedure analysing the interaction between the main molecules involved in the co-stimulatory system. Moreover, recent studies support the crescent idea of quantifying the triggering signal, from TCR stimulation to CD28 co-signal, as a cascade path which efficiency would depend on this triggering signal occurring faster than a dwell time for the contact between the APC and the T cell.

A general stochastic model presented in Figure 3.13 allows us to quantify how fast this co-stimulation process occurs depending on the concentrations of co-receptors CTLA-4 and CD28, and ligands B7-1 and B7-2 interacting within the synapse at different stages of T cell activation, and for a T cell interacting with an immature or mature APC. By making use of the compartmental model in Figure 3.13, we can analyse similar characteristics in the underlying Markov chain (regarding ligand depletion timescales, receptor-ligand complex formation and steady-state

characteristics) when the different four molecules are introduced and removed one at a time. When only compartment **A** is considered, these characteristics can be exactly analysed via the techniques developed in Section 3.3.2, and the corresponding Algorithms in Section 3.3.2.6. A particular feature of this analytical approach is that it allows us to study the impact that each kinetic rate has on the descriptors of interest, via the computation of partial derivatives. However, for the dynamics of the process when more than one compartment is considered in Figure 3.13, Gillespie simulations are implemented instead in order to compute our results, given the increasing complexity of this general model and computational limitations of algorithms in Section 3.3.2.6.

For model in Figure 3.13, a total number $n_R^{CD28} = 256$ of CD28 is considered on the synapse [30], and binding and dissociation rates for CD28 with ligand B7-1 and B7-2 are $\alpha_{1+}^{CD28} = 0.034s^{-1}$, $\alpha_{1-}^{CD28} = 1.6s^{-1}$, $\alpha_{2+}^{CD28} = 0.061s^{-1}$ and $\alpha_{2-}^{CD28} = 28s^{-1}$ [30]. In order to analyse the impact that introducing any other molecule (B7-2, CD28) has on the B7-1 ligand depletion dynamics, we compute in Figure 3.14 the analogous results than those ones in Figure 3.9 regarding the time to reach a threshold number $n_L^{B7-1} - I$ of internalised B7-1 ligands via CTLA-4 binding, where compartments **A**, **A+B**, **A+C** and **A+B+C+D** are considered for a T cell interacting with a mature APC, and with $R_S^{CTLA-4}(0) \in \{11, 110\}$. Ligand B7-2 (introduced by compartment **C**) seems to have a greater impact on the B7-1 ligand depletion dynamics in comparison with co-receptor CD28 (introduced by compartment **B**). However, it is worth to highlight how this mean time $E[T_{\mathbf{n}}^{n_L^{B7-1}-I}]$ is specially perturbed when both molecules are introduced at the same time (compartments **A+B+C+D**) compared to the slighter difference provoked by the individual presence of CD28 or B7-2. This suggests that there exists a significant synergy between the CD28 co-receptor and the B7-2 ligand for slowing down not only the binding (see Figure 3.15 where this synergistic behavior can also be identified for the receptor-ligand CTLA-4/B7-1 complexes formation), but also the internalisation dynamics of the CTLA-4/B7-1 bound complexes. The presence of competitor molecules CD28 and B7-2 can increase the time for total B7-1 ligand depletion from $\sim$ 9 minutes (compartment **A** in Figure 3.14 (top)) up to $\sim$ 43 minutes (compartments **A+B+C+D** in Figure 3.14 (top)). However, if synthesis of CTLA-4 receptor results in a 10-fold increase for the synapse receptor levels ($R_S^{CTLA-4}(0) = 110$), then this difference is highly attenuated: $\sim$ 7.5 minutes for total B7-1 ligand depletion for compartment **A** in Figure 3.14 (bottom), against $\sim$ 19 minutes for total B7-1 ligand depletion for compartments **A+B+C+D** in Figure 3.14 (bottom).

We analyse in Figure 3.15 how CTLA-4/B7-1 complex formation dynamics are affected by the

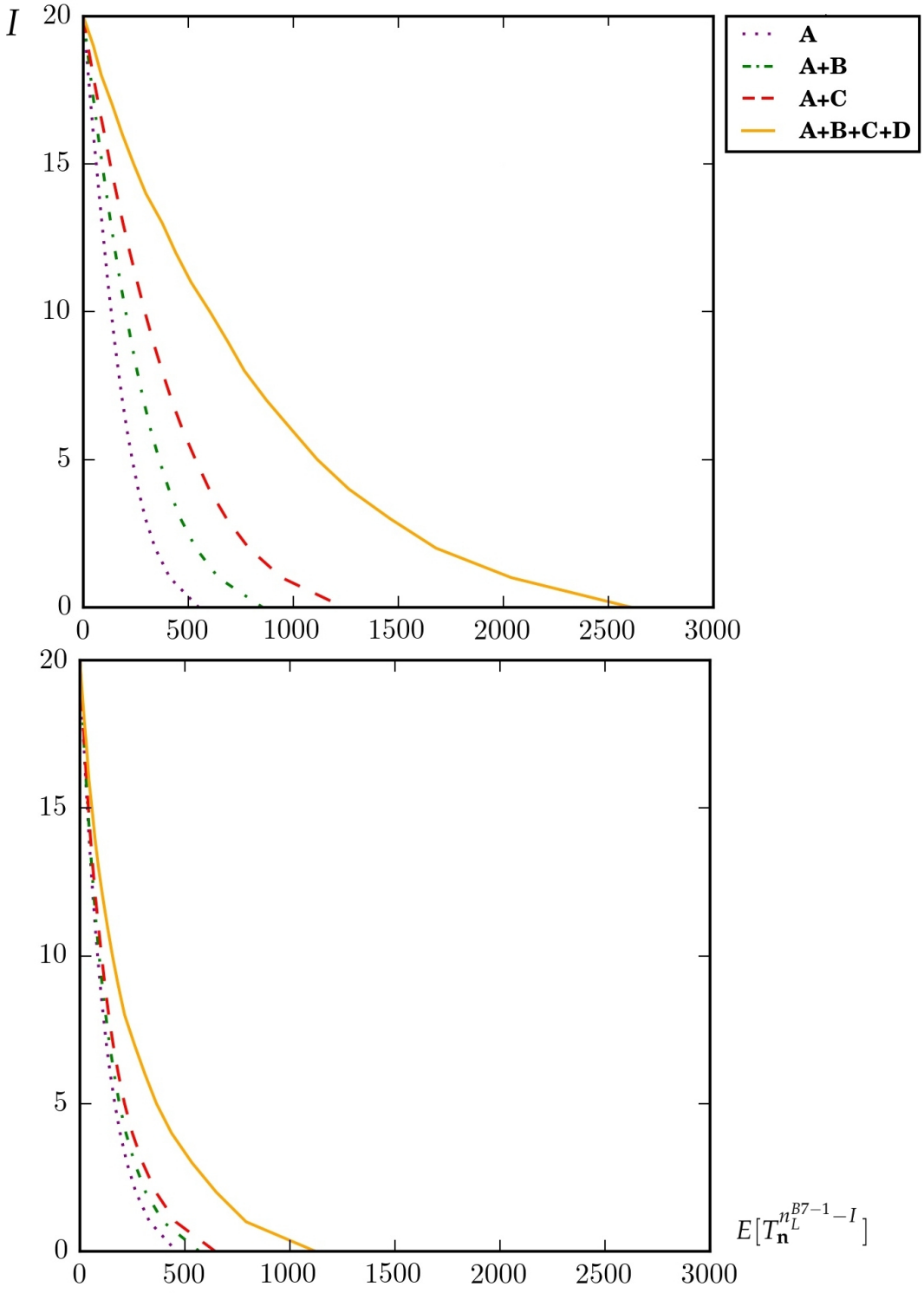

Figure 3.14: Mean time $E[T_{\mathbf{n}}^{n_L^{B7-1}-I}]$ (in *seconds*) to reach a threshold number $n_L^{B7-1} - I$ of internalised B7-1 ligands via CTLA-4 binding versus $1 \leq I \leq n_L^{B7-1}$, for compartments **A**, **A+B**, **A+C** and **A+B+C+D**. Initial conditions **n** for the total number of each molecule are taken from Tables 3.4-3.5. T cell interacting with a mature APC, for CTLA-4 receptor numbers initially on the synapse equal to 11 (*top*) and 110 (*bottom*).

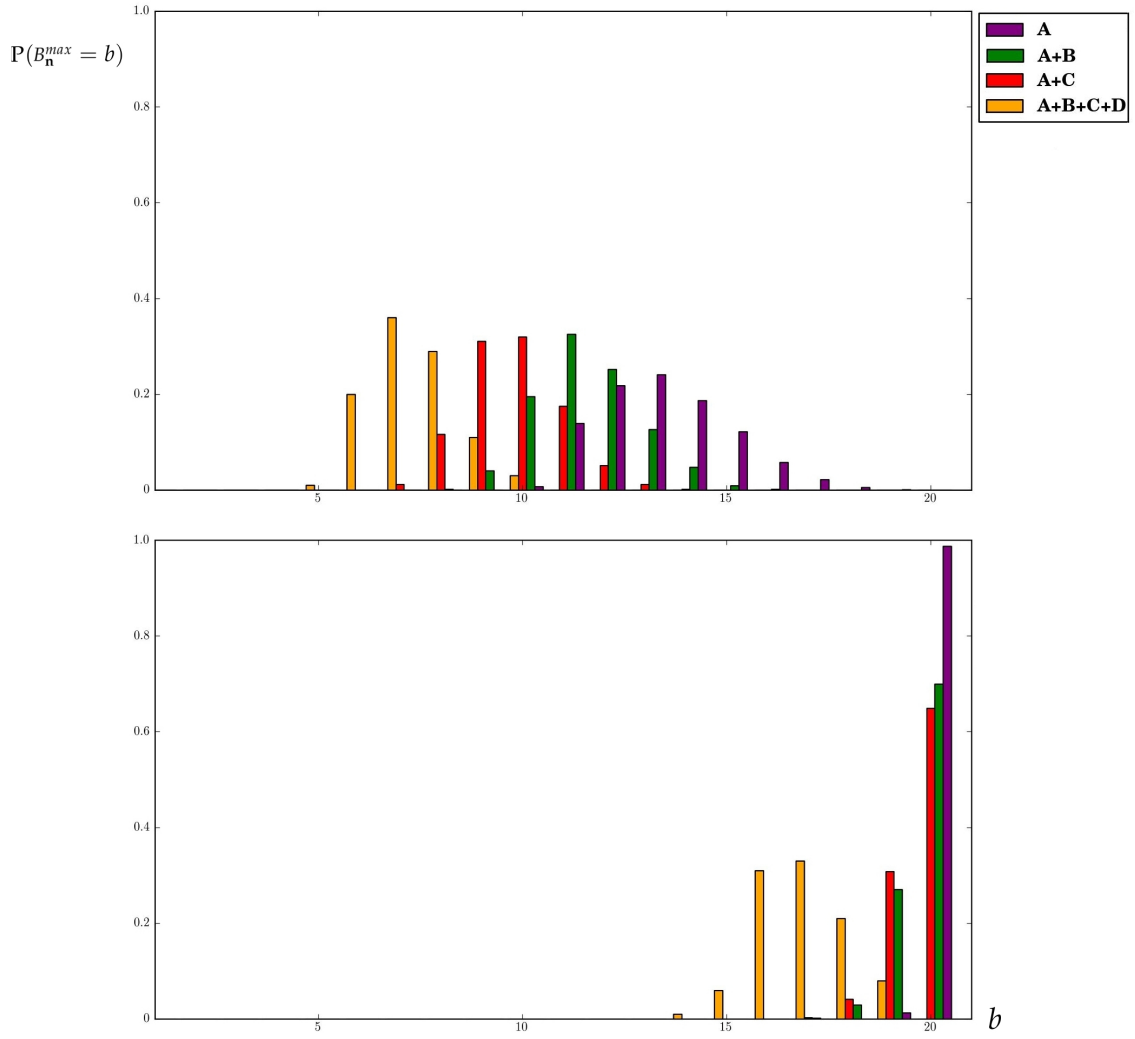

Figure 3.15: Probability mass function of the maximum number $B_{\mathbf{n}}^{max}$ of CTLA-4/B7-1 bound complexes simultaneously present on the synapse, for compartments **A**, **A+B**, **A+C** and **A+B+C+D**. Initial conditions **n** for the total number of each molecule are taken from Tables 3.4-3.5. T cell interacting with a mature APC, for initial CTLA-4 receptor numbers on the synapse equal to 11 (*top*) and 110 (*bottom*).

introduction of competitor molecules, by means of considering compartments **A** ,**A+B**, **A+C** and **A+B+C+D**. Main conclusion from these results is the synergistic behavior observed between co-receptor CD28 and ligand B7-2 for avoiding formation and internalisation of bound CTLA-4/B7-1 complexes. The internalisation timescales observed in these results represent an increase of around $2-3$ times for the time required to internalise B7-1 via CTLA-4 binding under scenario **A+B+C+D** compared to scenarios without CD28 and/or without B7-2.

$R_S(0)$	**Bound complex**	**CTLA-4/B7-1**	**CTLA-4/B7-2**	**CD28/B7-1**	**CD28/B7-2**
11	$E[B_{\mathbf{n}}^{max}]$	7.22	15.27	18.65	132.32
	$Var[B_{\mathbf{n}}^{max}]$	0.87	6.02	0.64	4.56
110	$E[B_{\mathbf{n}}^{max}]$	16.91	96.52	10.22	118.47
	$Var[B_{\mathbf{n}}^{max}]$	1.28	3.15	0.23	4.91

Table 3.9: Mean and variance of the maximum number $B_{\mathbf{n}}^{max}$ of bound complexes simultaneously present on the synapse for scenario **A+B+C+D**, and regarding bound complexes CTLA-4/B7-1, CTLA-4/B7-2, CD28/B7-1 and CD28/B7-2. **n** represents the initial state of process in Figure 3.13 given from Tables 3.4-3.5, and we consider a T cell interacting with a mature APC, for initial numbers of CTLA-4 receptors on the synapse equal to 11 and 110.

We can complement data in Figure 3.15 by results in Table 3.9, where we compute the mean and the variance of the maximum number of bound complexes CTLA-4/B7-1, CTLA-4/B7-2, CD28/B7-1 and CD28/B7-2 for both activation stages represented by $R_S(0) = 11$ and $R_S(0) = 110$, for a non-regulatory T cell interacting with a mature APC, and when the four molecules are considered within the synapse at the same time (scenario **A+B+C+D**). Our results suggest that the formation of complexes involving the B7-2 ligand is even more influenced by the initial surface receptor levels than when considering complex formation involving the B7-1 ligand. The significant formation of bound CD28/B7-2 complexes, which are the most common bound complexes in both scenarios, could be considered as contradictive with the synergistic effect observed before for CD28 and B7-2 in disrupting formation of CTLA-4/B7-1 complexes; that is, if co-receptor CD28 and ligand B7-2 tend to bind each other according to Table 3.9, it should be expected that the separate presence of each of them should affect more the dynamics of CTLA-4 and B7-1 than the presence of both of them at the same time. However, the unstable nature of bound CD28/B7-2 complexes represented by $\alpha_{2-}^{CD28} = 28s^{-1}$ needs to be taken into account.

Therefore, we can conclude that competitor molecules for B7-1 (*i.e.*, receptor CD28 and ligand B7-2) have a significant effect in B7-1 ligand depletion timescales. On the other hand, numerical results carried out but not reported here regarding B7-2 ligand depletion timescales suggest that these timescales are not so significantly affected by competitor molecules for B7-2 (B7-1 and CD28). Moreover, the introduction of B7-2 into the system has a higher effect than the introduction of CD28 on the dynamics of CTLA-4/B7-1, both regarding the B7-1 ligand depletion and the CTLA-4/B7-1 complex formation, but the introduction of both molecules (B7-2 and CD28) at the same time results into a synergistic effect significantly affecting CTLA-4/B7-1 dynamics.

3.4.1 Cell extrinsic regulator mediation

Once TCR signalling has been triggered by MHCp in the synapse area between a T cell and an APC, a competition process takes place between inhibitor CTLA-4 and CD28 co-receptors for ligands B7-1 and B7-2 from the APC. However, the strength of CD28 co-signal is thought to be limited by CTLA-4 not only because of the fact of sharing ligands but also for a cell extrinsic regulator process in which CTLA-4 would deplete ligands from and APC(B7-1,B7-2) in a way that this APC would become and APC*(B7-1,B7-2) with a presumably lower capacity for future stimulations due to a decrease of ligand expression.

Under this scenario, we want to quantify this loss of efficiency by measuring how molecules in the APC* were depleted depending on different conditions as the type of T cell that the APC interacted to or on the time of this interaction. With respect to the first condition, an important distinction has to be done between Regulatory and non-regulatory T cells. CD28 is considered to be, as the other three molecules, homogeneously distributed in the cells, and not to vary from one kind of T cell to the other. On the other hand, for the CTLA-4 receptor, we first note that its spatial distribution corresponds to $90\% - 10\%$ (endosome-surface) in non-regulatory T cells at any given time. Thus, and according to [30], which parameters regarding expression levels are gathered in Table 3.3, 400 CTLA-4 receptors are on the cell surface (of which $\sim$ 11 correspond to receptors on the synapse, according to synapse area and T cell radius), while 3600 are into the endosome ($\sim$ 100 corresponding to those ones trafficking to the synapse). Following T cell activation CTLA-4 is synthesised, resulting in a temporary proportional increase at the cell surface [68]. To represent different time instants after activation when synthesis may have occurred, we consider total numbers of CTLA-4 receptors within the synapse equal to 11, 22, 55 and 110 (representing 2-, 5- or 10-fold increases with respect steady-state conditions before activation, respectively). These assumptions yield the total number of co-receptors given in Table 3.4, and their initial spatial distribution. A similar analysis yields the total number of ligands provided by the donor cell, which is given in Table 3.5.

If we consider initial values for a mature APC(B7-1,B7-2) as appear in Table 3.5, for the different values of $R_S^{CTLA-4}(0)$, the mean number of molecules of each kind can be computed at different time points (900, 1800, 3600 s) which will indicate the time of contact between the regulatory T cell and the APC(B7-1,B7-2). The mean values of the ligands will be then the initial values of the new APC$^*(E[L^{B7-1}], E[L^{B7-2}])_{900}$, APC$^*(E[L^{B7-1}], E[L^{B7-2}])_{1800}$,APC$^*(E[L^{B7-1}], E[L^{B7-2}])_{3600}$. Table 3.10.

	110R			155R			210R		
	900s	1800s	3600s	900s	1800s	3600s	900s	1800s	3600s
$E[R_S^{CTLA-4}]$	0.82	1.21	2.39	1.5	2.63	7.51	3.27	6.27	20.06
$E[R^{CD28}]$	159.04	175.67	206.73	172.24	195.21	238.86	190.45	221.91	254.73
$E[L^{B7-1}]$	1.4	0.33	0.02	0.48	0.08	0	0.21	0	0
$E[L^{B7-2}]$	267.55	212.14	109.71	218.52	143.05	32.38	158.95	71.38	2
$E[B_1^{CTLA-4}]$	1.11	0.34	0.01	0.77	0.17	0	0.37	0.01	0
$E[B_2^{CTLA-4}]$	9.11	9.49	8.67	13.25	12.78	7.77	17.59	14.67	1.43
$E[B_1^{CD28}]$	4.37	1.03	0.06	1.83	0.17	0	0.73	0.02	0
$E[B_2^{CD28}]$	92.59	79.3	49.21	81.93	60.62	17.14	64.82	34.07	1.27
$E[L_{int}^{B7-1}]$	13.12	18.3	19.91	16.92	19.58	20	18.69	19.97	20
$E[L_{int}^{B7-2}]$	61.75	130.07	263.41	117.3	214.55	373.71	189.64	310.88	426.3

Table 3.10: Mean number of molecules and complexes in the synapse after 10^3 simulations of model in Figure 3.13 after 900, 1800 and 3600 s.for three different cases of number of total number of CTLA-4 $R_E^{CTLA-4}(0) + R_S^{CTLA-4}(0) = 110, 155, 210$. Initial values from Tables 3.4-3.5. The mean values of the ligands will be then the initial values of the new APCs. That is $\text{APC}^*(E[L^{B7-1}], E[L^{B7-2}])_{900}$, $\text{APC}^*(E[L^{B7-1}], E[L^{B7-2}])_{1800}$,$\text{APC}^*(E[L^{B7-1}], E[L^{B7-2}])_{3600}$.

With this in hand, Figures 3.16, 3.17 and 3.18 show the dynamics of ligand B7-2 over time under the different values of total CTLA-4, when CD28 fixed. Moreover, data from experiments done in [54] in which they measure the mean fluorescence intensity of B7-2 in both B7-2^+ cells and CTLA-4^+ cells was incorporated to our plots to follow the accuracy of our model. In particular, dots in our plots show the correspondance between the intensity of the green fluorescence marker for B7-2 on average for the APCs, with internalisation of such ligand in the T cells.

3.4.1.1 Varying the amount of both ligands.

In this Section, numerical results were obtained supposing that the number of ligands varies with respect to the amount of receptors. If, for instance, this number increases two times, in which case, $n_L^{B7\text{-}1} = 40$ and $n_L^{B7\text{-}2} = 862$, Figure 3.16 shows a plausible situation (according to internal discussions with experimentalists) in which an increase of ligands might have accidentally occurred.

Furthermore, when equally decreasing the amount of ligands by dividing rates in Table 3.5 (mature case) by two, what Figure 3.17 shows is a minor tracking of data from [54], which is here rescaled since it comes in relative terms as explained in Section 3.3.4. Given that the number of complexes is the same for both Figures 3.16 and 3.17, effectively there is a more inclined slope as the amount of ligands gets reduced.

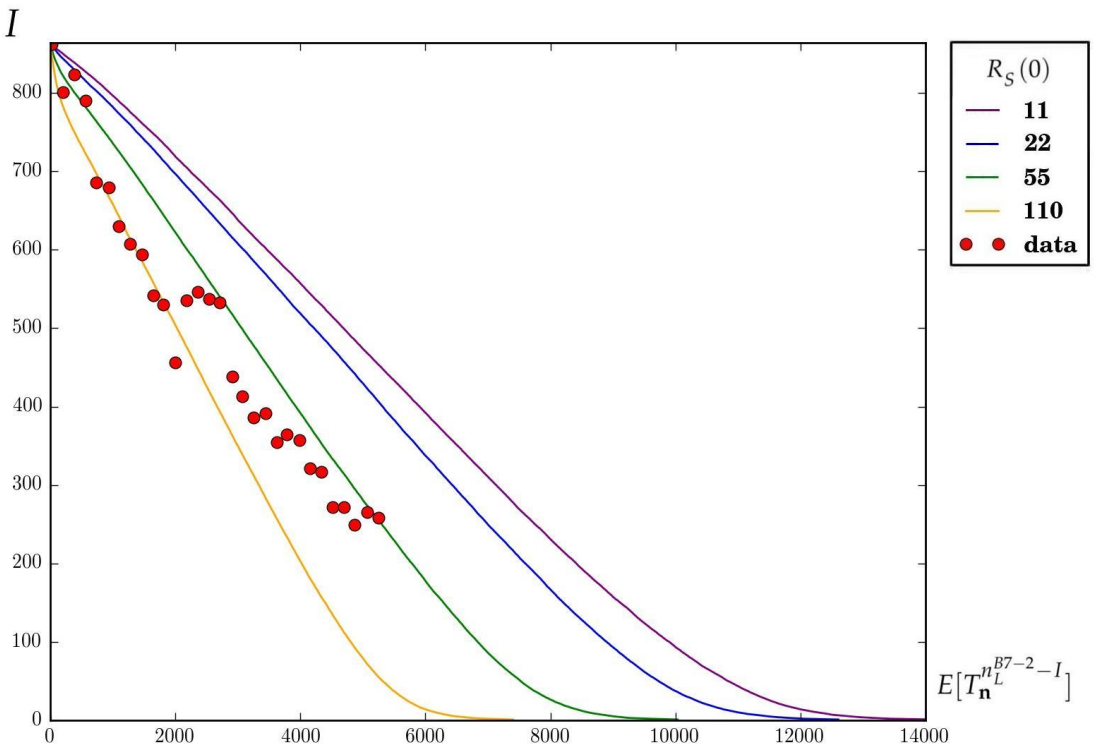

Figure 3.16: Time dynamics (in *seconds*) of B7-2 when the number of ligads given in Table 3.5 (mature case) is multiplied by two under different scenarios. Data from [54, Supplementary Material, Figure S4 B (left)] are also plotted with only first dot is fitted..

3.4.1.2 Varying the ratio $r_{\frac{1}{2}}$.

But it can also happen that what varies at a given time is the rate between the two ligands in charge of costimulation. Thus, if the total amount of ligands gets fixed as

$$n_L^T = n_L^{B7\text{-}1} + n_L^{B7\text{-}2} = 451,$$

for the initial scenario (Table 3.5, mature case), the ratio $r_{\frac{1}{2}} = \frac{n_L^{B7\text{-}1}}{n_L^{B7\text{-}2}}$ modifies to provide several possibilities in which the proportion of both ligands can be altered. Therefore, the amount of initial ligands in each case is given by

$$n_L^{B7\text{-}1} = r_{\frac{1}{2}} \cdot n_L^T$$
$$n_L^{B7\text{-}2} = (1 - r_{\frac{1}{2}}) \cdot n_L^T$$

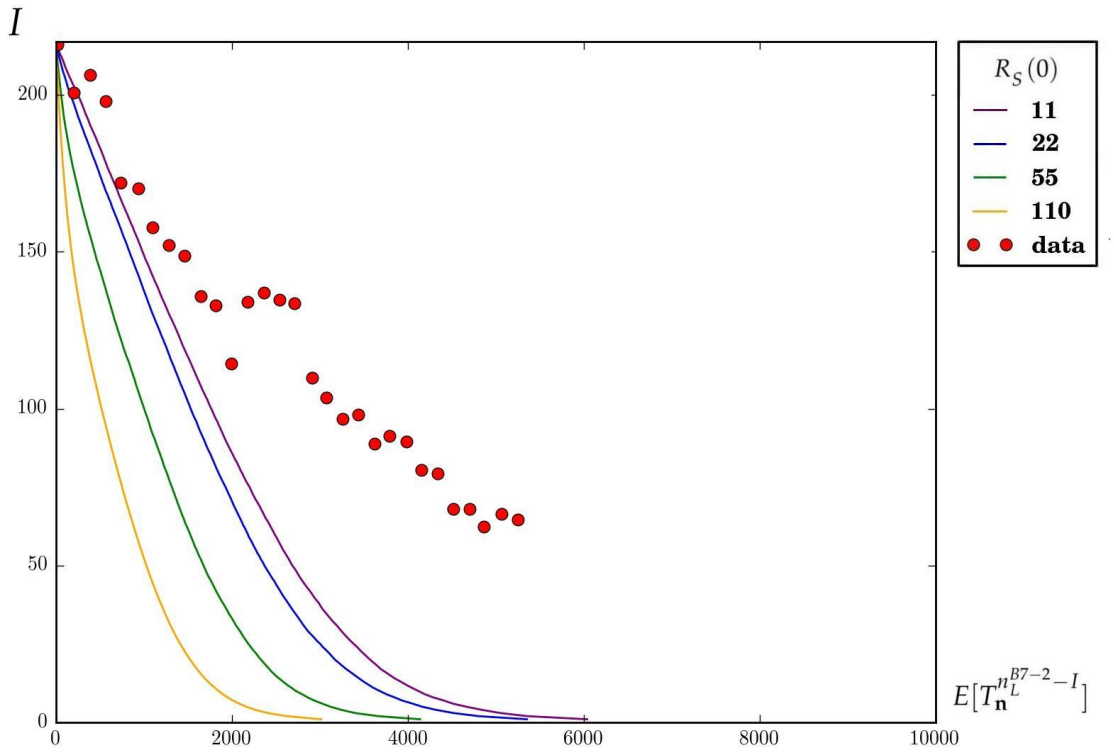

Figure 3.17: Time dynamics (in *seconds*) of B7-2 when the number of ligads given in Table 3.5 (mature case) is divided by two under different scenarios and. Data from [54, Supplementary Material, Figure S4 B (left)] are also plotted with only first dot is fitted.

And computing the model for the cases $r_{\frac{1}{2}} \in \{0.1, 0.25, 0.5, 0.75\}$ plots are given in Figure 3.18.

Figure 3.18 shows internalisation of B7-2 when varying the ratio $r_{\frac{1}{2}}$ according to expression (3.17). Interestingly, the time taken for the whole amount of B7-2 to become internalised is not significantly altered depending on the initial quantity of such type of ligand as long as there is a compensation of the amount of B7-1 involved in the process. This statement relies not only on the similar time for this process to finish (around $4 \cdot 10^3$ to $8 \cdot 10^3$ (*seconds*) depending on the initial amount of receptors on the surface $R_S(0)$ for the four plots in Figure 3.18) but on how different this time is from Figure 3.16 to Figure 3.15 (from around $1.4 \cdot 10^4$ to $6 \cdot 10^3$ (*seconds*) when $R_S(0) = 11$), where the amount of B7-1 is proportionally reduced or augment with the amount of B7-2. This seems to confirm that competition really exists and can be quantified having into account, as Figures 3.4 and 3.5 show, that each ligand has a constant amount of receptors occupied

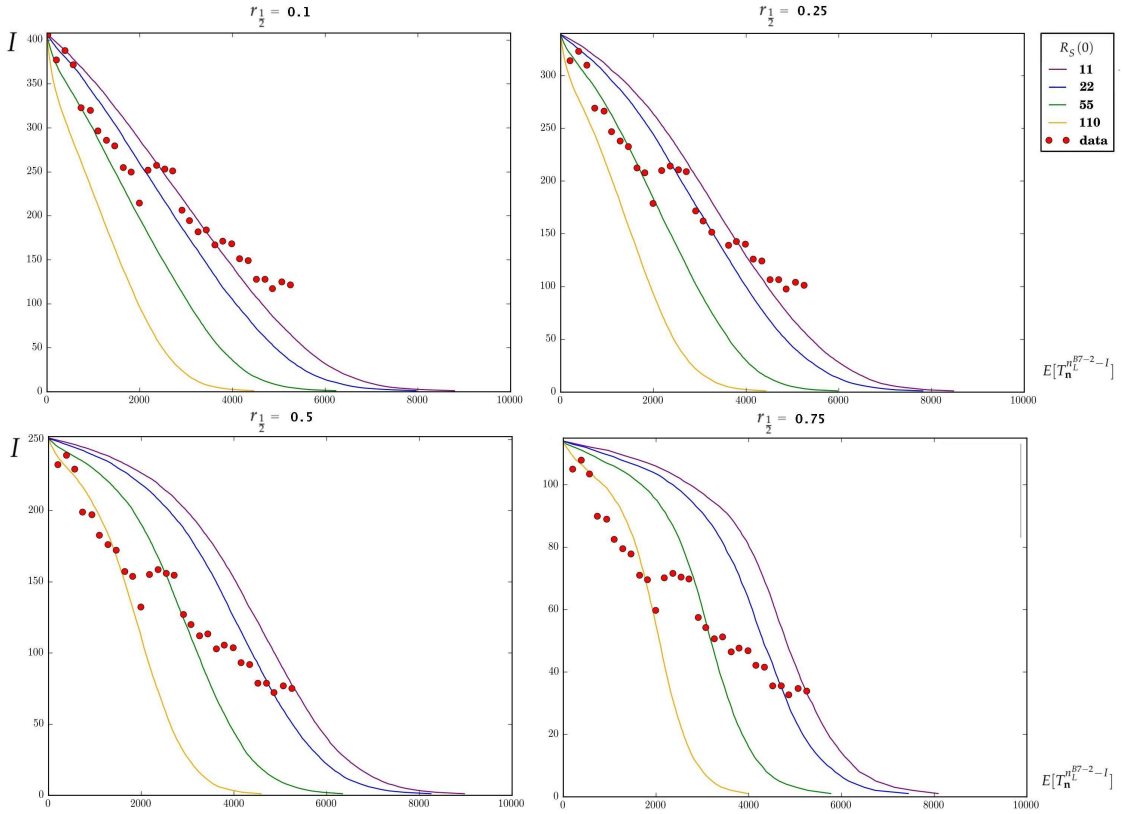

Figure 3.18: Time dynamics (in *seconds*) of B7-2 when varying the ratio $r_{\frac{1}{2}}$ and for different scenarios. Data from [54, Supplementary Material, Figure S4 B (left)] are also plotted with only first dot is fitted.

from very early and that free receptors, as long as there are ligands, do not last too long without binding.

On the other hand, the slope for each graph in Figure 3.18 is quite different depending on $r_{\frac{1}{2}}$. When the rate between B7-1 and B7-2 $r_{\frac{1}{2}}$ is high, case right down, it takes longer for the first B7-2 to internalise but after certain time the speen is higher than in other cases. However, as the rate $r_{\frac{1}{2}}$ gets reduced, B7-2 internalisation is more constant.

Chapter 4

Quorum-sensing model

4.1 Introduction

Regulatory $CD4^+$ T cells (**T regs**) play a central role in establishing self-tolerance and in preventing autoimmune diseases. The mechanisms in which this T cell subpopulation regulates the size number of the $CD4^+$ T cell pool have been recently hypothesised through different approaches [5, 60]. A quorum-sensing like model, in which homeostasis is based in the ability of certain populations to perceive their own expression levels proliferating consequently, is followed in this chapter.

As explained in Chapter 2, Interleukin 2 (IL-2), a cytokine mainly secreted for effector $CD4^+$ T cells (**IL-2 producer**), can bind with high affinity to receptor CD25, which characterises, together with transcriptor factor FOXP3, regulatory $CD4^+$ T cells [11]. Therefore, in this quorum-sensing mechanism three different T cells subpopulations are considered: IL-2 producers, regulatory T cells, which depend on IL-2 to proliferate and survive, and a third group of $CD4^+$ that excludes the other two (**Total $CD4^+$ -** {**IL-2 producer/T reg**}).

One of the main distinctive points about this chapter has to do with the fact that real data were specifically obtained for the common purpose of analysing the hypotheses explained beforehand in a shared project with immunologists from Pasteur Institute in Paris, as part of the European Network in Quantitative immunology (QuanTI Network). Data shown in the present chapter belong to Pasteur Institute and the University of Leeds group as was stated in the agreement.

The present chapter is organised in the following manner: First, a statistical analysis (Sections 4.2

and 4.3) is carried out based on a set of experiments done in Pasteur Institute of Paris regarding this phenomenon. In particular, two scenarios under different infections and conditions with the purpose of providing in vivo results to support or refute what has already been observed ex vivo. A deterministic mathematical model is introduced in Section 4.4 to contrast distinct hypotheses in the mechanisms that drive quorum-sensing, to provide estimations on which parts of the process might be more relevant or to observe if the behaviour obtained in the experiments can be reproduced, and under which circumstances. In order to do so, Section 4.5 brings a global sensitivity analysis to distinguish those parameters with a stronger effect to take into consideration for further analysis. Thus, once these parameters are identified, Section 4.6 explains a parameter estimation process in which Bayesian techniques are explained and used. Finally, some results and discussions follow in Sections 4.7 and 4.8.

4.2 Lymphopenia driven proliferation

A T-cell receptor (TCR) complex consists on two functional components: the TCR heterodimer, responsible for antigen recognition, and the CD3 complex, in charge of signal transduction. By a genetic technique, mice can have certain specific genes in-operated so, when compared to normal mice (control), conclusions about a specific gene role can be determined. CD3 is composed of one extracellular immunoglobulin-like domain CD3γ, CD3δ and two CD3ϵ chains which, together with the two intracellular ζ chains, drive the signalling capacity of T cells [16].

In the present lymphopenia driven proliferation (LDP) set of experiments, both CD3ϵ chains have been blocked in host mice ($CD3\epsilon^{-/-}$ mice) avoiding T cell development. Two different types of reporter mice were used to obtain the T cells injected in the hosts. Out of the four successive experiments following the levels of IL-2 producer T cells, T reg cells and Total $CD4^+$ (excluding IL-2 producers and T reg), $2 \cdot 10^4$ T cells coming from **Tg IL-2/GFP** mice were used for two of them (experiment 1 and experiment 2), whereas $2 \cdot 10^4$ and $5 \cdot 10^4$ T cells coming from **IL-2/Thy1.1** were applied for the two other trials (Figure 4.1).

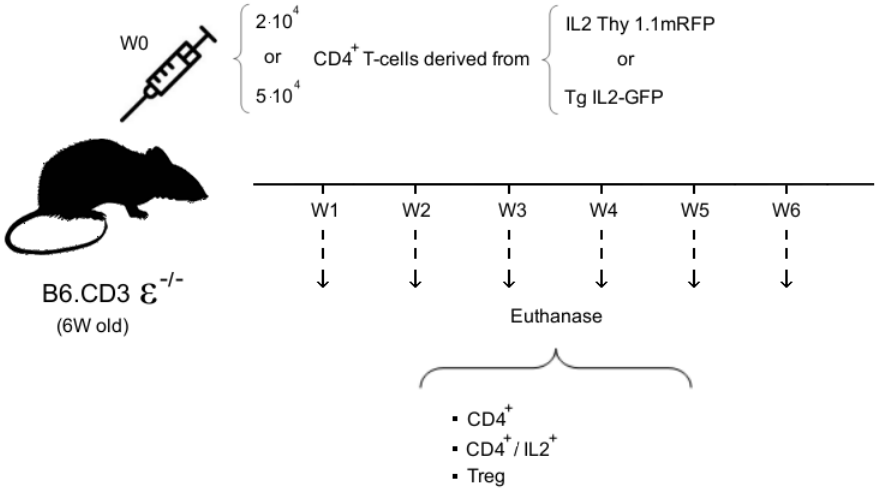

Figure 4.1: Time line for lymphopenia driven proliferation (LDP) experiment in which three or four mice are euthanised each week from the day of the injection until week 6. Each CD3 knockout mouse provides some amount of IL-2 producer cells, regulatory T cells and total $CD4^+$ excluding the previous two groups.

For each of these experiments, either three (experiment 2 and experiment 3) or four (experiment 1 and experiment 4) mice were used every week to analyse their lymphatic organs (spleen and inguinal regions, in this case) so every piece of data (Total $CD4^+$, IL-2 producer, T reg) belongs to a different mouse. In fact, the mouse needs to be killed for the obtaining of the data. Tables 4.1,4.2,4.3,4.4 show the data for the four different LDP experiments obtained in *Pasteur Institute*.

For the purpose of the statistical analysis, let us define

$$x_{ijk} = \text{“Number of } CD4^+ \text{ T cells excluding IL-2 producers and T reg cells for mouse } j, \text{ of experiment } k \text{ at week } i.\text{”}, \tag{4.1}$$

$$y_{ijk} = \text{“Number of IL-2 producers T cells for mouse } j \text{ of experiment } k \text{ at week } i.\text{”}, \tag{4.2}$$

$$z_{ijk} = \text{“Number of T reg cells for mouse } j \text{ of experiment } k \text{ at week } i\text{”}, \tag{4.3}$$

where $1 \leq k \leq 3$, $1 \leq j \leq 4$ (for $k = 1$), $1 \leq j \leq 3$ (for $k = 2, 3$) and $0 \leq i_0 < i_f \leq 6$ (5 for $k = 4$). Vectors can then be arranged as

$$(x_j)_k^{[i_0, i_f]} = (x_{ji_0}, x_{ji_0+1}, ..., x_{ji_f-1}, x_{ji_f})_k \tag{4.4}$$

and, defining $j_f = 3$ (when $k = 1$) or $j_f = 4$ (when $k = 2, 3$), the average value

$$E[x]_k^{[i_0,i_f]} = \frac{1}{j_f}\sum_{j=1}^{j_f}(x_j)_k^{[i_0,i_f]}, \tag{4.5}$$

and similarly for the other two variables y and z. So on, super-index $[k_0, k_f]$ will be skipped when $k_0 = 0$ and $k_f = 6$.

Week	Mouse	x_{ij1}	y_{ij1}	z_{ij1}
1	1	156353	3521	6808
	2	102995	1943	711
	3	51743	5952	501
	4	47772	3340	819
2	1	468609	41957	19880
	2	393237	23900	9630
	3	1222322	173879	61537
	4	475998	47420	3201
3	1	1266271	130700	176400
	2	813128	136521	70671
	3	392307	66010	55010
	4	396125	85487	71934
4	1	737624	102441	32575
	2	341650	50375	2689
	3	76333	11158	5602
	4	751773	81213	36026
5	1	2407178	409248	96311
	2	2148912	319652	119087
	3	1060051	263194	86828
	4	2227967	547476	71472
6	1	1032118	181490	74581
	2	3081450	426915	521068
	3	504651	89185	33496
	4	4588501	651678	188138

Table 4.1: Data obtained in *Pasteur Institute* for (LDP) experiment 1 where x, y and z represent the number of $CD4^+$, IL-2 producers and regulatory T cells, respectively, in a single mouse which is euthanised for such purpose.

Week	Mouse	x_{ij2}	y_{ij2}	z_{ij2}
1	1	124000	1876	1100
	2	141000	1654	1011
	3	127000	2341	988
2	1	452400	36915	9591
	2	308000	20543	13552
	3	414000	23184	12420
3	1	2315300	105809	104652
	2	1821600	92901	65031
	3	3548200	230633	124187
4	1	1680000	82320	206640
	2	3562500	146418	158175
	3	2170000	124558	164920
5	1	2632000	16780	34291
	2	2281600	159712	104954
	3	2974400	356928	130874
6	1	5324800	415334	23961
	2	9664000	1227600	128726
	3	5562700	310398	103460

Table 4.2: Data obtained in *Pasteur Institute* for (LDP) experiment 2 where x, y and z represent the number of $CD4^+$, IL-2 producers and regulatory T cells, respectively, in a single mouse which is euthanised for such purpose.

Week	Mouse	x_{ij3}	y_{ij3}	z_{ij3}
1	1	663000	1950	4501
	2	896000	3120	3876
	3	690000	2960	6102
2	1	1858896	29952	13104
	2	3358714	108346	27086
	3	3444210	72765	20790
3	1	6945575	206938	579425
	2	5529576	69841	242424
	3	3322200	73224	67800
4	1	9628990	316050	906010
	2	5989375	129500	485625
	3	3201600	113796	278400
5	1	4360500	91800	229500
	2	5593000	152320	357000
	3	7520000	229600	480000
6	1	5868720	209851	59280
	2	11800000	500303	215794
	3	8589848	322043	185153

Table 4.3: Data obtained in *Pasteur Institute* for (LDP) experiment 3 where x, y and z represent the number of $CD4^+$, IL-2 producers and regulatory T cells, respectively, in a single mouse which is euthanised for such purpose.

Week	Mouse	x_{ij4}	y_{ij4}	z_{ij4}
1	1	604000	51680	4256
	2	2031840	81600	8160
	3	671531	49567	7469
	4	709995	28600	5005
2	1	7355850	438045	909150
	2	12300000	517725	991643
	3	13000000	648600	772800
	4	10900000	301860	673380
3	1	16700000	35114	877850
	2	11600000	23808	321408
	3	15200000	47472	648784
	4	9928800	20160	151200
4	1	4590000	14520	251680
	2	5609520	11760	270480
	3	3817440	15840	142560
	4	6448400	13160	131600
5	1	4885920	26325	17908
	2	7857720	26910	11228
	3	15700000	33820	117520
	4	7621120	16640	69888

Table 4.4: Data obtained in *Pasteur Institute* for (LDP) experiment 4 where x, y and z represent the number of $CD4^+$, IL-2 producers and regulatory T cells, respectively, in a single mouse which is euthanised for such purpose.

Figure 4.2 shows the mean $\pm$ the standard deviation of these values for three of the experiments. The particularities of experiment 4, which in addition to having followed cell expression for just 5 weeks, instead of 6, as in the other three experiments, a different initial amount of cells is injected into mice; drove us to work from a comparative study of the first three experiments simultaneously. Before analysing the correlation between different types of cells for each experiment, one of the first targets is to quantify dissimilarities among them, mainly to find out if these are due to the different conditions that have already been explained.

Whereas in IL-2 producer cells a smaller difference appears from one experiment to another, either total $CD4^+$ and T reg cells show an important variability in terms of absolute numbers. At first sight, experiments 2 and 3 show a similar behaviour in the three variables whereas experiment 1 practically reverses monotony. This suggests that the sign of correlation between variables might be constant but, for each experiment, the time for the change of cycles differs and this variation has not much to do, according to Figure 4.2, with the kind of reporter mice from which injected cells proceed. Given that OVA and LCMV experiments in following sections will study quorum-sensing under non-natural conditions, we first need to quantify how this variability might happen

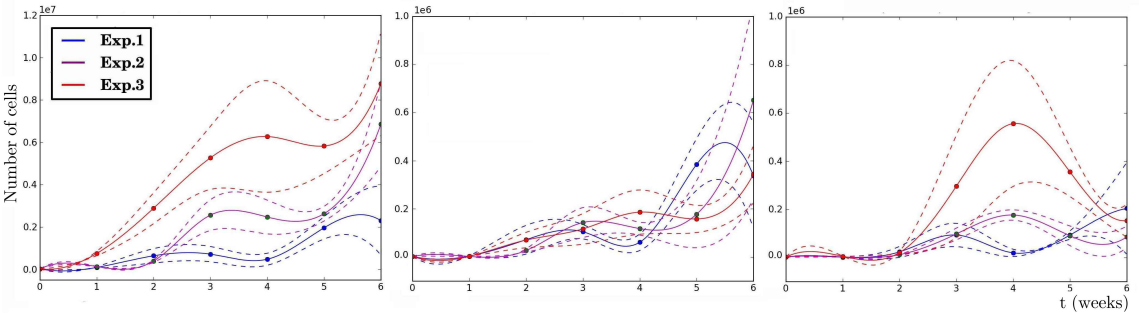

Figure 4.2: Three different experiments for the lymphopenia driven proliferation. From left to right, dots represent the average of the values of the actual data for total CD4$^+$, IL-2 and T reg cells, and curves a spline interpolation over time (in weeks). Dash curves represent the standard error.

due to experimental issues and noise.

Given this, let us make a comment about the main similarities between experiments regarding the correlation of the variables. Figure 4.3 shows a stronger linear correlation between $E[z]_2$ and $E[z]_3$ than between any of these two with $E[z]_1$ (Pearson correlation coefficient of 0.966 versus 0.333 and 0.175). This characteristic occurs, in a smaller proportion, with variables x and y. Moreover, 95% confidence intervals for experiments 2 and 3 also support this statement. In particular, (0.521, 0.988) between $E[x_j]_2$ and $E[x_j]_3$, (0.581, 0.990) between $E[y_j]_2$ and $E[y_j]_3$, and (0.781, 0.995) for $E[z_j]_2$ and $E[z_j]_3$. This intersection does not occur when comparing experiment 1 with either experiment 2 or 3. This suggests that the type of cells injected into mice do not seem to have a notable effect on the proliferation of these type of cells, given that cells from Tg IL-2/GFP mice were used for experiments 1 and 2 and T cells from IL-2/Thy1.1 mice, for experiments 2 and 3. Even when experiments 2 and 3 show a more similar behaviour, a smaller variability obtained within mice in experiment 1, in which four mice instead of the three from experiments 2 and 3 were taken every week, is observed in its standard deviation in Figure 4.2.

Let us now compare correlation between variables to see how this might vary from one experiment to another (Figure 4.4). Here, what seems to be predominant is the linear correlation observed between CD^+4 and IL-2 in the three experiments (Pearson correlation of 0.977, 0.975 and 0.960 for experiments 1, 2 and 3). Again, the respective 95% confidence intervals, (0.847, 0.997), (0.836, 0.996) and (0.747, 0.994) come to confirm this statement. The strength of this relation, given by the slope m of the blue dash lines, does not seem to be that clearly similar for the three experiments. The values of the slopes $m_1 = 0.17$, $m_2 = 0.09$ and $m_1 = 0.03$, when obtaining

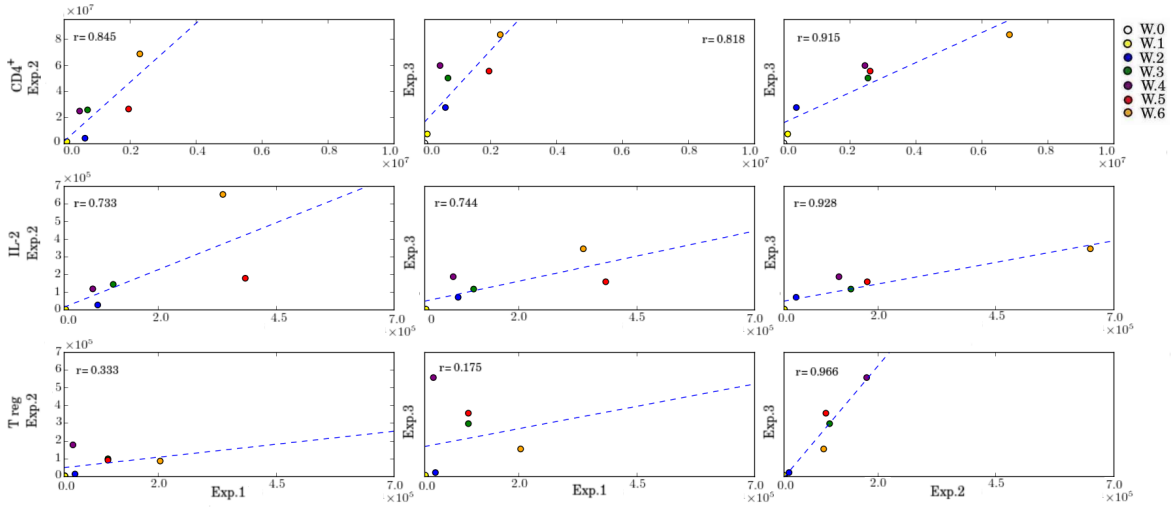

Figure 4.3: Linear correlation between every couple from CD4$^+$ ($(x_j)_1$), IL-2 producers ($(x_j)_2$), regulatory cells ($(x_j)_3$) (first row) and the other two variables y and z (second and third row) with their respective Pearson correlation coefficient (between $E[x]_1$, $E[x]_2$, $E[x]_3$ for the first row and similarly for y and z in second and third row). For every variable x,y and z, dots show the j different mouse with a different colour for every week i. Blue dash lines are regression lines.

the 95% confidence intervals for every couple, (0.129, 0.215), (0.067, 0.117) and (0.024, 0.049) respectively, suggests that how this linear relation between IL-2 and CD4$^+$ occurs is significantly different for each experiment. Additionally, Figure 4.4 shows that T reg cells do not seem to have a clear linear relation with the other two variables, as it was expected, and a deeper analysis is required. However, these values take into account vectors including every week $i \in [0, 6]$ which indicates the importance of measuring how this values depend on each week.

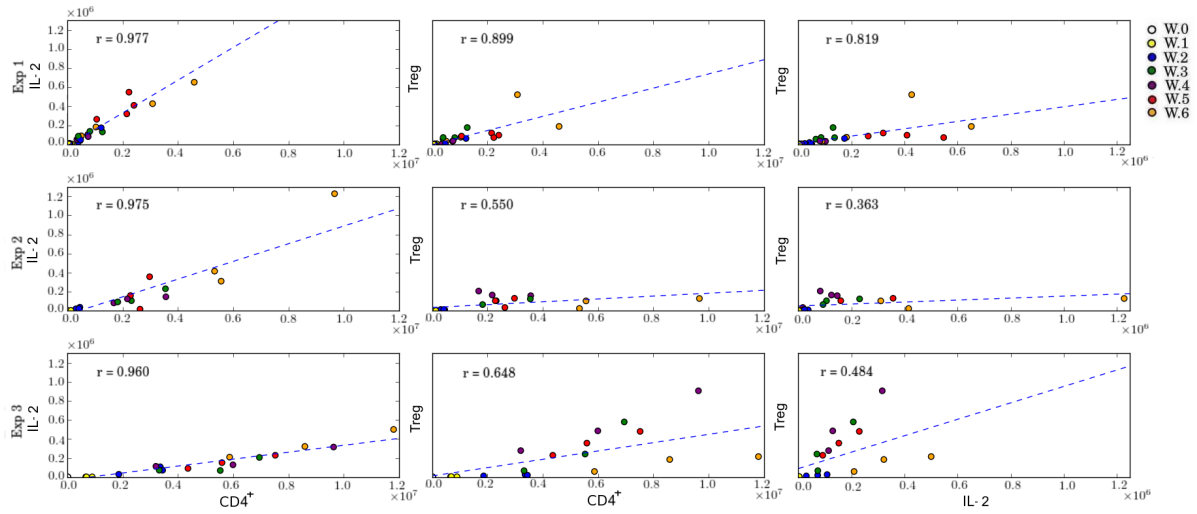

Figure 4.4: Linear correlation between $(x_j)_k$, $(y_j)_k$ and $(z_j)_k$ for every experiment k ($k = 1, 2, 3$ in the first, second and third row, respectively). For every experiment k, dots show the j different mouse with a different colour for every week i. P values in the top-left corner correspond to each pair $E[x]_k$, $E[y]_k$ and $E[z]_k$ for $k \, \epsilon [1, 3]$. Blue dash lines are regression lines.

Let us now focus on experiment 4. Given that a different amount of cells were injected for this case compared to the other three experiments, comparisons have been omitted so far. Notation can be maintained considering now $k = 4$. One advantage of this experiment, as occurs in the first one, is that a larger number of mice were used every week ($j \leq 4$). On the other hand, measurements took place for one week less than in the other cases ($0 \leq i \leq 5$). An equivalent table to the one shown in Figure 4.4 for previous experiments show a very different behaviour due to a drastic increase of T reg cells and, in particular, of IL-2 producer cells, in week 3. This particularity, provokes an imbalance in the decreasing tendency of the Pearson coefficient observed for previous experiments (from left to right in the columns of Figure 4.4). Again, no linear correlation can be strongly supported here.

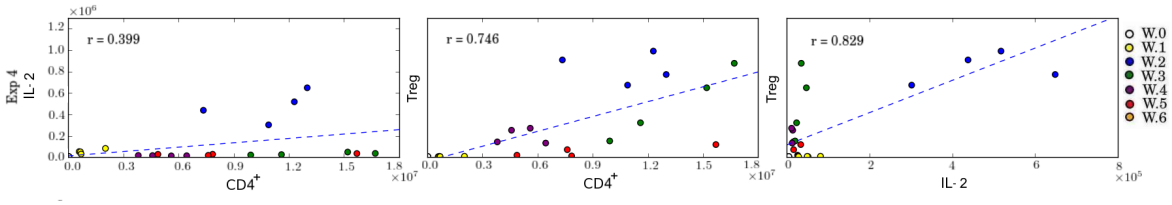

Figure 4.5: Linear correlation between $(x_j)_4$, $(y_j)_4$ and $(z_j)_4$. Dots show the j ($1 \leq j \leq 4$) mouse with a different colour for every week i ($0 \leq i \leq 5$). P values correspond to each pair $E[x]_4$, $E[y]_4$ and $E[z]_4$. Blue dash lines are regression lines.

Figure 4.6 shows an equivalence to Figure 4.3 but instead of total number of cells, it follows the rate of each group of cell to compare each pair of experiments. This would bring some light to a linear kind of relation between the percentages of the variables in use. Given that the amounts of each type of cells are relatively similar for each experiment, no much noise affects the conclusions shown in this plot (this would not be the case in Section 4.3). Figure 4.6 confirms the existing connection between experiments 2 and 3 also regarding population rates. For the other experiments, no linear correlation seems to be supported.

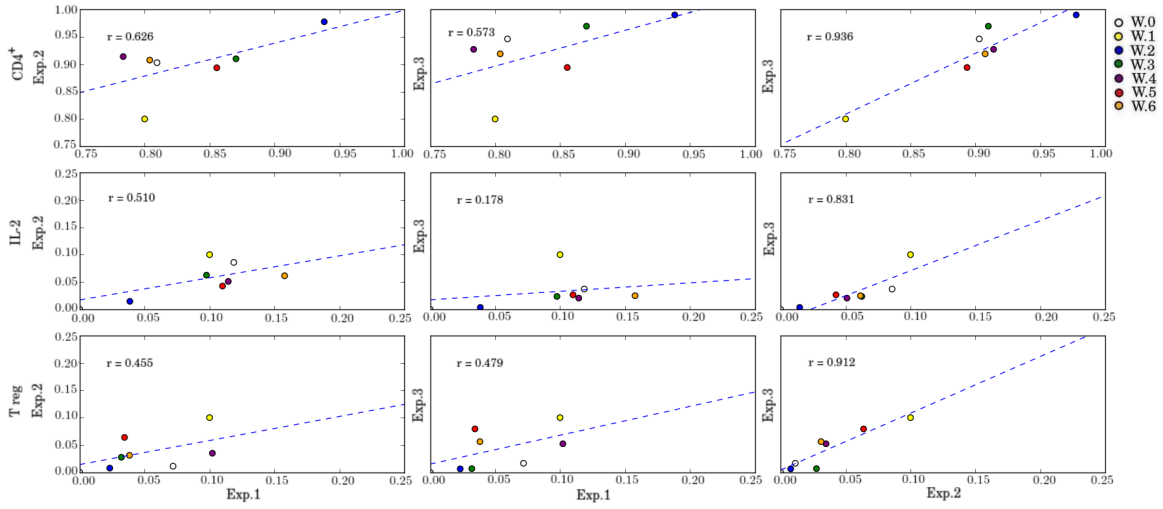

Figure 4.6: Linear correlation between $\frac{(x_j)_k}{(x_j)_k+(y_j)_k+(z_j)_k}$, $\frac{(y_j)_k}{(x_j)_k+(y_j)_k+(z_j)_k}$ and $\frac{(z_j)_k}{(x_j)_k+(y_j)_k+(z_j)_k}$ for every experiment k ($k = 1, 2, 3$ in the first, second and third column, respectively). For every experiment k, dots show the j different mouse with a different colour for every week i. P values correspond to each pair $\frac{E[x]_k}{E[x]_k+E[y]_k+E[z]_k}$, $\frac{E[y]_k}{E[x]_k+E[y]_k+E[z]_k}$ and $\frac{E[z]_k}{E[x]_k+E[y]_k+E[z]_k}$ for $k \in [1, 3]$. Blue dash lines represent regression lines.

Given that no significant linear correlation was found in most of the situations, a more specific observation follows separating vectors by slots of weeks, this is, considering Equations (4.4) and (4.5) without omitting super-index. Thus, in Table 4.5, a more specific analysis of the correlation between variables was done identifying when the main variation takes place for every experiment. Here, it can be observed that the four experiments follow a very similar behaviour before the fifth week and that from then, variability emerges, bringing distinct combinations between how variables interact. It is particularly noticeable the opposite adaptation of IL-2 and $CD4^+$ to T reg cells between experiments 2 and 3. Even when taken as a whole, they showed a clear linear relation (Figures 4.3 and 4.6), the negative feedback of regulatory T cells start at different moments depending on the experiment.

		Weeks 0-2	**Weeks 1-3**	**Weeks 2-4**	**Weeks 3-5**	**Weeks 4-6**
Exp 1	**CD4 vesusIL-2**	0.996	0.978	0.880	1	0.951
	CD4 vesusT reg	0.995	0.759	0.780	0.624	0.896
	IL-2 vesusT reg	1	0.879	0.984	0.602	0.715
Exp 2	**CD4 vesusIL-2**	0.954	0.998	0.985	0.984	0.997
	CD4 vesusT reg	0.927	1	0.861	-0.939	-0.565
	IL-2 vesusT reg	0.997	0.998	0.761	-0.863	-0.622
Exp 3	**CD4 vesusIL-2**	0.971	0.990	0.941	1	1
	CD4 vesusT reg	0.995	0.902	0.978	0.933	-0.787
	IL-2 vesusT reg	0.991	0.834	0.991	0.917	-0.787
Exp 4	**CD4 vesusIL-2**	1	0.289	0.261	0.973	N.A.
	CD4 vesusT reg	0.997	0.824	0.660	0.684	
	IL-2 vesusT reg	0.996	0.781	0.897	0.496	

Table 4.5: Pearson correlation coefficient between variables for every set of two weeks in each experiment.

However, cross-correlation is not symmetric and a delayed on the impact between variables can be analysed. For that purpose, it is convenient to have a constant unit of time in the measurements which allows us only to work for this case with the LDP experiment. What follow are all possible combinations between the correlation of one vector variable with a transposition of one other vector variable of 1 to a maximum of 4 weeks. Results have been obtained for absolute values and for percentages and, again, an important variability results among the different experiments (Tables 4.6 and 4.7).

Absolute numbers

	$E[x]_i^{[k'_0,6]}$					$E[y]_i^{[k'_0,6]}$					$E[z]_i^{[k'_0,6]}$				
k'_0	0	1	2	3	4	0	1	2	3	4	0	1	2	3	4
$E[x]_1^{[0,k_f]}$						.98	.60	.57	.96	.48	.90	.90	.18	.71	.95
$E[y]_1^{[0,k_f]}$	.98	.73	.58	.99	.66						.82	.88	.22	.83	0.93
$E[z]_1^{[0,k_f]}$	.80	.39	.55	.84	.65	.82	.28	.73	.66	.39					
$E[x]_2^{[0,k_f]}$						.98	.63	.70	.99	.98	.55	.73	.03	-.45	-.77
$E[y]_2^{[0,k_f]}$	.98	.83	.61	.99	1						.36	.70	.06	-.50	-.54
$E[z]_2^{[0,k_f]}$	.55	.47	.87	.99	.99	.36	.39	.91	1	.98					
$E[x]_3^{[0,k_f]}$						.96	.82	.84	.87	.92	.65	.72	.21	-.66	-.96
$E[y]_3^{[0,k_f]}$	.96	.85	.88	.80	.99						.48	.63	.09	-.72	-.87
$E[z]_3^{[0,k_f]}$	.65	.68	.80	.97	.96	.48	.64	.86	.96	.96					
$E[x]_4^{[0,k_f]}$						.40	-.54	-.63	.24	NA	.75	-.06	-.94	-.80	NA
$E[y]_4^{[0,k_f]}$	.40	.67	-.83	-.12	NA						.83	.37	-.42	-.81	NA
$E[z]_4^{[0,k_f]}$	.75	.49	-.95	-.03	NA	.83	-.51	-.57	.20	NA					

Table 4.6: Pearson correlation coefficient between one vector variable and a transposition from 0 to a maximum of 4 weeks (3 for experiment 4) of one other vector variable for each experiment for absolute values $k_f + k_0 = 6$ for $i \in [1, 3]$ and $k_f + k_0 = 5$ for $i = 4$).

Percentages

	$E[x]_i^{[k'_0,6]}$					$E[y]_i^{[k'_0,6]}$					$E[z]_i^{[k'_0,6]}$				
k'_0	0	1	2	3	4	0	1	2	3	4	0	1	2	3	4
$E[x]_1^{[0,k_f]}$						-.80	.20	-.38	.06	.94	-.77	.09	.81	-.82	.10
$E[y]_1^{[0,k_f]}$	-.80	-.34	.44	-.86	.61						.24	.33	-.77	.59	.39
$E[z]_1^{[0,k_f]}$	-.77	.66	.35	-.68	1	.24	-.58	.34	-.38	-.72					
$E[x]_2^{[0,k_f]}$						-.84	.68	-.30	-.02	.55	-.89	.42	.23	.39	-.72
$E[y]_2^{[0,k_f]}$	-.84	.74	-.21	.99	-.97						.50	-.40	.09	-.48	-.56
$E[z]_2^{[0,k_f]}$	-.89	.79	.06	.87	-.99	.50	-.67	.53	-.06	-.69					
$E[x]_3^{[0,k_f]}$						-.90	.60	-.19	.40	.30	-.93	.21	.84	.28	-.72
$E[y]_3^{[0,k_f]}$	-.90	.55	.72	.32	-.73						.68	-.35	-.67	-.11	.64
$E[z]_3^{[0,k_f]}$	-.93	.16	.85	.57	-.85	.68	-.36	.40	-.19	-.38					
$E[x]_4^{[0,k_f]}$						-.92	-.64	-.91	.68	NA	-.91	.43	-.92	-.12	NA
$E[y]_4^{[0,k_f]}$	-.92	-.48	-.98	-.60	NA						.68	-.11	.99	.61	NA
$E[z]_4^{[0,k_f]}$	-.91	.35	-.75	.23	NA	.68	.23	.78	-.38	NA					

Table 4.7: Pearson correlation coefficient between one vector variable and a traspostion from 0 to a maximum of 4 weeks (3 for experiment 4) of one other vector variable for each experiment for percentages ($k_f + k_0 = 6$ for $i \in [1, 3]$ and $k_f + k_0 = 5$ for $i = 4$).

4.3 Lymphocytic choriomeningitis virus (LCMV) experiment

A plaque-forming unit (PFU), in virology, is a measure that quantifies the number of particles that can forme plaques per unit volume. Theoretically, the plaque-forming unit includes only the infectious virus particles since a virus particle failing to infect a host cell would not be able to produce a plaque and would not be taking into account. Given that PFU includes only the particles capable of infecting cells on their own, one PFU means one event of dissolution (or one infectious virus particle).

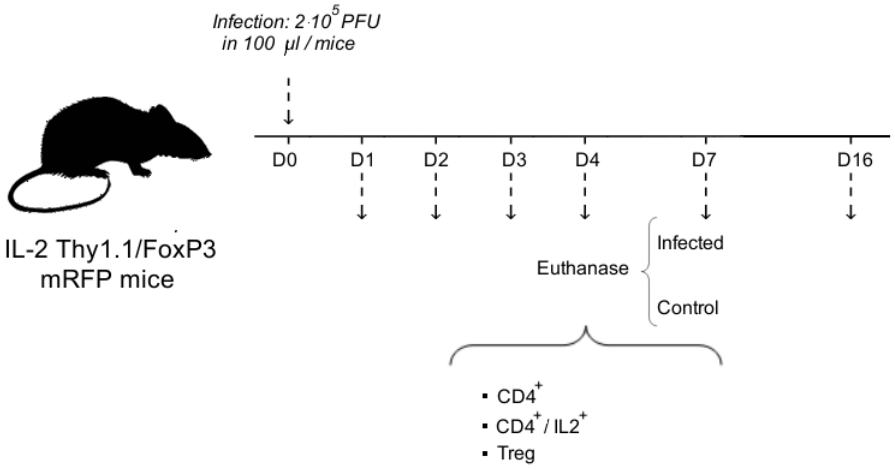

Figure 4.7: Time line for lymphocytic choriomeningitis virus LCMV experiment in which two or three mice (j) were killed for both control and infection. Each mouse provides some amount of IL-2 producer cells, regulatory T cells and total $CD4^+$ excluding the previous two groups

IL-2 Thy1.1/FoxP3 mRFP mice were infected with $2 \cdot 10^5$ plaque-forming units (PFU) of lymphocytic choriomeningitis virus (LCMV) and three mice were killed every time to measure the same variables as in LDP experiment in Section 4.2. As a control, two mice (three for the last day) were used to compare results. Figure 4.7 shows the time line for LCMV experiment. In this section, let us define x_{ij}^C and x_{ij}^I as the number of $CD4^+$ T cells (excluding both IL-2 producers and regulatory) in mouse j at day i (where $i = 1, 2, 3, 4, 7, (16)$ and $j = 1, 2, (3)$) for control case and virus infection, respectively. Note that every mouse j is independent for each day i. Similarly, y_{ij}^C, y_{ij}^I and z_{ij}^C, z_{ij}^I encode number of IL-2 producer and T reg cells directly from data as Table 4.8 shows.

	Control / Non-infected								
Days (i)	x_{i1}^C	x_{i2}^C	z_{i3}^C	y_{i1}^C	y_{i2}^C	y_{i3}^C	z_{i1}^C	z_{i2}^C	z_{i3}^C
1	$1.65 \cdot 10^7$	$1.96 \cdot 10^7$	–	$3.30 \cdot 10^3$	$7.84 \cdot 10^3$	–	$2.98 \cdot 10^6$	$2.33 \cdot 10^6$	–
2	$1.48 \cdot 10^7$	$1.72 \cdot 10^7$	–	$4.95 \cdot 10^4$	$8.16 \cdot 10^4$	–	$2.72 \cdot 10^6$	$3.08 \cdot 10^6$	–
3	$2.21 \cdot 10^7$	$2.03 \cdot 10^7$	–	$1.99 \cdot 10^4$	$1.42 \cdot 10^4$	–	$2.32 \cdot 10^6$	$3.24 \cdot 10^6$	–
4	$1.95 \cdot 10^7$	$1.68 \cdot 10^7$	–	$9.75 \cdot 10^4$	$2.18 \cdot 10^5$	–	$2.73 \cdot 10^6$	$2.52 \cdot 10^6$	–
7	$3.09 \cdot 10^7$	$1.48 \cdot 10^7$	$2.98 \cdot 10^7$	$3.09 \cdot 10^4$	$1.48 \cdot 10^4$	$8.95 \cdot 10^3$	$2.64 \cdot 10^6$	$1.93 \cdot 10^6$	NA
16	–	–	–	–	–	–	–	–	–
	LCMV Infection								
Days (i)	x_{i1}^I	x_{i2}^I	z_{i3}^I	y_{i1}^I	y_{i2}^I	y_{i3}^I	z_{i1}^I	z_{i2}^I	z_{i3}^I
1	$1.75 \cdot 10^7$	$1.85 \cdot 10^7$	$2.00 \cdot 10^7$	$1.00 \cdot 10^5$	$6.43 \cdot 10^4$	$2.25 \cdot 10^5$	$2.48 \cdot 10^6$	$2.96 \cdot 10^6$	$2.47 \cdot 10^6$
2	$1.60 \cdot 10^7$	$1.97 \cdot 10^7$	$1.37 \cdot 10^7$	$6.72 \cdot 10^5$	$6.98 \cdot 10^5$	$1.88 \cdot 10^6$	$3.23 \cdot 10^6$	$3.58 \cdot 10^6$	$2.95 \cdot 10^6$
3	$1.61 \cdot 10^7$	$1.85 \cdot 10^7$	$1.61 \cdot 10^7$	$1.89 \cdot 10^5$	$2.18 \cdot 10^5$	$3.84 \cdot 10^5$	$2.84 \cdot 10^6$	$3.26 \cdot 10^6$	$3.07 \cdot 10^6$
4	$2.30 \cdot 10^7$	$2.75 \cdot 10^7$	$2.53 \cdot 10^7$	$6.49 \cdot 10^6$	$5.26 \cdot 10^6$	$5.59 \cdot 10^6$	$4.06 \cdot 10^6$	$3.40 \cdot 10^6$	$4.12 \cdot 10^6$
7	$2.56 \cdot 10^7$	$2.38 \cdot 10^7$	$2.53 \cdot 10^7$	$1.38 \cdot 10^6$	$3.09 \cdot 10^6$	$2.82 \cdot 10^6$	$3.48 \cdot 10^6$	$3.55 \cdot 10^6$	$2.90 \cdot 10^6$
16	$1.68 \cdot 10^7$	$3.23 \cdot 10^7$	$2.42 \cdot 10^7$	$5.04 \cdot 10^5$	$3.23 \cdot 10^5$	$4.83 \cdot 10^5$	$9.58 \cdot 10^5$	$1.68 \cdot 10^6$	$1.88 \cdot 10^6$

Table 4.8: LCMV experiment data for both control and infection. Two or three mice were killed at days 1,2,3,4,7 and 16 for the obtaining of $CD4^+$ cells, IL-2 producers and regulatory cells. NA means not available due to experimental reasons.

Arranging vectors similarly to Section 4.2 (see Equations (4.4) and (4.5)), Figure 4.8 shows the correlation between $(x_j)^k$, $(y_j)^k$ and $(z_j)^k$ for every experiment k ($k = I, C$). This plots show how when the infection takes place, T reg cells suppression gets blocked when comparing to the control case (Pearson coefficient reduced from $r = -0.044$ to $r = -0.821$). Alternatively, there are some behaviours that might not be explained by this first approach like interactions between IL-2 producer cells and either total $CD4^+$ or T reg cells. Apparently, by looking at Figure 4.8, the infection strengthens IL-2 proliferative abilities. This might be also due to the small amount of data available which correlations miss to understand or that delay in which signals are traduced is not reflected in this analysis.

Similarly to the comparison done in LDP between Figures 4.4 and 4.6, a last example between correlations is shown in Figure 4.9 in which correlation between percentages are studied. Hence, correlation between $\frac{(x_j)^k}{(x_j)^k+(y_j)^k+(z_j)^k}$, $\frac{(y_j)^k}{(x_j)^k+(y_j)^k+(z_j)^k}$ and $\frac{(z_j)^k}{(x_j)^k+(y_j)^k+(z_j)^k}$ are analysed in an analogous manner to Figure 4.8. Here it can be observed a neater effect of T reg cells when suppressing $CD4^+$ and also how IL-2 producer cells lose their proliferative capacity when the infection take place. However, conclusions need to be analysed carefully. On one side, given that three variables are taken into account when parametrising, if the weight of the third variable is too high, that might affect the Pearson correlation term even when there is a reasonable strong linear correlation between the other two variables. On the other hand, if when comparing two

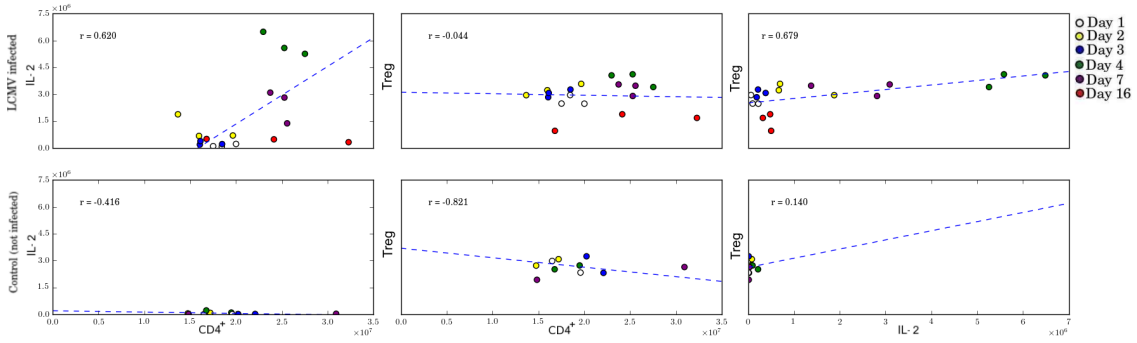

Figure 4.8: Linear correlation between $(x_j)^k$, $(y_j)^k$ and $(z_j)^k$ for every experiment k ($k = C, I$ in the first (infected mice) and second (control mice) column, respectively) in the LCMV experiment. For every experiment k, dots show the j different mouse with a different colour for every day i. P values correspond to each pair $E[x]^k$, $E[y]^k$ and $E[z]^k$ for $k = C, I$. Blue dash lines are regression lines.

variable the proportional rates are imbalanced, they might seem to follow a strong correlation which is only due to this lack of proportion. This can be the case between T reg cells and $CD4^+$ in the control case (Figure 4.9). However, given the relation between this two variables in term of numbers and proportions (same box in Figure 4.8), the suppressive influence of T reg cells over $CD4^+$ seems to have in principle supported when no infection is taken place.

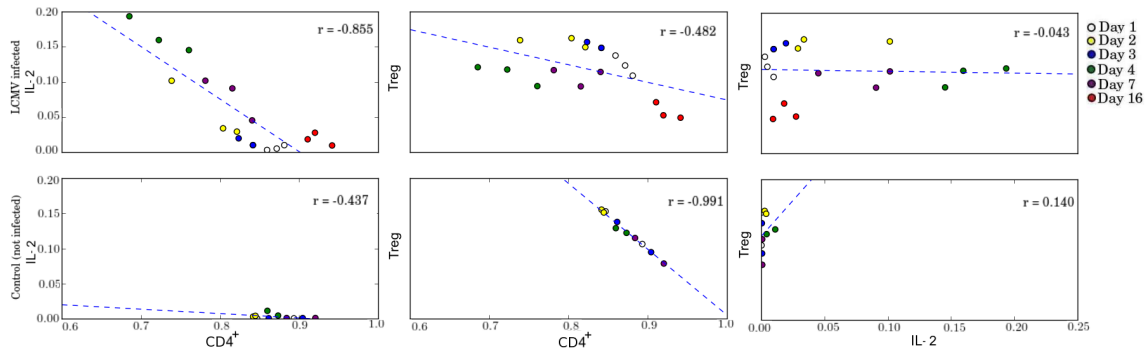

Figure 4.9: Linear correlation between $\frac{(x_j)^k}{(x_j)^k+(y_j)^k+(z_j)^k}$, $\frac{(y_j)^k}{(x_j)^k+(y_j)^k+(z_j)^k}$ and $\frac{(z_j)^k}{(x_j)^k+(y_j)^k+(z_j)^k}$ for every experiment k ($k = C, I$ in the first (infected mice) and second (control mice) column, respectively) in the LCMV experiment. For every experiment k, dots show the j different mouse with a different colour for every day i. P values correspond to each pair $\frac{E[x]^k}{E[x]^k+E[y]^k+E[z]^k}$, $\frac{E[y]^k}{E[x]^k+E[y]^k+E[z]^k}$ and $\frac{E[z]^k}{E[x]^k+E[y]^k+E[z]^k}$ for $k = C, I$. Blue dash lines are regression lines.

4.4 Two hypothesis tests for a quorum-sensing model

As mentioned in Section 1.1.3, a quorum-sensing model was already proposed in [5, 57]. For this chapter, several variations take place in the alluded model. In addition to this, by using some Bayesian techniques, data exposed in Section 4.3 for LCMV have been used to parametrise the model and to elucidate some yet hidden mechanisms behind this self-regulated process. Given the following T cell subpopulations, naive $CD4^+$ (n_1), IL-2 producer (n_2), memory (n_3) and regulatory (n_4) T cells, two different hypothesis in Models (I) and (II) regarding IL-2 fate via regulatory T cell suppression are given by equations below in a general scenario.

IL-2 death pathway (Model (I)):

$$\begin{aligned}
\frac{dn_1}{dt} &= \nu_1 + \lambda_1 n_1 \left(1 - \frac{n_1}{\kappa_1}\right) - \mu_1 n_1 - \alpha_1 n_1, \\
\frac{dn_2}{dt} &= \alpha_1 n_1 + \lambda_2 n_2 - \mu_2 n_2 - \alpha_2 n_2 - \beta n_2 n_4, \\
\frac{dn_3}{dt} &= \alpha_2 n_2 + \lambda_3 n_3 \left(1 - \frac{n_3}{\kappa_3}\right) - \mu_3 n_3, \\
\frac{dn_4}{dt} &= \nu_4 + \lambda_4 n_4 \left(1 - \frac{n_4}{\kappa_4}\right) - \mu_4 n_4 + \gamma_4 n_4 n_2.
\end{aligned} \tag{4.6}$$

IL-2 differentiation pathway (Model (II)):

$$\begin{aligned}
\frac{dn_1}{dt} &= \nu_1 + \lambda_1 n_1 \left(1 - \frac{n_1}{\kappa_1}\right) - \mu_1 n_1 - \alpha_1 n_1, \\
\frac{dn_2}{dt} &= \alpha_1 n_1 + \lambda_2 n_2 - \mu_2 n_2 - \alpha_2 n_2 - \beta n_2 n_4, \\
\frac{dn_3}{dt} &= \alpha_2 n_2 + \lambda_3 n_3 \left(1 - \frac{n_3}{\kappa_3}\right) - \mu_3 n_3 + \beta n_2 n_4, \\
\frac{dn_4}{dt} &= \nu_4 + \lambda_4 n_4 \left(1 - \frac{n_4}{\kappa_4}\right) - \mu_4 n_4 + \gamma_4 n_4 n_2.
\end{aligned} \tag{4.7}$$

Even when the concept of naive and memory cells where explained in the introduction (Section 1.1.1), given that in this section no distinction had been already done, it must be clarified that whereas naive T cells have not received any kind of activation, memory cells did at some point, but at the present moment are not activated any more. However, it is known that their time of reaction to a plausible response will take much less time to be produced [51]. Having said that, what in the experiments and so in previous sections were called total $CD4^+$, in this chapter they are separated into naive and memory.

Consequently, in both models, for the naive cells (n_1) there is a thymic input, ν_1, which is the rate at which naive cells are produced or more precisely, released to the periphery. Homeostasis proliferation, the rate at which naive T cells in normal conditions get divided, is encoded by λ_1 and it is limited by a carrying capacity κ_1 for naive cells. Death rate of naive cells is given by μ_1. And finally, an activation term, α_1, expresses how much of an immune response behaviour we have in a lymphopenic environment. This term is only present if an immune response has taken place and it will create two different scenarios in succeeding sections depending on if this term is, or not, considered.

Regarding IL-2 producing cells, there is a programme of proliferation, λ_2, which is turned on, when an immune response is taking place, a μ_2 death rate, with no carrying capacity, and a memory differentiation rate, α_2, which term is only present if an immune response takes place, just like α_1. These three terms are linearly proportional to the amount of IL-2 producing cells available. As a contrast, β rate, that is, the death regulated by regulatory cells in Model (I) and the differentiation into memory cells in Model (II) , is proportional to the amount of IL-2 producer cells (n_2) and to the number of T reg cells (n_4). Thus, the two hypotheses considered in the analysis mathematically speaking are: this term being a death term (so this term will not appear in the third equation regarding memory T cells), or the term being a suppression of IL-2 production for IL-2 producing cells to become part of the memory population, so by switching off IL-2 secretion and these cells would stop being n_2 (so the term would appear in the memory T cell equation with positive sign).

For the memory T cells or IL-2 non-producing T cells there is no thymic input. However, an homeostasis proliferation λ_3 is considered, that is, the rate at which memory T cells in normal conditions get divided. As occurred with n_1, a carrying capacity κ_3 for memory cells limits their expansion. As for the previous populations, n_3 death rate is given by μ_3.

Finally, regulatory T cells follow a thymic input ν_1 encoding the rate at which this subpopulation is released into the periphery. An homeostatic proliferation, λ_4, that should be considered as TCR signal induced more than cytokine induced which, as for n_1 and n_3 is limited by a carrying capacity κ_3, an n_4 death rate given by μ_4 and a γ_4 term for IL-2 driven proliferation, proportional to n_2 and n_4. Note that no γ_1 term was used for naive cells given that they do not upregulate CD25.

4.5 Sensitivity analysis

This section focuses on Model (I). The same procedure was followed for Model (II) and its not shown here due to similar output. As a way of analysing the weight that every single parameter has in the output when initial values are perturbed, a global sensitivity analysis was carried for model given by Equation (4.6). As in many other systems biology [45], once the influence of each input factor is quantified, further studies can be followed having into account the results obtained from sensitivity analysis. Those parameters which influence in the output appears to be considerably small can be then considered as fixed values and the system of open values shall be reduced, which will allow, in principle, a more accurate study on the remaining set of parameters, which are those supposed to be more relevant for the output.

As a starting point, a general approach over the whole set of $\{\theta\}$ is followed. The effect on each concentration of species of every parameter in $\{\theta\}$ at different time points, including steady state is simultaneously quantified, as

$$S_{ij} = \left(\frac{\partial n_i}{\partial \theta_j}\right) \cdot \left(\frac{n_i}{\theta_j}\right)^{-1}$$

This global sensitivity analysis provides a first conclusion when limiting the range of parameters to study in depth [63]. The following table shows a summary of the S_{ij} as a mean of the those obtained at different points, including steady state.

	n_1	n_2	n_3	n_4
$\left(\frac{\partial n_i}{\partial \lambda_1}\right) \cdot \left(\frac{n_i}{\lambda_1}\right)^{-1}$	-.129	-.001	-.000	-.001
$\left(\frac{\partial n_i}{\partial \lambda_3}\right) \cdot \left(\frac{n_i}{\lambda_3}\right)^{-1}$	0	.000	-.118	.000
$\left(\frac{\partial n_i}{\partial \mu_1}\right) \cdot \left(\frac{n_i}{\mu_1}\right)^{-1}$	-.034	-.000	-.000	-.000
$\left(\frac{\partial n_i}{\partial \mu_3}\right) \cdot \left(\frac{n_i}{\mu_3}\right)^{-1}$	0	.000	-.127	0
$\left(\frac{\partial n_i}{\partial \mu_4}\right) \cdot \left(\frac{n_i}{\mu_4}\right)^{-1}$	0	.000	.000	.000
$\left(\frac{\partial n_i}{\partial \nu_1}\right) \cdot \left(\frac{n_i}{\nu_1}\right)^{-1}$	.181	.001	.000	.001
$\left(\frac{\partial n_i}{\partial \nu_4}\right) \cdot \left(\frac{n_i}{\nu_4}\right)^{-1}$	0	-.000	-.000	.000

Table 4.9: Summary of the elasticities from the sensitivity analysis of S_{ij} where $j \in \{\theta_F\}$.

Given that the influence for all the variables which respect to every parameter in $\{\theta_F\}$ is always

smaller than $|0.135|$, it seems reasonable to fix these values according to literature and keep the analysis with the rest of the parameters. For the carrying capacities κ_1 and κ_4 which have been obtained from data in homeostasis, the influence given by the sensitivity analysis is much higher and will vary depending on the variable. Table 4.11 summaries these values

	n_1	n_2	n_3	n_4
$\left(\frac{\partial n_i}{\partial \kappa_1}\right) \cdot \left(\frac{n_i}{\kappa_1}\right)^{-1}$	.819	.005	.001	.005
$\left(\frac{\partial n_i}{\partial \kappa_4}\right) \cdot \left(\frac{n_i}{\kappa_4}\right)^{-1}$	0	$\approx$ -1	-.258	.006

Table 4.10: Summary of the elasticities for the sensitivity analysis of κ_1 and κ_4.

Interestingly, variations in κ_4 inputs show a very strong inverse correlation with the output of n_2. In the case of κ_1 it seems to be the one with the highest impact on the output of n_1 given that the rest of the rest of the rates, (only those with sub index 1 will have something to do with the output), have a relationship of less than $|0.2|$. Finally, the set of parameters of $\{\theta_V\}$ which will be under the Bayesian study verifies: A previous knowledge about the process they encode being particularly important, or not sufficiently understood; This relates also to the fact of a lack of information relating to the exact values of the parameters; And finally, as the output of the sensitivity analysis arises, altering parameters in $\{\theta_V\}$ tends to have more weight on the output than those in $\{\theta_F\}$ as it is shown below.

	n_1	n_2	n_3	n_4
$\left(\frac{\partial n_i}{\partial \alpha_1}\right) \cdot \left(\frac{n_i}{\alpha_1}\right)^{-1}$	-.017	.006	.001	.006
$\left(\frac{\partial n_i}{\partial \alpha_2}\right) \cdot \left(\frac{n_i}{\alpha_2}\right)^{-1}$	0	-.035	.237	-.033
$\left(\frac{\partial n_i}{\partial \beta}\right) \cdot \left(\frac{n_i}{\beta}\right)^{-1}$	0	-.010	-.003	-.009
$\left(\frac{\partial n_i}{\partial \lambda_2}\right) \cdot \left(\frac{n_i}{\lambda_2}\right)^{-1}$	0	≈ 1	.317	≈ 1
$\left(\frac{\partial n_i}{\partial \lambda_4}\right) \cdot \left(\frac{n_i}{\lambda_4}\right)^{-1}$	0	.994	.244	-.006
$\left(\frac{\partial n_i}{\partial \kappa_3}\right) \cdot \left(\frac{n_i}{\kappa_3}\right)^{-1}$	0	.000	.754	0
$\left(\frac{\partial n_i}{\partial \gamma_4}\right) \cdot \left(\frac{n_i}{\gamma_4}\right)^{-1}$	0	-.991	-.243	.006
$\left(\frac{\partial n_i}{\partial \mu_2}\right) \cdot \left(\frac{n_i}{\mu_2}\right)^{-1}$	0	-.210	-.051	-.198

Table 4.11: Summary of the elasticities for sensitivity analysis of parameters in $\{\theta_V\}$.

Clearly, those parameters that are more subjected to variability are λ_2, λ_4, κ_3 and γ_4. Given that, at the same time, the information relating to this rate in literature is not strong enough, these four

parameters will undergo the Bayesian process. Moreover, α_1 and α_2 are considered to play a key role on the activation process. As it will be seen in Section 4.6, they will be also conditioned to a variable recording the time in which activation take place an, lastly, they take different values when there is no immune response, as it was seen before. μ_2 is also considered in the Bayesian analysis since it should not be assured that its weight, approximately -0.2 for several variables, can be despicable. Additionally, and given that n_2 is the only variable without a carrying capacity in the model, changes on degradation rate need to be followed. Finally, β plays a central role when studying the two different models hypothesised in which the preference for the system to whether IL-2 producer cells become memory cells or are degraded when activation process has finished, wants to be quantified.

4.6 Parameter estimation

Still showing results only for Model (I), System (4.6) encodes LCMV dynamics for the IL-2 death pathway. As discussed in Section 4.5, some of these parameters $\{\theta_F\}$, gathered in Table:4.12, are obtained from literature [5] whereas the rest of them $\{\theta_V\}$ were either deterministically compute from the equations or they go under an ABC parameter estimation process (see Definition 4.6.1). Therefore, $\{\theta\} = \{\theta_F\} \cup \{\theta_V\}$.

Parameter	*Value*	*Units*
λ_1	$2 \cdot 10^{-2}$	h^{-1}
λ_3	$5 \cdot 10^{-2}$	h^{-1}
μ_1	$1 \cdot 10^{-3}$	h^{-1}
μ_3	$1 \cdot 10^{-2}$	h^{-1}
μ_4	$1 \cdot 10^{-2}$	h^{-1}
ν_1	$2.5 \cdot 10^{6}$	$cell \cdot day^{-1}$
ν_4	$2.5 \cdot 10^{5}$	$cell \cdot day^{-1}$

Table 4.12: Parameters $\{\theta_F\}$ obtained from literature [5].

Given that data show CD4$^+$ both naive (n_1) and memory (n_3) together, a coefficient $q_0 \in]0,1]$ might be included to split them. The rate naive/memory T cells is not rigorously established in literature and it is subjected to variabilities from homeostasis. This distinction, however, will be only considered for obtaining initial conditions and carrying capacities in $\{\theta_F\}$ given that for obtaining parameters in $\{\theta_V\}$ both memory and naive T cells will be gathered together for comparing with CD4$^+$ data, as it will be explained. Consequently, the following relations, for instance, for the control case, hold:

$$
\begin{aligned}
n_1^C(i,j) &= q_0 \cdot x_{ij}^C, \\
n_2^C(i,j) &= y_{ij}^C, \\
n_3^C(i,j) &= (1-q_0) \cdot x_{ij}^C, \\
n_4^C(i,j) &= z_{ij}^C.
\end{aligned}
\tag{4.8}
$$

Therefore, the values of the parameters in $\{\theta_V\}$ will be q_0 dependent as it is described in Section 4.6.1. Time dynamics of the three populations given in data are shown with a cube spline interpolation in Figure 4.10.

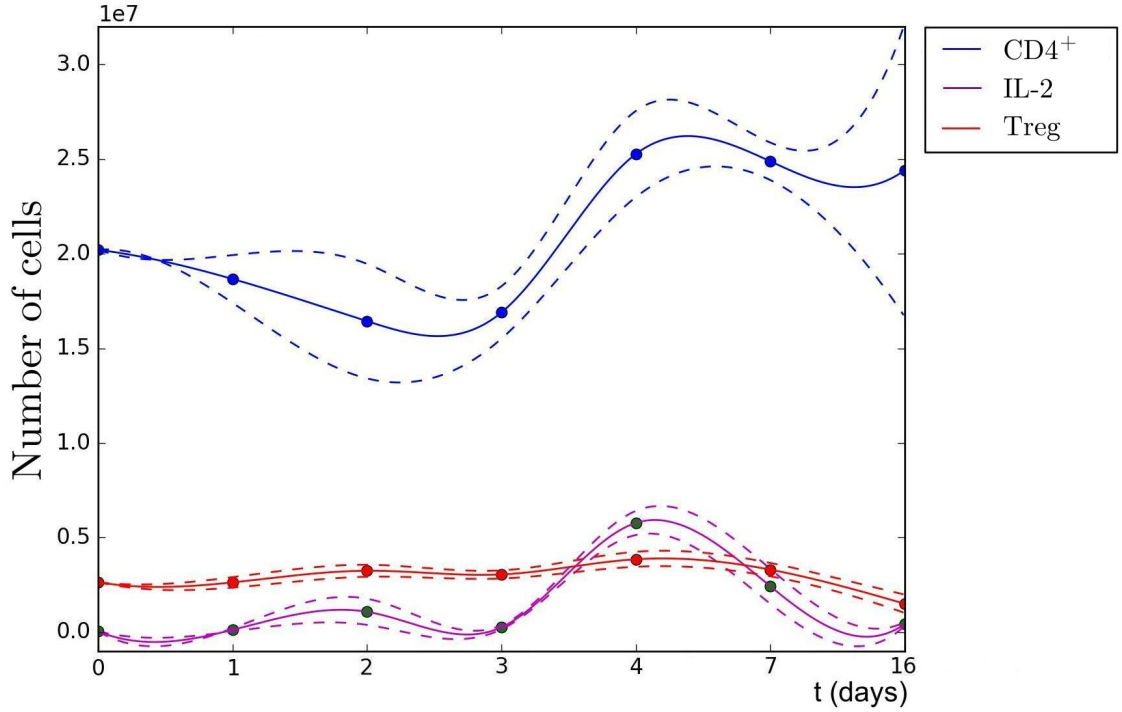

Figure 4.10: Spline for the infection case for CD4$^+$ (both naive and memory), IL-2 producers and regulatory T cells. Dash lines are the standard deviation. Time in days.

4.6.1 κ_1 and $\kappa_4 \in \{\theta_V\}$ estimation. No immune response

LCMV control data will be used to estimate the carrying capacity rates κ_1 and $\kappa_4 \in \{\theta_V\}$ and initial conditions. For this purpose, when no immune response is taking place, $\alpha_1 = \alpha_2 = 0$ can be assumed, so no differentiation from naive into IL-2 producers nor from IL-2 producers to

memory T cells will be considered. Thus, from System (4.6), it holds:

$$0 = \nu_1 + \lambda_1\, n_1 \left(1 - \frac{n_1}{\kappa_1}\right) - \mu_1\, n_1, \tag{4.9}$$

$$0 = \lambda_3 n_3 \left(1 - \frac{n_3}{\kappa_3}\right) - \mu_3 n_3. \tag{4.10}$$

For this subsection, and given that no particular immune response is taken place, no discernment will be done from mice at different days. Therefore, κ_1 can be obtained from system above taking $n_1 = \text{mean}(n_1^C(i,j))$, that is

$$\kappa_1 = \frac{\lambda_1\, mean(n_1^C(i,j))^2}{\nu_1 + (\lambda_1 - \mu_1)\, mean(n_1^C(i,j))}. \tag{4.11}$$

κ_4 is supposed to keep the relation 1:10 with κ_1 as for the synthesis of naive and regulatory T cells, so

$$\kappa_4 = 0.1 \cdot \kappa_1. \tag{4.12}$$

Initial conditions were then obtained as $n_s(0)$ =mean$(n_s^C(i,j))$ with $s = 1,2,3,4$, $i = 1,2,3,4,7$ and $j = 1,2,(3)$. Thus, for example, for $q_0 = 1$, and given parameters from Table 4.12,

Parameter	*Value*	*Units*
κ_1	16730840	*cell*
κ_4	1673084	*cell*
$n_1(0)$	20206727	*cell*
$n_2(0)$	49686	*cell*
$n_3(0)$	0	*cell*
$n_4(0)$	2648488	*cell*

Table 4.13: Initial conditions and $\kappa_s \in \{\theta_V\}$ with $(s = 1,4)$ for $q_0 = 1$.

4.6.2 Bayesian estimation for $\{\theta_V\}$

When analysing a statistical model, one of the crucial points relies on the properties deduced from the underlying probability distribution of the data. This process of inference normally needs a function of the parameter, likelihood function, to quantify the support data [12]. An alternative way of approximating this likelihood, when for instance its analytical expression cannot be obtained, follows a class of computational methods under the name of Approximate

Bayesian Computation (ABC)-based methods [9].

A prior distribution $\pi(\theta)$ represents the beliefs about parameter θ before data is available. If θ^* is a sample from this prior distribution, a dataset n^S is generated by a conditional probability distribution $f(n^S|\theta^*)$ or likelihood function as a solution of a given statistical model. Therefore, both n^S and the experimental data, n^I, can be compared under a proposed distance d which if it is sufficiently small, θ^* will be accepted. The posterior distribution $\pi(\theta|n^I)$ is then the set of accepted $\theta \in \pi(\theta|n^I)$. A summary of this rejection sampler, which is one of the more used examples of ABC-based methods, is given in the following definition.

Definition 4.6.1 *The* **Approximate Bayesian computation (ABC) rejection sampler** *[52] follows the following steps:*

1. *Sample θ^* from $\pi(\theta)$.*
2. *Simulate a dataset n^S from $f(n^S|\theta^*)$.*
3. *If $d(n^S, n^I) \leq \varepsilon$, accept θ^*, otherwise reject.*
4. *Return to step 1.*

ABC-based methods then filter the most appropriate values sampled from prior distributions for a given set of parameters by means of a distance d between certain approximations of the likelihood function and the observed data. But before applying this methodology to model given by Equation (4.6), several definitions are needed which will be used as prior distributions later on.

Definition 4.6.2 *A random variable X has an* **uniform distribution**, $X \sim U(a, b)$, *if its probability density function is given by:*

$$f(x) = \frac{1}{b-a}, \quad a < x < b, \tag{4.13}$$

where a and b are fixed constants.

Definition 4.6.3 *For a given positive integer n, the* **gamma function**, Γ *is an extension of the factorial function, shifting arguments down by 1. That is*

$$\Gamma(n) = (n-1)! = (n-1) \cdot (n-2) \cdots \tag{4.14}$$

Definition 4.6.4 *A random variable X defined over the interval $[0,1]$ has a* **beta distribution** *with parameters α and β, $X \sim$ **Beta**(α,β), if its probability distribution function is given by*

$$\mathcal{F}(x) = \frac{x^{\alpha-1}(1-x)^{\beta-1}}{B(\alpha,\beta)}, \quad 0 \leq x \leq 1, \tag{4.15}$$

where α and β are positive parameters and $B(\alpha,\beta) = \frac{\Gamma(\alpha)\Gamma(\beta)}{\Gamma(\alpha+\beta)}$ (Γ is gamma function).

Recapitulating, parameters $\{\alpha_1,\ \alpha_2,\ \beta,\ \lambda_2,\ \lambda_4,\ \kappa_3,\ \gamma_4,\ \mu_2\} \in \{\theta_V\}$ are obtained for a first approximation from System (4.6) using the control case data. However, the more than probable diverse manner of the Immune System to behave with and without a challenge activation guides us towards considerations found in literature as well as intuition to choose the intervals of the uniform prior distribution $\pi(\theta_V)$ for each of these parameters under the infection scenario. For this purpose, sufficiently wide intervals broadly considering a range which contemplates successive and reasonable speeds of reaction are taken under two alternatives procedures. One of them choosing the prior over the parameter itself and, the other, over the inverse of the parameter, that is, over a time scale.

So far, there are four different scenarios for our analysis of parameters:

- U_ρ: When $\pi(\theta_V)$ follows a uniform distribution over parameters θ_V.
- U_τ: When $\pi(\theta_V)$ follows a uniform distribution over the exponent of the intervals of the parameters θ_V.
- $Beta_\rho$: When $\pi(\theta_V)$ follows a $Beta(\frac{1}{2},\frac{1}{2})$ over parameters θ_V.
- $Beta_\tau$: When $\pi(\theta_V)$ follows a $Beta(\frac{1}{2},\frac{1}{2})$ over the exponent of the intervals of the parameters θ_V.

Other four similar scenarios when the priors are taken over the time (the inverse of the parameters) were also studied although results are not shown here. Now, given the sample $\theta_i^* = (\alpha_1^*, \alpha_2^*, \beta^*, \lambda_2^*, \lambda_4^*, \kappa_3^*, \gamma_4^*, \mu_2^*)_i \in \{\theta_V\}$, for $i = 1, 2, ...N$, prior distributions can be defined as:

The U_ρ (left column) and U_τ (right column) cases:

$$\begin{aligned}
&\alpha_1 \sim U[10^{-5}, 10^{0}](h^{-1}), && \alpha_1 \sim 10^{U[-5,0]}(h^{-1}),\\
&\alpha_2 \sim U[10^{-5}, 10^{0}](h^{-1}), && \alpha_2 \sim 10^{U[-5,0]}(h^{-1}),\\
&\beta \sim U[10^{-10}, 10^{-3}](h^{-1}\cdot cell^{-1}), && \beta \sim 10^{U[-10,-3]}(h^{-1}\cdot cell^{-1}),\\
&\lambda_2 \sim U[10^{-2}, 10^{2}](h^{-1}), && \lambda_2 \sim 10^{U[-2,2]}(h^{-1}),\\
&\lambda_4 \sim U[10^{-2}, 10^{2}](h^{-1}), && \lambda_4 \sim 10^{U[-2,2]}(h^{-1}),\\
&\kappa_3 \sim U[10^{4}, 10^{8}](cell), && \kappa_3 \sim 10^{U[4,8]}(cell),\\
&\gamma_4 \sim U[10^{-10}, 10^{-3}](h^{-1}\cdot cell^{-1}), && \gamma_4 \sim 10^{U[-10,-3]}(h^{-1}\cdot cell^{-1}),\\
&\mu_2 \sim U[10^{-4}, 10^{-1}](h^{-1}), && \mu_2 \sim 10^{U[-4,-1]}(h^{-1}).
\end{aligned} \tag{4.16}$$

where U represents the uniform distribution. The $Beta_\rho$ (left column) and $Beta_\tau$ (right column) cases:

$$\begin{aligned}
&\alpha_1 \sim Beta[10^{-5}, 10^{0}](h^{-1}), && \alpha_1 \sim 10^{Beta[-5,0]}(h^{-1}),\\
&\alpha_2 \sim Beta[10^{-5}, 10^{0}](h^{-1}), && \alpha_2 \sim 10^{Beta[-5,0]}(h^{-1}),\\
&\beta \sim Beta[10^{-10}, 10^{-3}](h^{-1}\cdot cell^{-1}), && \beta \sim 10^{Beta[-10,-3]}(h^{-1}\cdot cell^{-1}),\\
&\lambda_2 \sim Beta[10^{-2}, 10^{2}](h^{-1}), && \lambda_2 \sim 10^{Beta[-2,2]}(h^{-1}),\\
&\lambda_4 \sim Beta[10^{-2}, 10^{2}](h^{-1}), && \lambda_4 \sim 10^{Beta[-2,2]}(h^{-1}),\\
&\kappa_3 \sim Beta[10^{4}, 10^{8}](cell), && \kappa_3 \sim 10^{Beta[4,8]}(cell),\\
&\gamma_4 \sim Beta[10^{-10}, 10^{-3}](h^{-1}\cdot cell^{-1}), && \gamma_4 \sim 10^{Beta[-10,-3]}(h^{-1}\cdot cell^{-1}),\\
&\mu_2 \sim Beta[10^{-4}, 10^{-1}](h^{-1}), && \mu_2 \sim 10^{Beta[-4,-1]}(h^{-1}).
\end{aligned} \tag{4.17}$$

where $Beta$ represents $Beta(\frac{1}{2}, \frac{1}{2})$ distribution. Then, an ABC estimation (Definition 4.6.1) was computed for obtaining the posterior distributions of these parameters using the distance

$$d(n^{S_i}, n^I) = \sqrt{\sum_{j=1}^{6}\sum_{k=1}^{4}\left(\frac{n_k^{S_i}(j) - mean(n_k^I(j))}{sd(n_k^I(j))}\right)^2}, \tag{4.18}$$

where n^{S_i} is the solution of System (4.6) for every sample θ_i^* over either θ or τ_θ. For this purpose,

the set of accepted values **A** can be defined as:

$$\mathbf{A} = \{\theta_i^*; d(n^{S_i}, n^I) < \delta\}, \tag{4.19}$$

for a given fixed $\delta \in \Re^+$. For this first approach, best combination of values θ_{min} from all θ_i in **A** (given by the minimum value of $d(n^{S_i}, n^I)$) was used to plot curves $n_s(t)$ for $s = 1, 2, 3, 4$. This would give so far the best fit to data $n_s^I(i, j)$, for $s = 1, 2, 3, 4$. However either the first set of dots was fairly reproduced and then the curves for regulatory and IL-2 producer cells do not reach a peak within the 16 days time or there were another bunch of accepted parameters which gave a reasonable accuracy for the second half of the dots without reproducing the peak around the third day (results not shown here).

4.6.3 LCMV challenge model

This vicissitude suggested a next step in which the strength of the challenge signal would be progressively reduced, in a linear manner, starting at a certain time of the activation process t_0 until it extinguishes after an interval Δt that will be given by $t_{chall} = t_0 + \Delta t$. This LCMV challenge affects only parameters α_1, α_2 and λ_2. Therefore, the two new priors that were considered in the *ABC* analysis

$$\begin{aligned} t_0 &\sim U[12, 96](h) \\ \Delta t &\sim U[1, 72](h). \end{aligned} \tag{4.20}$$

Our new set of parameters is now called $\Theta_V = \{\alpha_1, \alpha_2, \beta, \lambda_2, \lambda_4, \kappa_3, \gamma_4, \mu_2, t_0, t_{chall}\}$. For each of the N proposed set of parameters θ_i^* in Θ_V taken from the prior distributions, System (4.6) is solved for $t \in [0, t_{0_i}[$ for $i = 1, 2, 3...N$. The code jumps then for $t \in [t_{0_i}, t_{chall_i}[$ $(i = 1, 2, 3...N)$ to solve System (4.21)

$$\begin{aligned} \frac{dn_1}{dt} &= \nu_1 + \lambda_1 n_1 \left(1 - \frac{n_1}{\kappa_1}\right) - \mu_1 n_1 - g(t; t_0, t_{chall})\alpha_1 n_1, \\ \frac{dn_2}{dt} &= g(t; t_0, t_{chall})\alpha_1 n_1 + g(t; t_0, t_{chall})\lambda_2 n_2 - \mu_2 n_2 - g(t; t_0, t_{chall})\alpha_2 n_2 - \beta n_2 n_4, \\ \frac{dn_3}{dt} &= g(t; t_0, t_{chall})\alpha_2 n_2 + \lambda_3 n_3 \left(1 - \frac{n_3}{\kappa_3}\right) - \mu_3 n_3, \\ \frac{dn_4}{dt} &= \nu_4 + \lambda_4 n_4 \left(1 - \frac{n_4}{\kappa_4}\right) - \mu_4 n_4 + \gamma_4 n_4 n_2. \end{aligned} \tag{4.21}$$

where $g(t; t_0, t_{chall}) = \frac{t_{chall}-t}{t_{chall}-t_0}$ and similarly for Model (II) in System (4.7). Finally, once the virus is cleared, this is, α_1,α_2, $\lambda_2 \to 0$, for $t = [t_{chall_i}, 16 \cdot 24]$ (h), the code jumps to solve System (4.22),

$$\begin{aligned}
\frac{dn_1}{dt} &= \nu_1 + \lambda_1 n_1 \left(1 - \frac{n_1}{\kappa_1}\right) - \mu_1 n_1, \\
\frac{dn_2}{dt} &= -\mu_2 n_2 - \beta n_2 n_4, \\
\frac{dn_3}{dt} &= \lambda_3 n_3 \left(1 - \frac{n_3}{\kappa_3}\right) - \mu_3 n_3, \\
\frac{dn_4}{dt} &= \nu_4 + \lambda_4 n_4 \left(1 - \frac{n_4}{\kappa_4}\right) - \mu_4 n_4 + \gamma_4 n_4 n_2,
\end{aligned} \tag{4.22}$$

and similarly for Model (II) in System (4.7). This is, the strength of the activation signal vanishes progressively from t_0 to t_{chall} and this is reflected on parameters α_1, α_2 and λ_2 which, after $t = t_{chall_i}$ will be equal to 0. So far, the results of the posterior distributions obtained when using the priors over the parameter or over the time can be compared. For this comparison to be realistic, in both cases the same amount of proposals were taken, $N = 10^6$, and so the same threshold of acceptance, $\delta = 29$. In this way, it can be compared not only the differences in the distributions, but the amount of accepted proposal N_A for each case and the best fit(s) given by the minimum value(s) of $d(n^{S_i}, n^I)$, being the output of each approach our accepted matrix in Equation (4.19)

$$\mathbf{A} = \begin{pmatrix}
(\alpha_1^*)_1 & (\alpha_1^*)_2 & \dots & (\alpha_1^*)_{N_A} \\
(\alpha_2^*)_1 & (\alpha_2^*)_2 & \dots & (\alpha_2^*)_{N_A} \\
(\beta^*)_1 & (\beta^*)_2 & \dots & (\beta^*)_{N_A} \\
\vdots & \vdots & \ddots & \vdots \\
(t_0^*)_1 & (t_0^*)_2 & \dots & (t_0^*)_{N_A} \\
(t_{chall}^*)_1 & (t_{chall}^*)_2 & \dots & (t_{chall}^*)_{N_A}
\end{pmatrix}, \tag{4.23}$$

Still, the curve for IL-2 producer cells do not seem to reflect the behaviour given by the data in what the highest value concerns (results not shown here). This seem to be due to the convenience of the distance measure to give priority the proximity to dots excluding day 3. However, and given the difficulty in measuring the expression levels which might happen in shorter slots of time than 24 hours, the Bayesian fitting was computed again ignoring the results obtained in day 3, which could perhaps not represent rigorously the time scales of what is happening, to somehow force the curve to reach the high peak at the following day. The same plots as for the previous

case were obtained and here it is shown (Figure 4.22) how the curve now follows a more similar behaviour to expected experimentally. A summary of the characteristics of each approach (also for Model (II)) is shown in the following table

	MODEL I Death pathway		MODEL II Differentiation pathway	
	‰ acceptance	Min($d(n^{S_i}, n^I)$)	‰ acceptance	Min($d(n^{S_i}, n^I)$)
U_τ over θ	2.28	22.550	1.68	21.514
$Beta_\rho$ over θ	0.10	24.647	0.11	23.672
$Beta_\tau$ over θ	1.90	22.543	1.78	22.361
U_ρ over τ_θ	0.50	24.008	0.51	21.719
U_τ over τ_θ	2.23	22.741	1.65	21.143
$Beta_\rho$ over τ_θ	3.29	23.606	3.33	23.392
$Beta_\tau$ over τ_θ	2.01	23.368	1.76	21.641

Table 4.14: Summary of the eight different approaches U_ρ,U_τ,$Beta_\rho$,$Beta_\tau$ all over θ and over τ_θ regarding the number of trials N_T (for $\delta = 29$) and for Models (I) and (II). Data from U_ρ was not possible to obtain under this value of δ for computational reasons.

4.7 Results

Out of the ten different posterior distributions, one for each parameter, that are obtained from each approach, let us focus on those which present a higher disagreement among them. Figure 4.11, shows these dissimilarities for α_1 in a coupled way when comparing the four cases U_τ, $Beta_\tau$ (Model (I)), U_τ^*, $Beta_\tau^*$ (Model (II)) when the prior distributions are considered over the parameters. It can be observed how the posterior distribution, plotted in light blue, seems to follow a bimodal shape when *Beta* distribution is used as the prior for computing the distance whereas it looks more uni-modal when using a uniform prior. This suggests that the inclusion of weight on the sides, which is what the *Beta* distribution does, would bring two alternative pathways to minimise the distance of the curves to the data. Nevertheless, the only two parameters which can increase the proliferation of IL-2 producers are the differentiation of naive cells into IL-2 producers, recorded by α_1, and the proliferation of the latter, given by λ_2. However, correlations between this two variables, shown in Figure 4.20, indicates that when the model accepts high values for λ_2, instead of compensating with smaller values for α_1, it tends to accept values of α_1 in the middle of its prior interval, which is what produces this accumulation of values in the posterior distribution.

Broadly speaking, two different types of behaviour can be observed when comparing prior

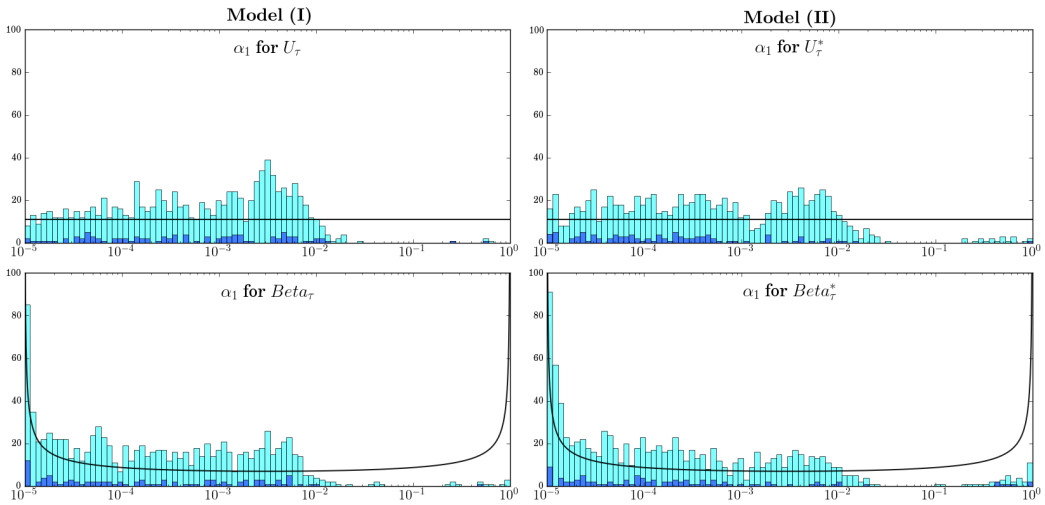

Figure 4.11: α_1 for U_τ,U^*_τ,$Beta_\tau$,$Beta^*_\tau$ prior (black curve) and posterior distributions (light blue). Dark blue bars correspond to the 10% of the accepted values **A** which gives the smallest distance d.

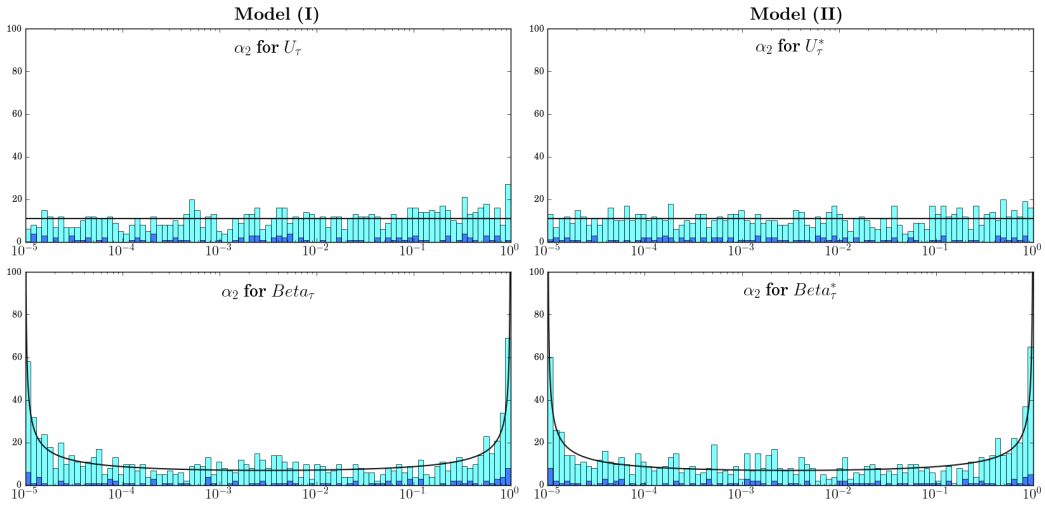

Figure 4.12: α_2 for U_τ,U^*_τ,$Beta_\tau$,$Beta^*_\tau$ prior (black curve) and posterior distributions (light blue). Dark blue bars correspond to the 10% of the accepted values **A** which gives the smallest distance d.

to posterior distributions in the parameters. Mainly for α_1, λ_2, β and γ_4, some noticeable dependency between the learning and the prior distribution can be observed, when taking together the uniform and the beta distributions (Figures 4.11,4.13,4.15,4.16). Even when these alterations are not very significant, they have to be taken into account when comparing how the respective variations in the other parameters are almost negligible, supporting the idea that these

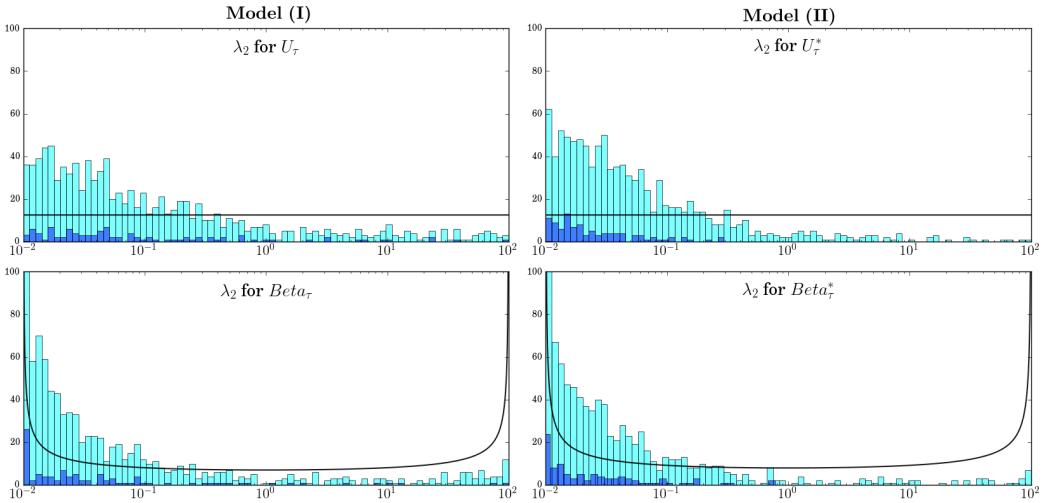

Figure 4.13: λ_2 for U_τ,U^*_τ,$Beta_\tau$,$Beta^*_\tau$ prior (black curve) and posterior distributions (light blue). Dark blue bars correspond to the 10% of the accepted values **A** which gives the smallest distance d.

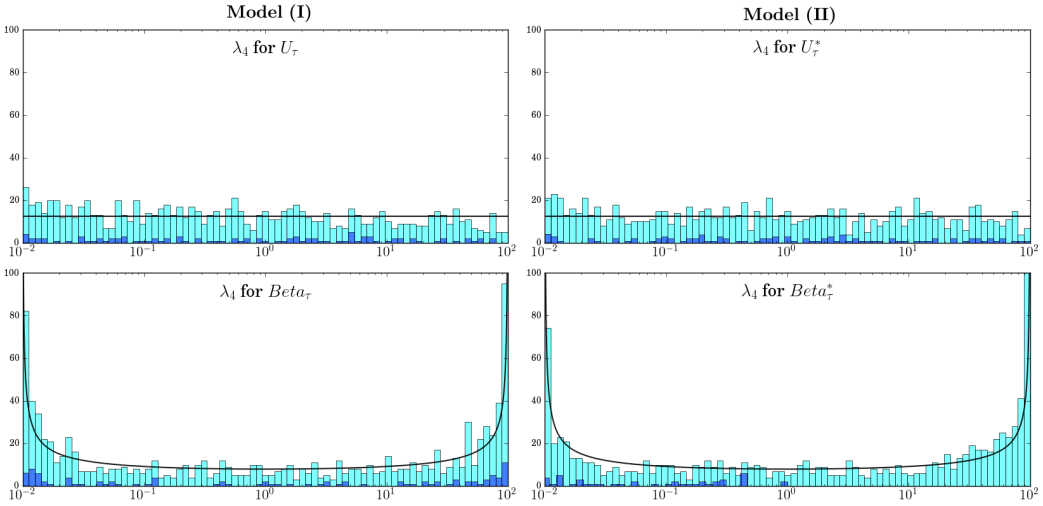

Figure 4.14: λ_4 for U_τ,U^*_τ,$Beta_\tau$,$Beta^*_\tau$ prior (black curve) and posterior distributions (light blue). Dark blue bars correspond to the 10% of the accepted values **A** which gives the smallest distance d.

four parameters are those driving the Bayesian learning.

Regarding the posterior distribution of λ_2, Figure 4.13 does not show much difference between the diverse approaches further the amount of accepted values that are reflected also in the prior distribution and given in Table 4.14. Taking these two plots together the output clusters

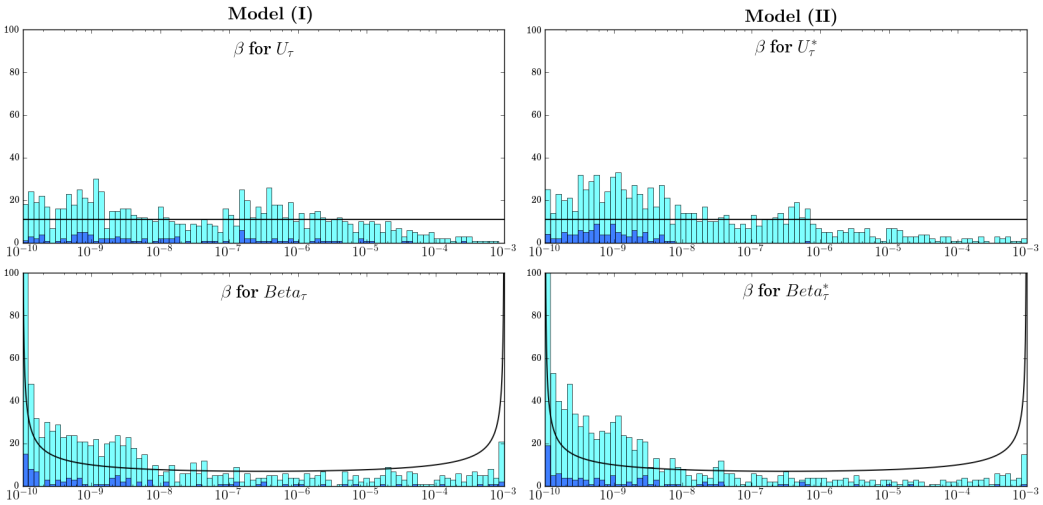

Figure 4.15: β for U_τ,U_τ^*,$Beta_\tau$,$Beta_\tau^*$ prior (black curve) and posterior distributions (light blue). Dark blue bars correspond to the 10% of the accepted values **A** which gives the smallest distance d.

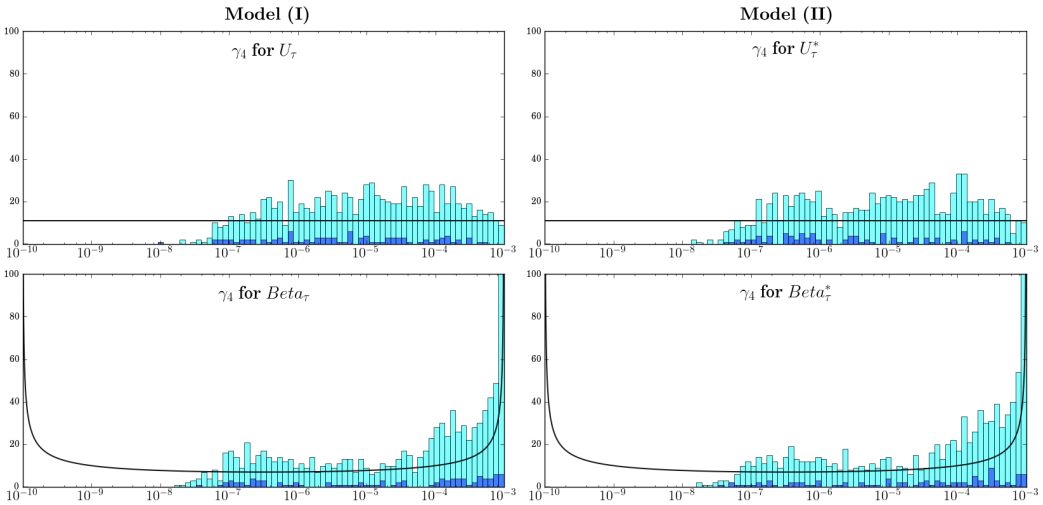

Figure 4.16: γ_4 for U_τ,U_τ^*,$Beta_\tau$,$Beta_\tau^*$ prior (black curve) and posterior distributions (light blue). Dark blue bars correspond to the 10% of the accepted values **A** which gives the smallest distance d.

the truthfulness of the model in two different groups characterised by the strength of naive differentiation into IL-2 producers. This behaviour can also be appreciated in the most of the other parameters (see for instance β posterior distributions in Figure 4.15). This approximation to the best fit might act as a support of the robustness of the model.

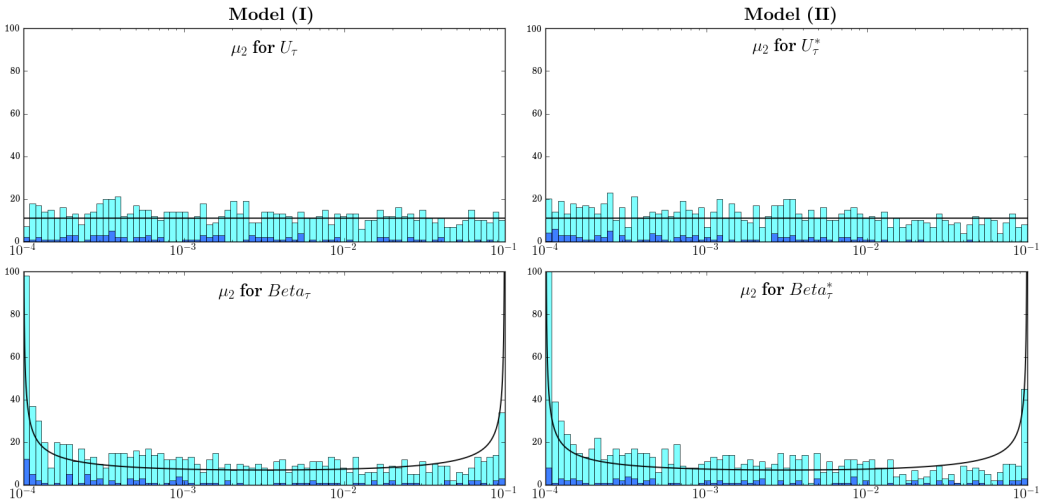

Figure 4.17: μ_2 for U_τ,U_τ^*,$Beta_\tau$,$Beta_\tau^*$ prior (black curve) and posterior distributions (light blue). Dark blue bars correspond to the 10% of the accepted values **A** which gives the smallest distance d.

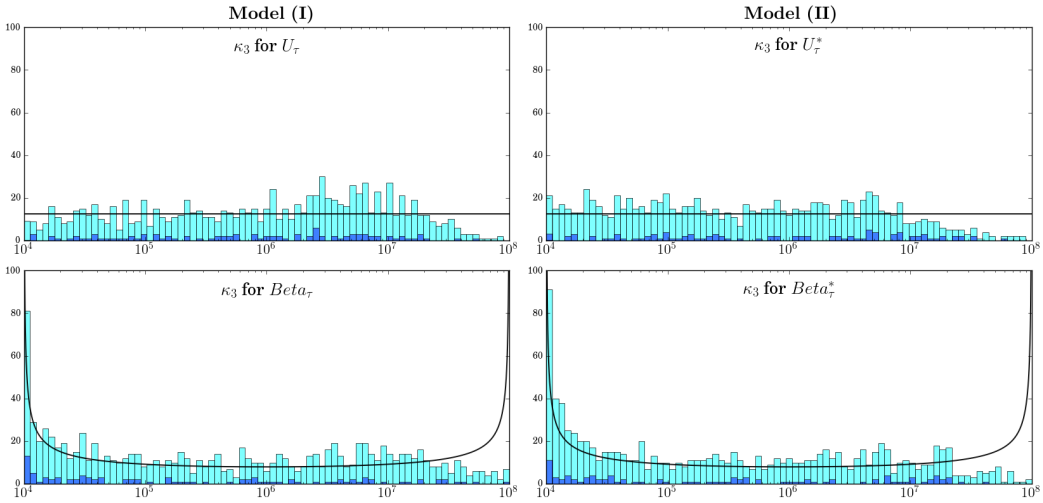

Figure 4.18: κ_3 for U_τ,U_τ^*,$Beta_\tau$,$Beta_\tau^*$ prior (black curve) and posterior distributions (light blue). Dark blue bars correspond to the 10% of the accepted values **A** which gives the smallest distance d.

		Mean	*Std. Dev.*	*Min*	*Median*	*Max*
α_1	U_τ	$3.98 \cdot 10^{-3}$	$3.21 \cdot 10^{-2}$	$1.01 \cdot 10^{-5}$	$6.42 \cdot 10^{-4}$	$6.16 \cdot 10^{-1}$
	U_τ^*	$1.16 \cdot 10^{-2}$	$7.35 \cdot 10^{-2}$	$1.00 \cdot 10^{-5}$	$4.08 \cdot 10^{-4}$	$9.37 \cdot 10^{-1}$
	$Beta_\tau$	$8.35 \cdot 10^{-3}$	$6.99 \cdot 10^{-2}$	$1.00 \cdot 10^{-5}$	$1.85 \cdot 10^{-4}$	$9.87 \cdot 10^{-1}$
	$Beta_\tau^*$	$2.51 \cdot 10^{-2}$	$1.31 \cdot 10^{-1}$	$1.00 \cdot 10^{-5}$	$1.28 \cdot 10^{-4}$	$9.99 \cdot 10^{-1}$
α_2	U_τ	$1.17 \cdot 10^{-1}$	$2.22 \cdot 10^{-1}$	$1.01 \cdot 10^{-5}$	$6.71 \cdot 10^{-3}$	$9.97 \cdot 10^{-1}$
	U_τ^*	$1.06 \cdot 10^{-1}$	$2.13 \cdot 10^{-1}$	$1.01 \cdot 10^{-5}$	$3.58 \cdot 10^{-3}$	$9.95 \cdot 10^{-1}$
	$Beta_\tau$	$1.69 \cdot 10^{-1}$	$3.05 \cdot 10^{-1}$	$1.00 \cdot 10^{-5}$	$2.65 \cdot 10^{-3}$	1.00
	$Beta_\tau^*$	$1.74 \cdot 10^{-1}$	$3.06 \cdot 10^{-1}$	$1.00 \cdot 10^{-5}$	$2.15 \cdot 10^{-3}$	1.00

Table 4.15: Summary of posterior distributions when uniform prior is taken over the logarithm of the parameters and β term represents death of IL-2 producer cells (case U_τ).

		Mean	*Std. Dev.*	*Min*	*Median*	*Max*
λ_2	U_τ	2.83	$1.13 \cdot 10$	$1.00 \cdot 10^{-2}$	$5.17 \cdot 10^{-2}$	$9.85 \cdot 10$
	U_τ^*	$7.61 \cdot 10^{-1}$	5.36	$1.00 \cdot 10^{-2}$	$3.48 \cdot 10^{-2}$	$9.00 \cdot 10$
	$Beta_\tau$	3.86	$1.53 \cdot 10$	$1.00 \cdot 10^{-2}$	$2.19 \cdot 10^{-2}$	$1.00 \cdot 102$
	$Beta_\tau^*$	1.73	$1.05 \cdot 10$	$1.00 \cdot 10^{-2}$	$2.12 \cdot 10^{-2}$	$9.96 \cdot 10$
λ_4	U_τ	7.75	$1.67 \cdot 10$	$1.00 \cdot 10^{-2}$	$5.11 \cdot 10^{-1}$	$9.86 \cdot 10$
	U_τ^*	9.03	$1.81 \cdot 10$	$1.00 \cdot 10^{-2}$	$6.74 \cdot 10^{-1}$	$9.92 \cdot 10$
	$Beta_\tau$	$2.28 \cdot 10$	$3.38 \cdot 10$	$1.00 \cdot 10^{-2}$	1.28	$1.00 \cdot 10^2$
	$Beta_\tau^*$	$2.59 \cdot 10$	$3.51 \cdot 10$	$1.00 \cdot 10^{-2}$	2.52	$1.00 \cdot 10^2$

Table 4.16: Summary of posterior distributions when uniform prior is taken over the log of the parameters and β term represents death of IL-2 producer cells (case U_τ).

		Mean	*Std. Dev.*	*Min*	*Median*	*Max*
β	U_τ	$9.15 \cdot 10^{-6}$	$4.98 \cdot 10^{-5}$	$1.01 \cdot 10^{-10}$	$3.38 \cdot 10^{-8}$	$7.84 \cdot 10^{-4}$
	U_τ^*	$1.00 \cdot 10^{-5}$	$6.75 \cdot 10^{-5}$	$1.00 \cdot 10^{-10}$	$4.52 \cdot 10^{-9}$	$9.06 \cdot 10^{-4}$
	$Beta_\tau$	$4.26 \cdot 10^{-5}$	$1.64 \cdot 10^{-4}$	$1.00 \cdot 10^{-10}$	$1.38 \cdot 10^{-9}$	$9.99 \cdot 10^{-4}$
	$Beta_\tau^*$	$3.17 \cdot 10^{-5}$	$1.44 \cdot 10^{-4}$	$1.00 \cdot 10^{-10}$	$7.03 \cdot 10^{-10}$	$1.00 \cdot 10^{-3}$
γ_4	U_τ	$8.43 \cdot 10^{-5}$	$1.67 \cdot 10^{-4}$	$1.05 \cdot 10^{-8}$	$1.02 \cdot 10^{-5}$	$9.90 \cdot 10^{-4}$
	U_τ^*	$8.04 \cdot 10^{-5}$	$1.62 \cdot 10^{-4}$	$1.39 \cdot 10^{-8}$	$9.89 \cdot 10^{-6}$	$9.71 \cdot 10^{-4}$
	$Beta_\tau$	$2.51 \cdot 10^{-4}$	$3.25 \cdot 10^{-4}$	$1.63 \cdot 10^{-8}$	$8.37 \cdot 10^{-5}$	$1.00 \cdot 10^{-3}$
	$Beta_\tau^*$	$2.58 \cdot 10^{-4}$	$3.26 \cdot 10^{-4}$	$1.79 \cdot 10^{-8}$	$8.94 \cdot 10^{-5}$	$1.00 \cdot 10^{-3}$

Table 4.17: Summary of posterior distributions when uniform prior is taken over the log of the parameters and β term represents death of IL-2 producer cells (case U_τ).

		Mean	*Std. Dev.*	*Min*	*Median*	*Max*
μ_2	U_τ	$1.25 \cdot 10^{-2}$	$2.13 \cdot 10^{-2}$	$1.00 \cdot 10^{-4}$	$2.26 \cdot 10^{-3}$	$9.85 \cdot 10^{-2}$
	U_τ^*	$1.07 \cdot 10^{-2}$	$1.96 \cdot 10^{-2}$	$1.00 \cdot 10^{-4}$	$1.97 \cdot 10^{-3}$	$9.70 \cdot 10^{-2}$
	$Beta_\tau$	$1.30 \cdot 10^{-2}$	$2.51 \cdot 10^{-2}$	$1.00 \cdot 10^{-4}$	$1.01 \cdot 10^{-3}$	$1.00 \cdot 10^{-1}$
	$Beta_\tau^*$	$1.19 \cdot 10^{-2}$	$2.52 \cdot 10^{-2}$	$1.00 \cdot 10^{-4}$	$9.42 \cdot 10^{-4}$	$1.00 \cdot 10^{-1}$
κ_3	U_τ	$5.15 \cdot 10^6$	$9.42 \cdot 10^6$	$1.01 \cdot 10^4$	$1.21 \cdot 10^6$	$8.31 \cdot 10^7$
	U_τ^*	$3.43 \cdot 10^6$	$8.59 \cdot 10^6$	$1.00 \cdot 10^4$	$4.28 \cdot 10^5$	$8.26 \cdot 10^7$
	$Beta_\tau$	$6.48 \cdot 10^6$	$1.46 \cdot 10^7$	$1.00 \cdot 10^4$	$3.73 \cdot 10^5$	$9.96 \cdot 10^7$
	$Beta_\tau^*$	$4.72 \cdot 10^6$	$1.14 \cdot 10^7$	$1.00 \cdot 10^4$	$2.37 \cdot 10^5$	$9.41 \cdot 10^7$

Table 4.18: Summary of posterior distributions when uniform prior is taken over the log of the parameters and β term represents death of IL-2 producer cells (case U_τ).

		Mean	*Std. Dev.*	*Min*	*Median*	*Max*
t_0	U_τ	66.85	22.89	12	72	95
	U_τ^*	63.45	23.21	12	69	95
	$Beta_\tau$	63.82	28.59	12	73	95
	$Beta_\tau^*$	60.60	29.84	12	68	95

Table 4.19: Summary of posterior distributions when uniform prior is taken over the log of the parameters and β term represents death of IL-2 producer cells (case U_τ).

Regarding the strength of the signal for the activation, results seem to suggest a delay of between 62 and 67 hours average, depending on the approach that has been followed (U_τ, $Beta_\tau$, U^*_τ or $Beta^*_\tau$ (Table 4.19). Even when the acceptance criteria must consider the election of a vector with 10 different proposed parameters, from the prior uniform distribution which interval, for t_0, is $[12, 96]$, Figure 4.19 show the posterior distribution of this parameter with a clear slope to the right for every case. However when only the 10% of the accepted values giving the minimum distance are considered, the distribution looks more homogeneous and, specially for the IL-2 death pathway, the optimal value is obtained when α_1, α_2 and λ_2 start to decrease between the first and the second day.

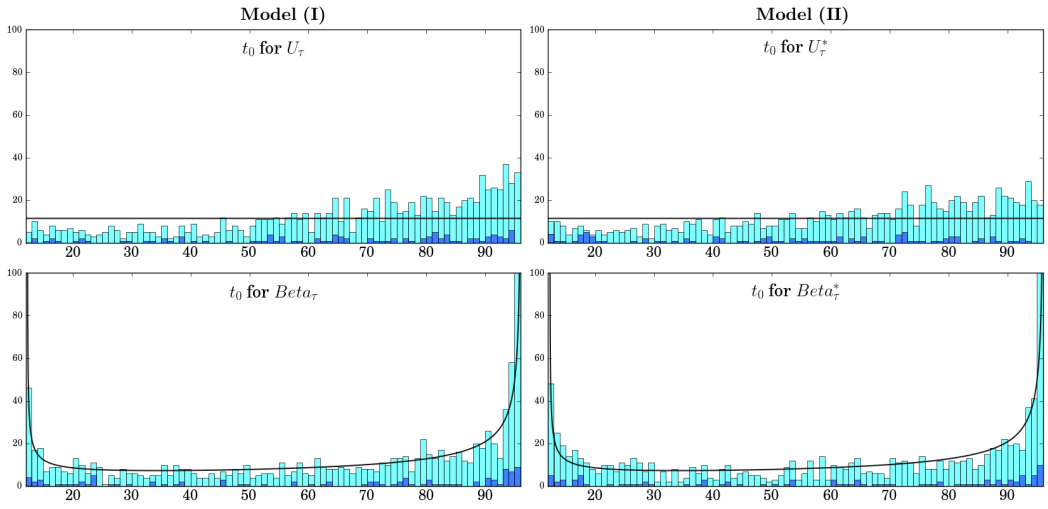

Figure 4.19: t_0 prior (black curve) and posterior distributions (light blue). Dark blue bars correspond to the 10% of the accepted values **A** which gives the smallest distance d.

4.7.1 Model selection

The tendency for preferring the differentiation path or the death one for IL-2 producer cells does not seem to be strongly supported by the model comparison in which the ‰of acceptances was contrasted in both scenarios. On the other hand, the robustness of the model is also seconded by the relatively small different appearing regarding the different approach that has been followed, according to the values below. Let us call p =‰of acceptances for model (I) and p^* = ‰of acceptances for model (II) for every single approach. Then, it can be concluded:

- For U_τ over θ versus U^*_τ: $\frac{p^*_{UL}}{(p^*_{UL}+p_{UL})} = 0.425$

- For $Beta_\rho$ over θ versus $Beta^*_\rho$: $\frac{p^*_B}{(p^*_B+p_B)} = 0.511$
- For $Beta_\tau$ over θ versus $Beta^*_\tau$: $\frac{p^*_{BL}}{(p^*_{BL}+p_{BL})} = 0.483$
- For U_ρ over τ_θ versus U^*_ρ: $\frac{p^*_U}{(p^*_U+p_U)} = 0.505$
- For U_τ over τ_θ versus U^*_τ: $\frac{p^*_{UL}}{(p^*_{UL}+p_{UL})} = 0.426$
- For $Beta_\rho$ over τ_θ versus $Beta^*_\rho$: $\frac{p^*_B}{(p^*_B+p_B)} = 0.505$
- For $Beta_\tau$ over τ_θ versus $Beta^*_\tau$: $\frac{p^*_{BL}}{(p^*_{BL}+p_{BL})} = 0.466$

4.8 Discussion

This chapter goes through an adapted model for quorum-sensing mechanism involving $CD4^+$ T cells, IL-2 producer cells and T reg cells. The first part (Sections 4.2 and 4.3) mainly analyses from a statistical point of view several experiments in which under different scenarios population levels were tracked. First, a lymphopenia driven proliferation set of experiments shows, with variability occurring from one condition to another, that negative feedback from T reg cells to the other cells cannot be explained in a linear way as clearly as the positive signal from IL-2 (Figures 4.3-4.6). Among other observations explained in Section 4.2, it is reasonable as a first approach to analyse these correlations from a relative and a total point of view before making further conclusions.

After this, Section 4.4 propose a quorum-sensing model for trying to reproduce the mechanisms observed in data. Once the model is introduced, the first step is to localise those parameters that mainly drive the output of the model. For this purpose, Section 4.5 identifies such rates that would be used afterwards in the Bayesian estimation and fix those which would be taken from literature. In this Bayesian analysis in Section 4.6.2, the methodology behind the ABC algorithm and so the justification on the election of prior distributions and intervals are explained.

As an attempt of improving our model, once the first results were obtained, we introduced some alterations regarding the variability of some of the rates. Given that the strength in cell signalling might be monotonously reduced [72], we include in Section 4.6.3 two new variables,t_0 and $t_{chall} = t_0 + \Delta t$, in the Bayesian analysis to identify when the activation pathway starts to decrease, encoded by α_1, α_2 and λ_2, and when it would be completely over. Which means that from time 0 to time t_0, these three parameters would take the values obtained in the estimation, and from t_0 to t_{chall}, they would linearly decrease until 0.

Some conclusions about this Bayesian analysis can be observed in Figures 4.11-4.19. There are some parameters for which the learning done by the Bayesian analysis is more relevant than others. For instance, we see that the selection of α_1, λ_2, β and γ_4 has a strong impact on the resultant distance d. For the first three of them, α_1, λ_2, β, small values result in smaller distance, whereas for γ_4 the model tends to choose values higher than 10^{-7}. We can also conclude that there is no significant learning for values α_2 and λ_4. Finally, there is just a preference for not choosing too high values for κ_3 and μ_2, for the latter, specially when using a *Beta* distribution for the prior. It seems then, that the most sensitive reactions for this model to track are related to effector cells production (α_1 and λ_2) and iteractions between regulatory T cells and effector cells, which would be studied in more detail in Chapter 5.

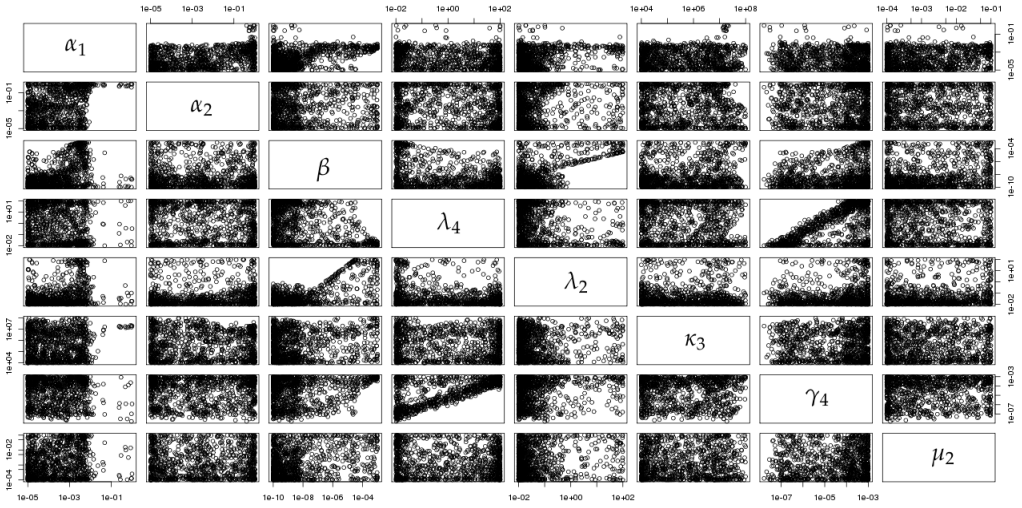

Figure 4.20: Correlations of accepted parameters from $\{\theta_V\}$ for case $Beta_\tau$.

Moreover, Figure 4.20 shows correlations between all different dots in the set of accepted values for case $Beta_\tau$ as a representative example of all of them. In fact, and as it could be predicted from the posterior distributions, differences between approaches do not seem to indicate a significance influence on the output from the election of the prior distribution. A first noticeable thing to comment comes from the vertical and horizontal gaps that some parameters show regardless their correspondence with the others. This is specially evident for α_1 and in a smaller proportion for γ_4 or κ_3, and reflects well with what was observed in the probability distribution plots for the posterior of the parameters which shifts the preference of certain values to a specific side. A more interesting result that cannot be appreciated in the previous plots shows a very strong correlation between λ_4 and γ_4 and, on the other side, between β and λ_2. The first of them suggests that

proliferation of regulatory T cells seems to be somehow balanced by both the influence of IL-2 producer cells and self-development signals and when one of them tends to spread that forces the increase of the other. The second case indicates that from a specific value of λ_2, the same which splits in every correlation the dots into crowded and non-crowded region, the value of β will increase with λ_2, suggesting that IL-2 producer cells would balance their expression levels by the control of the regulatory T cells.

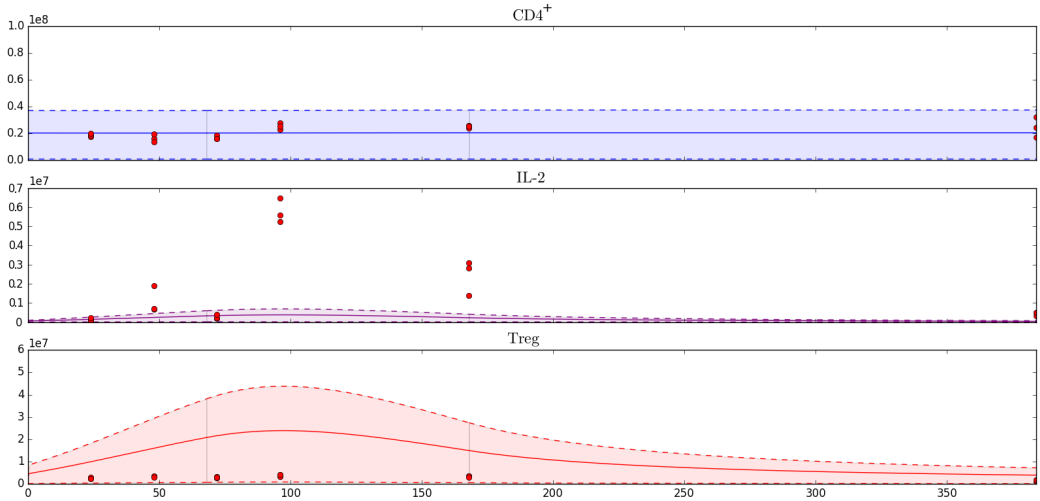

Figure 4.21: Time course of model given by Equation (4.6) for the median values of parameters $\{\theta_V\}$ (shown in Table 4.18) for case $Beta^*_\tau$ with 95% confident interval. Vertical lines reflect the time points where the system jumps from model given by Equation (4.6) to model given by Equation (4.21) and then to model given by Equation (4.22) as explained in Section 4.6.3.

Finally, the median of the values given in Table 4.18 was plotted for the model $Beta^*_\tau$ in Figures 4.21 and 4.22. Both of them show the 95% confident interval and it can be observed that when the whole approach is followed without taking into account dots of day 3 (Figure 4.21), the model seems to better describe the shape of the experimental data. However, due to the particularities of the data and the limitations of the model, the comments made throughout the chapter suggest further study is needed.

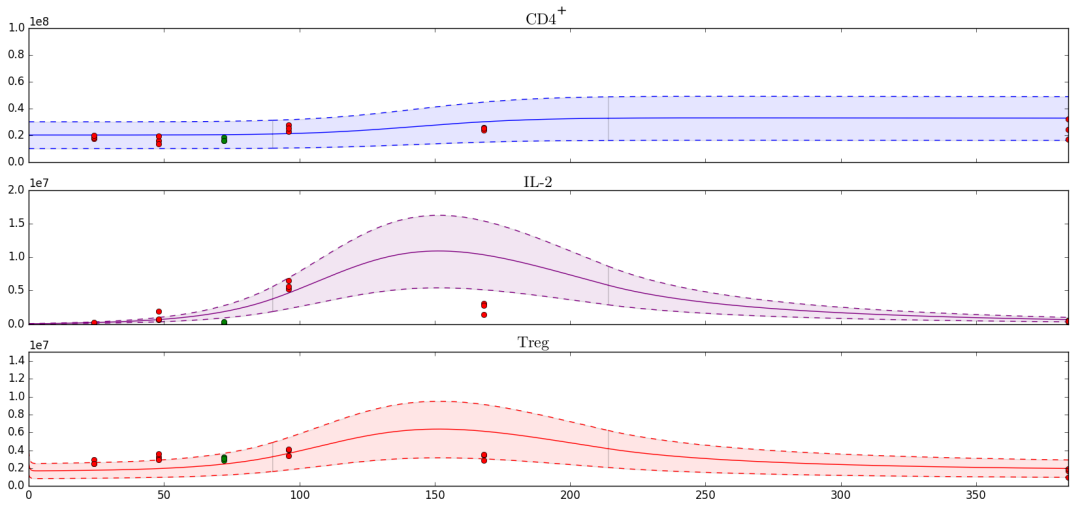

Figure 4.22: Time course of model given by Equation (4.6) for the median values of parameters $\{\theta_V\}$, excluding day 3, for case $Beta^*_\tau$ with 95% confident interval. Vertical lines reflect the time points where the system jumps from model given by Equation (4.6) to model given by Equation (4.21) and then to model given by Equation (4.22) as explained in Section 4.6.3.

Chapter 5

A probabilistic approach to tumour prognosis

5.1 Introduction

In previous chapters, the role of regulatory $CD4^+$T cells suppressing effector T cells (IL-2 producing cells) was explained. From a molecular point of view, in Chapter 3 we explained how CTLA-4 high expression on the surface of T reg cells leads to an acceleration on the blockade of cells proliferation by a cell extrinsic behaviour that depletes triggering molecules on APCs. Moreover, the quorum-sensing mechanism between these two types of cells analysed in Chapter 4 suggests that the relative number of naive, effector, memory and T reg $CD4^+$ T cells determines the mechanism that regulates population levels. In fact, in a cancer scenario, it has been observed [59] that the relative number of effector and T reg cells, as well as IL-2 expression levels, are an indicator of disease progression.

In this Chapter, we consider a tumour scenario to further investigate the role of quorum-sensing. To this end, we only take into account two types of cells; T reg cells and IL-2 producing $CD8^+$ T cells. It has been studied that in malignant tumour, regulatory T cells suppress effective antitumour immunity, causing tumour progression ([70] or [49] among others). To mathematically check this, two different models are proposed for Sections 5.2 and 5.3 encoding interactions between this two subpopulations of cells. Each of these models will be studied both deterministic and stochastically. Moreover, for each of these models, some mathematical results

are used to guarantee the extinction of one of the populations depending on the parameter rates. Finally, Section 5.4 shows some conclusions regarding the results obtained from each approach.

5.2 Toy model

In this section, a basic toy model is considered for two interacting populations of T cells: cytotoxic effector $CD8^+$ T cells (IL-2 producing) and regulatory T cells. $n_E(t)$ and $n_R(t)$ represent the amount of cytotoxic and regulatory T cells, respectively, at time $t \geq 0$. Reactions considered in Equation (5.1) represent linear and non-linear death in both populations (μ_E, μ_R, ν_E and ν_R), where, in the spirit of [4], ν_E and ν_R also act as "carrying capacities"; proliferation due to TCR (λ_E and λ_R), proliferation due to IL-2 (α_E and α_R) and suppression of effector T cells by regulatory T cells (χ).

By focusing on the stochastic version of this model, and considering a continuous-time Markov chain $\mathcal{X} = \{(N_E(t), N_R(t)) : t \geq 0\}$ defined over $\mathbb{N}_0^2$, transitions and infinitesimal transition rates are given by

$$q_{(n_E,n_R),(n'_E,n'_R)} = \begin{cases} \lambda_E n_E + \alpha_E n_E^2, & \text{if } (n'_E, n'_R) = (n_E + 1, n_R), \\ \mu_E n_E + \nu_E n_E^2 + \chi n_E n_R, & \text{if } (n'_E, n'_R) = (n_E - 1, n_R), \\ \lambda_R n_R + \alpha_R n_E n_R, & \text{if } (n'_E, n'_R) = (n_E, n_R + 1), \\ \mu_R n_R + \nu_R n_R^2, & \text{if } (n'_E, n'_R) = (n_E, n_R - 1). \end{cases} \tag{5.1}$$

This represents a bivariate Markov process over $\mathcal{S} = \mathbb{N}_0^2$ that, starting at a given state $(n_E, n_R) \in \mathbb{N}^2$, it may eventually hit one of the axis

$$A_E = \{(n_E, 0) : n_E \in \mathbb{N}\}, \quad A_R = \{(0, n_R) : n_R \in \mathbb{N}\},$$

meaning that one of the T cell populations becomes extinct. Once one population becomes extinct, the surviving species will evolve according to a one-dimensional birth-and-death process; see, for example, [4, Section 6.2].

5.2.1 Probability of extinction and mean time until extinction

A fundamental question is whether this process hits or not one of the axis; that is, whether one of the T cell populations becomes extinct in a finite time or not, with probability one. In order to analyse this, for which we will use some results in [56] and [29], one may consider from now on that A_E and A_R are two sub-sets of absorbing states. Then, we structure the state space of $\mathcal{X}$ as

$$\mathcal{S} \;=\; \mathcal{C} \cup A_E \cup A_R \;=\; \mathcal{C} \cup \mathcal{C}_0, \tag{5.2}$$

with $\mathcal{C}_0$ being an absorbing set of states in an axis and $\mathcal{C} = \mathbb{N}^2$ being an irreducible infinite class of non-absorbing states. Thus, we have Theorem 5.1.

Theorem 5.1. Let $\alpha_{(n_E,n_R)}$, with $(n_E, n_R) \in \mathcal{C}$, be the probability of reaching some state in $\mathcal{C}_0$, from (n_E, n_R), in a finite time, and $\tau_{(n_E,n_R)}$ the mean time until this occurs. Under parameter Regimes A, B or C, $\alpha_{(n_E,n_R)} = 1$ and $\tau_{(n_E,n_R)} < +\infty$ for any initial state $(n_E, n_R) \in \mathcal{C}$. Where

Regime A**:**	**Regime** B**:**	**Regime** C**:**
$\mu_E = \mu_R$,	$\mu_E = \mu_R$,	$\mu_E = \mu_R$,
$\lambda_E > \lambda_R$,	$\lambda_E > \lambda_R$,	$\lambda_E > \lambda_R$,
$\alpha_R > \alpha_E$,	$\alpha_R > \alpha_E$,	$\alpha_R > \alpha_E$,
$\nu_E > \alpha_E > \frac{\alpha_R}{2}$,	$\nu_E > \alpha_E > \frac{\alpha_R}{2}$,	$\nu_E = \nu_R = \nu > \alpha_E > \frac{\alpha_R}{2}$,
$2\nu_E < \chi < \nu_E + \nu_R$.	$2\nu_R > \chi > \nu_E + \nu_R$.	$2\nu < \chi$.

Proof.

We prove this result by means of [56, Criterion C]. In particular, this criterion states:

> *[56, Criterion C]: Lets suppose that $\mathcal{X}$ is a regular process defined over $\mathcal{S} = \mathcal{C} \cup \mathcal{C}_0$ where $\mathcal{C}$ is a set of non-absorbing states and $\mathcal{C}_0$ is a set of absorbing states. Let $\alpha_{(n_E,n_R)}$, with $(n_E, n_R) \in \mathcal{C}$, be the probability of reaching some state in $\mathcal{C}_0$, from (n_E, n_R), in a finite time, and $\tau_{(n_E,n_R)}$ the mean time until this occurs. If there exists a set of constants $u_{(n'_E,n'_R)} \geq 0$ for $(n'_E, n'_R) \in \mathcal{C}$ such that*
>
> $$\sum_{(n'_E,n'_R)\in\mathcal{S}} q_{(n_E,n_R),(n'_E,n'_R)} u_{(n'_E,n'_R)} \;\leq\; -1, \quad \forall (n_E, n_R) \in \mathcal{C},$$

then $\alpha_{(n_E,n_R)} = 1$ *and* $\tau_{(n_E,n_R)} \leq u_{(n_E,n_R)} < +\infty$.

The utility of this criterion is partially limited by the fact that it is not trivial to find these constants $u_{(n_E,n_R)}$. *We may instead follow the results in [29] where alternative sufficient conditions are given. In order to use results in [29], we first organise* $\mathcal{C}$ *by levels as*

$$\mathcal{C} = \bigcup_{k=2}^{+\infty} \mathcal{C}(k), \quad \mathcal{C}(k) = \{(n_E, n_R) \in \mathcal{C} : \ n_E + n_R = k\}.$$

For each level $\mathcal{C}(k)$, *we define the global birth-and-death rates as*

$$\begin{aligned} \lambda_k &= \max_{(n_E,n_R)\in\mathcal{C}(k)} \{q_{(n_E,n_R),(n_E+1,n_R)} + q_{(n_E,n_R),(n_E,n_R+1)}\}, \\ \mu_k &= \min_{(n_E,n_R)\in\mathcal{C}(k)} \{q_{(n_E,n_R),(n_E-1,n_R)} + q_{(n_E,n_R),(n_E,n_R-1)}\}. \end{aligned}$$

Finally, if we define

$$\begin{aligned} \sigma_2 &= 1, \\ \sigma_k &= \frac{\lambda_3 \cdots \lambda_k}{\mu_3 \cdots \mu_k}, \quad k \geq 3, \end{aligned}$$

then, [29, Theorem 3] states that $\alpha_{(n_E,n_R)} = 1$ *for all* $(n_E, n_R) \in \mathcal{C}$ *if (sufficient condition)*

$$\sum_{k=2}^{+\infty} \frac{1}{\lambda_k \sigma_k} = +\infty.$$

Moreover, if $\alpha_{(n_E,n_R)} = 1$ *for all* $(n_E, n_R) \in \mathcal{C}$, *then [29, Theorem 4] states that* $\tau_{(n_E,n_R)} < +\infty$ *if (sufficient condition)*

$$\sum_{k=2}^{+\infty} \sigma_k < +\infty.$$

In our particular process, since give $(n_E, n_R) \in \mathcal{C}(k)$, $n_R = k - n_E$, *we get*

$$\begin{aligned} \lambda_k &= \max_{n_E\in[1,k-1]} \{(\alpha_E - \alpha_R)n_E^2 + (\lambda_E - \lambda_R + \alpha_R k)n_E + \lambda_R k\}, \\ \mu_k &= \min_{n_E\in[1,k-1]} \{(\nu_E + \nu_R - \chi)n_E^2 + (\chi - 2\nu_R)kn_E + (\mu_R + \nu_R k)k + (\mu_E - \mu_R)n_E\},. \end{aligned}$$

We prove now that, at least under three different regimes, $\alpha_{(n_E,n_R)} = 1$ *and* $\tau_{(n_E,n_R)} < +\infty$.

Regime A

For simplicity, and given that data in literature (see, for instance, References [5] and [6]) seems to support this hypothesis, we will assume for now on that $\mu = \mu_E = \mu_R$. *We can write first* λ_k *and* μ_k *as*

$$\lambda_k \;=\; \max_{n_E\in[1,k-1]}\{f_k(n_E)\}, \quad \mu_k \;=\; \min_{n_E\in[1,k-1]}\{g_k(n_E)\}, \quad k \geq 2,$$

with $f_k(\cdot)$ *and* $g_k(\cdot)$ *two continuous functions defined over* $n_E \in [1, k-1]$ *as*

$$f_k(n_E) \;=\; (\alpha_E - \alpha_R)n_E^2 + (\lambda_E - \lambda_R + \alpha_R k)n_E + \lambda_R k, \tag{5.3}$$

$$g_k(n_E) \;=\; (\nu_E + \nu_R - \chi)n_E^2 + (\chi - 2\nu_R)kn_E + (\mu + \nu_R k)k. \tag{5.4}$$

We first note that, under Regime A, $f_k(\cdot)$ *and* $g_k(\cdot)$ *are monotonically increasing and decreasing, respectively, with respect to* $n_E \in [1, k-1]$. *In particular:*

- $f_k'(n_E) = 2(\alpha_E - \alpha_R)n_E + (\lambda_E - \lambda_R + \alpha_R k) > 0 \Leftrightarrow n_E < \frac{\lambda_E - \lambda_R + \alpha_R k}{2(\alpha_E - \alpha_R)}$, *since* $\alpha_R > \alpha_E$. *Now, since* $k(\alpha_R - 2\alpha_E) < 0 < \lambda_E - \lambda_R + 2(\alpha_R - \alpha_E)$, *we have that*

  $$n_E \;\leq\; k-1 \;<\; \frac{\lambda_E - \lambda_R + \alpha_R k}{2(\alpha_R - \alpha_E)},$$

  so that $f_k'(n_E) < 0$ *for all* $n_E \in [1, k-1]$.

- $g_k'(n_E) = 2(\nu_E + \nu_R - \chi)n_E + (\chi - 2\nu_R)k < 0 \Leftrightarrow n_E < \frac{(2\nu_R - \chi)k}{2(\nu_E + \nu_R - \chi)}$, *since* $\nu_E + \nu_R > \chi$. *Now, since* $n_E \leq k-1$ *and*

  $$k-1 \;<\; \frac{(2\nu_R - \chi)k}{2(\nu_E + \nu_R - \chi)} \;\Leftrightarrow\; (2\nu_E - \chi)k < 2(\nu_E + \nu_R - k) \;\Leftrightarrow\; k > \frac{2(\nu_E + \nu_R - k)}{2\nu_E - \chi},$$

  which holds since $2\nu_E < \chi$, *we have that* $g_k'(n_E) < 0$ *for all* $n_E \in [1, k-1]$.

Then, $f_k(\cdot)$ and $g_k(\cdot)$ reach their maximum and minimum, respectively, at $n_E = k-1$. Thus,

$$\begin{aligned}\lambda_k &= \alpha_E k^2 + (\alpha_R - 2\alpha_E + \lambda_E)k + \alpha_E - \alpha_R + \lambda_R - \lambda_E,\\ \mu_k &= \nu_E k^2 + (\mu + \chi - 2\nu_E)k + \nu_E + \nu_R - \chi.\end{aligned}$$

In order to prove $\alpha_{(n_E,n_R)} = 1$ for all $(n_E, n_R) \in \mathcal{C}$, we now analyse the convergence of

$$\sum_{k=2}^{+\infty} \frac{1}{\lambda_k \sigma_k} = \sum_{k=2}^{+\infty} a_k.$$

We use here D'Alembert criterion:

$$\begin{aligned}\lim_{k\to+\infty} \frac{a_{k+1}}{a_k} &= \lim_{k\to+\infty} \frac{\prod_{p=3}^{k+1} \mu_p \left(\prod_{p=2}^{k+1} \lambda_p\right)^{-1}}{\prod_{p=3}^{k} \mu_p \left(\prod_{p=2}^{k} \lambda_p\right)^{-1}} = \lim_{k\to+\infty} \frac{\mu_{k+1}}{\lambda_{k+1}}\\ &= \lim_{k\to+\infty} \frac{\nu_E(k+1)^2 + (\mu+\chi-2\nu_E)(k+1) + \nu_E + \nu_R - \chi}{\alpha_E(k+1)^2 + (\alpha_R - 2\alpha_E + \lambda_E)(k+1) + \alpha_E - \alpha_R + \lambda_R - \lambda_E}\\ &= \frac{\nu_E}{\alpha_E} > 1,\end{aligned}$$

so that $\sum_{k=2}^{+\infty} \frac{1}{\lambda_k\sigma_k} = +\infty$ and $\alpha_{(n_E,n_R)} = 1$ for all $(n_E, n_R) \in \mathcal{C}$. Moreover, by applying [29, Theorem 4] we can prove that $\tau_{(n_E,n_R)} < +\infty$ by proving that

$$\sum_{k=2}^{+\infty} \sigma_k = \sum_{k=2}^{+\infty} a_k \tag{5.5}$$

converges. By D'Alembert criterion again, we have that

$$\begin{aligned}\lim_{k\to+\infty} \frac{a_{k+1}}{a_k} &= \lim_{k\to+\infty} \frac{\prod_{p=3}^{k+1} \lambda_p \left(\prod_{p=3}^{k+1} \mu_p\right)^{-1}}{\prod_{p=3}^{k} \lambda_p \left(\prod_{p=3}^{k} \mu_p\right)^{-1}} = \lim_{k\to+\infty} \frac{\lambda_{k+1}}{\mu_{k+1}}\\ &= \lim_{k\to+\infty} \frac{\alpha_E(k+1)^2 + (\alpha_R - 2\alpha_E + \lambda_E)(k+1) + \alpha_E - \alpha_R + \lambda_R - \lambda_E}{\nu_E(k+1)^2 + (\mu+\chi-2\nu_E)(k+1) + \nu_E + \nu_R - \chi}\\ &= \frac{\alpha_E}{\nu_E} < 1,\end{aligned}$$

so that $\sum_{k=2}^{+\infty} \sigma_k$ *converges and* $\tau_{(n_E,n_R)} < +\infty$ *for all* $(n_E, n_R) \in \mathcal{C}$.

Regime *B*

We point out here that, since $f_k(n_E)$ *only involves parameters* α_E, α_R, λ_E *and* λ_R, *which satisfy same inequalities as in Regime A, we have that*

$$\lambda_k \;=\; \alpha_E k^2 + (\alpha_R - 2\alpha_E + \lambda_E)k + \alpha_E - \alpha_R + \lambda_R - \lambda_E.$$

On the other hand, it can be proved in an analogous way as in Regime A that $g_k'(n_E) < 0$ *for all* $n_E \in [1, k-1]$, *so that*

$$\mu_k \;=\; \nu_E k^2 + (\mu + \chi - 2\nu_E)k + \nu_E + \nu_R - \chi.$$

Then, since λ_k *and* μ_k *have the same expressions than in Regime A, and* $\nu_E > \alpha_E$ *also in Regime B:*

$$\sum_{k=2}^{+\infty} \frac{1}{\lambda_k \sigma_k} \;=\; +\infty, \quad \sum_{k=2}^{+\infty} \sigma_k \;<\; +\infty,$$

so that $\alpha_{(n_E,n_R)} = 1$ *and* $\tau_{(n_E,n_R)} < +\infty$ *for all* $(n_E, n_R) \in \mathcal{C}$.

Regime *C*:

By following same argument than for Regimes A and B, we can obtain $\lambda_k = \alpha_E k^2 + (\alpha_R - 2\alpha_E + \lambda_E)k + \alpha_E - \alpha_R + \lambda_R - \lambda_E$ *also under this regime. We also note that under Regime C,* $\nu = \nu_E = \nu_R$, *so that*

$$\begin{aligned}
g_k(1) &= g_k(k-1) \;=\; \nu k^2 + (\mu + \chi - 2\nu)k + 2\nu - \chi, \\
g_k'(1) &= (\chi - 2\nu)(k-2) \;>\; 0, \quad k \geq 3, \\
g_k'(k-1) &= (2\nu - \chi)(k-2) \;<\; 0, \quad k \geq 3, \\
g_k'(n_E) &= 0 \;\Leftrightarrow\; n_E \;=\; \frac{k}{2}, \\
g_k''(k/2) &= 2(2\nu - \chi) \;<\; 0.
\end{aligned}$$

That is, $g_k(\cdot)$ reaches its maximum in $n_E = k/2$ and its minimum in $n_E \in \{1, k-1\}$ (both with same value). Since $\mu_k = \min_{n_E \in [1,k-1]} \{g_k(n_E)\}$, $k \geq 2$, we get

$$\mu_k = \nu k^2 + (\mu + \chi - 2\nu)k + 2\nu - \chi,$$

which is the same expression than in previous regimes but with $\nu_E = \nu_R = \nu$. Thus, since $\nu > \alpha_E$, by same arguments than before, it is clear that

$$\sum_{k=2}^{+\infty} \frac{1}{\lambda_k \sigma_k} = +\infty, \quad \sum_{k=2}^{+\infty} \sigma_k < +\infty,$$

so that $\alpha_{(n_E,n_R)} = 1$ and $\tau_{(n_E,n_R)} < +\infty$ for all $(n_E, n_R) \in \mathcal{C}$. □

5.2.2 A probabilistic approach to predicting tumour prognosis

Once we have proved in Theorem 5.1 that, at least under some parameter regimes, process $\mathcal{X}$ goes to absorption into some of the axis with probability one and in a finite mean time, our aim in this Section is to provide a probabilistic measure of the predicted outcome of tumour-specific immune responses, which is dictated by the ratio T_{eff}/T_{reg} [59, Figure 1]. In particular, we focus here on analysing the probability of reaching different regions of the state space defined according to this ratio, corresponding to *Poor Prognosis* or *Better Prognosis*. This poor prognosis corresponds to smaller chances for the immune system to recover from the tumour than in the better prognosis case. Various approaches shown in [70] or [62] correlate small ratios of effector $CD8^+$ T cells to regulatory $CD4^+$ T cells with poor prognosis in several types of human cancers and a better prognosis is related to high amounts of effector $CD8^+$ T cells in almost every type of cancer under study [20, Table 1] (see Figure 5.1).

Thus, our regions can be described in terms of parameters $0 < K_1 < K_2$, by splitting the state space $\mathcal{S}$ into three regions of states (n_E, n_R) according to the value of $\frac{n_E}{n_R}$ $(= \frac{T_{eff}}{T_{reg}})$: $(n_E, n_R) \in \mathbb{PP}^{K_1,K_2}$ (poor prognosis) if $\frac{n_E}{n_R} \leq K_1$; $(n_E, n_R) \in \mathbb{BP}^{K_1,K_2}$ (better prognosis) if $\frac{n_E}{n_R} \geq K_2$; and $(n_E, n_R) \in \mathbb{R}^{K_1,K_2}$ (rest) if $K_1 < \frac{n_E}{n_R} < K_2$. Regions $\mathbb{PP}^{K_1,K_2}$, $\mathbb{BP}^{K_1,K_2}$ and $\mathbb{R}^{K_1,K_2}$ depend on the particular values of K_1 and K_2; see Figure 5.2.

Given an initial state $(N_E, N_R) \in \mathbb{R}^{K_1,K_2}$ our interest is in computing the *poor prognosis probability*

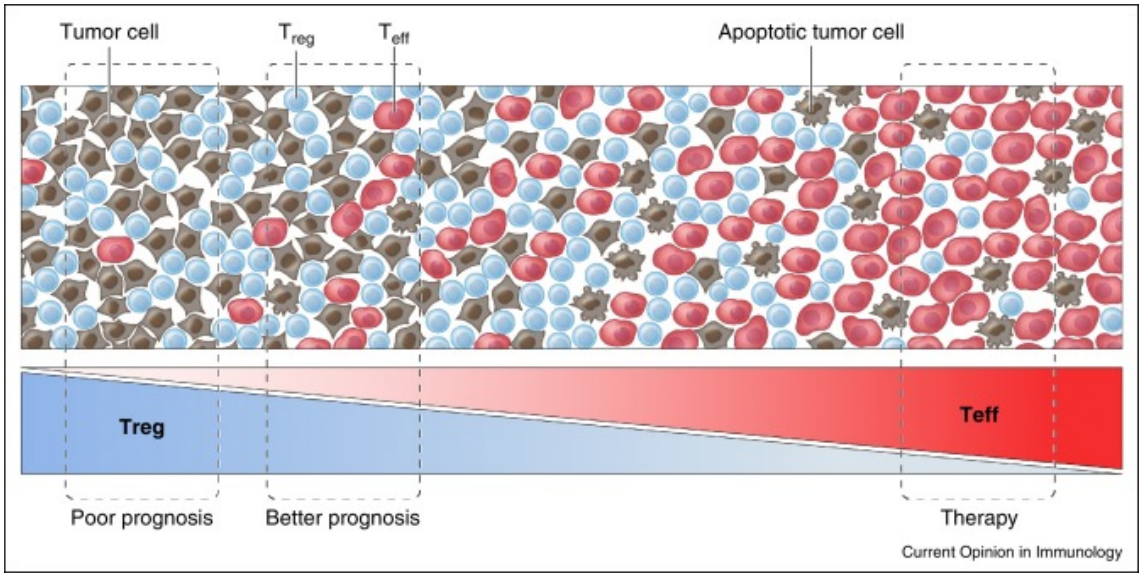

Figure 5.1: Tumour prognosis depends on the ratio T_{eff}/T_{reg}. Figure taken from [59]. The x axis just representatively indicates that for a region of values $T_{eff}/T_{reg} \approx 1$, prognosis is better.

defined as

$$p^{K_1,K_2}_{(N_E,N_R)} = \text{“}\textit{Probability of process } \mathcal{X} \textit{ of reaching region } \mathbb{PP}^{K_1,K_2} \textit{ before region } \mathbb{BP}^{K_1,K_2}\textit{, given the initial state } (N_E,N_R) \in \mathbb{R}^{K_1,K_2}\text{”}.$$

which represents the probability that the process drifts towards poor prognosis instead of better prognosis. We point out here that, since our process $\mathcal{X}$ reaches one of the axis in finite time with probability one, at least under some parameter regimes, $\mathcal{X}$ can not stay in $\mathbb{R}^{K_1,K_2}$ indefinitely and one of the prognosis regions (poor or better) has to be reached. Thus, in these regimes,

$$1 - p^{K_1,K_2}_{(N_E,N_R)} = \text{“}\textit{Probability of process } \mathcal{X} \textit{ of reaching region } \mathbb{BP}^{K_1,K_2} \textit{ before region } \mathbb{PP}^{K_1,K_2}\textit{, given the initial state } (N_E,N_R) \in \mathbb{R}^{K_1,K_2}\text{”}.$$

We can compute this probability by following a first-step argument. In particular, this probability

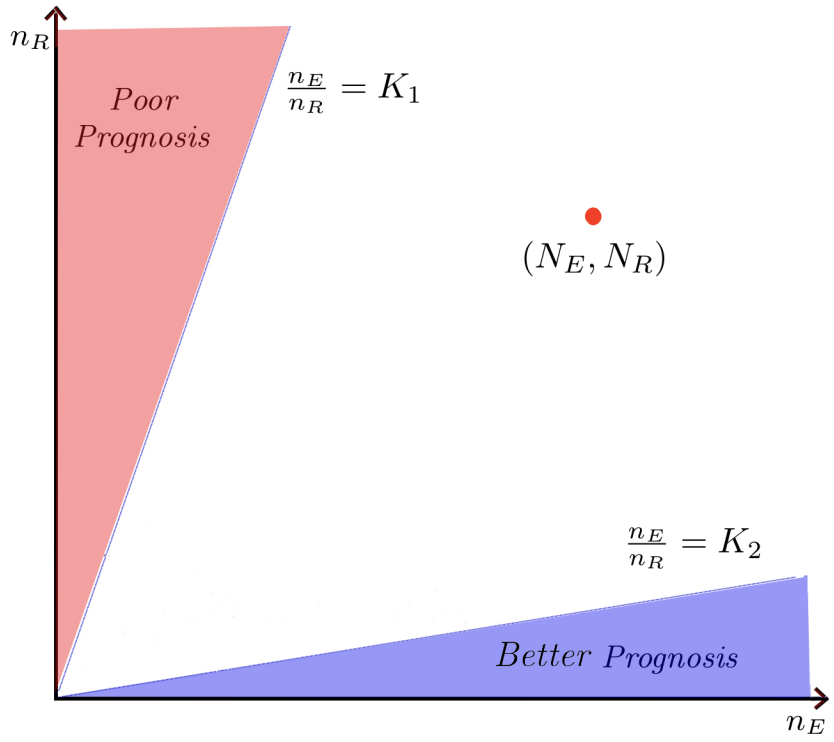

Figure 5.2: Poor and Better prognosis regions defined in the spirit of [59], and according to parameter values $0 < K_1 < K_2$. Initial state (N_E, N_R).

for all values $(n_E, n_R) \in \mathbb{R}^{K_1,K_2}$ verifies

$$\begin{aligned}\Delta_{(n_E,n_R)} p^{K_1,K_2}_{(n_E,n_R)} &= (\lambda_E + \alpha_E n_E) n_E p^{K_1,K_2}_{(n_E+1,n_R)} + (\mu_E + \nu_E n_E + \chi n_R) n_E p^{K_1,K_2}_{(n_E-1,n_R)} \\ &\quad + (\lambda_R + \alpha_R n_E) n_R p^{K_1,K_2}_{(n_E,n_R+1)} + (\mu_R + \nu_R n_R) n_R p^{K_1,K_2}_{(n_E,n_R-1)}, \end{aligned} \tag{5.6}$$

with $\Delta_{(n_E,n_R)} = (\lambda_E + \alpha_E n_E + \mu_E + \nu_E n_E + \chi n_R) n_E + (\lambda_R + \alpha_R n_E + \mu_R + \nu_R n_R) n_R$, and with boundary conditions given by

$$\begin{aligned} p^{K_1,K_2}_{(n_E,n_R)} &= 1, \quad \text{if } \tfrac{n_E}{n_R} \leq K_1, \\ p^{K_1,K_2}_{(n_E,n_R)} &= 0, \quad \text{if } \tfrac{n_E}{n_R} \geq K_2. \end{aligned}$$

However, the infinite number of states in $\mathbb{R}^{K_1,K_2}$ translates into an infinite system of equations given by Equation (5.6), which seems to be analytically intractable. We propose here to follow a similar approximative approach than the one in [23], and analyse Equation (5.6) by truncating

the set $\mathbb{R}^{K_1,K_2}$ so that a finite system of equations is obtained that approximates the infinite one, a truncation that can be carried out following a probabilistic criteria.

We first organise region $\mathbb{R}^{K_1,K_2}$ by levels as

$$\mathbb{R}^{K_1,K_2} = \bigcup_{k=2}^{+\infty} \mathbb{R}^{K_1,K_2}(k),$$

with

$$\begin{aligned}\mathbb{R}^{K_1,K_2}(k) = & \left\{ \left(\left\lceil \frac{K_2 k}{K_2+1} \right\rceil - 1, \left\lfloor \frac{k}{K_2+1} \right\rfloor + 1 \right), \right. \\ & \left. \left(\left\lceil \frac{K_2 k}{K_2+1} \right\rceil - 2, \left\lfloor \frac{k}{K_2+1} \right\rfloor + 2 \right), \ldots, \left(\left\lfloor \frac{K_1 k}{K_1+1} \right\rfloor + 1, \left\lceil \frac{k}{K_1+1} \right\rceil - 1 \right) \right\},\end{aligned}$$

where $\lceil x \rceil$ and $\lfloor x \rfloor$ amount to the upper and lower integer part of x, respectively. That is, $\mathbb{R}^{K_1,K_2}(k)$ contains all the states $(n_E, n_R) \in \mathbb{R}^{K_1,K_2}$ that verify $n_E + n_R = k$; see Figure 5.3. Thus, it is clear that level $\mathbb{R}^{K_1,K_2}(k)$ contains

$$J^{K_1,K_2}(k) = \#\mathbb{R}^{K_1,K_2}(k) = \left\lceil \frac{K_2 k}{K_2+1} \right\rceil - \left\lfloor \frac{K_1 k}{K_1+1} \right\rfloor - 1$$

states.

Observation: State $\left(\left\lceil \frac{K_2 k}{K_2+1} \right\rceil - 1, \left\lfloor \frac{k}{K_2+1} \right\rfloor + 1 \right)$ is at position 1 within level $\mathbb{R}^{K_1,K_2}(k)$ (when this level is not empty), state $\left(\left\lfloor \frac{K_1 k}{K_1+1} \right\rfloor + 1, \left\lceil \frac{k}{K_1+1} \right\rceil - 1 \right)$ is at position $\left\lceil \frac{K_2 k}{K_2+1} \right\rceil - \left\lfloor \frac{K_1 k}{K_1+1} \right\rfloor - 1$ within this level (when this level is not empty), and any other state $(n_E, n_R) \in \mathbb{R}^{K_1,K_2}(k)$ is at position $Pos_k(n_E) = \left\lceil \frac{K_2 k}{K_2+1} \right\rceil - n_E$ within this level.

We propose now to truncate $\mathbb{R}^{K_1,K_2}$ in terms of the random variable

$$\begin{aligned}X^{max,K_1,K_2}_{(n_E,n_R)} = & \text{ “Maximum cell population size (that is, maximum level } \mathbb{R}^{K_1,K_2}(k)\text{) reached by process} \\ & \mathcal{X} \text{ before reaching prognosis regions } \mathbb{PP}^{K_1,K_2} \cup \mathbb{BP}^{K_1,K_2}\text{, given the initial state } (n_E, n_R)\text{”} \\ = & \max_{t \in [0,T]} \{N_E(t) + N_R(t)\},\end{aligned}$$

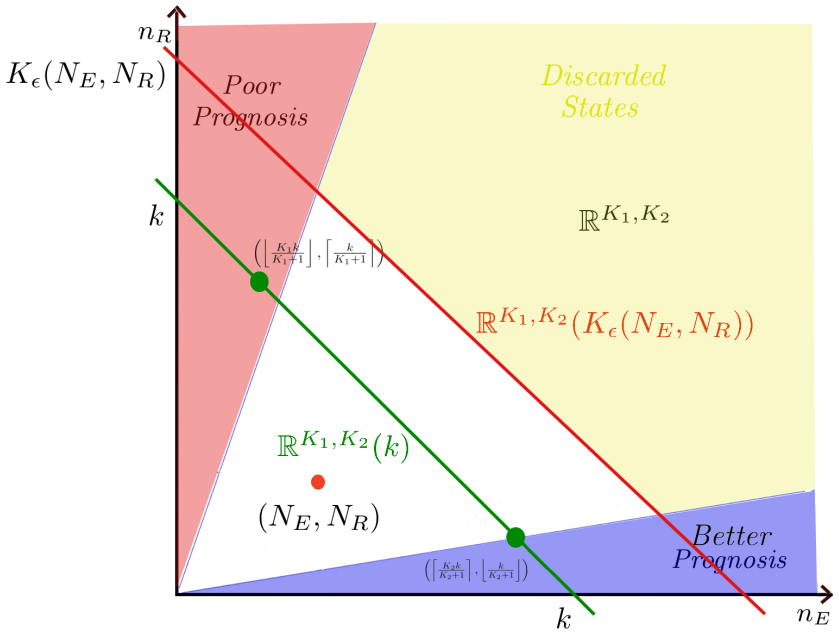

Figure 5.3: Region $\mathbb{R}^{K_1,K_2}$ organised in levels $\mathbb{R}^{K_1,K_2}(k)$, $k \geq 2$. Each level $\mathbb{R}^{K_1,K_2}(k)$ contains states $(n_E, n_R) \in \mathbb{R}^{K_1,K_2}$ such that $n_E + n_R = k$. Truncating level $\mathbb{R}^{K_1,K_2}(K_\epsilon(N_E, N_R))$.

where $T = \inf\{t \geqslant 0 : (N_E(t), N_R(t)) \in \mathbb{PP}^{K_1,K_2} \cup \mathbb{BP}^{K_1,K_2}\}$. Since we are interested in the dynamics of $\mathcal{X}$ until regions $\mathbb{PP}^{K_1,K_2}$ or $\mathbb{BP}^{K_1,K_2}$ are reached, we propose to choose a truncating level $\mathbb{R}^{K_1,K_2}(K_\epsilon(N_E, N_R))$ by choosing the smallest value $K_\epsilon(N_E, N_R)$ such that

$$\mathbb{P}\left(X^{max,K_1,K_2}_{(N_E,N_R)} \geqslant K_\epsilon(N_E, N_R)\right) \quad < \quad \epsilon,$$

for the initial state $(N_E, N_R) \in \mathbb{R}^{K_1,K_2}$, and $\epsilon > 0$ small enough.

Once $K_\epsilon(N_E, N_R)$ is selected for a given initial state (N_E, N_R) of interest, and for a small value $\epsilon > 0$, we propose to analyse the dynamics of $\mathcal{X}$ within states in

$$\bigcup_{k=2}^{K_\epsilon(N_E,N_R)-1} \mathbb{R}^{K_1,K_2}(k),$$

since states at and above level $\mathbb{R}^{K_1,K_2}(K_\epsilon(N_E, N_R))$ are only visited by process $\mathcal{X}$ with probability smaller than ϵ, which acts here as an error control parameter. Thus, states at and above level $\mathbb{R}^{K_1,K_2}(K_\epsilon(N_E, N_R))$ and transitions from level $\mathbb{R}^{K_1,K_2}(K_\epsilon(N_E, N_R) - 1)$ to states at level $\mathbb{R}^{K_1,K_2}(K_\epsilon(N_E, N_R))$ are discarded, and $\mathcal{X}$ evolves now among a finite number of states.

$K_\epsilon(N_E, N_R)$, chosen as the $(1-\epsilon)$ percentile of $X^{max,K_1,K_2}_{N_E,N_R}$, can be identified by computing probabilities

$$p^{max,K_1,K_2}_{(N_E,N_R)}(k) \quad = \quad \mathbb{P}(X^{max,K_1,K_2}_{(N_E,N_R)} \geqslant k),$$

for all $k \geq N_E + N_R$. These probabilities, for any initial state $(n_E, n_R) \in \mathbb{R}^{K_1,K_2}$, can be computed by means of the system of equations given by Equation (5.6) (replacing probabilities $p^{K_1,K_2}_{(n_E,n_R)}$ by probabilities $p^{max,K_1,K_2}_{(n_E,n_R)}$), with boundary conditions

$$\begin{aligned} p^{max,K_1,K_2}_{(n_E,n_R)}(k) &= 0, \quad \textit{if } \tfrac{n_E}{n_R} \leq K_1 \textit{ or } \tfrac{n_E}{n_R} \geq K_2, \\ p^{max,K_1,K_2}_{(n_E,n_R)}(k) &= 1, \quad \textit{if } n_E + n_R = k,\ K_1 < \tfrac{n_E}{n_R} < K_2. \end{aligned}$$

Thus, the percentile $K_\epsilon(N_E, N_R)$ can be obtained, for a given initial state (N_E, N_R), by computing $p^{max,K_1,K_2}_{(N_E,N_R)}(k)$ for $k = N_E + N_R + 1$ and sequentially increasing the value of k until we reach $p^{max,K_1,K_2}_{(N_E,N_R)}(k) < \epsilon$. We note here that convergence is ensured, at least in Regimes A, B and C, given that it has been proved in Theorem 5.1 that the probability to extinction of one of the populations is equal to one.

In order to solve this system of equations, for probabilities $p^{max,K_1,K_2}_{(N_E,N_R)}(k)$, we work in matrix form and store these probabilities in a vector

$$\mathbf{p}^{max,K_1,K_2}(k) \quad = \quad \begin{pmatrix} \mathbf{p}_2^{max,K_1,K_2}(k) \\ \mathbf{p}_3^{max,K_1,K_2}(k) \\ \vdots \\ \mathbf{p}_{k-1}^{max,K_1,K_2}(k) \end{pmatrix},$$

with

$$\mathbf{p}_r^{max,K_1,K_2}(k) \quad = \quad \begin{pmatrix} p^{max,K_1,K_2}_{\left(\left\lceil \frac{K_2 r}{K_2+1} \right\rceil - 1, \left\lfloor \frac{r}{K_2+1} \right\rfloor + 1\right)}(k) \\ \vdots \\ p^{max,K_1,K_2}_{\left(\left\lfloor \frac{K_1 r}{K_1+1} \right\rfloor + 1, \left\lceil \frac{r}{K_1+1} \right\rceil - 1\right)}(k) \end{pmatrix}, \quad 2 \leq r \leq k-1.$$

Then, this system of equations can be written in matrix form as

$$\mathbf{p}^{max,K_1,K_2}(k) \quad = \quad \mathbf{A}^{K_1,K_2}(k)\mathbf{p}^{max,K_1,K_2}(k) + \mathbf{b}^{max,K_1,K_2}(k) \tag{5.7}$$

with coefficient matrix given by

$$\mathbf{A}^{K_1,K_2}(k) \quad = \quad \begin{pmatrix} \mathbf{0} & \mathbf{A}_{23}^{K_1,K_2} & \mathbf{0} & \dots & \mathbf{0} & \mathbf{0} \\ \mathbf{A}_{32}^{K_1,K_2} & \mathbf{0} & \mathbf{A}_{34}^{K_1,K_2} & \dots & \mathbf{0} & \mathbf{0} \\ \mathbf{0} & \mathbf{A}_{43}^{K_1,K_2} & \mathbf{0} & \dots & \mathbf{0} & \mathbf{0} \\ \vdots & \vdots & \vdots & \ddots & \vdots & \vdots \\ \mathbf{0} & \mathbf{0} & \mathbf{0} & \dots & \mathbf{0} & \mathbf{A}_{k-2,k-1}^{K_1,K_2} \\ \mathbf{0} & \mathbf{0} & \mathbf{0} & \dots & \mathbf{A}_{k-1,k-2}^{K_1,K_2} & \mathbf{0} \end{pmatrix}, \tag{5.8}$$

where each matrix $\mathbf{A}_{r,r'}^{K_1,K_2}$ corresponds to transitions from states at level $\mathbb{R}^{K_1,K_2}(r)$ to states at level $\mathbb{R}^{K_1,K_2}(r')$. We note that:

- Dimensions of $\mathbf{A}_{r,r-1}^{K_1,K_2}$: $J^{K_1,K_2}(r) \times J^{K_1,K_2}(r-1) = \left(\left\lceil \frac{K_2 r}{K_2+1} \right\rceil - \left\lfloor \frac{K_1 r}{K_1+1} \right\rfloor - 1\right) \times \left(\left\lceil \frac{K_2(r-1)}{K_2+1} \right\rceil - \left\lfloor \frac{K_1(r-1)}{K_1+1} \right\rfloor - 1\right)$.
- Dimensions of $\mathbf{A}_{r,r+1}^{K_1,K_2}$: $J^{K_1,K_2}(r) \times J^{K_1,K_2}(r+1) = \left(\left\lceil \frac{K_2 r}{K_2+1} \right\rceil - \left\lfloor \frac{K_1 r}{K_1+1} \right\rfloor - 1\right) \times \left(\left\lceil \frac{K_2(r+1)}{K_2+1} \right\rceil - \left\lfloor \frac{K_1(r+1)}{K_1+1} \right\rfloor - 1\right)$.

These matrices are given as follows:

- For $3 \leq r \leq k-1$:

$$\left(\mathbf{A}_{r,r-1}^{K_1,K_2}\right)_{ij} \quad = \quad \begin{cases} \frac{(\mu_E+\nu_E n_E+\chi n_R)n_E}{\Delta_{(n_E,n_R)}}, & \text{if } j = Pos_{r-1}(n_E-1), \\ \frac{(\mu_R+\nu_R n_R)n_R}{\Delta_{(n_E,n_R)}}, & \text{if } j = Pos_{r-1}(n_E), \\ 0, & \text{otherwise}, \end{cases}$$

  with $(n_E, n_R) = \left(\left\lceil \frac{K_2 r}{K_2+1} \right\rceil - i, \left\lfloor \frac{r}{K_2+1} \right\rfloor + i\right)$, for $1 \leq i \leq J^{K_1,K_2}(r)$;

- For $2 \leq r \leq k-2$:

$$\left(\mathbf{A}_{r,r+1}^{K_1,K_2}\right)_{ij} \quad = \quad \begin{cases} \frac{(\lambda_E+\alpha_E n_E)n_E}{\Delta_{(n_E,n_R)}}, & \text{if } j = Pos_{r+1}(n_E+1), \\ \frac{(\lambda_R+\alpha_R n_E)n_R}{\Delta_{(n_E,n_R)}}, & \text{if } j = Pos_{r+1}(n_E), \\ 0, & \text{otherwise}, \end{cases}$$

$$\text{with } (n_E, n_R) = \left(\left\lceil \frac{K_2 r}{K_2+1} \right\rceil - i, \left\lfloor \frac{r}{K_2+1} \right\rfloor + i \right), \text{ for } 1 \leq i \leq J^{K_1,K_2}(r);$$

Finally, the vector of independent terms is given as

$$\mathbf{b}^{max,K_1,K_2}(k) \quad = \quad \begin{pmatrix} \mathbf{0}_{J^{K_1,K_2}(2)} \\ \mathbf{0}_{J^{K_1,K_2}(3)} \\ \vdots \\ \mathbf{0}_{J^{K_1,K_2}(k-2)} \\ \mathbf{b}_{k-1}^{max,K_1,K_2} \end{pmatrix},$$

with $\mathbf{b}_{k-1}^{max,K_1,K_2} = \mathbf{A}_{k-1,k}^{K_1,K_2} \mathbf{1}_{J^{K_1,K_2}(k)}$, where $\mathbf{1}_{J^{K_1,K_2}(k)}$ is a column vector of ones with dimension $J^{K_1,K_2}(k)$. Finally, our system of equations can be solved algorithmically via Algorithm 5.1

Algorithm 5.1

$\mathbf{H}_2 = 1;$

For $r = 3, \ldots, k-1$:

$$\mathbf{H}_r = \mathbf{I}_{J^{K_1,K_2}(r)} - \mathbf{A}_{r,r-1}^{K_1,K_2} \mathbf{H}_{r-1}^{-1} \mathbf{A}_{r-1,r}^{K_1,K_2};$$

$$\mathbf{p}_{k-1}^{max,K_1,K_2}(k) = \mathbf{H}_{k-1}^{-1} \mathbf{b}_{k-1}^{max,K_1,K_2};$$

For $r = k-2, \ldots, 2$:

$$\mathbf{p}_r^{max,K_1,K_2}(k) = \mathbf{H}_r^{-1} \mathbf{A}_{r,r+1}^{K_1,K_2} \mathbf{p}_{r+1}^{max,K_1,K_2}(k);$$

Once $K_\epsilon(N_E, N_R)$ is chosen by starting at $k = N_E + N_R + 1$ and sequentially increasing k until $p_{(N_E,N_R)}^{max,K_1,K_2}(k) < \epsilon$, the system of equations given by Equation (5.6) for the desired probabilities $p_{(n_E,n_R)}^{K_1,K_2}$ can be solved also in a matrix way:

$$\mathbf{p}^{K_1,K_2}(K_\epsilon(N_E,N_R)) \quad = \quad \mathbf{A}^{K_1,K_2}(K_\epsilon(N_E,N_R)) \mathbf{p}^{K_1,K_2}(K_\epsilon(N_E,N_R)) + \mathbf{b}^{K_1,K_2}(K_\epsilon(N_E,N_R)) \quad (5.9)$$

with

$$\mathbf{b}^{K_1,K_2}(K_\epsilon(N_E,N_R)) = \begin{pmatrix} \mathbf{b}_2^{K_1,K_2} \\ \mathbf{b}_3^{K_1,K_2} \\ \vdots \\ \mathbf{b}_{K_\epsilon(N_E,N_R)-1}^{K_1,K_2} \end{pmatrix},$$

where sub-vector $\mathbf{b}_r^{K_1,K_2}$ has zeros everywhere except for any element corresponding to a state (n_E, n_R) such that $\frac{n_E}{n_R+1} \leq K_1$ or $\frac{n_E-1}{n_R} \leq K_1$ (that is, a state (n_E, n_R) that has one-step transition access to poor prognosis region $\mathbb{PP}^{K_1,K_2}$), which is equal to

$$\frac{1}{\Delta_{(n_E,n_R)}}\left((\lambda_R+\alpha_R n_E)n_R\delta_{\{\frac{n_E}{n_R+1}\leq K_1\}}+(\mu+\nu_E n_E+\chi n_R)n_E\delta_{\{\frac{n_E-1}{n_R}\leq K_1\}}\right),$$

where $\delta_{\{A\}}$ is equal to 1 if A is satisfied, and 0 otherwise. This system can be solved by adapting Algorithm 5.1

5.2.3 Deterministic approach to the model

We have just presented the matrix-analytic methods to study the effector and T reg cells system from a stochastic point of view. From a deterministic perspective, this process is described by

$$\begin{aligned} \frac{dn_E}{dt} &= -\mu_E n_E - \nu_E n_E^2 + \lambda_E n_E + \alpha_E n_E^2 - \chi n_E n_R, \\ \frac{dn_R}{dt} &= -\mu_R n_R - \nu_R n_R^2 + \lambda_R n_R + \alpha_R n_E n_R, \end{aligned} \tag{5.10}$$

where $n_E(t)$ and $n_R(t)$ represent, as previously, the amount of cytotoxic (or effector) and regulatory T cells, respectively, at time $t \geq 0$, and rates are defined as in Section 5.2. The focus here is in analysing the mathematical model defined in Section 5.2 from a deterministic perspective. First, we compute the steady states of this process by setting the derivatives of the population dynamics equal to 0:

$$\begin{aligned} -\mu_E n_E - \nu_E n_E n_E + \lambda_E n_E + \alpha_E n_E n_E - \chi_R n_E n_R &= 0, \\ -\mu_R n_R + \lambda_R n_R + \alpha_R n_E n_R - \nu_R n_R n_R &= 0, \end{aligned} \tag{5.11}$$

which leads to four steady states

$$
\begin{aligned}
SS_1: &\quad (n_E^{(1)}, n_R^{(1)}) = (0,0), \quad \textbf{extinction.} \\
SS_2: &\quad (n_E^{(2)}, n_R^{(2)}) = \left(0, \frac{\lambda_R - \mu_R}{\nu_R}\right), \quad \textbf{poor prognosis.} \\
SS_3: &\quad (n_E^{(3)}, n_R^{(3)}) = \left(\frac{\mu_E - \lambda_E}{\alpha_E - \nu_E}, 0\right), \quad \textbf{better prognosis.} \\
SS_4: &\quad (n_E^{(4)}, n_R^{(4)}) = \left(\frac{\chi(\lambda_R - \mu_R) - \nu_R(\lambda_E - \mu_E)}{\nu_R(\alpha_E - \nu_E) - \alpha_R\chi}, \frac{(\alpha_E - \nu_E)(\lambda_R - \mu_R) + \alpha_R(\mu_E - \lambda_E)}{\nu_R(\alpha_E - \nu_E) - \alpha_R\chi}\right), \quad \textbf{tolerance.}
\end{aligned}
\tag{5.12}
$$

For these steady states, we carry out a stability analysis by means of computing the corresponding Jacobian matrix $J(n_E, n_R)$, which is given by

$$
J(n_E, n_R) \quad = \quad \begin{pmatrix} 2n_E\alpha_E + \lambda_E - \mu_E - 2n_E\nu_E - n_R\chi_R & -n_E\chi_R \\ n_R\alpha_R & n_E\alpha_R + \lambda_R - \mu_R - 2n_R\nu_R \end{pmatrix},
$$

so that a given steady state $(n_E^{(i)}, n_R^{(i)})$ ($i \in \{1,2,3,4\}$) is asymptotically stable if and only if the eigenvalues of $J(n_E^{(i)}, n_R^{(i)})$ have strictly negative real part.

Steady state SS_1: $(n_E^{(1)}, n_R^{(1)}) = (0,0)$ - Extinction

Steady state SS_1 represents that both populations go to extinction in the late times. Evaluating the Jacobian matrix at the steady state, we get:

$$
J(n_E^{(1)}, n_R^{(1)}) \quad = \quad \begin{pmatrix} \lambda_E - \mu_E & 0 \\ 0 & \lambda_R - \mu_R \end{pmatrix},
$$

with eigenvalues

$$
\begin{aligned}
\sigma_1^{(1)} &= \lambda_E - \mu_E, \\
\sigma_2^{(1)} &= \lambda_R - \mu_R.
\end{aligned}
$$

Thus, SS_1 is stable if and only if the stability conditions

$$
SC_1: \qquad \mu_E > \lambda_E, \quad \mu_R > \lambda_R \tag{5.13}
$$

are satisfied.

Steady state SS_2: $(n_E^{(2)}, n_R^{(2)}) = (0, \frac{\lambda_R - \mu_R}{\nu_R})$ - Poor prognosis

Steady state SS_2 represents survival of the regulatory T cell population in the late times, while the population of effector T cells goes to extinction, moving the system towards the *poor prognosis* area. Evaluating the Jacobian matrix at SS_2 we obtain

$$J(n_E^{(2)}, n_R^{(2)}) = \begin{pmatrix} \mu_E - \lambda_E + \frac{(-\lambda_R + \mu_R)\chi_R}{\nu_R} & 0 \\ -\frac{\alpha_R(-\lambda_R + \mu_R)}{\nu_R} & \mu_R - \lambda_R \end{pmatrix},$$

with eigenvalues

$$\begin{aligned} \sigma_1^{(2)} &= -\lambda_R + \mu_R, \\ \sigma_2^{(2)} &= \frac{\lambda_E \nu_R - \mu_E \nu_R - \lambda_R \chi + \mu_R \chi}{\nu_R}. \end{aligned}$$

Thus, steady state SS_2 is stable if and only if the stability conditions

$$SC_2: \qquad \lambda_R > \mu_R, \quad \lambda_E \nu_R + (-\lambda_R + \mu_R)\chi < \mu_E \nu_R \tag{5.14}$$

are satisfied. It is easy to check that stability conditions SC_1 and SC_2 are incompatible, so that steady states SS_1 and SS_2 can not be stable at the same time.

Steady state SS_3: $(n_E^{(3)}, n_R^{(3)}) = (\frac{\mu_E - \lambda_E}{\alpha_E - \nu_E}, 0)$ - Better prognosis

Steady state SS_3 represents the process going in the late times towards the *better prognosis* area, with the population of regulatory T cells going to extinction. The Jacobian matrix for this steady state is

$$J(n_E^{(3)}, n_R^{(3)}) = \begin{pmatrix} \lambda_E - \mu_E & \frac{(\lambda_E - \mu_E)\chi_R}{\alpha_E - \nu_E} \\ 0 & \lambda_R - \mu_R - \frac{\alpha_R(\lambda_E - \mu_E)}{\alpha_E - \nu_E} \end{pmatrix},$$

with eigenvalues

$$\begin{aligned}\sigma_1^{(3)} &= -\lambda_E + \mu_E, \\ \sigma_2^{(3)} &= \frac{-\alpha_R\lambda_E + \alpha_E\lambda_R + \alpha_R\mu_E - \alpha_E\mu_R - \lambda_R\nu_E + \mu_R\nu_E}{\alpha_E - \nu_E}.\end{aligned}$$

Thus, steady state SS_3 is stable if and only if the stability conditions

$$SC_3: \qquad \lambda_E > \mu_E, \quad (\alpha_R(-\lambda_E + \mu_E) + (\lambda_R - \mu_R)(\alpha_E - \nu_E))(\alpha_E - \nu_E) < 0 \tag{5.15}$$

are satisfied. Again, stability conditions SC_1 and SC_3 are incompatible, so that steady states SS_1 and SS_3 can not be stable at the same time. In fact, SC_2 and SC_3 are also incompatible when imposing that $n_E^{(2)}, n_R^{(2)}, n_E^{(3)}, n_R^{(3)} \geqslant 0$, which are physical conditions. This allows to conclude that, only under parameter regimes SC_1, SC_2 or SC_3, initial states will not affect long-term dynamics, and the steady states will only depend on the ratios between parameters given by stability conditions SC_i, with $i \in \{1, 2, 3\}$.

Steady state SS_4: $(n_E^{(4)}, n_R^{(4)}) = \left(\frac{\chi(\lambda_R-\mu_R)-\nu_R(\lambda_E-\mu_E)}{\nu_R(\alpha_E-\nu_E)-\alpha_R\chi}, \frac{(\alpha_E-\nu_E)(\lambda_R-\mu_R)+\alpha_R(\mu_E-\lambda_E)}{\nu_R(\alpha_E-\nu_E)-\alpha_R\chi}\right)$ - Tolerance

Steady state SS_4 represents both populations surviving in the late times. This can lead to late times poor or better prognosis depending on the particular value of $(n_E^{(4)}, n_R^{(4)})$ which, at the same time, depends on the particular values of the parameters in the model. The Jacobian matrix in this case is given by

$$J(n_E^{(4)}, n_R^{(4)}) = \begin{pmatrix} -\frac{(\nu_E-\alpha_E)(\nu_R(\lambda_E-\mu_E)+\chi(-\lambda_R+\mu_R))}{\nu_E\nu_R-\nu_R\alpha_E+\chi\alpha_R} & \frac{\chi(\nu_R(-\lambda_E+\mu_E)+\chi(\lambda_R-\mu_R))}{\nu_E\nu_R-\nu_R\alpha_E+\chi\alpha_R} \\ \frac{\alpha_R(\alpha_R(\lambda_E-\mu_E)+(\nu_E-\alpha_E)(\lambda_R-\mu_R))}{\nu_E\nu_R-\nu_R\alpha_E+\chi\alpha_R} & \frac{\nu_R(\alpha_R(-\lambda_E+\mu_E)-(\nu_E-\alpha_E)(\lambda_R-\mu_R))}{\nu_E\nu_R-\nu_R\alpha_E+\chi\alpha_R} \end{pmatrix},$$

and the eigenvalues as

$$\begin{aligned}\sigma_1^{(4)}, \sigma_2^{(4)} &= \frac{1}{2(\nu_E\nu_R - \nu_R\alpha_E + \chi\alpha_R)}\Big[\chi(\nu_E - \alpha_E)(\lambda_R - \mu_R) + \nu_R\big(\alpha_R(-\lambda_E + \mu_E) + \alpha_E(\lambda_E + \lambda_R - \mu_E - \mu_R) + \nu_E(-\lambda_E - \lambda_R + \mu_E + \mu_R)\big) \\ &\pm \Big(-4(\nu_E\nu_R - \nu_R\alpha_E + \chi\alpha_R)\big(\alpha_R(\lambda_E - \mu_E) + (\nu_E - \alpha_E)(\lambda_R - \mu_R)\big)\big(\nu_R(\lambda_E - \mu_E) + \chi(-\lambda_R + \mu_R)\big) \\ &+ \Big(\chi\alpha_E(\lambda_R - \mu_R) + \nu_E\big(\nu_R(\lambda_E + \lambda_R - \mu_E - \mu_R) + \chi(-\lambda_R + \mu_R)\big) + \nu_R\big(\alpha_R(\lambda_E - \mu_E) + \alpha_E(-\lambda_E - \lambda_R + \mu_E + \mu_R)\big)\Big)^2\Big)^{\frac{1}{2}}\Big],\end{aligned}$$

which implies that steady state SS_4 is stable if and only if $\sigma_1^{(4)}$ and $\sigma_2^{(4)}$ have strictly negative real part. However, a general analysis of stability and parameter conditions, without setting these parameters to some specific values, does not seem feasible from an analytical point of view. However, different scenarios will be considered in Section 5.2.4 depending on the ratio $\frac{n_E^{(4)}}{n_R^{(4)}}$. Thus, depending on this ratio being smaller, equal or grater than one, time dynamics of effector and regulatory T cells will be studied, exploring how the probability of reaching poor or better prognosis is altered when varying this ratio.

5.2.4 Results

The parameter values for our deterministic studies were obtained from [5]. Some small perturbations were implemented for reaching the diversity of steady states, as it will be explained later, by identifying, and minimising the difference of only those parameters responsible of changing the steady state.

Parameter	μ_E	μ_R	ν_E	ν_R	λ_E	λ_R	α_E	α_R	χ
from [5]	$1 \cdot 10^{-2}$	$1 \cdot 10^{-2}$	$1 \cdot 10^{-4}$	$1 \cdot 10^{-4}$	$2 \cdot 10^{-2}$	$2 \cdot 10^{-2}$	$5 \cdot 10^{-5}$	$1 \cdot 10^{-4}$	$2 \cdot 10^{-4}$
SC_1	$2 \cdot 10^{-2}$	$2 \cdot 10^{-2}$	$1 \cdot 10^{-4}$	$3 \cdot 10^{-4}$	$1.5 \cdot 10^{-2}$	$1 \cdot 10^{-2}$	$5 \cdot 10^{-5}$	$7.5 \cdot 10^{-5}$	$5 \cdot 10^{-4}$
SC_2	$1 \cdot 10^{-3}$	$1 \cdot 10^{-3}$	$1 \cdot 10^{-4}$	$3 \cdot 10^{-4}$	$1.5 \cdot 10^{-2}$	$1 \cdot 10^{-2}$	$5 \cdot 10^{-5}$	$7.5 \cdot 10^{-5}$	$5 \cdot 10^{-4}$
SC_3	$1 \cdot 10^{-2}$	$1 \cdot 10^{-2}$	$1 \cdot 10^{-4}$	$3 \cdot 10^{-4}$	$1.5 \cdot 10^{-2}$	$2 \cdot 10^{-3}$	$5 \cdot 10^{-5}$	$7.5 \cdot 10^{-5}$	$5 \cdot 10^{-4}$
$SC_{4(n_R^{(4)} > n_E^{(4)})}$	$1 \cdot 10^{-2}$	$1 \cdot 10^{-2}$	$1 \cdot 10^{-4}$	$1 \cdot 10^{-4}$	$5 \cdot 10^{-2}$	$2 \cdot 10^{-2}$	$5 \cdot 10^{-5}$	$1 \cdot 10^{-4}$	$2 \cdot 10^{-4}$
$SC_{4(n_R^{(4)} = n_E^{(4)})}$	$1 \cdot 10^{-2}$	$1 \cdot 10^{-2}$	$1 \cdot 10^{-4}$	$1 \cdot 10^{-4}$	$5 \cdot 10^{-2}$	$1 \cdot 10^{-2}$	$5 \cdot 10^{-5}$	$1 \cdot 10^{-4}$	$2 \cdot 10^{-4}$
$SC_{4(n_R^{(4)} < n_E^{(4)})}$	$1 \cdot 10^{-2}$	$1 \cdot 10^{-2}$	$1 \cdot 10^{-4}$	$1 \cdot 10^{-4}$	$8 \cdot 10^{-2}$	$1 \cdot 10^{-3}$	$5 \cdot 10^{-5}$	$1 \cdot 10^{-4}$	$2 \cdot 10^{-4}$
Units	h^{-1}	h^{-1}	$cell^{-1}h^{-1}$	$Cell^{-1}h^{-1}$	h^{-1}	h^{-1}	$Cell^{-1}h^{-1}$	$cell^{-1}h^{-1}$	$cell^{-1}h^{-1}$

Table 5.1: Parameter values used for model in Equation (5.10). Values from [5] satisfy stability conditions for SS_2. Modifications of some identified values result in the stability of the other steady states as given.

Regarding values K_1 and K_2 which delimit poor and better prognosis areas, results given in References [62] and [70] suggest that the poor prognosis is reached when numbers of effector and regulatory T cells stablish equally or when T reg cells are found in higher proportion, which drives us to consider $K_1 = 1$, according also to [59]. On the other hand, the better prognosis is indicated for a proportion of 1:10 for T reg/effector, so we set $K_2 = 10$. These two values will remain fixed for the whole chapter. Regarding the initial state, we will use a value $(N_E, N_R) \in \mathbb{R}^{K_1,K_2}$ in between these two regions, in a relation of 1:2 for T reg/effector. Therefore, and having into account computational limitations, for now on the initial state $(N_E, N_R) = (50, 25)$ will be used.

- **Steady state SS_1: $(n_E^{(1)}, n_R^{(1)}) = (0,0)$ - Extinction**

  Based on stability conditions SC_1, ($\mu_E > \lambda_E$ and $\mu_R > \lambda_R$), both cell populations would reach extinction in the late times. This can be obtained by only slightly perturbing parameters μ_R and μ_E from those in [5], as reported in Table 5.1.

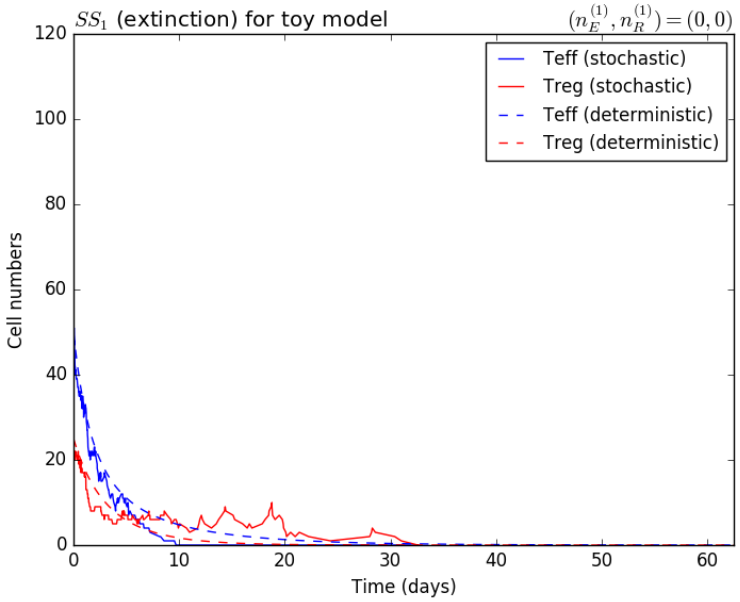

Figure 5.4: Time dynamics for effector and regulatory T cells when reaching $SS_1 = (0,0)$ under parameters given in Table 5.1 for SC_1. (Python code for obtaining this figure is included in Appendix C).

Figure 5.4 shows together deterministic time dynamics, and Gillespie simulations of model given in Equation (5.10) when steady state $(n_E^{(1)}, n_R^{(1)}) = (0,0)$ is reached. We can see that whereas the deterministic simulation supports that regulatory T cell number always remains below effector's, and so their extinction also becomes earlier, the stochastic simulation sample (blue and red solid lines) shows that this fact can be altered, specially in low expression levels examples as it is the case. The mean time until reaching steady state for both populations is of the order of 30 days, which is relatively shorter than the following cases.

Regarding the probability of reaching poor or better prognosis areas, Figure 5.5 shows the results of the methodology followed in Section 5.2.2. Thus, these analytical results indicate that under stability conditions SC_1 given in Table 5.1, when $K_1 = 1$, $K_2 = 10$ and $(N_E, N_R) = (50, 25)$ is the initial state, the probability of entering to poor prognosis

area through each state (n_E, n_R) is given by red bars in the histogram and through states (n_E, n_R) in the better prognosis, by blue bars. When adding up all the probabilities of entering from every state for each area we obtain the total probability of reaching either poor prognosis area $p^{1,10}_{(50,25)} = 0.6544$ or better prognosis area $1 - p^{1,10}_{(50,25)} = 0.3456$. The stochastic simulation plotted in Figure 5.4 shows for instance a sample in which poor prognosis is reached first and through state $(n_E, n_R) = (7,7)$. This stochastic approach has the advantage, with respect to a deterministic model, that it can track how probability changes from state to state, which can be particularly interesting for detecting wide distribution as the poor prognosis one in Figure 5.5.

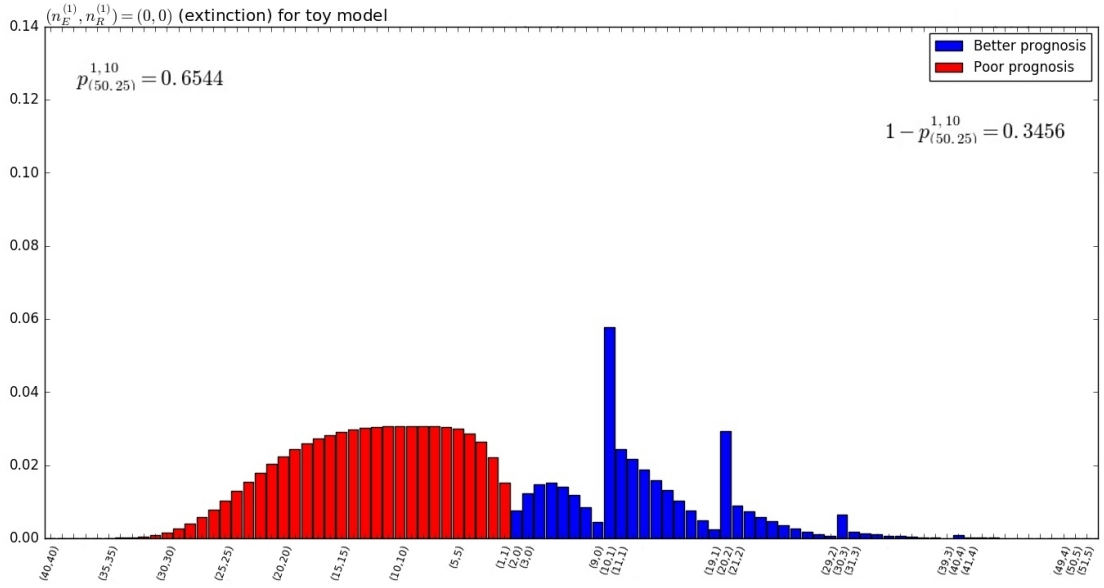

Figure 5.5: Probabilities of reaching poor and better prognosis regions through each potential state (n_E, n_R). Initial state $(N_E, N_R) = (50,25)$. $K_1 = 1$, $K_2 = 10$. Parameters satisfying SC_1 in Table 5.1. (Python code for obtaining this figure is included in Appendix B).

- **Steady state SS_2: $(n_E^{(2)}, n_R^{(2)}) = (0, \frac{\lambda_R - \mu_R}{\nu_R})$ - Poor Prognosis**

  Stability conditions SC_2 represent populations $(n_E(t), n_R(t))$ reaching poor prognosis steady state $(0, \frac{\lambda_R - \mu_R}{\nu_R})$, allowing the disease condition to prevail, see Figure 5.6. This plot also shows that regulatory T cells expression level overtakes effector cells number around day $4-5$. Moreover, whereas T reg cells seem to reach steady state in a similar range of time to SS_1 case, effector cells will not extinct, in the deterministic case, before day 60. However, stochastic simulations might bring cases, as the one plotted, in which this extinction occurs

at a different time, as in three weeks time in such plot.

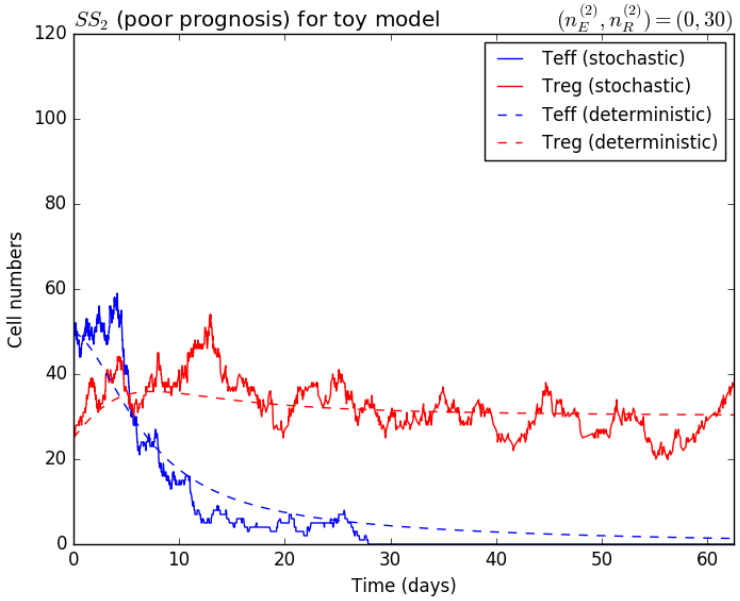

Figure 5.6: Time dynamics for effector and regulatory T cells when reaching $SS_2 = (0, 30)$ under parameters given in Table 5.1 for SC_2.

Regarding the probability of reaching poor and better prognosis regions plotted in Figure 5.7, we can see this a case in which poor prognosis region will be reached in almost 100% of the cases. Given that the process ends up in state $(n_E, n_R) = (0, 30)$, located quite inside the poor prognosis area, the chances of reaching better prognosis first are almost negligible. The closer to zero that n_R is in the steady state $SS_2 = (0, \frac{\lambda_R - \mu_R}{\nu_R})$, the bigger that probability of reaching better prognosis $1 - p^{1,10}_{(50,25)}$ will become, with a maximum value given for the extinction case; $1 - p^{1,10}_{(50,25)} = 0.3456$. The stochastic simulation plotted in Figure 5.6 also shows one of the cases with more probability, which is the one reaching poor prognosis around state $(n_E, n_R) = (35, 35)$.

- **Steady state SS_3: $(n_E^{(3)}, n_R^{(3)}) = (\frac{\mu_E - \lambda_E}{\alpha_E - \nu_E}, 0)$ - Better prognosis**

  This steady state represents a T cell environment which favours the killing of cancerous cells, by increasing the effector T cell population. In order for the system to reach this steady state in the long-term, parameters need to satisfy SC_3 conditions. These conditions can be satisfied by slightly decreasing values α_R and λ_R from [5], as represented in Table 5.1. In Figure 5.8 we plot time dynamics of these two species, with steady state $(n_E^{(3)}, n_R^{(3)}) = (2 \cdot 10^2, 0)$. In a situation like this, after a simultaneous decrease of both populations during

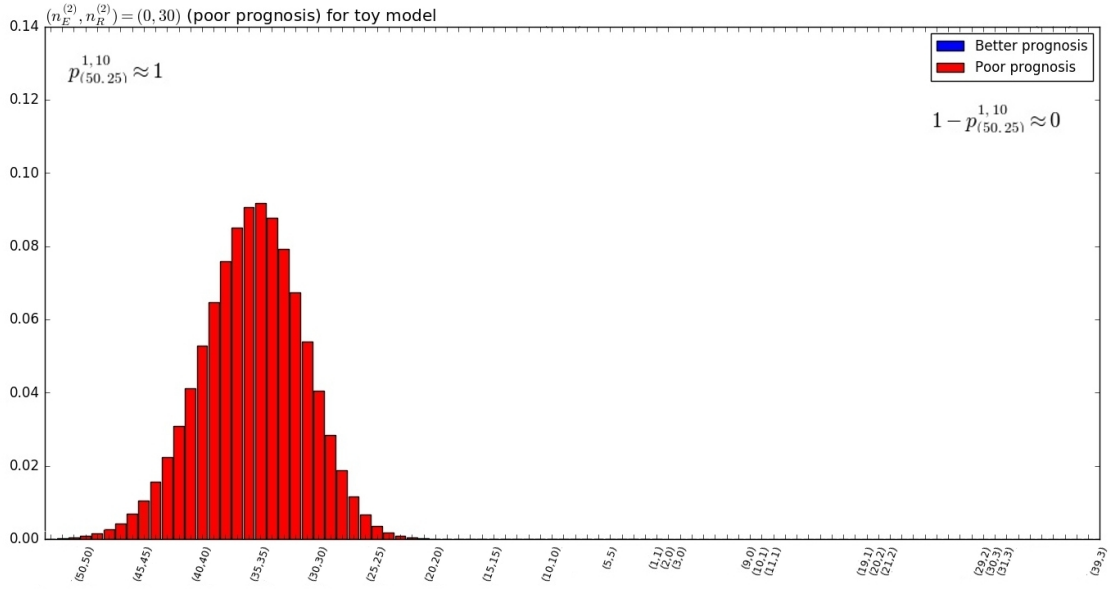

Figure 5.7: Probabilities of reaching poor and better prognosis regions through each potential state (n_E, n_R). Initial state $(N_E, N_R) = (50, 25)$. $K_1 = 1$, $K_2 = 10$. Parameters satisfying SC_2 in Table 5.1.

the first week, effector T cells start increasing until steady state $n_E = 100$ while regulatory cells keep going down until extinction.

In this better prognosis scenario, there is, as for SS_2 case, a clear tendency for the process to reach first the region where the steady state is allocated. Nevertheless, Figure 5.9 shows that when $SS_3 = (100, 0)$, probability of entering in poor prognosis region $p^{1,10}_{(50,25)}$ is slightly higher than the chances of entering in the better prognosis area in the previous case. This could be the case of the stochastic simulation in Figure 5.8 if both effector and regulatory T cells Gillepie simulation touch at any time. The peculiar shape of the histogram for better prognosis, alternating a higher value of probability every ten states, has to do with the fact that these states $\{(n_E, n_R) = (10 \cdot i, i) \in \mathbb{BP}^{1,10}\}$ are reachable for the process from two different transition rates, as Equation (5.1) shows, whereas the rest of the states in the better prognosis region (which are connected by transitions to at least one state outside this region), are only reachable by one transition rate.

- **Steady state SS_4: $(n_E^{(4)}, n_R^{(4)}) = \left(\frac{\chi(\lambda_R - \mu_R) - \nu_R(\lambda_E - \mu_E)}{\nu_R(\alpha_E - \nu_E) - \alpha_R \chi}, \frac{(\alpha_E - \nu_E)(\lambda_R - \mu_R) + \alpha_R(\mu_E - \lambda_E)}{\nu_R(\alpha_E - \nu_E) - \alpha_R \chi} \right)$ - Tolerance**

  The final steady state occurs when both cell populations reach stable non-zero steady state values. Depending on the particular values of parameter considered (see Table 5.1) steady

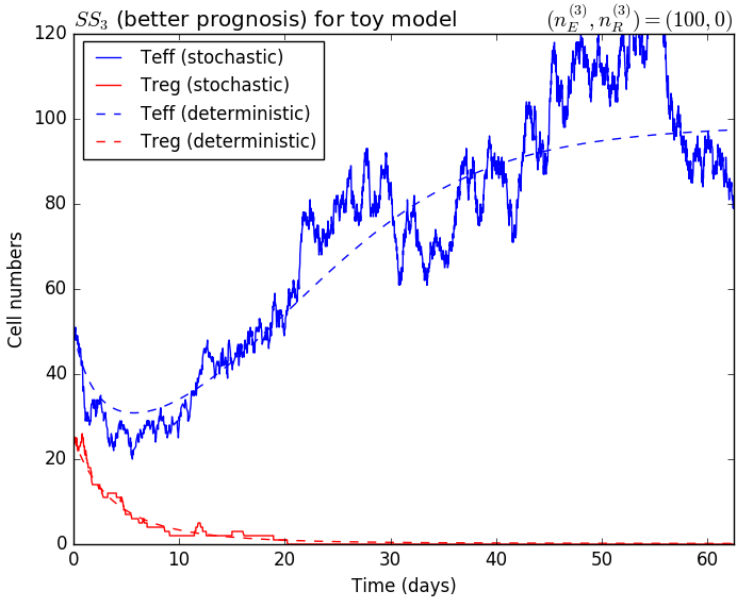

Figure 5.8: Time dynamics for effector and regulatory T cells when reaching $SS_3 = (100, 0)$ under parameters given in Table 5.1 for SC_3.

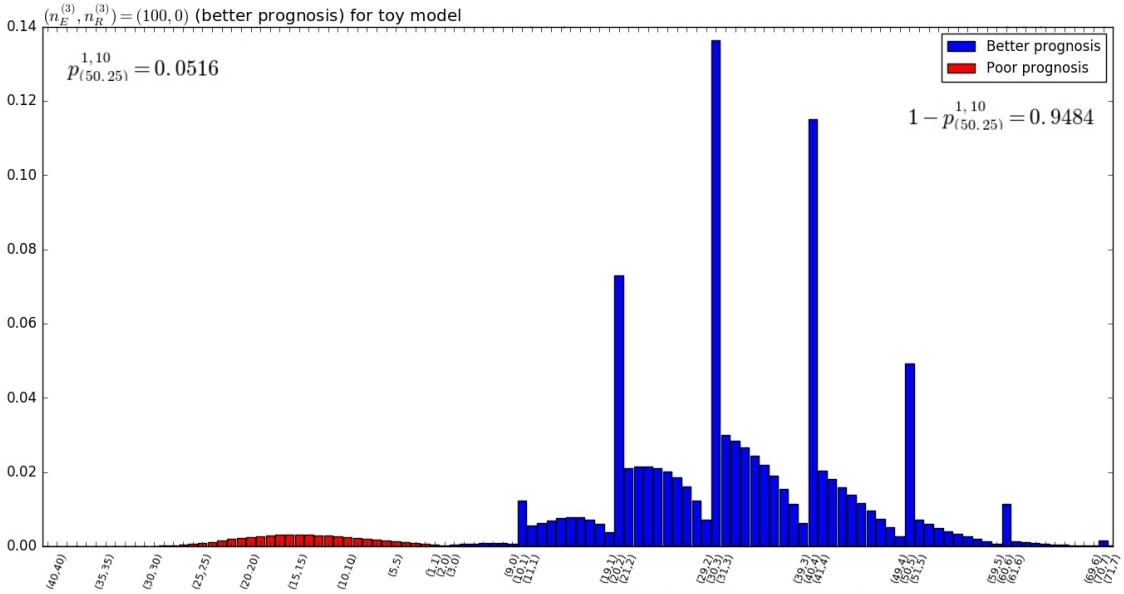

Figure 5.9: Probabilities of reaching poor and better prognosis regions through each potential state (n_E, n_R). Initial state $(N_E, N_R) = (50, 25)$. $K_1 = 1$, $K_2 = 10$. Parameters satisfying SC_3 in Table 5.1.

state $(n_E^{(4)}, n_R^{(4)})$ can amount to a larger number of effector T cells or of regulatory T cells. In particular, by considering different parameter values satisfying SC_4, one can obtain $n_E^{(4)} > n_R^{(4)}, n_E^{(4)} = n_R^{(4)}$ or $n_E^{(4)} < n_R^{(4)}$; see Figures 5.10-5.15.

i) When $n_E^{(4)} > n_R^{(4)}$

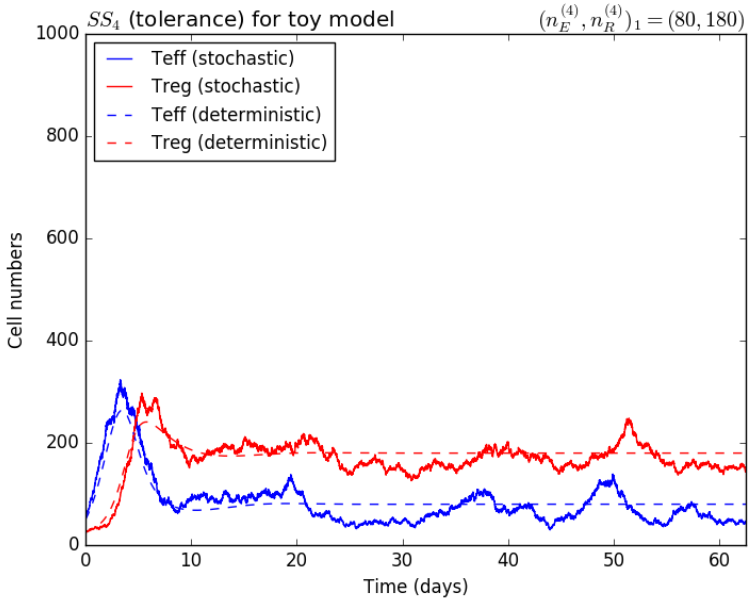

Figure 5.10: Time dynamics for effector and regulatory T cells when reaching $(n_E^{(4)}, n_R^{(4)})$ with $n_E^{(4)} > n_R^{(4)}$ under parameters given in Table 5.1 for $SC_{4(n_E^{(4)} > n_R^{(4)})}$.

ii) When $n_E^{(4)} = n_R^{(4)}$

iii) When $n_E^{(4)} < n_R^{(4)}$

The time dynamics of the process when steady state $SS_4 = (n_E^{(4)}, n_R^{(4)})$ is reached show similar behaviour in the three different cases $SC_{4(n_E^{(4)} > n_R^{(4)})}$, $SC_{4(n_E^{(4)} = n_R^{(4)})}$ and $SC_{4(n_E^{(4)} < n_R^{(4)})}$. In all of them (Figures 5.10, 5.12 and 5.14) both populations arrive to steady state in around two weeks, faster than in the other steady states. Regardless of the ratio $\frac{n_E^{(4)}}{n_R^{(4)}}$, regulatory T cells maximum value is always only slightly higher that its steady state whereas effector cells reach up to more than twice its steady state value as Figure 5.14 shows, from 352 to approximately 800. The behaviour of the stochastic simulations for n_E and n_R populations, Figures 5.10, 5.12 and 5.14, suggests that effector cells have a short time impact on regulatory T cells, as the similar path (but shifted to right in T reg cells) for both of them show.

Finally, Figures 5.11, 5.13 and 5.15 encode the probability of reaching SS_4 in the three

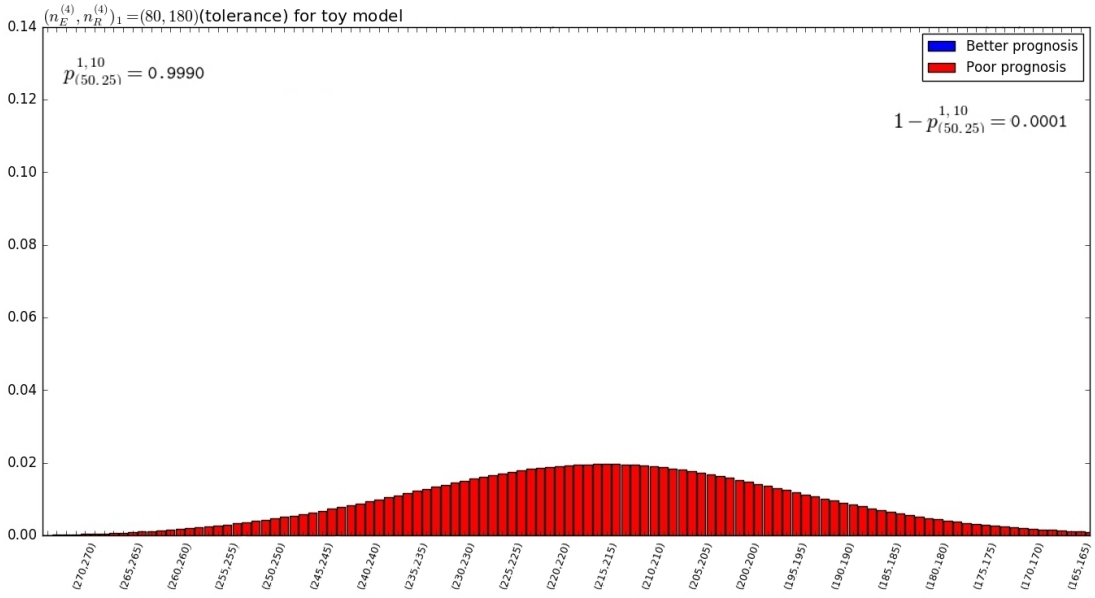

Figure 5.11: Probabilities of reaching poor and better prognosis regions through each potential state (n_E, n_R). Initial state $(N_E, N_R) = (50, 25)$. $K_1 = 1$, $K_2 = 10$. Parameters satisfying $SC_{4(n_E^{(4)} > n_R^{(4)})}$ in Table 5.1.

different scenarios described before. Poor prognosis histograms in Figures 5.11 and 5.13 show almost the same behaviour where their similar mean values are also reflected in the intersection between effector and regulatory T cells curves in their respective Gillespie samples shown in Figures 5.10 and 5.12. Better prognosis histogram is not shown in Figure 5.11 since $1 - p^{1,10}_{(50,25)}$ is almost negligible in this case. As the ratio $\frac{n_E^{(4)}}{n_R^{(4)}}$ increases, not only $1 - p^{1,10}_{(50,25)}$ does but also the mean value of any of the two variables in the state of entry in the poor prognosis area and the difference between the probability of entering in the better prognosis region through states $\{(n_E, n_R) = (10 \cdot i, i); (n_E, n_R) \in \mathbb{BP}^{1,10}\}$ and the probability of entering through the rest of the states in this $\mathbb{BP}$ region.

5.3 Fas/FasL induced-death and role of IL-2 in T reg cells death

Fas ligand (FasL) is a transmembrane protein which, once secreted mainly by an effector cell, might induce apoptosis when binding with its receptor (Fas). Fas/FasL interactions have

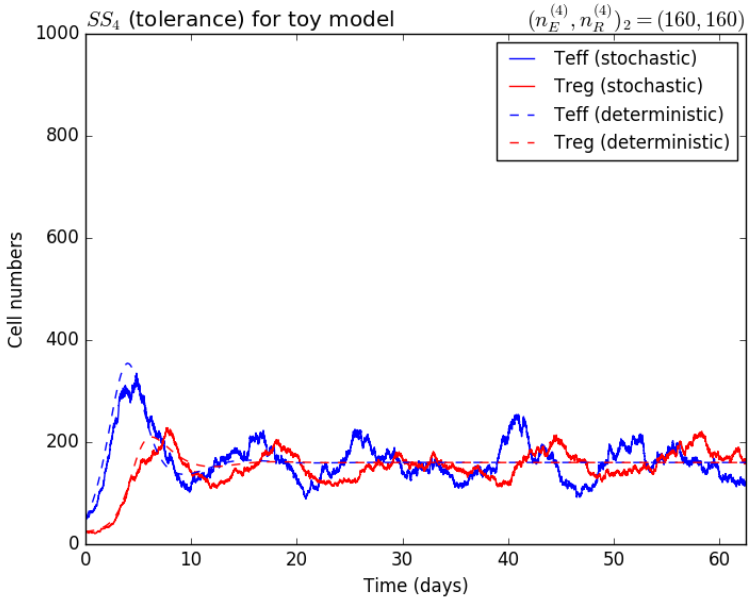

Figure 5.12: Time dynamics for effector and regulatory T cells when reaching $(n_E^{(4)}, n_R^{(4)})$ with $n_E^{(4)} = n_R^{(4)}$ under parameters given in Table 5.1 for $SC_{4(n_E^{(4)}=n_R^{(4)})}$.

a crucial role when regulating the immune system and particularly in cancer progression [59]. This alternative model tries to reproduce how tumour prognosis will be affected by the fact that these ligand/receptor interactions are considered in the model. Consequently, in this section, the relations between effector and regulatory T cells are slightly modified with respect to those in the model given in Equation (5.10).

In such scenario, effector T cells die with rate μ_E, they die by Fas/FasL induced-death due to Fas expressed on effector T cells and FasL expressed on effector T cells with rate ν_{EE}, they die by Fas/FasL induced-death due to Fas expressed on effector T cells and FasL expressed on regulatory T cells with rate ν_{ER}, they proliferate due to TCR with rate λ_E, they proliferate due to IL-2 secreted by effector T cells with rate α_E and they are suppressed by regulatory T cells with rate χ. Regulatory T cells die with rate μ_R and this death rate depends on the cytokine IL-2 available, and modulated as $\frac{\kappa_E}{\kappa_E + n_E}$, they die by Fas/FasL induced-death due to Fas expressed on regulatory T cells and FasL expressed on effector T cells with rate ν_{RE}, they die by Fas/FasL induced-death due to Fas expressed on regulatory T cells and FasL expressed on regulatory T cells with rate ν_{RR}, they proliferate due to TCR with rate λ_R and they proliferate due to IL-2 secreted by effector T cells with rate α_R.

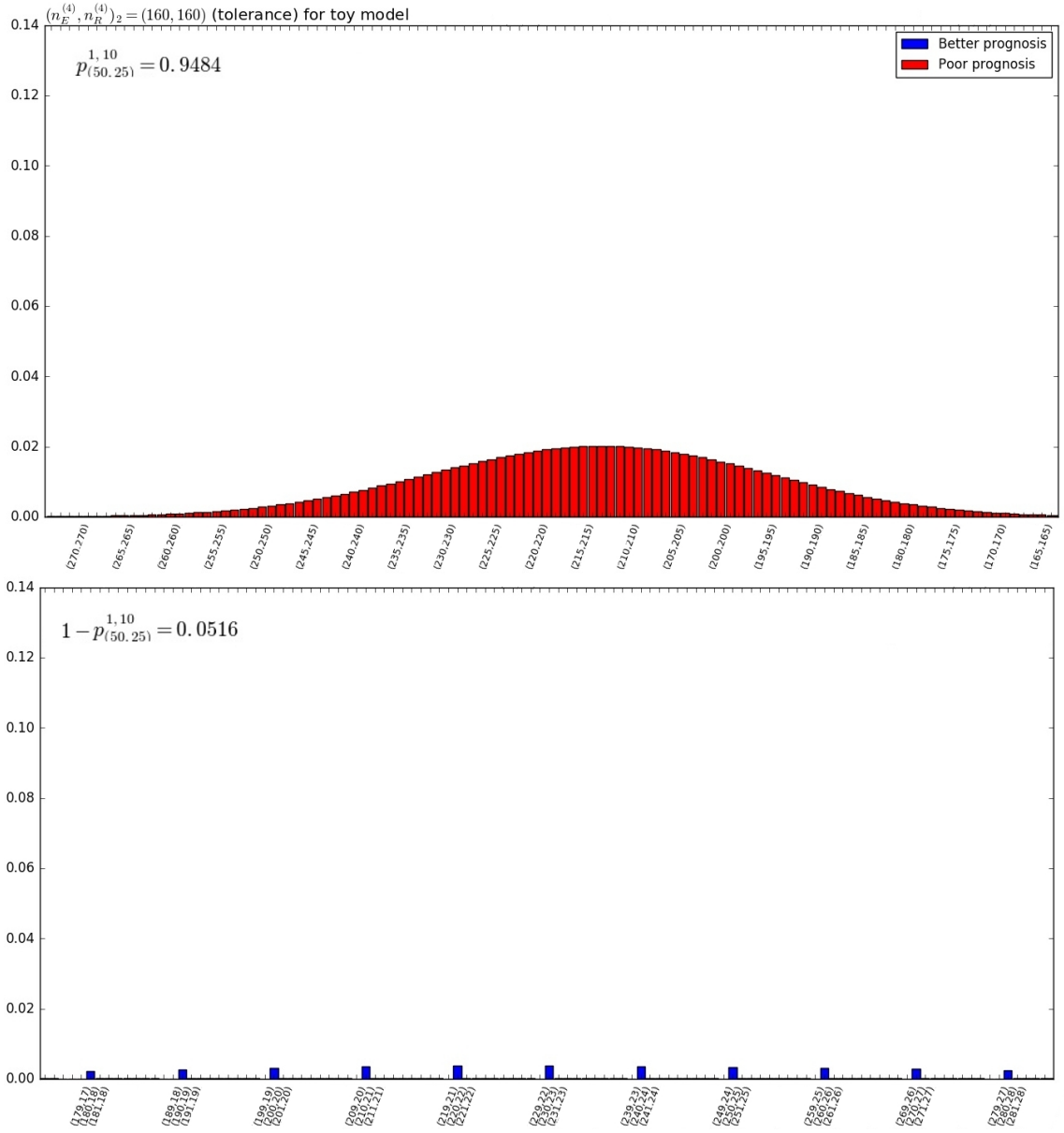

Figure 5.13: Probabilities of reaching poor and better prognosis regions through each potential state (n_E, n_R). Initial state $(N_E, N_R) = (50, 25)$. $K_1 = 1$, $K_2 = 10$. Parameters satisfying $SC_{4(n_E^{(4)}=n_R^{(4)})}$ in Table 5.1.

These reactions can be modelled, like in Section 5.2, as a continuous-time Markov chain $\tilde{\mathcal{X}} = \{(N_E(t), N_R(t)) : t \geq 0\}$ defined over $\mathbb{N}_0^2$, where transitions and infinitesimal transition

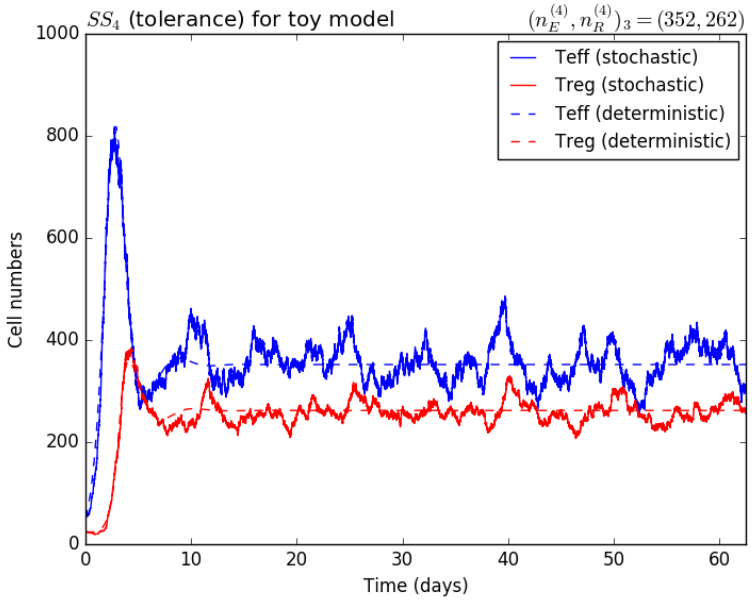

Figure 5.14: Time dynamics for effector and regulatory T cells when reaching $(n_E^{(4)}, n_R^{(4)})$ with $n_E^{(4)} < n_R^{(4)}$ under parameters given in Table 5.1 for $SC_{4(n_E^{(4)} < n_R^{(4)})}$.

rates are given by

$$\bar{q}_{(n_E,n_R),(n'_E,n'_R)} = \begin{cases} \lambda_E n_E + \alpha_E n_E^2, & \text{if } (n'_E, n'_R) = (n_E + 1, n_R), \\ \mu_E n_E + \nu_{EE} n_E^2 + (\nu_{ER} + \chi) n_E n_R, & \text{if } (n'_E, n'_R) = (n_E - 1, n_R), \\ \lambda_R n_R + \alpha_R n_E n_R, & \text{if } (n'_E, n'_R) = (n_E, n_R + 1), \\ \mu_R \frac{\kappa_E}{\kappa_E + n_E} n_R + \nu_{RR} n_R^2 + \nu_{RE} n_R n_E, & \text{if } (n'_E, n'_R) = (n_E, n_R - 1). \end{cases} \tag{5.16}$$

Note that these transitions satisfy, as those in Equation (5.1), that from any given state (n_E, n_R) only adjacent states $(n_E + 1, n_R), (n_E - 1, n_R), (n_E, n_R + 1)$ and $(n_E, n_R - 1)$ are directly accessible in one jump. This implies that the probabilistic approach in Section 5.3.2 of this model can be constructed by using the structure of states explained in Section 5.2.2.

5.3.1 Probability of extinction and mean time until extinction

Following the reasoning in Section 5.2.1, some parameter regimes are looked in the present Section for model given by reactions described in Equation (5.16). For this purpose, Theorem 5.2 holds.

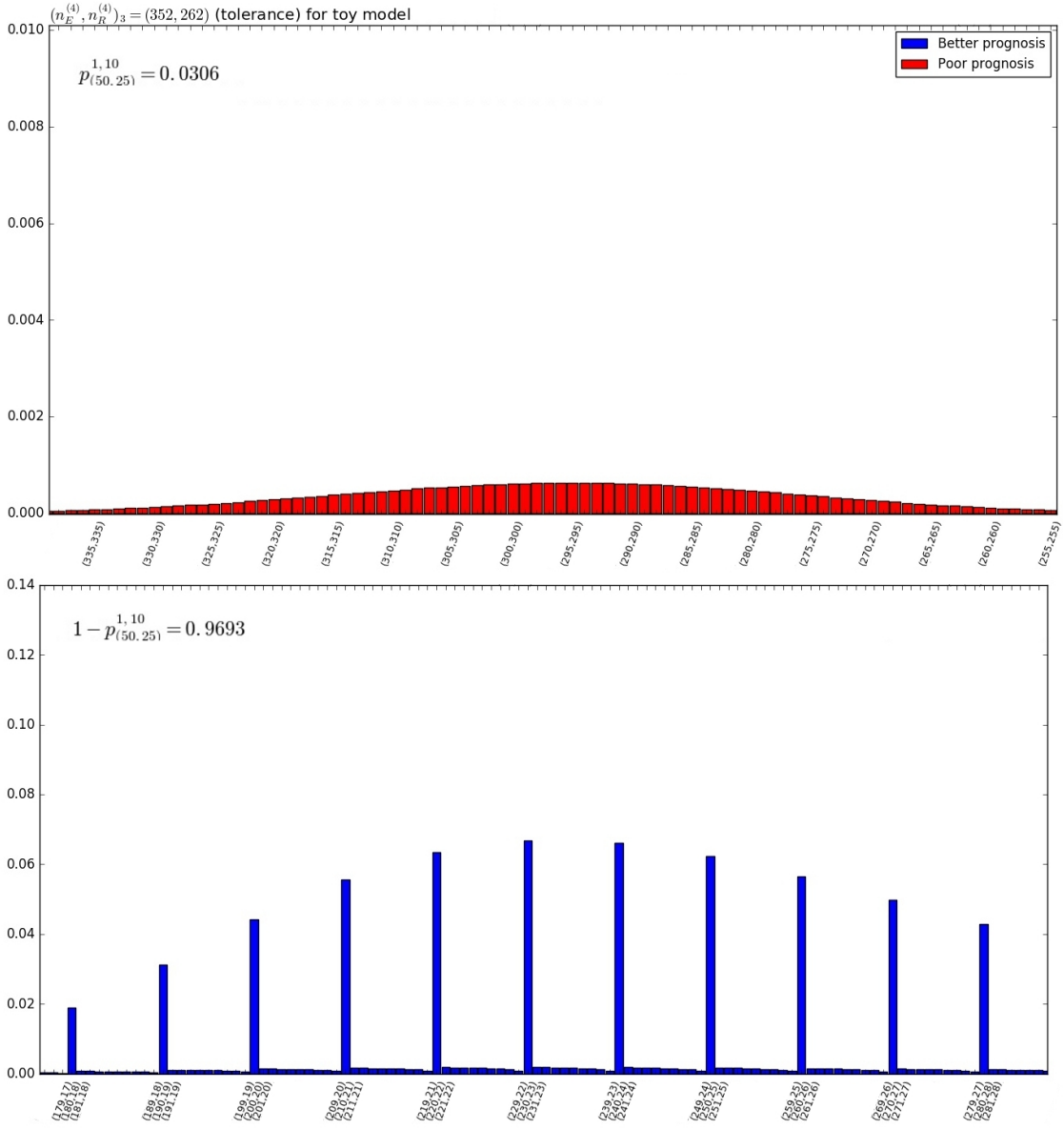

Figure 5.15: Probabilities of reaching poor and better prognosis regions through each potential state (n_E, n_R). Initial state $(N_E, N_R) = (50, 25)$. $K_1 = 1$, $K_2 = 10$. Parameters satisfying $SC_{4(n_E^{(4)} < n_R^{(4)})}$ in Table 5.1.

Theorem 5.2. Let $\alpha_{(n_E,n_R)}$, with $(n_E, n_R) \in \mathcal{C}$, be the probability of reaching some state in $\mathcal{C}_0$, from (n_E, n_R), in a finite time, and $\tau_{(n_E,n_R)}$ the mean time until this occurs. Under parameter Regimes $\bar{A}$ or $\bar{B}$, $\alpha_{(n_E,n_R)} = 1$ and $\tau_{(n_E,n_R)} < +\infty$ for any initial state $(n_E, n_R) \in \mathcal{C}$. Where

Regime $\bar{A}$:

$\mu := \mu_E$

$\nu_{EE} + \nu_{RR} > \nu_{ER} + \nu_{RE} + \chi > 2\nu_{RR} + \frac{\mu}{\kappa_E}$

Regime $\bar{B}$:

$\mu := \mu_E$

$\nu_{EE} + \nu_{RR} < \nu_{ER} + \nu_{RE} + \chi < 2\nu_{EE}$,

$2\nu_{EE} + \nu_{ER} + \nu_{RE} + \chi > 4\nu_{RR} + 3\frac{\mu}{\kappa_E}$.

Proof.

Following the same reasoning as for Theorem 5.1, the global brith-and-death rates for each level $\mathcal{C}(k)$, $k = n_R + n_E$, are given in this case as

$$\begin{aligned} \lambda_k &= \max_{n_E \in [1,k-1]} \{\bar{f}_k(n_E)\}, \\ \mu_k &= \min_{n_E \in [1,k-1]} \{\bar{g}_k(n_E)\}, \end{aligned}$$

with, in this case,

$$\begin{aligned} \bar{f}_k(n_E) &= (\alpha_E - \alpha_R)n_E^2 + (\lambda_E - \lambda_R + \alpha_R k)n_E + \lambda_R k, \\ \bar{g}_k(n_E) &= (\nu_{EE} - \nu_{ER} + \nu_{RR} + \nu_{RE} - \chi)n_E^2 \\ &+ (\mu_E + k\nu_{ER} + k\chi - 2k\nu_{RR} - \mu_R \frac{\kappa_E}{\kappa_E + n_E} + \nu_{RE}k)n_E + (\mu_R \frac{\kappa_E}{\kappa_E + n_E} + \nu_{RR}k)k. \end{aligned}$$

Note that $\bar{f}_k(n_E)$ has the same expression as $f_k(n_E)$ in Equation (5.3) and that the more complicated expression of $\bar{g}_k(n_E)$ will make harder to find some regimes to verify uniqueness of solution. In order to find such regimes, some assumptions need to be taken into account so these conditions can be used. Then, we set the minimum for $\bar{g}_k(n_E)$ to be in in either $n_E = 1$ or $n_E = k - 1$ and, if the function monotonically increases or decreases, respectively, our assumption will hold. Since

$$\begin{aligned} \bar{g}_k(1) &= \nu_{EE} + \nu_{RR}(k-1)^2 + \mu_E + \mu_R \frac{\kappa_E}{\kappa_E + 1}(k-1) + \nu_{RE}(k-1) + (\nu_{ER} + \chi)(k-1), \\ \bar{g}_k(k-1) &= \nu_{EE}(k-1)^2 + \nu_{RR} + \mu_E(k-1) + \mu_R \frac{\kappa_E}{\kappa_E + k - 1} + \nu_{RE}(k-1) + (\nu_{ER} + \chi)(k-1), \end{aligned}$$

for $k > 2$, $\bar{g}_k(1) \gtrless \bar{g}_k(k-1)$ is equivalent to

$$\begin{aligned} \nu_{EE} + \nu_{RR}(k-1)^2 + \mu_E + \mu_R \frac{\kappa_E}{\kappa_E + 1}(k-1) &\gtrless \nu_{EE}(k-1)^2 + \nu_{RR} + \mu_E(k-1) + \mu_R \frac{\kappa_E}{\kappa_E + k - 1}, \\ \nu_{RR}(k^2 - 2k) - \nu_{EE}(k^2 - 2k) - \mu_E(k-2) + \mu_R(k-2)\frac{\kappa_E(\kappa_E + k)}{(\kappa_E + k - 1)(\kappa_E - 1)} &\gtrless 0. \end{aligned}$$

Note that when $k = 2$, $\bar{g}_k(1) = \bar{g}_k(k-1)$. So dividing last expression by $(k-2)$,

$$(\nu_{RR} - \nu_{EE})k - \mu_E + \mu_R \frac{\kappa_E(\kappa_E + k)}{(\kappa_E + k - 1)(\kappa_E + 1)} \gtrless 0.$$

Let us consider $\mu = \mu_E = \mu_R$ for this section, given that $\mu_E = \mu_R$ in both parameter regimes A and B. Since

$$\frac{\kappa_E(\kappa_E + k)}{(\kappa_E + k - 1)(\kappa_E + 1)} < 1,$$

if

$$\nu_{EE} > \nu_{RR} \Rightarrow \bar{g}_k(1) < \bar{g}_k(k-1).$$

And the second condition is then that $\bar{g}_k'(n_E) > 0 \; \forall n_E \in [1, k-1]$. Since

$$\bar{g}_k'(n_E) = 2\nu_{EE}n_E + 2\nu_{RR}(n_E - k) + (\nu_{ER} + \nu_{RE} + \chi)(k - 2n_E) + \mu\left(\frac{3\kappa_E n_E + n_E^2 - \kappa_E k}{(\kappa_E + n_E)^2}\right). \quad (5.17)$$

In order to deal with this expression, a classification depending of the values of n_E needs to be done due to the variations of sign of each of the four terms in Equation (5.17). In order to have $\bar{g}_k'(n_E) > 0$ $\forall n_E \in [1, k-1]$, we can study what will happen under

- **Case i)** *When $n_E \in [0, \frac{k}{3})$.*
- **Case ii)** *When $n_E \in [\frac{k}{3}, \frac{k}{2})$.*
- **Case iii)** *When $n_E \in [\frac{k}{2}, k)$.*

Last term of Equation (5.17) can now be minimized. For cases ii) and iii), $\mu(\frac{3\kappa_E n_E + n_E^2 - \kappa_E k}{(\kappa_E + n_E)^2}) > 0$, but most of the times negligible when compared to the other terms. In case i), $\mu(\frac{3\kappa_E n_E + n_E^2 - \kappa_E k}{(\kappa_E + n_E)^2}) \geqslant \frac{-k\mu}{\kappa_E}$. Let us start by working with case iii). From

$$2\nu_{EE}n_E > |2\nu_{RR}(n_E - k) + (\nu_{ER} + \nu_{RE} + \chi)(k - 2n_E)|$$

it follows that either one of this two conditions needs to be satisfied:

- $\overline{SC_1}$: $\nu_{EE} + \nu_{RR} > \nu_{ER} + \nu_{RE} + \chi$ *or*
- $\overline{SC_2}$: $\nu_{EE} + \nu_{RR} < \nu_{ER} + \nu_{RE} + \chi < 2\nu_{EE}$.

With this two options in hand for $n_E \in [\frac{k}{2}, k)$ we need to check if Equation (5.17) is also satisfied for the other two cases i) and ii). Case ii) gives a less strict condition for uniqueness than case iii) so nothing new appears from it. From case i) the regime that insterests us has to verify both

- $\overline{SC_1} : \nu_{EE} + \nu_{RR} > \nu_{ER} + \nu_{RE} + \chi$ *and*
- $\overline{SC_2} : 2\nu_{EE} + \nu_{ER} + \nu_{RE} + \chi > 4\nu_{RR} + 3\frac{\mu}{\kappa_E}$.

So, in conclusion, for $\bar{g}_k'(n_E) > 0 \; \forall n_E \in [1, k-1]$, regimes $\bar{A}$ and $\bar{B}$ hold. □

These two regimes $\bar{A}$ and $\bar{B}$ for System (5.18), together with the regimes found in previous sections for $\bar{f}_k(n_E)$ and with the convergence of $\sum_{k=2}^{+\infty} \frac{1}{\lambda_k \sigma_k}$, can be gathered in Table 5.2 which resumes the two scenarios where existence and uniqueness of extinction are guaranteed.

Regime $\bar{A}$	Regimen $\bar{B}$
$\nu_{EE} + \nu_{RR} > \nu_{ER} + \nu_{RE} + \chi > 2\nu_{RR} + \frac{\mu}{\kappa_E}$	$\nu_{EE} + \nu_{RR} < \nu_{ER} + \nu_{RE} + \chi < 2\nu_{EE}$
	$2\nu_{EE} + \nu_{ER} + \nu_{RE} + \chi > 4\nu_{RR} + 3\frac{\mu}{\kappa_E}$
$\nu_{EE} > \nu_{RR} > \alpha_E, \quad \alpha_E < \alpha_R < 2\alpha_E, \quad \lambda_E < \lambda_R$	

Table 5.2: Summary of the regimes where existence and uniqueness of extinction are guaranteed for model (5.18).

5.3.2 A probabilistic approach for predicting tumour prognosis

Process $\bar{\mathcal{X}}$ starts in a given initial state $(N_E(0), N_R(0)) = (N_E, N_R)$ and it is defined on the same state space $\mathcal{S}$ as the model in Section 5.2, which is structured by levels $\mathbb{R}^{K_1,K_2}(k)$. Given that infinitesimal transition rates $q_{(n_E,n_R),(n_E',n_R')}$ and $\bar{q}_{(n_E,n_R),(n_E',n_R')}$ in Equations (5.1) and (5.16) have the same structure, that is, they represent the same kind of transitions to adjacent states, most of the probabilistic approach explained in Section 5.2.2 can be equally implemented for the Fas/FasL model.

In order to carry out the truncation of $\mathbb{R}^{K_1,K_2}$ as in Section 5.2.2, by means of the probabilities defined by the system of equations given in Equation (5.7), we define

$$\bar{X}^{max,K_1,K_2}_{(n_E,n_R)} = \text{“Maximum cell population size (that is, maximum level } \mathbb{R}^{K_1,K_2}(k)\text{) reached by process } \bar{\mathcal{X}} \text{ before reaching prognosis regions } \mathbb{PP}^{K_1,K_2} \cup \mathbb{BP}^{K_1,K_2}\text{, given the initial state } (n_E, n_R)\text{”} = \max_{t\in[0,T]} \{N_E(t) + N_R(t)\},$$

where $T = \inf\{t \geqslant 0 : (N_E(t), N_R(t)) \in \mathbb{PP}^{K_1,K_2} \cup \mathbb{BP}^{K_1,K_2}\}$, with associated probabilities

$$\bar{p}^{max,K_1,K_2}_{(N_E,N_R)}(k) \quad = \quad \mathbb{P}(\bar{X}^{max,K_1,K_2}_{(N_E,N_R)} \geqslant k),$$

for all $k \geqslant N_E + N_R$. The objective is to choose a truncation value k such that

$$\bar{p}^{max,K_1,K_2}_{(N_E,N_R)}(k) < \epsilon,$$

for ϵ small enough. Probabilities $\bar{p}^{max,K_1,K_2}_{(N_E,N_R)}(k)$ can be computed by firststep arguments leading to an analogous system to the one given by Equation (5.7). In particular, matrices $\mathbf{A}^{K_1,K_2}_{r,r'}$ need to be substituted by matrices $\bar{\mathbf{A}}^{K_1,K_2}_{r,r'}$, which are defined as follows:

- For $3 \leq r \leq k-1$:

$$\left(\bar{\mathbf{A}}^{K_1,K_2}_{r,r-1}\right)_{ij} \quad = \quad \begin{cases} \frac{\mu n_E + \nu_{EE} n_E^2 + (\nu_{ER}+\chi) n_E n_R}{\bar{\Delta}_{(n_E,n_R)}}, & \text{if } j = Pos_{r-1}(n_E - 1), \\ \frac{\mu_R \frac{\kappa_E}{\kappa_E + n_E} n_R + \nu_R n_R^2 + \nu_{RE} n_R n_E}{\bar{\Delta}_{(n_E,n_R)}}, & \text{if } j = Pos_{r-1}(n_E), \\ 0, & \text{otherwise}, \end{cases}$$

  with $(n_E, n_R) = \left(\left\lceil \frac{K_2 r}{K_2+1} \right\rceil - i, \left\lfloor \frac{r}{K_2+1} \right\rfloor + i\right)$, for $0 \leq i \leq J^{K_1,K_2}(r)$, and where now $\bar{\Delta}_{(n_E,n_R)} = (\lambda_E + \alpha_E n_E + \mu_E + \nu_{EE} n_E + \nu_{ER} n_R + \chi n_R) n_E + (\lambda_R + \alpha_R n_E + \mu_R \frac{\kappa_E}{\kappa_E + n_E} + \nu_{RR} n_R + \nu_{RE} n_E) n_R$.

- For $2 \leq r \leq k-2$,

$$\left(\bar{\mathbf{A}}^{K_1,K_2}_{r,r+1}\right)_{ij} \quad = \quad \left(\mathbf{A}^{K_1,K_2}_{r,r+1}\right)_{ij},$$

  where $0 \leq i \leq J^{K_1,K_2}(r)$.

Finally, the vector of independent terms $\mathbf{b}^{max,K_1,K_2}(k)$ in Equation (5.7) needs to be replaced by

$$\bar{\mathbf{b}}^{max,K_1,K_2}(k) \quad = \quad \begin{pmatrix} \mathbf{0}_{J^{K_1,K_2}(2)} \\ \mathbf{0}_{J^{K_1,K_2}(3)} \\ \vdots \\ \mathbf{0}_{J^{K_1,K_2}(k-2)} \\ \bar{\mathbf{b}}^{max,K_1,K_2}_{k-1} \end{pmatrix},$$

with $\bar{\mathbf{b}}_{k-1}^{max,K_1,K_2} = \bar{\mathbf{A}}_{k-1,k}^{K_1,K_2}\mathbf{1}_{J^{K_1,K_2}(k)}$, where $\mathbf{1}_{J^{K_1,K_2}(k)}$ is a column vector of ones with dimension $J^{K_1,K_2}(k)$. Finally, the resulting alternative version of Equation (5.7), with matrices $\bar{\mathbf{A}}_{r,r-1}^{K_1,K_2}$ and vector $\bar{\mathbf{b}}_{k-1}^{max,K_1,K_2}$ can be iteratively solved via Algorithm 5.1 which allows to truncate the state space for the Fas/FasL model described by transition rates given in Equation (5.16) as Figure 5.3 shows.

Once $K_\epsilon(N_E,N_R)$ is chosen by starting at $k = N_E + N_R + 1$ and sequentially increasing k until $\bar{p}_{(N_E,N_R)}^{max,K_1,K_2}(k) < \epsilon$, process $\bar{\mathcal{X}}$ can be analysed on a truncated state space for levels $\bigcup_{k=2}^{K_\epsilon(N_E,N_R)} \mathbb{R}^{K_1,K_2}(k)$. The objective, as in Section 5.2.2, is to compute probabilities

$$\bar{p}_{(N_E,N_R)}^{K_1,K_2} = \text{“}\textit{Probability of process } \bar{\mathcal{X}} \textit{ of reaching region } \mathbb{PP}^{K_1,K_2} \textit{ before region } \mathbb{BP}^{K_1,K_2}, \textit{ given the initial state } (N_E,N_R) \in \mathbb{R}^{K_1,K_2}\text{”}.$$

which can be obtained in a matrix way by solving the system

$$\bar{\mathbf{p}}^{K_1,K_2}(K_\epsilon(N_E,N_R)) = \bar{\mathbf{A}}^{K_1,K_2}(K_\epsilon(N_E,N_R))\bar{\mathbf{p}}^{K_1,K_2}(K_\epsilon(N_E,N_R)) + \bar{\mathbf{b}}^{K_1,K_2}(K_\epsilon(N_E,N_R))$$

where vector $\bar{\mathbf{p}}^{K_1,K_2}$ has the same structure as vector $\mathbf{p}^{K_1,K_2}$ in Section 5.2.2, matrix $\bar{\mathbf{A}}^{K_1,K_2}$ has the same structure as matrix $\mathbf{A}^{K_1,K_2}$ defined in Equation (5.8) but substituting matrices $\mathbf{A}_{r,r'}^{K_1,K_2}$ by matrices $\bar{\mathbf{A}}_{r,r'}^{K_1,K_2}$, and with

$$\bar{\mathbf{b}}^{K_1,K_2}(K_\epsilon(N_E,N_R)) = \begin{pmatrix} \bar{\mathbf{b}}_2^{K_1,K_2} \\ \bar{\mathbf{b}}_3^{K_1,K_2} \\ \vdots \\ \bar{\mathbf{b}}_{K_\epsilon(N_E,N_R)-1}^{K_1,K_2} \end{pmatrix},$$

where sub-vector $\bar{\mathbf{b}}_r^{K_1,K_2}$ has zeros everywhere except for any element corresponding to a state (n_E,n_R) such that $\frac{n_E}{n_R+1} \leq K_1$ or $\frac{n_E-1}{n_R} \leq K_1$ (that is, a state (n_E,n_R) that has one-step transition access to poor prognosis region $\mathbb{PP}^{K_1,K_2}$), which is equal to

$$\frac{1}{\bar{\Delta}_{(n_E,n_R)}}\left((\lambda_R + \alpha_R n_E)n_R\delta_{\{\frac{n_E}{n_R+1}\leq K_1\}} + (\mu_E n_E + \nu_{EE}n_E^2 + (\nu_{ER}+\chi)n_E n_R)\delta_{\{\frac{n_E-1}{n_R}\leq K_1\}}\right),$$

where $\delta_{\{A\}}$ is equal to 1 if A is satisfied, and 0 otherwise. This system can be solved by adapting Algorithm 5.1.

5.3.3 Deterministic approach to the model

The equations for the deterministic model are given by

$$\begin{aligned}\frac{dn_E}{dt} &= -\mu_E n_E - \nu_{EE} n_E^2 - \nu_{ER} n_E n_R + \lambda_E n_E + \alpha_E n_E^2 - \chi n_E n_R, \\ \frac{dn_R}{dt} &= -\mu_R \frac{\kappa_E}{\kappa_E + n_E} n_R - \nu_{RE} n_R n_E - \nu_{RR} n_R^2 + \lambda_R n_R + \alpha_R n_R n_E, \end{aligned} \tag{5.18}$$

As for the original model, four steady states $\overline{SS}_i$ with $i \in \{1,2,3,4\}$ can be obtained for the Fas/FasL model by computing

$$\begin{aligned} -\mu_E n_E - \nu_{EE} n_E^2 - \nu_{ER} n_E n_R + \lambda_E n_E + \alpha_E n_E^2 - \chi n_E n_R &= 0, \\ -\mu_R \frac{\kappa_E}{\kappa_E + n_E} n_R - \nu_{RE} n_R n_E - \nu_{RR} n_R^2 + \lambda_R n_R + \alpha_R n_R n_E &= 0. \end{aligned} \tag{5.19}$$

Therefore,

$$\begin{aligned} &\overline{SS}_1: && (n_E^{(1)}, n_R^{(1)}) = (0,0), && \textbf{extinction.} \\ &\overline{SS}_2: && (n_E^{(2)}, n_R^{(2)}) = \left(0, \frac{\lambda_R - \mu_R}{\nu_{RR}}\right), && \textbf{poor prognosis.} \\ &\overline{SS}_3: && (n_E^{(3)}, n_R^{(3)}) = \left(\frac{\mu_E - \lambda_E}{\alpha_E - \nu_{EE}}, 0\right), && \textbf{better prognosis.} \end{aligned} \tag{5.20}$$

Observation: Given that the stability analysis of $\overline{SS}_4$ does not seem feasible from an analytical perspective and not even its formulae looks tractable, we will focus on the other three.

Equivalently to the study done in Section 5.2.3, a stability analysis by means of analysing the corresponding Jacobian matrix $\bar{J}(n_E, n_R)$ can be done, where

$$\bar{J}(n_E, n_R) = \begin{pmatrix} 2(\alpha_E - \nu_{EE})n_E - (\nu_{ER} + \chi)n_R + \lambda_E - \mu_E & -(\nu_{ER} + \chi)n_E \\ \frac{\mu_R \kappa_E n_R}{(\kappa_E + n_E)^2} + (\alpha_R - \nu_{RE})n_R & \frac{-\mu_R \kappa_E}{\kappa_E + n_E} + (\alpha_R - \nu_{RE})n_E - 2\nu_{RR} n_R + \lambda_R \end{pmatrix}.$$

Thus, a given steady state $(n_E^{(i)}, n_R^{(i)})$ ($i \in \{1,2,3\}$) is asymptotically stable if and only if the eigenvalues of $\bar{J}(n_E^{(i)}, n_R^{(i)})$ have strictly negative real part.

Steady state $\overline{SS}_1$: $(n_E^{(1)}, n_R^{(1)}) = (0,0)$ - Extinction

Steady state $\overline{SS}_1$ represents that both populations go to extinction in the late times. Evaluating the Jacobian matrix at the steady state, we get:

$$\bar{J}(n_E^{(1)}, n_R^{(1)}) = \begin{pmatrix} \lambda_E - \mu_E & 0 \\ 0 & \lambda_R - \mu_R \end{pmatrix},$$

with eigenvalues

$$\begin{aligned} \bar{\sigma}_1^{(1)} &= \lambda_E - \mu_E, \\ \bar{\sigma}_2^{(1)} &= \lambda_R - \mu_R. \end{aligned}$$

Thus, $\overline{SS}_1$ is stable if and only if the stability conditions

$$\overline{SC}_1 : \qquad \mu_E > \lambda_E, \quad \mu_R > \lambda_R \tag{5.21}$$

are satisfied.

Steady state $\overline{SS}_2$: $(n_E^{(2)}, n_R^{(2)}) = (0, \frac{\lambda_R - \mu_R}{\nu_{RR}})$ - Poor prognosis

Steady state $\overline{SS}_2$ represents survival of the regulatory T cell population in the late times, while the population of effector T cells goes to extinction, moving the system towards the *poor prognosis* area. The Jacobian matrix evaluated at $\overline{SS}_2$ can be obtained as

$$\bar{J}(n_E^{(2)}, n_R^{(2)}) = \begin{pmatrix} \lambda_E - \mu_E + \frac{(\mu_R - \lambda_R)(\nu_{ER} + \chi_R)}{\nu_{RR}} & 0 \\ \frac{(\lambda_R - \mu_R)(\mu_R + \alpha_R \kappa_E - \nu_{RE} \kappa_E)}{\kappa_E \nu_{RR}} & \mu_R - \lambda_R \end{pmatrix},$$

from which the following eigenvalues hold

$$\begin{aligned} \bar{\sigma}_1^{(2)} &= -\lambda_R + \mu_R, \\ \bar{\sigma}_2^{(2)} &= \frac{(\lambda_E - \mu_E)\nu_{RR} + (\mu_R - \lambda_R)(\nu_{ER} + \chi)}{\nu_{RR}}. \end{aligned}$$

Thus, we can conclude that steady state $\overline{SS}_2$ is stable if and only if the stability conditions

$$\overline{SC}_2 : \qquad \lambda_R > \mu_R, \quad \nu_{RR}\lambda_E + (\nu_{ER} + \chi)\mu_R < \nu_{RR}\mu_E + (\nu_{ER} + \chi)\lambda_R \tag{5.22}$$

are satisfied.

Steady state $\overline{SS}_3$: $(n_E^{(3)}, n_R^{(3)}) = (\frac{\mu_E-\lambda_E}{\alpha_E-\nu_{EE}}, 0)$ - Better prognosis

Steady state $\overline{SS}_3$ represents the process going in the late times towards the *better prognosis* area, with the population of regulatory T cells going to extinction. The Jacobian matrix for this steady state is

$$\bar{J}(n_E^{(3)}, n_R^{(3)}) = \begin{pmatrix} \lambda_E - \mu_E & \frac{(\lambda_E-\mu_E)(\nu_{ER}+\chi)}{\alpha_E-\nu_{EE}} \\ 0 & \lambda_R - \mu_R \frac{\kappa_E(\alpha_E-\nu_{EE})}{\kappa_E\alpha_E-\kappa_E\nu_{EE}+\mu_E-\lambda_E} + \frac{(\alpha_R-\nu_{RE})(\mu_E-\lambda_E)}{\alpha_E-\nu_{EE}} \end{pmatrix},$$

with eigenvalues

$$\begin{aligned} \bar{\sigma}_1^{(3)} &= -\lambda_E + \mu_E, \\ \bar{\sigma}_2^{(3)} &= \lambda_R - \mu_R \frac{\kappa_E(\alpha_E-\nu_{EE})}{\kappa_E\alpha_E-\kappa_E\nu_{EE}+\mu_E-\lambda_E} + \frac{(\alpha_R-\nu_{RE})(\mu_E-\lambda_E)}{\alpha_E-\nu_{EE}}. \end{aligned}$$

Thus, steady state $\overline{SS}_3$ is stable if and only if the stability conditions

$$\overline{SC}_3: \qquad \lambda_E > \mu_E, \quad \left(\lambda_R - \mu_R \frac{\kappa_E(\alpha_E-\nu_{EE})}{\kappa_E\alpha_E-\kappa_E\nu_{EE}+\mu_E-\lambda_E} + \frac{(\alpha_R-\nu_{RE})(\mu_E-\lambda_E)}{\alpha_E-\nu_{EE}}\right) < 0 \quad (5.23)$$

are satisfied. Moreover, stability conditions $\overline{SC}_1$ and $\overline{SC}_2$ are incompatible, so that steady states $\overline{SS}_1$ and $\overline{SS}_2$ can not be stable at the same time. This also happens between $\overline{SC}_1$ and $\overline{SC}_3$ but not necessary between $\overline{SC}_2$ and $\overline{SC}_3$. This means that steady states $\overline{SS}_2$ and $\overline{SS}_3$ could be reached under the same parameter regimes depending on the initial value (N_E, N_R) for the process.

5.3.4 Results

Table 5.3 shows parameter regimes leading to stability of each of the steady states above. First row indicates the values as appear in [5]. However, we note that since λ_R is not included in this reference, it has been taken for a first approach as λ_E and we consider $\nu_{EE} = \nu_{ER} = \nu_{RE} = \nu_{RR} = \nu_E$.

Parameter	μ_E	μ_R	ν_{EE}	ν_{ER}	ν_{RE}	ν_{RR}
In the spirit of [5]	$1\cdot10^{-2}$	$1\cdot10^{-2}$	$1\cdot10^{-4}$	$1\cdot10^{-4}$	$1\cdot10^{-4}$	$1\cdot10^{-4}$
$\overline{SC}_1$	$1\cdot10^{-2}$	$1\cdot10^{-2}$	$1\cdot10^{-3}$	$1\cdot10^{-4}$	$1\cdot10^{-4}$	$1\cdot10^{-4}$
$\overline{SC}_2$	$1\cdot10^{-2}$	$1\cdot10^{-2}$	$1\cdot10^{-3}$	$1\cdot10^{-4}$	$1\cdot10^{-4}$	$1\cdot10^{-4}$
$\overline{SC}_3$	$1\cdot10^{-3}$	$1\cdot10^{-3}$	$4\cdot10^{-4}$	$1.5\cdot10^{-4}$	$1.5\cdot10^{-4}$	$1\cdot10^{-4}$
Units	h^{-1}	h^{-1}	$cell^{-1}h^{-1}$	$cell^{-1}h^{-1}$	$cell^{-1}h^{-1}$	$cell^{-1}h^{-1}$
Parameter	λ_E	λ_R	α_E	α_R	χ	κ_E
In the spirit of [5]	$2\cdot10^{-2}$	$2\cdot10^{-2}$	$5\cdot10^{-5}$	$1\cdot10^{-4}$	$2\cdot10^{-4}$	10^2
$\overline{SC}_1$	$2\cdot10^{-3}$	$8\cdot10^{-3}$	$7.5\cdot10^{-5}$	$1\cdot10^{-4}$	$2\cdot10^{-4}$	10^2
$\overline{SC}_2$	$2\cdot10^{-2}$	$3\cdot10^{-2}$	$7.5\cdot10^{-5}$	$1\cdot10^{-4}$	$2\cdot10^{-4}$	10^2
$\overline{SC}_3$	$5\cdot10^{-3}$	$5\cdot10^{-4}$	$7.5\cdot10^{-5}$	$1\cdot10^{-4}$	$2\cdot10^{-4}$	10^2
Units	h^{-1}	h^{-1}	$cell^{-1}h^{-1}$	$cell^{-1}h^{-1}$	$cell^{-1}h^{-1}$	$cell$

Table 5.3: Parameter values used for Fas/FasL model described by Equation (5.18).

Steady state $\overline{SS}_1$: $(n_E^{(1)}, n_R^{(1)}) = (0,0)$ - Extinction

In this case, slight alterations from [5] of certain parameters were implemented having into account stability conditions $\overline{SC}_1$, and the regimes where existence and uniqueness of extinction are guaranteed, Regimen A in Table 5.2, leading to steady state $(n_E^{(1)}, n_R^{(1)}) = (0,0)$.

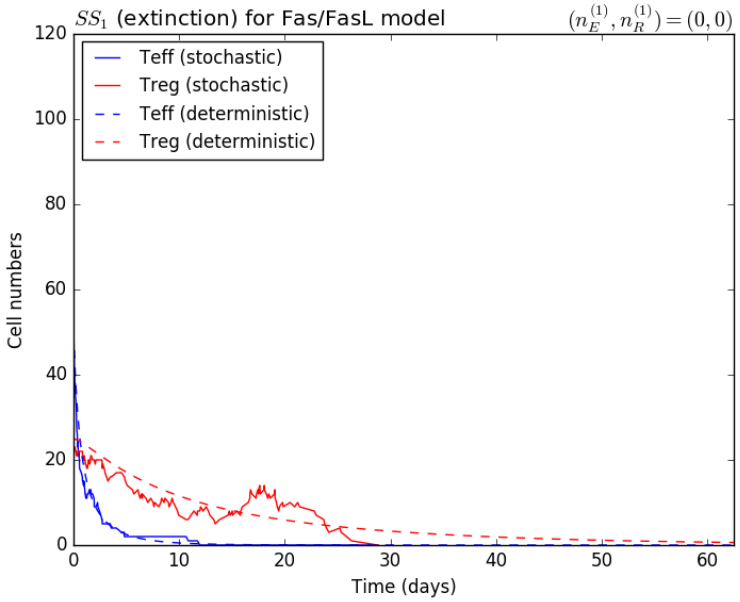

Figure 5.16: Time dynamics for effector and regulatory T cells when reaching $\overline{SS}_1 = (0,0)$ under parameters given in Table 5.2 for $\overline{SC}_1$.

Figure 5.16 shows stochastic and deterministic time dynamics of Fas/FasL model under parameter regime $\overline{SC}_1$, in which extinction takes place. As a contrast to what happened to the extinction case in the toy model, see Figure 5.4, effector cells tend to become extinguish much quicker than regulatory cells, which survive longer with respect to the previous model. Successive simulations with other parameter regimes confirm that this different is not only due to the election of the rate values but for the impact that Fas/FasL dynamics have in inducing apoptosis.

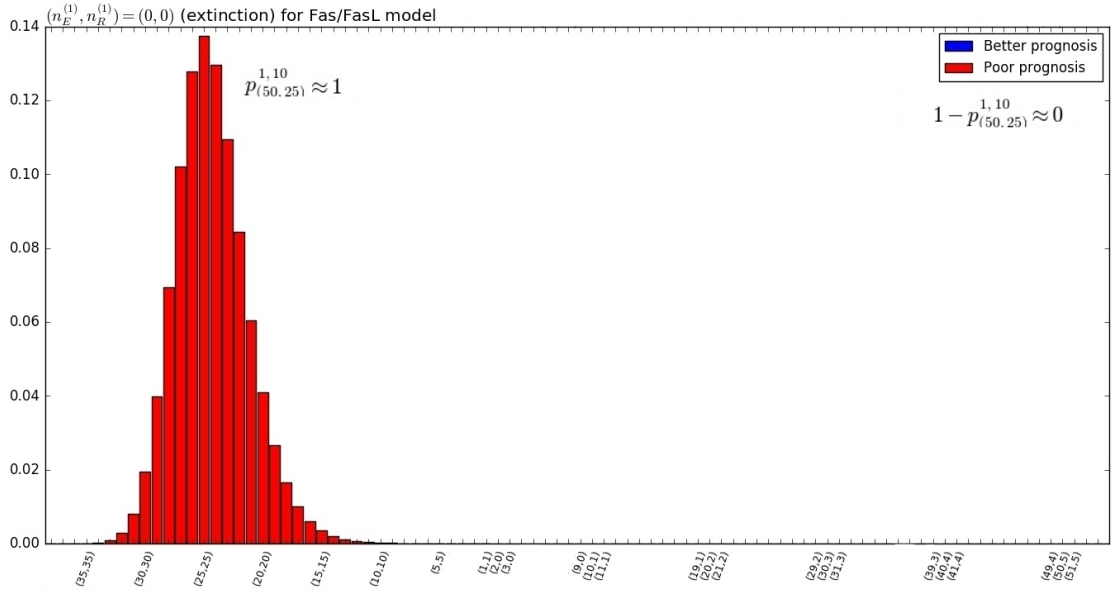

Figure 5.17: Probabilities of reaching poor and better prognosis regions through each potential state (n_E, n_R). Initial state $(N_E, N_R) = (50, 25)$. $K_1 = 1$, $K_2 = 10$. Parameters satisfying $\overline{SC}_1$ in Table 5.3.

As a consequence of this new behaviour, some alterations also related to the probability of reaching poor and better prognosis regions could be predicted when comparing toy and Fas/FasL models. Figure 5.17 shows how $1 - p^{1,10}_{(50,25)}$ reduces from 0.3456 in the former (Figure 5.5) to almost 0 in the latter. From Figures 5.16 and 5.17 together we can deduce that the process in this scenario very soon reaches poor prognosis regimes and around states very close to the initial state (N_E, N_R), being the one with more probability (≈ 0.14) state $(n_E, n_R) = (25, 25)$.

Steady state $\overline{SS}_2$: $(n_E^{(2)}, n_R^{(2)}) = (0, \frac{\lambda_R - \mu_R}{\nu_{RR}})$ - Poor prognosis

Under parameters satisfying stability conditions $\overline{SC}_2$, the process reaches a scenario in which tumour progression is believed to take place. Figure 5.18 is an example of the time dynamics when parameters satisfy these $\overline{SC}_2$, values given in Table 5.2. Similarly to the extinction case, effector cells go very quickly to extinction whereas regulatory cells expand until reaching steady state $n_R = 200$, in around two weeks mean time.

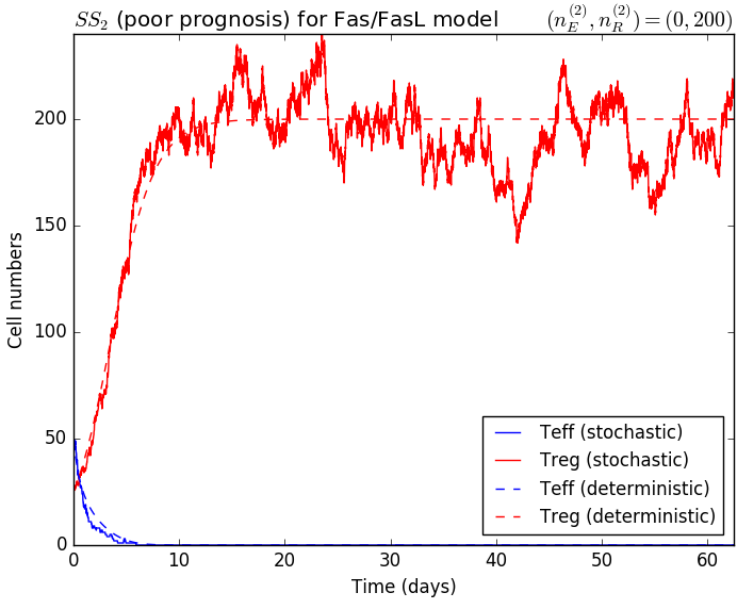

Figure 5.18: Time dynamics for effector and regulatory T cells when reaching $\overline{SS}_2 = (0, 200)$ under parameters given in Table 5.2 for $\overline{SC}_2$.

Histograms shown in Figure 5.19 for the probabilities of reaching poor and better prognosis regions in this scenario are almost identical to the extinction case. However, since T reg cells are proliferating much faster here, the state of entry in the poor prognosis region has slightly increased now (in ≈ 7 states). Moreover, the probability distributions for poor prognosis in the Fas/FasL model tends to be more symmetric in the firt two steady states when compared to the ones in the toy model.

Steady state $\overline{SS}_3$: $(n_E^{(3)}, n_R^{(3)}) = (\frac{\mu_E - \lambda_E}{\alpha_E - \nu_{EE}}, 0)$ - Better prognosis

Finally, parameter regimes given by $\overline{SC}_3$ would potentially drive the proccess into regulatory T cell extinction and the maintenance of effectors in the late times. For the

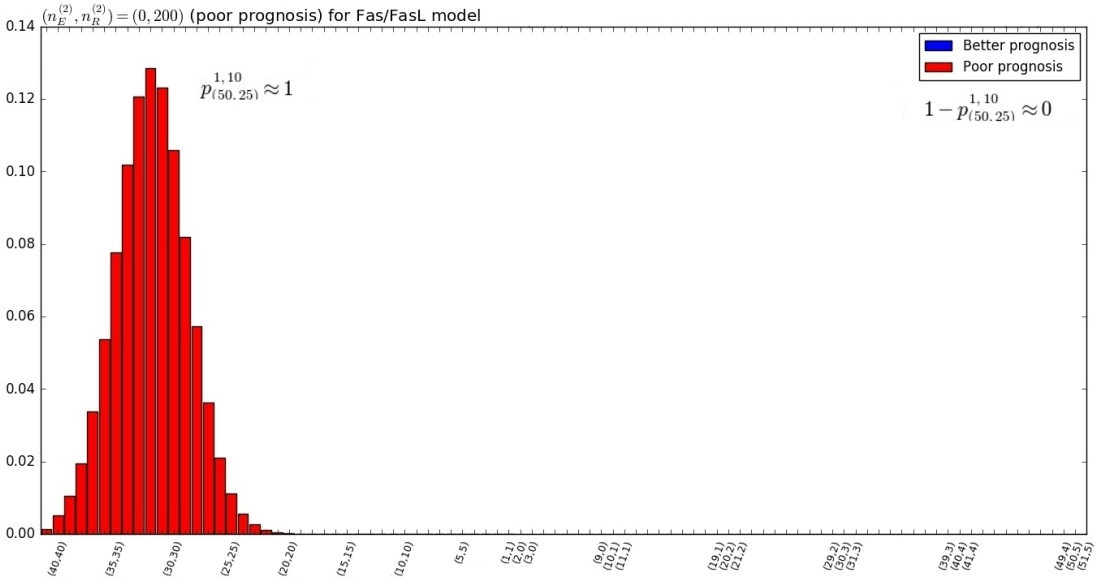

Figure 5.19: Probabilities of reaching poor and better prognosis regions through each potential state (n_E, n_R). Initial state $(N_E, N_R) = (50, 25)$. $K_1 = 1$, $K_2 = 10$. Parameters satisfying $\overline{SC}_2$ in Table 5.3.

particular case in which such parameters are fixed as given in Table 5.2, The steady state $\overline{SS}_3$ would be given as $(n_E^{(3)}, n_R^{(3)}) = (12, 0)$.

In this particular case, time dynamics for effector and regulatory T cells in Figure 5.20 show that the deterministic curves intersect twice, and the stochastic curves many more. This, together to the fact that population levels are very close, implies that the probability of reaching better prognosis first $1 - p^{1,10}_{(50,25)}$, even when the steady state $\overline{SS}_3 \approx (12.31, 0)$ is allocated in the poor prognosis area, is smaller than 0.02 (Figure 5.21). in fact, if we compute these histograms just perturbing the initial state, let us say reducing the initial value of regulatory cells, this probability $1 - p^{1,10}_{(50,25)}$ progressively increases until being one, when $(N_E, N_R) = (50, 5)$. For instance, the initial state that splits probability of reaching poor or better prognosis in approximately two halves is $(N_E, N_R) = (50, 9)$.

5.4 Conclusions

This Chapter introduces two versions of a tumour prognosis model from different perspectives. With the intention of elucidating how the ratio T_{eff}/T_{reg} between effector

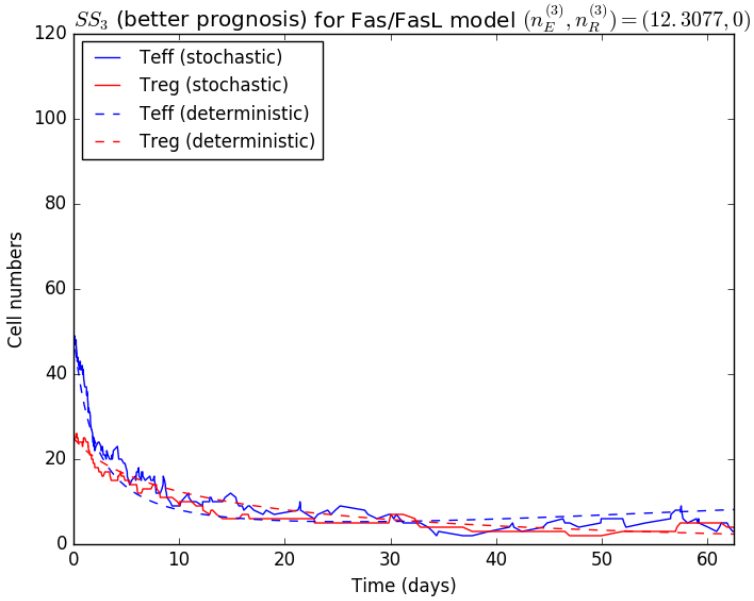

Figure 5.20: Time dynamics for effector and regulatory T cells when reaching $\overline{SS}_3 \approx (12.31, 0)$ under parameters given in Table 5.2 for $\overline{SC}_3$.

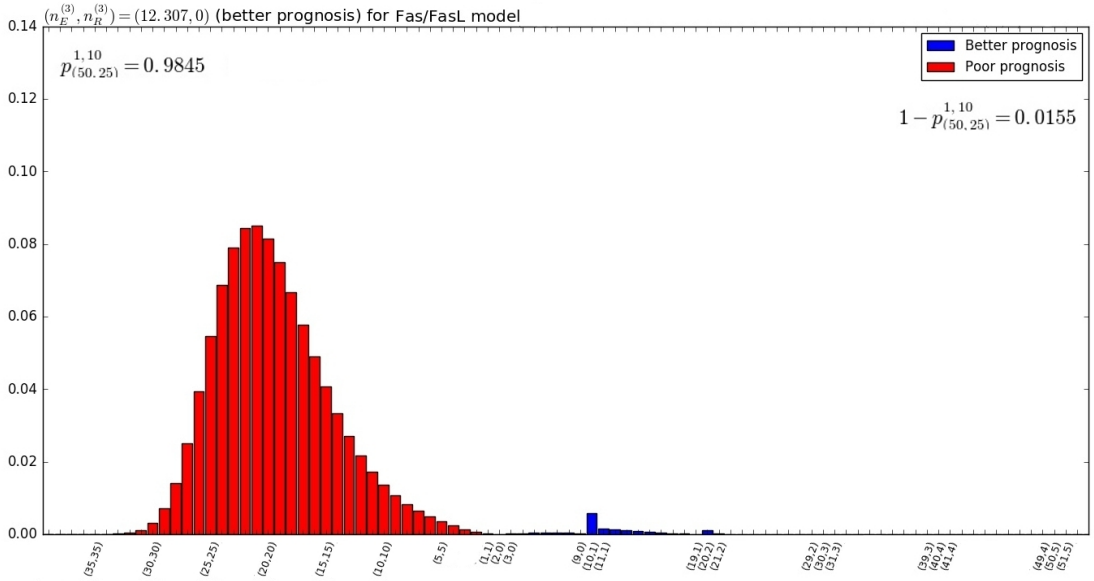

Figure 5.21: Probabilities of reaching poor and better prognosis regions through each potential state (n_E, n_R). Initial state $(N_E, N_R) = (50, 25)$. $K_1 = 1$, $K_2 = 10$. Parameters satisfying $\overline{SC}_3$ in Table 5.3.

$CD8^+$ T cells and regulatory T cells determines tumour progression, we studied, for each of these two models, some parameter regimes in which extinction and uniqueness of extinction are guaranteed. For our toy model and for the Fas/FasL version, regimes given in Theorem 5.1 and Theorem 5.2 in Sections 5.2.1 and 5.3.1 guarantee that the respective process will reach poor or better prognosis with probability one.

With this in hand, stochastic descriptors, over a conveniently defined state space are used in the stochastic version of our models to study in Sections 5.2.2 and 5.3.2 the probability of reaching poor or better prognosis depending on the values of the parameters and so the probability of entering to each of these two regions by any specific state. Moreover, a deterministic approach follows in both Sections 5.2.3 and 5.3.3 for analysing the steady states of the systems and their stability.

When studying the toy model, results in Section 5.2.4 shows how the tendency of probability of reaching poor and better prognosis varies as the parameter conditions SC_i, with $i = 1, 2, 3, 4$, are changed. When observing the histograms with the probability of entering through every state, the patterns followed in the case of poor and better prognosis are quite different, see for instance Figure 5.5. Whereas for the poor prognosis the shape of the distribution is more constant, and seems to follow a gamma distribution, for the better prognosis distribution certain states have a much higher probability of being reached than their neighbours. In particular, those states $(n_E, n_R) \in K_2$. This is because they can be reached by one transition more than those $(n_E, n_R) \notin K_2$ but which belong to $\mathbb{BP}^{K_1,K_2}$.

When comparing the different probability distributions, it can be observed that the steady state location determines the distribution of the two types of prognosis. However, this condition is not complete for the steady state $SS_3 = (100, 0)$. Even when it is located in the better prognosis area, Figure 5.9 shows how the process sometimes reaches first a poor prognosis region (more than 5 times out of 100) before ending up in SS_3. When SS_4 is analysed, again this steady state location affects both distributions. When the steady state is located in the poor prognosis region, the probability of reaching better prognosis $1 - p^{1,10}_{(50,25)}$ is negligible (Figure 5.11), and this probability increases as the steady state approaches to the better prognosis area. It is also interesting to notice how the region of values for the poor prognosis distribution increases as the probability of reaching this area decreases (odd figures from Figure 5.5 to 5.15).

Regarding the time dynamics, stochastic and deterministic simulations are plotted for every steady state (even figures from Figure 5.4 to Figure 5.14), using values in Table 5.1. The

time needed for the process to reach each steady state is significantly different. If for the three distinct cases of SS_4, this steady state is reached in around 10 days (Figures 5.10,5.12 and 5.14), at least 60 days are needed for the system to stay at steady state for the better prognosis scenario (Figure 5.8). This gives and indicator of the time that the system needs to become in homeostais when tumour cells have good prognosis to be depleted. Figures 5.10, 5.12 and 5.14 also show better how effector cells and T reg cells interacts in time. By observing the stochastic dynamics these three plots suggest that regulatory T cells reproduce the behaviour of effector cells dynamics from which we could conclude that the formers have more impact on the latter than the other way round, disregarding the amount of cells of each type.

When introducing the Fas/FasL model, the main differences occur when the steady state reaches either extinction or the better prognosis region. In the first case, Figure 5.17 shows that when $\overline{SS_1} = (0,0)$ is reached, the different paths observed of the toy model are always the poor prognosis one ($1 - p^{1,10}_{(50,25)} \approx 0$). Actually, by comparing the time dynamics of both models in the extinction case (Figures 5.4 and Figure 5.16), we can see that whereas effector cells decreases the time to extinction (from 30 to 10 days), regulatory T cells delay the time needed to vanish in the Fas/FasL model (from 30 to more than 60 days).

Regarding $\overline{SS_3}$, Figures 5.20 and 5.21 both together indicate that even when the steady state is located in the better prognosis area, the poor prognosis region is almost always reached first. This is due to the long time that the process stays around similar values of effector and T reg cells 5.20 and also to the small value of regulatory T cells in steady state SS_3.

Finally, further results for the matrix-analytic approach for both models include a different way of ordering the poor and the better prognosis areas. This would consist on squares instead of triangles and could be more appropriate for certain types of cancers as it is suggested in [59]. Finally, the times needed to reach every state in the boundary conditions can be also analytically obtained with the same approach developed in Sections 5.2.3 and 5.3.2.

Chapter 6

Conclusions

Understanding the mechanisms by which the immune system self-regulates lymphocytes expression levels is believed to be nowadays a crucial aspect for plenty of immunologists. Focused on the role that regulatory $CD4^+$ T cells have in such a matter, the present work has analysed, at different levels, diverse features about this cell sub-population to find out more about their quantitative effect in controlling T cell pool in both homeostasis and cancerous scenarios. To this purpose, the main part of the work was organised from a stochastic perspective which has, among others, the advantage of taking into account the intrinsic randomness of a system and so identifying some less deterministic behaviours that might not be tracked, for instance, by differential equations.

Starting from a molecular approach, Chapters 2 and 3 develop, by means of matrix-analytic methods, two different stochastic models to quantify receptor/ligand dynamics between different types of cells. The apparatus driven by cytokine IL-2 for regulatory T cell stimulation, is studied in Chapter 2. Our model suggests that CD25 (IL-2 high affinity receptor) synthesis rate is fairly affected by the number of IL-2/IL-2R complexes and so that, when these complexes are both intracellular and extracellularly located, those driving the receptor rates are located on the cell surface. Numerical results explained throughout this Chapter also illustrate how time dynamics of these molecules get affected by initial conditions and different hypothesis.

Regulatory T cells are characterised by CD4, transcription factor FOXP3, and CD25. However, another of their characteristic is the location of the inhibitory co-receptor CTLA-4. The fact that most of these molecules are located in the cell surface, in contrast to what

occurs in conventional T cells, implies that their ability to suppress T cell activation is much higher than non-regulatory cells. Chapter 3 compare the the co-stimulatory system dynamics between conventional T cells and APCs and regulatory T-cells with APCs. In terms of cell intrinsic behaviours, results obtained indicate some saturation phenomena when approaching to regulatory cells scenarios, related to higher amount of initial CTLA-4 receptors on the cell surface. When only CTLA-4 is considered versus one kind of ligand, for the maximum amount of complexes simultaneously on the cell surface, this variations are more relevant with mature APCs interactions whereas for the time until having certain amount of ligands internalised, it almost remains the same. When talking about cell extrinsic behaviours, clear differences are quantified depending on if the APC^* that for a second time is stimulating a T cell, stayed in a first stimulation with a regulatory or a conventional T cell and for how long, because of the B7 ligands that the APC^* might have lost in the first one. Additionally, the possibility of sequentially including ligands or receptors in our model, allows us to describe a significant synergy when CD28, CTLA-4, B7-1 and B7-2 are considered together to described the two main characteristics explained above.

There are, however, certain limitations that need to be taken into account when dealing with the type of analytic models used for Chapters 2 and 3. The computational costs of dealing with these matrix algorithms reduce the complexity of our models, which only allows to track the short amount of dynamics considered in them and with small initial conditions. Even when this fact can be compensated with the use of simulations, these should not be too different to the analytic versions if we want to identify where the possible variations arise.

From a population level, Chapter 4 introduces a quorum-sensing model in which interactions between naive, IL-2 producer (effector) cells, memory and regulatory $CD4^+$ cells take place together. For this purpose, some experimental data is used to try to stablish a hierarchy in the reactions involved in the model. As hypothesis for selecting a better model which explains how regulatory cells inhibit effector cells proliferation, we study one pathway in which these effector cells would become memory by T reg cells intervention, and another one in which this intervention would induce effector cells apoptosis. Results from Bayesian analysis with different approaches conclude that, in spite of the robustness of the model, no preference pathway is supported by the model comparison. Moreover, the efficiency of such models is also discussed for the different approaches and so the

identification of those parameters which perturbations might affect more the output of these models.

Results suggest that certain reactions, such as the differentiation/death pathway of IL-2 producers or the IL-2 driven proliferation of regulatory cells, mainly drive the output of the systems and that also these parameters are those in which the learning might be affected by the kind of prior distribution chosen. A complete study of these Bayesian techniques together with a statistical analysis allow to understand the main dynamics of this quorum-sensing mechanism. However, this approach still brings some limitations. In first place, the problems of tracking with accuracy the influence that a short and noisy data has in the output. On the other hand, the fact of tracking together two subpopulations experimentally, when the models split them, suggest that restrictions of the model replicating data might be due to this fact.

Finally, this quorum-sensing mechanism is studied in more detail to analyse tumour prognosis. For this purpose, only regulatory T cells and effector $CD8^+$ cells are taken into account. By means of matrix-analytic methods and a deterministic approach, two different models were compared to elucidate some conditions, under which the cancer might have a poor or a better prognosis. Taking together the stochastic and the deterministic approach, our models analyse how this system might reach each steady state and, with more accuracy, the probability of ending up in any of these areas of prognosis, and so under which parameter regimes, the existence and uniqueness of extinction is guaranteed.

Regarding the limitations of this analysis of tumour prognosis, we would mention that given the non-linear terms of our models, the parameter regimes for which we can verify the existence and uniqueness of solution are quite restricted. However, the values found in literature for these parameters seem to fit well in those regimes. On the other hand, the stability of the steady states for the Fas/FasL model, does not allow to work with the tolerance case from an analytic point of view. This does not allow to compare the if the tolerance state can be reached under the same parameter regimes that one of the other states, varying initial conditions.

Future work that could be done to complete the study developed in some of the chapters includes: for Chapter 2 and Chapter 3, taking into account the mobility of the molecules to quantify how this would affect the output of the systems. In addition to this, it would have been very interesting to model TCR + CTLA-4^+ dynamics for Chapter 3 for which, the possibility of using experimental data would have been great to include to carry out

Bayesian analysis. For Chapter 4, the fact that memory cells and naive cells were included together in the data, but separated in the models (and that these models cannot always reproduce the data) motivates to implement a different version of the model or, preferably, manage to obtain pieces of data that split these two species. Finally, for Chapter 5, we are trying to include some clinical data for completing the analysis and a different way of dividing *bad* and *better prognosis* regions that could perhaps be more adequate depending of different scenarios experimentally observed.

Appendices

A representative selection of codes have been included in this appendices, with references to figures obtained as a result. At the same time, throughout the thesis, an indication of the correspondent code included here is made. For the sake of the space, those lines starting with "]" in the codes are a continuation of the previous line.

A Python code for mean time ± standard deviation to reach a threshold B of complexes on the cell surface. Chapter 2.

```
# For Figure 2.3 (bottom), blue curve.

import random, math
import numpy as np
from numpy import linalg

#Matrix definition:

def Build_ApkkMinus1z(ApkkMinus1z,p,k,z):
        for j in range(nmax-k+1):
                for i in range(j*(2*nmax-2*k-j+3)/2,(j+1)*(2*nmax-2*k-(j+1)+3)/2):
                        if i<(j+1)*(2*nmax-2*k-(j+1)+3)/2-1:
                                Airk=v0+v1*((k+(i-j*(2*nmax-2*k-j+3)/2))**3)
]/((k+(i-j*(2*nmax-2*k-j+3)/2))**3+Kc**3)+ks*j+(ke+delta)
]*(i-j*(2*nmax-2*k-j+3)/2)+kon*j*nl+(koff+gamma)*k
                        else:
                                Airk=ks*j+(ke+delta)*(i-j*(2*nmax-2*k-j+3)/2)
]+kon*j*nl+(koff+gamma)*k
                        ApkkMinus1z[i,j*(2*nmax-2*(k-1)-j+3)/2+i-j*(2*nmax-2*k-j+3)/2+1]
]=((float)(((-1)**p)*math.factorial(p)))/((float)(Airk**p))*((float)(gamma*k))/((float)(z+Airk))
                        ApkkMinus1z[i,(j+1)*(2*nmax-2*(k-1)-(j+1)+3)/2+i-j*(2*nmax-2*k-j+3)/2]
]=((float)(((-1)**p)*math.factorial(p)))/((float)(Airk**p))*((float)(koff*k))/((float)(z+Airk))

def Build_Apkkz(Apkkz,p,k,z):
```

```
        j=0
        for i in range(j*(2*nmax-2*k-j+3)/2,(j+1)*(2*nmax-2*k-(j+1)+3)/2):
                if i<(j+1)*(2*nmax-2*k-(j+1)+3)/2-1:
                        Airk=v0+v1*((k+(i-j*(2*nmax-2*k-j+3)/2))**3)
]/((k+(i-j*(2*nmax-2*k-j+3)/2))**3+Kc**3)+ks*j+(ke+delta)
]*(i-j*(2*nmax-2*k-j+3)/2)+kon*j*nl+(koff+gamma)*k
                else:
                        Airk=ks*j+(ke+delta)*(i-j*(2*nmax-2*k-j+3)/2)
]+kon*j*nl+(koff+gamma)*k
                Apkkz[i,i-1]=((float)(((-1)**p)*math.factorial(p)))
]/((float)(Airk**p))*((float)(ke*(i-j*(2*nmax-2*k-j+3)/2)))/((float)(z+Airk))
                if i<(j+1)*(2*nmax-2*k-(j+1)+3)/2-1:
                        Apkkz[i,i+(nmax-k-j+1)]=((float)(((-1)**p)*math.factorial(p)))
]/((float)(Airk**p))*((float)(v0+v1*((k+(i-j*(2*nmax-2*k-j+3)/2))**3)
]/((k+(i-j*(2*nmax-2*k-j+3)/2))**3+Kc**3)))/((float)(z+Airk))
                Apkkz[i,i+(nmax-k-j+1)-1]=((float)(((-1)**p)*math.factorial(p)))
]/((float)(Airk**p))*((float)(delta*(i-j*(2*nmax-2*k-j+3)/2)))/((float)(z+Airk))
        for j in range(1,nmax-k):
                for i in range(j*(2*nmax-2*k-j+3)/2,(j+1)*(2*nmax-2*k-(j+1)+3)/2):
                        if i<(j+1)*(2*nmax-2*k-(j+1)+3)/2-1:
                                Airk=v0+v1*((k+(i-j*(2*nmax-2*k-j+3)/2))**3)
]/((k+(i-j*(2*nmax-2*k-j+3)/2))**3+Kc**3)+ks*j+(ke+delta)*(i-j*(2*nmax-2*k-j+3)/2)
]+kon*j*nl+(koff+gamma)*k
                        else:
                                Airk=ks*j+(ke+delta)*(i-j*(2*nmax-2*k-j+3)/2)
]+kon*j*nl+(koff+gamma)*k
                        Apkkz[i,i-(nmax-k-(j-1)+1)]=((float)(((-1)**p)*math.factorial(p)))
]/((float)(Airk**p))*((float)(ks*j))/((float)(z+Airk))
                        Apkkz[i,i-1]=((float)(((-1)**p)*math.factorial(p)))
]/((float)(Airk**p))*((float)(ke*(i-j*(2*nmax-2*k-j+3)/2)))/((float)(z+Airk))
                        if i<(j+1)*(2*nmax-2*k-(j+1)+3)/2-1:
                                Apkkz[i,i+(nmax-k-j+1)]=((float)(((-1)**p)*math.factorial(p)))
]/((float)(Airk**p))*((float)(v0+v1*((k+(i-j*(2*nmax-2*k-j+3)/2))**3)
]/((k+(i-j*(2*nmax-2*k-j+3)/2))**3+Kc**3)))/((float)(z+Airk))
                        Apkkz[i,i+(nmax-k-j+1)-1]=((float)(((-1)**p)*math.factorial(p)))
]/((float)(Airk**p))*((float)(delta*(i-j*(2*nmax-2*k-j+3)/2)))/((float)(z+Airk))
        j=nmax-k
        for i in range(j*(2*nmax-2*k-j+3)/2,(j+1)*(2*nmax-2*k-(j+1)+3)/2):
                if i<(j+1)*(2*nmax-2*k-(j+1)+3)/2-1:
                        Airk=v0+v1*((k+(i-j*(2*nmax-2*k-j+3)/2))**3)
]/((k+(i-j*(2*nmax-2*k-j+3)/2))**3+Kc**3)+ks*j+(ke+delta)*(i-j*(2*nmax-2*k-j+3)/2)
]+kon*j*nl+(koff+gamma)*k
                else:
                        Airk=ks*j+(ke+delta)*(i-j*(2*nmax-2*k-j+3)/2)+kon*j*nl+(koff+gamma)*k
                Apkkz[i,i-(nmax-k-(j-1)+1)]=((float)(((-1)**p)*math.factorial(p)))
]/((float)(Airk**p))*((float)(ks*j))/((float)(z+Airk))
                Apkkz[i,i-1]=((float)(((-1)**p)*math.factorial(p)))
]/((float)(Airk**p))*((float)(ke*(i-j*(2*nmax-2*k-j+3)/2)))/((float)(z+Airk))

def Build_ApkkPlus1z(ApkkPlus1z,p,k,z):
```

```
        for j in range(1,nmax-k+1):
                for i in range(j*(2*nmax-2*k-j+3)/2,(j+1)*(2*nmax-2*k-(j+1)+3)/2):
                        if i<(j+1)*(2*nmax-2*k-(j+1)+3)/2-1:
                                Airk=v0+v1*((k+(i-j*(2*nmax-2*k-j+3)/2))**3)
]/((k+(i-j*(2*nmax-2*k-j+3)/2))**3+Kc**3)+ks*j+(ke+delta)*(i-j*(2*nmax-2*k-j+3)/2)
]+kon*j*nl+(koff+gamma)*k
                        else:
                                Airk=ks*j+(ke+delta)*(i-j*(2*nmax-2*k-j+3)/2)
]+kon*j*nl+(koff+gamma)*k
                        ApkkPlus1z[i,(j-1)*(2*nmax-2*(k+1)-(j-1)+3)/2+i-j*(2*nmax-2*k-j+3)/2]
]=((float)(((-1)**p)*math.factorial(p)))/((float)(Airk**p))
]*((float)(kon*j*nl))/((float)(z+Airk))


values=[0]
values2=[0]
values3=[0]
jumps=[0]
nl=50

B=1
T=0
kmax=1000
while B<34:
        nmax=90
        nr=15
        Kc=10
        v0=0.1667
        v1=1.3333
        kon=0.001029
        koff=0.0138
        delta=0.15
        ke=0.0833
        ks=0.0107
        gamma=0.0283
        z=0
        l=2
        Hrkz=[np.asmatrix(np.zeros((((nmax-k+1)*(nmax-k+2))/2,((nmax-k+1)*(nmax-k+2))/2)))
] for k in range(B)]
        invHrkz=[np.asmatrix(np.zeros((((nmax-k+1)*(nmax-k+2))/2,((nmax-k+1)*(nmax-k+2))/2)))
] for k in range(B)]
        Jjrkz=[[np.asmatrix(np.zeros((((nmax-k+1)*(nmax-k+2))/2,1))) for k in range(B)]
]for j in range(l+1)]
        grkz=[np.asmatrix(np.zeros((((nmax-k+1)*(nmax-k+2))/2,1))) for k in range(B)]
        mjrk=[[np.asmatrix(np.zeros((((nmax-k+1)*(nmax-k+2))/2,1))) for k in range(B)]
]for j in range(l+1)]
        mtildejrk=[[np.asmatrix(np.zeros((((nmax-k+1)*(nmax-k+2))/2,1))) for k in range(B)]
]for j in range(l+1)]
        s=0
        k=0
```

```
        Apkkz=np.asmatrix(np.zeros((((nmax-k+1)*(nmax-k+2))/2,((nmax-k+1)*(nmax-k+2))/2)))
        Build_Apkkz(Apkkz,s,k,z)
        Hrkz[k]=np.asmatrix(np.identity(((nmax-k+1)*(nmax-k+2))/2))-Apkkz
        del Apkkz
        invHrkz[k]=Hrkz[k].I
        Jjrkz[s][k]=np.matrix(np.zeros((nmax-k+1,1)))
        for k in range(1,B):
                #print "k",k
                Apkkz=np.asmatrix(np.zeros((((nmax-k+1)*(nmax-k+2))/2,
](nmax-k+1)*(nmax-k+2))/2)))
                Build_Apkkz(Apkkz,s,k,z)
                ApkkMinus1z=np.asmatrix(np.zeros((((nmax-k+1)*(nmax-k+2))/2,
](nmax-k+2)*(nmax-k+3))/2)))
                Build_ApkkMinus1z(ApkkMinus1z,s,k,z)
                ApkkPlus1z=np.asmatrix(np.zeros((((nmax-k+2)*(nmax-k+3))/2,
](nmax-k+1)*(nmax-k+2))/2)))
                Build_ApkkPlus1z(ApkkPlus1z,s,k-1,z)
                Hrkz[k]=np.asmatrix(np.identity(((nmax-k+1)*(nmax-k+2))/2))
]-Apkkz-ApkkMinus1z*invHrkz[k-1]*ApkkPlus1z
                invHrkz[k]=Hrkz[k].I
                del Apkkz,ApkkMinus1z,ApkkPlus1z
        k=B-1
        ApkkPlus1z=np.asmatrix(np.zeros((((nmax-k+1)*(nmax-k+2))/2,((nmax-k)*(nmax-k+1))/2)))
        Build_ApkkPlus1z(ApkkPlus1z,s,k,z)
        ek=np.asmatrix(np.ones((((nmax-k)*(nmax-k+1))/2,1)))
        grkz[k]=invHrkz[k]*ApkkPlus1z*ek
        mjrk[s][k]=grkz[k]
        del ApkkPlus1z
        for k in reversed(range(B-1)):
                #print "kreverse",k
                ApkkPlus1z=np.matrix(np.zeros((((nmax-k+1)*(nmax-k+2))/2,
](nmax-k)*(nmax-k+1))/2)))
                Build_ApkkPlus1z(ApkkPlus1z,s,k,z)
                grkz[k]=invHrkz[k]*ApkkPlus1z*grkz[k+1]
                del ApkkPlus1z
                mjrk[s][k]=grkz[k]
        for k in range(B):
                for j in range(nmax-k+1):
                        for i in range(j*(2*nmax-2*k-j+3)/2,(j+1)*(2*nmax-2*k-(j+1)+3)/2):
                                if i<(j+1)*(2*nmax-2*k-(j+1)+3)/2-1:
                                        Airk=v0+v1*((k+(i-j*(2*nmax-2*k-j+3)/2))**3)
](k+(i-j*(2*nmax-2*k-j+3)/2))**3+Kc**3)+ks*j+(ke+delta)
]*(i-j*(2*nmax-2*k-j+3)/2)+kon*j*nl+(koff+gamma)*k
                                else:
                                        Airk=ks*j+(ke+delta)*(i-j*(2*nmax-2*k-j+3)/2)
]+kon*j*nl+(koff+gamma)*k
                                mtildejrk[s][k][i,0]=mjrk[s][k][i,0]/((float)(Airk))
        for s in range(1,l+1):
                #print "s",s
                k=0
```

```
                Jjrkz[s][k]=s*mtildejrk[s-1][k]
                for k in range(1,B):
                        ApkkMinus1z=np.asmatrix(np.zeros((((nmax-k+1)*(nmax-k+2))/2,
](nmax-k+2)*(nmax-k+3))/2)))
                        Build_ApkkMinus1z(ApkkMinus1z,0,k,z)
                        Jjrkz[s][k]=ApkkMinus1z*invHrkz[k-1]*Jjrkz[s][k-1]+s*mtildejrk[s-1][k]
                k=B-1
                mjrk[s][k]=invHrkz[k]*Jjrkz[s][k]
                for k in reversed(range(B-1)):
                        ApkkPlus1z=np.matrix(np.zeros((((nmax-k+1)*(nmax-k+2))/2
],((nmax-k)*(nmax-k+1))/2)))
                        Build_ApkkPlus1z(ApkkPlus1z,0,k,z)
                        mjrk[s][k]=invHrkz[k]*(Jjrkz[s][k]+ApkkPlus1z*mjrk[s][k+1])
                for k in range(B):
                        for j in range(nmax-k+1):
                                for i in range(j*(2*nmax-2*k-j+3)/2,(j+1)*(2*nmax-2*k-(j+1)+3)/2):
                                        if i<(j+1)*(2*nmax-2*k-(j+1)+3)/2-1:
                                                Airk=v0+v1*((k+(i-j*(2*nmax-2*k-j+3)/2))**3)
]/((k+(i-j*(2*nmax-2*k-j+3)/2))**3+Kc**3)+ks*j+(ke+delta)*(i-j*(2*nmax-2*k-j+3)/2)
]+kon*j*nl+(koff+gamma)*k
                                        else:
                                                Airk=ks*j+(ke+delta)*(i-j*(2*nmax-2*k-j+3)/2)
]+kon*j*nl+(koff+gamma)*k
                                        mtildejrk[s][k][i,0]=mjrk[s][k][i,0]/((float)(Airk))
        jumps.append(B)
        values.append(mjrk[1][0][nr*(2*nmax-2*0-nr+3)/2,0])
        values2.append(mjrk[1][0][nr*(2*nmax-2*0-nr+3)/2,0]+math.sqrt(mjrk[2][0]
][nr*(2*nmax-2*0-nr+3)/2,0]-mjrk[1][0][nr*(2*nmax-2*0-nr+3)/2,0]
]*mjrk[1][0][nr*(2*nmax-2*0-nr+3)/2,0]))
        values3.append(mjrk[1][0][nr*(2*nmax-2*0-nr+3)/2,0]-math.sqrt(mjrk[2][0]
][nr*(2*nmax-2*0-nr+3)/2,0]-mjrk[1][0][nr*(2*nmax-2*0-nr+3)/2,0]
]*mjrk[1][0][nr*(2*nmax-2*0-nr+3)/2,0]))
        print B
        B += 1
        print mjrk[1][0][nr*(2*nmax-2*0-nr+3)/2,0]  # (Figure 2.3 (bottom), blue curve.)
        print values2[B-1]
        print values3[B-1]
```

B Python code for Probability of reaching poor and beeter prognosis. Chapter 5.

```
#Histograms for Figure 5.5

import matplotlib.pyplot as plt
import random, math
import numpy as np
from numpy import linalg
import collections
```

```
eps=1e-7
def J(k1,k2,k):
        return int(math.ceil(((float)(k2*k))/((float)(k2+1))-eps))
]-int(((float)(k1*k))/((float)(k1+1))+eps)-1
def J2(k1,k2,k):
        return int(math.ceil(((float)(k2*(k+0.99)))/((float)(k2+1))-eps))
]-int(((float)(k1*(k+0.99)))/((float)(k1+1))+eps)-1

def Pos(k,nE):
        return int(math.ceil(((float)(k2*k))/((float)(k2+1))-eps))-nE

def Delta(nE,nR):
        return (muE+nuE*nE+xi*nR+lE+alE*nE)*nE+(muR+nuR*nR+lR+alR*nE)*nR

def DeltaTruncated(nE,nR):
        return (muE+nuE*nE+xi*nR)*nE+(muR+nuR*nR)*nR

def Build_AkkMinus1k1k2(AkkMinus1k1k2,k,k1,k2):
        for i in range(1,J(k1,k2,k)+1):
                nE=int(math.ceil(((float)(k2*k))/((float)(k2+1))-eps))-i
                nR=int(((float)(k))/((float)(k2+1))+eps)+i
                j=Pos(k-1,nE-1)
                if j>=1 and j<J(k1,k2,k-1)+1:
                        AkkMinus1k1k2[i-1,j-1]=(muE+nuE*nE+xi*nR)*nE/(Delta(nE,nR))
                j=Pos(k-1,nE)
                if j>=1 and j<J(k1,k2,k-1)+1:
                        AkkMinus1k1k2[i-1,j-1]=(muR+nuR*nR)*nR/(Delta(nE,nR))

def Build_AkkMinus1k1k2Truncated(AkkMinus1k1k2,k,k1,k2):
        for i in range(1,J(k1,k2,k)+1):
                nE=int(math.ceil(((float)(k2*k))/((float)(k2+1))-eps))-i
                nR=int(((float)(k))/((float)(k2+1))+eps)+i
                j=Pos(k-1,nE-1)
                if j>=1 and j<J(k1,k2,k-1)+1:
                        AkkMinus1k1k2[i-1,j-1]=(muE+nuE*nE+xi*nR)*nE/(DeltaTruncated(nE,nR))
                j=Pos(k-1,nE)
                if j>=1 and j<J(k1,k2,k-1)+1:
                        AkkMinus1k1k2[i-1,j-1]=(muR+nuR*nR)*nR/(DeltaTruncated(nE,nR))

def Build_AkkPlus1k1k2(AkkPlus1k1k2,k,k1,k2):
        for i in range(1,J(k1,k2,k)+1):
                nE=int(math.ceil(((float)(k2*k))/((float)(k2+1))-eps))-i
                nR=int(((float)(k))/((float)(k2+1))+eps)+i
                j=Pos(k+1,nE+1)
                if j>=1 and j<J(k1,k2,k+1)+1:
                        AkkPlus1k1k2[i-1,j-1]=(lE+alE*nE)*nE/(Delta(nE,nR))
                j=Pos(k+1,nE)
                if j>=1 and j<J(k1,k2,k+1)+1:
                        AkkPlus1k1k2[i-1,j-1]=(lR+alR*nE)*nR/(Delta(nE,nR))
```

```
def Build_bkk1k2(bkk1k2,k,k1,k2):
        for i in range(1,J(k1,k2,k)+1):
                nE=int(math.ceil(((float)(k2*k))/((float)(k2+1))-eps))-i
                nR=int(((float)(k))/((float)(k2+1))+eps)+i
                if ((float)(nE))/((float)(nR+1))<=k1:
                        bkk1k2[i-1,0]=(lR+alR*nE)*nR/(Delta(nE,nR))
                if ((float)(nE-1))/((float)(nR))<=k1:
                        bkk1k2[i-1,0]+=(muE+nuE*nE+xi*nR)*nE/(Delta(nE,nR))

def Build_bkk1k2Truncated(bkk1k2,k,k1,k2):
        for i in range(1,J(k1,k2,k)+1):
                nE=int(math.ceil(((float)(k2*k))/((float)(k2+1))-eps))-i
                nR=int(((float)(k))/((float)(k2+1))+eps)+i
                if ((float)(nE))/((float)(nR+1))<=k1:
                        bkk1k2[i-1,0]=(lR+alR*nE)*nR/(DeltaTruncated(nE,nR))
                if ((float)(nE-1))/((float)(nR))<=k1:
                        bkk1k2[i-1,0]+=(muE+nuE*nE+xi*nR)*nE/(DeltaTruncated(nE,nR))
def Build_bkk1k2_poor(bkk1k2,k,k1,k2,j):
        for i in range(1,J(k1,k2,k)+1):
                nE=int(math.ceil(((float)(k2*k))/((float)(k2+1))-eps))-i
                nR=int(((float)(k))/((float)(k2+1))+eps)+i
                if nE==int(((float)(k1*j))/((float)(k1+1)))
]and nR+1==int(math.ceil(((float)(j))/((float)(k1+1))-eps)):
                        bkk1k2[i-1,0]=(lR+alR*nE)*nR/(Delta(nE,nR))
                if nE-1==int(((float)(k1*j))/((float)(k1+1)))
]and nR==int(math.ceil(((float)(j))/((float)(k1+1))-eps)):
                        bkk1k2[i-1,0]+=(muE+nuE*nE+xi*nR)*nE/(Delta(nE,nR))

def Build_bkk1k2Truncated_poor(bkk1k2,k,k1,k2,j):
        for i in range(1,J(k1,k2,k)+1):
                nE=int(math.ceil(((float)(k2*k))/((float)(k2+1))-eps))-i
                nR=int(((float)(k))/((float)(k2+1))+eps)+i
                if nE-1==int(((float)(k1*j))/((float)(k1+1)))
]and nR==int(math.ceil(((float)(j))/((float)(k1+1))-eps)):
                        bkk1k2[i-1,0]+=(muE+nuE*nE+xi*nR)*nE/(DeltaTruncated(nE,nR))

def Build_bkk1k2_better(bkk1k2,k,k1,k2,j):
        for i in range(1,J(k1,k2,k)+1):
                nE=int(math.ceil(((float)(k2*k))/((float)(k2+1))-eps))-i
                nR=int(((float)(k))/((float)(k2+1))+eps)+i
                if nE==int(math.ceil(((float)(k2*j))/((float)(k2+1))-eps))
]and nR-1==int(((float)(j))/((float)(k2+1))+eps):
                        bkk1k2[i-1,0]=(muR+nuR*nR)*nR/(Delta(nE,nR))
                if nE+1==int(math.ceil(((float)(k2*j))/((float)(k2+1))-eps))
]and nR==int(((float)(j))/((float)(k2+1))+eps):
                        bkk1k2[i-1,0]+=(lE+alE*nE)*nE/(Delta(nE,nR))

def Build_bkk1k2Truncated_better(bkk1k2,k,k1,k2,j):
        for i in range(1,J(k1,k2,k)+1):
```

```
                    nE=int(math.ceil(((float)(k2*k))/((float)(k2+1))-eps))-i
                    nR=int(((float)(k))/((float)(k2+1))+eps)+i
                    if nE==int(math.ceil(((float)(k2*j))/((float)(k2+1))-eps))
]and nR-1==int(((float)(j))/((float)(k2+1))+eps):
                                bkk1k2[i-1,0]=(muR+nuR*nR)*nR/(DeltaTruncated(nE,nR))

#Parameter values:
NE=50
NR=25
k1=1
k2=10
lE=0.015
lR=0.01
nuE=0.0001
nuR=0.0003
alE=0.00005
alR=0.000075
muE=0.02
muR=0.02
xi=0.0005


Kepsilon=NE+NR+1
probability=1
Epsilon=0.02

# Maximum level for truncation:

while probability>Epsilon:
        Kepsilon+=1
        Hk1k2=[np.matrix(np.zeros((J2(k1,k2,k),J2(k1,k2,k)))) for k in range(2,Kepsilon+1)]
        invHk1k2=[np.matrix(np.zeros((J2(k1,k2,k),J2(k1,k2,k)))) for k in range(2,Kepsilon+1)]
        pmaxk1k2=[np.matrix(np.zeros((J2(k1,k2,k),1))) for k in range(2,Kepsilon+1)]

        Hk1k2[0]=np.asmatrix(np.eye((3-2)))
        invHk1k2[0]=Hk1k2[0].I
        for k in range(3,Kepsilon+1):
                AkkMinus1k1k2=np.asmatrix(np.zeros((J2(k1,k2,k),J2(k1,k2,k-1))))
                Build_AkkMinus1k1k2(AkkMinus1k1k2,k,k1,k2)
                AkkPlus1k1k2=np.asmatrix(np.zeros((J2(k1,k2,k-1),J2(k1,k2,k))))
                Build_AkkPlus1k1k2(AkkPlus1k1k2,k-1,k1,k2)
                Hk1k2[k-2]=np.asmatrix(np.eye((J2(k1,k2,k))))-
]AkkMinus1k1k2*invHk1k2[k-3]*AkkPlus1k1k2
                invHk1k2[k-2]=Hk1k2[k-2].I
        k=Kepsilon
        AkkPlus1k1k2=np.asmatrix(np.zeros((J2(k1,k2,k),J2(k1,k2,k+1))))
        Build_AkkPlus1k1k2(AkkPlus1k1k2,k,k1,k2)
        pmaxk1k2[k-2]=invHk1k2[k-2]*AkkPlus1k1k2*np.asmatrix(np.ones((J2(k1,k2,Kepsilon+1),1)))
        for k in reversed(range(2,Kepsilon)):
                AkkPlus1k1k2=np.asmatrix(np.zeros((J2(k1,k2,k),J2(k1,k2,k+1))))
```

```
                Build_AkkPlus1k1k2(AkkPlus1k1k2,k,k1,k2)
                pmaxk1k2[k-2]=invHk1k2[k-2]*AkkPlus1k1k2*pmaxk1k2[k-1]
        probability=pmaxk1k2[NE+NR-2][Pos(NE+NR,NE)-1,0]
        print(Kepsilon,probability)

print("Kepsilon: ", Kepsilon)
print("Probability of exceeding the Kepsilon level: ",probability)


# Probabilities of Poor and Better prognosis

pk1k2=[np.matrix(np.zeros((J2(k1,k2,k),1))) for k in range(2,Kepsilon+1)]
Pk1k2=[np.matrix(np.zeros((J2(k1,k2,k),J2(k1,k2,k)))) for k in range(2,Kepsilon+1)]

for k in range(Kepsilon,Kepsilon+1):
        AkkMinus1k1k2=np.asmatrix(np.zeros((J2(k1,k2,k),J2(k1,k2,k-1))))
        Build_AkkMinus1k1k2Truncated(AkkMinus1k1k2,k,k1,k2)
        AkkPlus1k1k2=np.asmatrix(np.zeros((J2(k1,k2,k-1),J2(k1,k2,k))))
        Build_AkkPlus1k1k2(AkkPlus1k1k2,k-1,k1,k2)
        Hk1k2[k-2]=np.asmatrix(np.eye((J2(k1,k2,k)))-AkkMinus1k1k2*invHk1k2[k-3]*AkkPlus1k1k2
        invHk1k2[k-2]=Hk1k2[k-2].I

k=2
Build_bkk1k2(Pk1k2[k-2],k,k1,k2)
for k in range(3,Kepsilon+1):
        AkkMinus1k1k2=np.asmatrix(np.zeros((J2(k1,k2,k),J2(k1,k2,k-1))))
        if k==Kepsilon:
                Build_AkkMinus1k1k2Truncated(AkkMinus1k1k2,k,k1,k2)
        else:
                Build_AkkMinus1k1k2(AkkMinus1k1k2,k,k1,k2)
        bkk1k2=np.asmatrix(np.zeros((J2(k1,k2,k),1)))
        if k==Kepsilon:
                Build_bkk1k2Truncated(bkk1k2,k,k1,k2)
        else:
                Build_bkk1k2(bkk1k2,k,k1,k2)
        Pk1k2[k-2]=AkkMinus1k1k2*invHk1k2[k-3]*Pk1k2[k-3]+bkk1k2

k=Kepsilon
pk1k2[k-2]=invHk1k2[k-2]*Pk1k2[k-2]
for k in reversed(range(2,Kepsilon)):
        AkkPlus1k1k2=np.asmatrix(np.zeros((J2(k1,k2,k),J2(k1,k2,k+1))))
        Build_AkkPlus1k1k2(AkkPlus1k1k2,k,k1,k2)
        pk1k2[k-2]=invHk1k2[k-2]*(AkkPlus1k1k2*pk1k2[k-1]+Pk1k2[k-2])


print("Probability of reaxing Poor Prognosis Region: ", pk1k2[NE+NR-2][Pos(NE+NR,NE)-1,0])
print("Probability of reaxing Better Prognosis Region: ", 1-pk1k2[NE+NR-2][Pos(NE+NR,NE)-1,0])

pk1k2poor=[[np.matrix(np.zeros((J2(k1,k2,k),1))) for k in range(2,Kepsilon+1)]
]for j in range(1,Kepsilon+1)]
```

```
histogramx=[]
histogramy=[]
histogram2x=[]
histogram2y=[]

#Probability of entry through each state (nE,nR):

check1=0
for j in range(1,Kepsilon+1):
        Pk1k2=[np.matrix(np.zeros((J2(k1,k2,k),J2(k1,k2,k)))) for k in range(2,Kepsilon+1)]
        k=2
        Build_bkk1k2_poor(Pk1k2[k-2],k,k1,k2,j)
        for k in range(3,Kepsilon+1):
                AkkMinus1k1k2=np.asmatrix(np.zeros((J2(k1,k2,k),J2(k1,k2,k-1))))
                if k==Kepsilon:
                        Build_AkkMinus1k1k2Truncated(AkkMinus1k1k2,k,k1,k2)
                else:
                        Build_AkkMinus1k1k2(AkkMinus1k1k2,k,k1,k2)
                bkk1k2=np.asmatrix(np.zeros((J2(k1,k2,k),1)))
                if k==Kepsilon:
                        Build_bkk1k2Truncated_poor(bkk1k2,k,k1,k2,j)
                else:
                        Build_bkk1k2_poor(bkk1k2,k,k1,k2,j)
                Pk1k2[k-2]=AkkMinus1k1k2*invHk1k2[k-3]*Pk1k2[k-3]+bkk1k2
        k=Kepsilon
        pk1k2poor[j-1][k-2]=invHk1k2[k-2]*Pk1k2[k-2]
        for k in reversed(range(2,Kepsilon)):
                AkkPlus1k1k2=np.asmatrix(np.zeros((J2(k1,k2,k),J2(k1,k2,k+1))))
                Build_AkkPlus1k1k2(AkkPlus1k1k2,k,k1,k2)
                pk1k2poor[j-1][k-2]=invHk1k2[k-2]*(AkkPlus1k1k2*pk1k2poor[j-1][k-1]+Pk1k2[k-2])
        if pk1k2poor[j-1][NE+NR-2][Pos(NE+NR,NE)-1,0]>0:
                print("(",int(((float)(k1*j))/((float)(k1+1))+eps), ",",
]int(math.ceil(((float)(j))/((float)(k1+1))-eps)),"),",pk1k2poor[j-1][NE+NR-2][Pos(NE+NR,NE)-1,0])
                histogramx=np.append(histogramx,str("(")+str(int(((float)(k1*j))/
](((float)(k1+1))+eps))+str(",")+str(int(math.ceil(((float)(j))/((float)(k1+1))-eps)))+str(")"))
                histogram2x=np.append(histogram2x,str("(")+str(int(((float)(k1*j))/
](((float)(k1+1))+eps))+str(",")+str(int(math.ceil(((float)(j))/((float)(k1+1))-eps)))+str(")"))
                histogramy=np.append(histogramy,0)
                histogram2y=np.append(histogram2y,pk1k2poor[j-1][NE+NR-2][Pos(NE+NR,NE)-1,0])
        check1+=pk1k2poor[j-1][NE+NR-2][Pos(NE+NR,NE)-1,0]
print("Total Poor Prognosis Region AGAIN: ", check1)
pk1k2better=[[np.matrix(np.zeros((J2(k1,k2,k),1))) for k in range(2,Kepsilon+1)]
]for j in range(1,Kepsilon+1)]
check2=0

for j in range(1,Kepsilon+1):
        Pk1k2=[np.matrix(np.zeros((J2(k1,k2,k),J2(k1,k2,k)))) for k in range(2,Kepsilon+1)]
        k=2
        Build_bkk1k2_better(Pk1k2[k-2],k,k1,k2,j)
        for k in range(3,Kepsilon+1):
```

```
                    AkkMinus1k1k2=np.asmatrix(np.zeros((J2(k1,k2,k),J2(k1,k2,k-1))))
                    if k==Kepsilon:
                            Build_AkkMinus1k1k2Truncated(AkkMinus1k1k2,k,k1,k2)
                    else:
                            Build_AkkMinus1k1k2(AkkMinus1k1k2,k,k1,k2)
                    bkk1k2=np.asmatrix(np.zeros((J2(k1,k2,k),1)))
                    if k==Kepsilon:
                            Build_bkk1k2Truncated_better(bkk1k2,k,k1,k2,j)
                    else:
                            Build_bkk1k2_better(bkk1k2,k,k1,k2,j)
                    Pk1k2[k-2]=AkkMinus1k1k2*invHk1k2[k-3]*Pk1k2[k-3]+bkk1k2
            k=Kepsilon
            pk1k2better[j-1][k-2]=invHk1k2[k-2]*Pk1k2[k-2]
            for k in reversed(range(2,Kepsilon)):
                    AkkPlus1k1k2=np.asmatrix(np.zeros((J2(k1,k2,k),J2(k1,k2,k+1))))
                    Build_AkkPlus1k1k2(AkkPlus1k1k2,k,k1,k2)
                    pk1k2better[j-1][k-2]=invHk1k2[k-2]*(AkkPlus1k1k2*pk1k2better[j-1][k-1]+Pk1k2[k-2])
            if pk1k2better[j-1][NE+NR-2][Pos(NE+NR,NE)-1,0]>0:
                    print("(",int(math.ceil(((float)(k2*j))/((float)(k2+1))-eps)), ",",
]int(((float)(j))/((float)(k2+1))+eps),"),", pk1k2better[j-1][NE+NR-2][Pos(NE+NR,NE)-1,0])
                    histogramx=np.append(histogramx,str("(")+str(int(math.ceil(((float)(k2*j))/
](((float)(k2+1))-eps)))+str(",")+str(int(((float)(j))/((float)(k2+1))+eps))+str(")"))
                    histogramy=np.append(histogramy,pk1k2better[j-1][NE+NR-2][Pos(NE+NR,NE)-1,0])
            check2+=pk1k2better[j-1][NE+NR-2][Pos(NE+NR,NE)-1,0]
print("Total Better Prognosis Region AGAIN: ", check2)

# Do both add up to 1?:

print(check1+check2)

integers=[i for i in range(len(histogramx))]
integers2=[i for i in range(len(histogram2x))]
poor=round(check1,4)
better=round(check2,4)

plt.bar(integers, histogramy,width=0.9,color='b',align='center',label='Better prognosis')
plt.bar(integers2, list(reversed(histogram2y)),width=0.9,color='red',
]align='center',label='Poor prognosis')

plt.xticks(fontsize=9,rotation=70)
plt.ylim((0,0.14))

histogramnew=[]
histogramnew2=[]

for i in range(len(integers2)):
        histogramnew=np.append(histogramnew,histogramx[i])
for i in range((len(integers)-len(integers2))):
        histogramnew2=np.append(histogramnew2,histogramx[i+len(integers2)])
```

```
Finalhistogram=list(reversed(histogramnew))+list(histogramnew2)
plt.xticks(integers, Finalhistogram)

plt.xlim((-0.5,90))

plt.title(r'$(n^{(1)}_E,n^{(1)}_R)=(0,0)$ (extinction) for toy model', loc='left')
plt.title(r'$p_{(50,25)}^{1,10}=0.6544$', loc='center')
plt.title(r'$1-p_{(50,25)}^{1,10}=0.3456$', loc='right')
plt.legend(loc=1, prop={'size':12})
plt.show()
```

C Python code for time dynamics of effector and regulatory T cells. Chapter 5

```
#Time dynamics for Figure 5.4

import random, math
import numpy as np
from scipy.integrate import odeint
from scipy import integrate
import matplotlib.pyplot as plt

# Gillespie simulation:

alE=0.00005
alR=0.000075
lbE=0.015
lbR=0.01
muE=0.02
muR=0.02
xi=0.0005
nuE=0.0001
nuR=0.0003
L=0

k=0
k1=1
nEp=[0]
K1=0.25
while k1<2:
        while k<100:
                t = 0
                nE = 50
                l=0
                nR = 25
                jumps=[0]
                valuesnE=[0]
```

```
valuesnR=[0]
while t<1500:
        # nE + 1
        if nE>0:
                q1 = nE*nE*alE+nE*lbE
                u1 = random.random()
                e1 = -(float(1)/float(q1))*math.log(1-u1)
        else:
                e1 = float('inf')
        # nE - 1
        if nE>0:
                q2 = nE*nE*nuE+nE*muE+nE*nR*xi
                u2 = random.random()
                e2 = -(float(1)/float(q2))*math.log(1-u2)
        else:
                e2 = float('inf')
        # nR + 1
        if nR>0:
                q3 = nR*lbR+nE*nR*alR
                u3 = random.random()
                e3 = -(float(1)/float(q3))*math.log(1-u3)
        else:
                e3 = float('inf')
        # nR - 1
        if nR>0:
                q4 = nR*nR*nuR+nR*muR
                u4 = random.random()
                e4 = -(float(1)/float(q4))*math.log(1-u4)
        else:
                e4 = float('inf')
        minimum = e1
        i=1
        if minimum>e2:
                minimum=e2
                i=2
        if minimum>e3:
                minimum=e3
                i=3
        if minimum>e4:
                minimum=e4
                i=4
        if i==1:
                nE=nE+1
        if i==2:
                nE=nE-1
        if i==3:
                nR=nR+1
        if i==4:
                nR=nR-1
        t += minimum
```

```
                        jumps.append(float(float(t)/float(24.)))
                        valuesnE.append(nE)
                        valuesnR.append(nR)
                        if (nE<K1*nR) and L<1:
                                L=L+1
                                nEp=[nE,nR]
                        l=l+1
                k += 1
        print nEp
        plt.plot(jumps,valuesnE,color = 'blue',label = 'Teff (stochastic)')
        plt.plot(jumps,valuesnR,color = 'red',label = 'Treg (stochastic)')
        plt.xlabel('Time (days)')
        plt.ylabel('Cell numbers')
        plt.title(r'$SS_1$ (extinction) for toy model', loc='left')
        plt.title(r'$(n^{(1)}_E,n^{(1)}_R)=(0,0)$', loc='right')
        plt.axis([0, 1500/24., 0, 120])
        k1=k1+1

# Deterministic simulation:

#=====================================================
def eq(par,initial_cond,start_t,end_t,incr):
    #-time-grid-------------------------------
    t  = np.linspace(start_t, end_t,incr)
    #differential-eq-system-------------------
    def funct(y,t):
       NE=y[0]
       NR=y[1]
       muE,nuE,lbE,alE,xi,muR,nuR,lbR,alR,NE,NR
       # the model equations
       f0 = -muE*NE-nuE*NE*NE+lbE*NE+alE*NE*NE-xi*NE*NR
       f1 = -muR*NR-nuR*NR*NR+lbR*NR+alR*NE*NR
       return [f0, f1]
    #integrate--------------------------------
    ds = integrate.odeint(funct,initial_cond,t)
    return (ds[:,0],ds[:,1],t)
#=====================================================

#parameters

NE=50
NR=25
k1=1
k2=10
muE=0.02
muR=0.02

nuE=0.0001
nuR=0.0003
```

```
lbE=0.015
lbR=0.01

alE=0.00005
alR=0.000075

xi=0.0005
rates=(muE,nuE,lbE,alE,xi,muR,nuR,lbR,alR,NE,NR)
# initial conditions
S0 = NE
Z0 = NR
y0 = [S0, Z0]

F0,F1,T=eq(rates,y0,0,5000.,1000)

plt.plot(T/24.,F0,'--b',label = 'Teff (deterministic)')
plt.plot(T/24.,F1,'--r',label = 'Treg (deterministic)')
plt.legend(loc=1, prop={'size':12})

plt.show()
```

Bibliography

[1] J Abate and W Whitt, *Numerical inversion of laplace transforms of probability distributions*, ORSA Journal on computing **7** (1995), no. 1, 36–43.

[2] T Alarcón and KM Page, *Stochastic models of receptor oligomerization by bivalent ligand*, Journal of The Royal Society Interface **3** (2006), no. 9, 545–559.

[3] M-L Alegre, KA Frauwirth, and CB Thompson, *T-cell regulation by cd28 and ctla-4*, Nature Reviews Immunology **1** (2001), no. 3, 220–228.

[4] LJS Allen, *An introduction to stochastic processes with applications to biology*, CRC Press, 2010.

[5] ARM Almeida, IF Amado, J Reynolds, J Berges, G Lythe, C Molina-París, and AA Freitas, *Quorum-sensing in cd4 t cell homeostasis: a hypothesis and a model*, The Molecular Mechanisms of Regulatory T cell Immunosuppression (2012), 66.

[6] ARM Almeida, N Legrand, M Papiernik, and AA Freitas, *Homeostasis of peripheral cd4+ t cells: Il-2rα and il-2 shape a population of regulatory cells that controls cd4+ t cell numbers*, The Journal of Immunology **169** (2002), no. 9, 4850–4860.

[7] ARM Almeida, B Zaragoza, and AA Freitas, *Indexation as a novel mechanism of lymphocyte homeostasis: the number of cd4+ cd25+ regulatory t cells is indexed to the number of il-2-producing cells*, The Journal of Immunology **177** (2006), no. 1, 192–200.

[8] ARM Almeida, B Zaragoza, and AA Freitas, *Stochastic descriptors to study the fate and potential of naive t cell clonotypes in the periphery*, Journal of Mathematical Biology. Under review (2015).

[9] MA Beaumont, *Approximate bayesian computation in evolution and ecology*, Annual review of ecology, evolution, and systematics **41** (2010), 379–406.

[10] Golan Bel, Brian Munsky, and Ilya Nemenman, *The simplicity of completion time distributions for common complex biochemical processes*, Physical biology **7** (2009), no. 1, 016003.

[11] O Boyman and J Sprent, *The role of interleukin-2 during homeostasis and activation of the immune system*, Nature Reviews Immunology **12** (2012), no. 3, 180–190.

[12] RJ Boys, DJ Wilkinson, and TBL Kirkwood, *Bayesian inference for a discretely observed stochastic kinetic model*, Statistics and Computing **18** (2008), no. 2, 125–135.

[13] D Busse, *Dynamics of the il-2 cytokine network and t-cell proliferation*, Logos Verlag Berlin GmbH, 2010.

[14] H Caswell, *Perturbation analysis of continuous-time absorbing markov chains*, Numerical Linear Algebra with Applications **18** (2011), no. 6, 901–917.

[15] PG Ciarlet, B Miara, and JM Thomas, *Introduction to numerical linear algebra and optimisation*, Cambridge University Press, 1989.

[16] VP Dave, *Hierarchical role of cd3 chains in thymocyte development*, Immunological reviews **232** (2009), no. 1, 22–33.

[17] SK Dower, SR Kronheim, CJ March, PJ Conlon, TP Hopp, S Gillis, and DL Urdal, *Detection and characterization of high affinity plasma membrane receptors for human interleukin 1.*, The Journal of Experimental Medicine **162** (1985), no. 2, 501–515.

[18] A Economou, A Gómez-Corral, and M López-García, *A stochastic sis epidemic model with heterogeneous contacts*, Physica A: Statistical Mechanics and its Applications **421** (2015), 78–97.

[19] ML Ford, AB Adams, and TC Pearson, *Targeting co-stimulatory pathways: transplantation and autoimmunity*, Nature Reviews Nephrology **10** (2014), no. 1, 14–24.

[20] WH Fridman, F Pagès, C Sautès-Fridman, and J Galon, *The immune contexture in human tumours: impact on clinical outcome*, Nature Reviews Cancer **12** (2012), no. 4, 298–306.

[21] RN Germain, *T-cell development and the cd4-cd8 lineage decision*, Nature reviews. Immunology **2** (2002), no. 5, 309.

[22] DT Gillespie, *Exact stochastic simulation of coupled chemical reactions*, The Journal of Physical Chemistry **81** (1977), no. 25, 2340–2361.

[23] A Gómez-Corral and M López García, *Extinction times and size of the surviving species in a two-species competition process*, Journal of mathematical biology **64** (2012), no. 1-2, 255–289.

[24] A Gómez-Corral and M López-García, *On the number of births and deaths during an extinction cycle, and the survival of a certain individual in a competition process*, Computers & Mathematics with Applications **64** (2012), no. 3, 236–259.

[25] A Gómez-Corral and M López-García, *Perturbation analysis in finite LD-QBD processes and applications to epidemic models*, Numerical Linear Algebra with Applications (Under review).

[26] C Guihenneuc-Jouyaux, S Richardson, and IM Longini, *Modeling markers of disease progression by a hidden markov process: application to characterizing cd4 cell decline*, Biometrics **56** (2000), no. 3, 733–741.

[27] KG Gurevich, PS Agutter, and DN Wheatley, *Stochastic description of the ligand–receptor interaction of biologically active substances at extremely low doses*, Cellular Signalling **15** (2003), no. 4, 447–453.

[28] QM He, *Fundamentals of matrix-analytic methods*, Springer, 2014.

[29] DL Iglehart, *Multivariate competition processes*, The Annals of Mathematical Statistics **35** (1964), no. 1, 350–361.

[30] A Jansson, E Barnes, P Klenerman, M Harlén, P Sørensen, SJ Davis, and P Nilsson, *A theoretical framework for quantitative analysis of the molecular basis of costimulation*, The Journal of Immunology **175** (2005), no. 3, 1575–1585.

[31] NG van Kampen, *A power series expansion of the master equation*, Canadian Journal of Physics **39** (1961), no. 4, 551–567.

[32] D Klatzmann and AK Abbas, *The promise of low-dose interleukin-2 therapy for autoimmune and inflammatory diseases*, Nature reviews. Immunology **15** (2015), no. 5, 283.

[33] S Krishnaswamy, MH Spitzer, M Mingueneau, SC Bendall, O Litvin, E Stone, D Pe'er, and GP Nolan, *Conditional density-based analysis of t cell signaling in single-cell data*, Science **346** (2014), no. 6213, 1250689.

[34] VG Kulkarni, *Modeling and analysis of stochastic systems*, CRC Press, 2009.

[35] G Latouche and V Ramaswami, *Introduction to matrix analytic methods in stochastic modeling*, vol. 5, Siam, 1999.

[36] DJ Lenschow, TL Walunas, and JA Bluestone, *Cd28/b7 system of t cell costimulation*, Annual review of immunology **14** (1996), no. 1, 233–258.

[37] M López-García, *Stochastic descriptors in an sir epidemic model for heterogeneous individuals in small networks*, Mathematical Biosciences. Under review (2015).

[38] M López-García, M Nowicka, C Bendtsen, G Lythe, S Ponnambalam, and C Molina-París, *Stochastic models of the binding kinetics of vegf-a to vegfr1 and vegfr2 in endothelial cells*, Journal of Theoretical Biology. Under review (2015).

[39] JR Magnus and H Neudecker, *Matrix differential calculus with applications to simple, hadamard, and kronecker products*, Journal of Mathematical Psychology **29** (1985), no. 4, 474–492.

[40] JR Magnus and H Neudecker, *Matrix differential calculus with applications in statistics and econometrics*, (1995).

[41] TR Malek and I Castro, *Interleukin-2 receptor signaling: at the interface between tolerance and immunity*, Immunity **33** (2010), no. 2, 153–165.

[42] TR Malek, BO Porter, EK Codias, P Scibelli, and A Yu, *Normal lymphoid homeostasis and lack of lethal autoimmunity in mice containing mature t cells with severely impaired il-2 receptors*, The Journal of Immunology **164** (2000), no. 6, 2905–2914.

[43] TR Malek, A Yu, V Vincek, P Scibelli, and L Kong, *Cd4 regulatory t cells prevent lethal autoimmunity in il-2rβ-deficient mice: implications for the nonredundant function of il-2*, Immunity **17** (2002), no. 2, 167–178.

[44] TR Malek, A Yu, L Zhu, T Matsutani, D Adeegbe, and AL Bayer, *Il-2 family of cytokines in t regulatory cell development and homeostasis*, Journal of Clinical Immunology **28** (2008), no. 6, 635–639.

[45] S Marino, IB Hogue, CJ Ray, and DE Kirschner, *A methodology for performing global uncertainty and sensitivity analysis in systems biology*, Journal of theoretical biology **254** (2008), no. 1, 178–196.

[46] R Medzhitov and CA Janeway, *Innate immunity: impact on the adaptive immune response*, Current opinion in immunology **9** (1997), no. 1, 4–9.

[47] C Moler and C Van Loan, *Nineteen dubious ways to compute the exponential of a matrix, twenty-five years later*, SIAM review **45** (2003), no. 1, 3–49.

[48] K Murphy and C Weaver, *Janeway's immunobiology*, Garland Science, 2016.

[49] N Nagarsheth, MS Wicha, and W Zou, *Chemokines in the cancer microenvironment and their relevance in cancer immunotherapy*, Nature Reviews Immunology (2017).

[50] MF Neuts, *Matrix-analytic methods in queuing theory*, European Journal of Operational Research **15** (1984), no. 1, 2–12.

[51] C Park and TS Kupper, *The emerging role of resident memory t cells in protective immunity and inflammatory disease*, Nature medicine **21** (2015), no. 7, 688.

[52] JK Pritchard, MT Seielstad, A Perez-Lezaun, and MW Feldman, *Population growth of human y chromosomes: a study of y chromosome microsatellites.*, Molecular biology and evolution **16** (1999), no. 12, 1791–1798.

[53] OS Qureshi, S Kaur, TZ Hou, LE Jeffery, NS Poulter, Z Briggs, R Kenefeck, AK Willox, SJ Royle, JZ Rappoport, and DM Sansom, *Constitutive clathrin-mediated endocytosis of ctla-4 persists during t cell activation*, Journal of Biological Chemistry **287** (2012), no. 12, 9429–9440.

[54] OS Qureshi, Y Zheng, K Nakamura, K Attridge, C Manzotti, EM Schmidt, J Baker, LE Jeffery, S Kaur, Z Briggs, et al., *Trans-endocytosis of cd80 and cd86: a molecular basis for the cell-extrinsic function of ctla-4*, Science **332** (2011), no. 6029, 600–603.

[55] C Rangel, J Angus, Z Ghahramani, M Lioumi, E Sotheran, A Gaiba, D L Wild, and F Falciani, *Modeling t-cell activation using gene expression profiling and state-space models*, Bioinformatics **20** (2004), no. 9, 1361–1372.

[56] GEH Reuter, *Competition processes*, Proc. 4th Berkeley Symp. Math. Statist. Prob, vol. 2, 1961, pp. 421–430.

[57] J Reynolds, IF Amado, AA Freitas, G Lythe, and C Molina-París, *A mathematical perspective on cd4+ t cell quorum-sensing*, Journal of theoretical biology **347** (2014), 160–175.

[58] SA Rosenberg, *Il-2: the first effective immunotherapy for human cancer*, The Journal of Immunology **192** (2014), no. 12, 5451–5458.

[59] R Roychoudhuri, RL Eil, and NP Restifo, *The interplay of effector and regulatory t cells in cancer*, Current opinion in immunology **33** (2015), 101–111.

[60] S Sakaguchi, *Regulatory t cells: key controllers of immunologic self-tolerance*, Cell **101** (2000), no. 5, 455–458.

[61] S Sakaguchi, T Yamaguchi, T Nomura, and M Ono, *Regulatory t cells and immune tolerance*, Cell **133** (2008), no. 5, 775–787.

[62] P Salama, M Phillips, F Grieu, M Morris, N Zeps, D Joseph, C Platell, and B Iacopetta, *Tumor-infiltrating foxp3+ t regulatory cells show strong prognostic significance in colorectal cancer*, Journal of clinical oncology **27** (2009), no. 2, 186–192.

[63] A Saltelli, K Chan, EM Scott, et al., *Sensitivity analysis*, vol. 1, Wiley New York, 2000.

[64] JA Schmid, *The acidic environment in endocytic compartments.*, Biochemical Journal **303** (1994), no. Pt 2, 679.

[65] KT Schultz and F Grieder, *Structure and function of the immune system*, Toxicologic pathology **15** (1987), no. 3, 262–264.

[66] K Shortman, D Vremec, and M Egerton, *The kinetics of t cell antigen receptor expression by subgroups of cd4+ 8+ thymocytes: delineation of cd4+ 8+ 3 (2+) thymocytes as post-selection intermediates leading to mature t cells.*, The Journal of Experimental Medicine **173** (1991), no. 2, 323–332.

[67] LM Sompayrac, *How the immune system works*, John Wiley & Sons, 2015.

[68] B Soskic, OS Qureshi, T Hou, and DM Sansom, *A transendocytosis perspective on the cd28/ctla-4 pathway.*, Advances in immunology **124** (2013), 95–136.

[69] B Sulzer, RJ De Boer, and AS Perelson, *Cross-linking reconsidered: binding and cross-linking fields and the cellular response.*, Biophysical journal **70** (1996), no. 3, 1154.

[70] Y Takeuchi and H Nishikawa, *Roles of regulatory t cells in cancer immunity*, International immunology **28** (2016), no. 8, 401–409.

[71] T Taniguchi and Y Minami, *The il-2il-2 receptor system: a current overview*, Cell **73** (1993), no. 1, 5–8.

[72] JJ Tyson, KC Chen, and B Novak, *Sniffers, buzzers, toggles and blinkers: dynamics of regulatory and signaling pathways in the cell*, Current opinion in cell biology **15** (2003), no. 2, 221–231.

[73] E Valk, CE Rudd, and H Schneider, *Ctla-4 trafficking and surface expression*, Trends in immunology **29** (2008), no. 6, 272–279.

[74] NG van Kampen, *The expansion of the master equation*, Adv. Chem. Phys **34** (1976), 245–309.

[75] NG Van Kampen, *Stochastic processes in physics and chemistry*, vol. 1, Elsevier, 1992.

[76] L Walker and DM Sansom, *The emerging role of ctla4 as a cell-extrinsic regulator of t cell responses*, Nature reviews Immunology **11** (2011), no. 12, 852–863.

[77] J Zhang, LT Watson, and Y Cao, *A modified uniformization method for the solution of the chemical master equation*, Computers & Mathematics with Applications **59** (2010), no. 1, 573–584.